The resistances of stud shear connectors with profiled sheeting

by

Hui Yuan
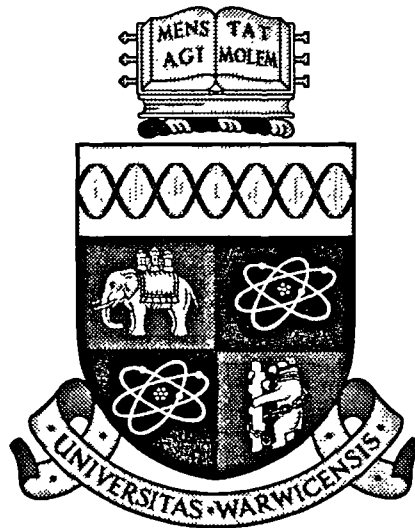
Department of Engineering

University of Warwick

Coventry CV4 7AL

The United Kingdom

A thesis submitted to the University of Warwick for the degree of

DOCTOR OF PHILOSOPHY

December, 1996

TO MY PARENTS

Contents

List of Tables

List of Figures

Abstract

This thesis presents the study of the static behaviour of stud shear connectors welded through profiled sheeting and the fatigue resistances of the connectors in composite bridges.

In the presence of profiled sheeting in a composite beam, the resistance of stud connectors to static shear is influenced by the geometry of the ribs and the position of the studs within them. This is allowed for in the existing methods by applying a reduction factor to the resistance of the stud in a solid slab, but a study of the results of 203 push-out tests showed that the influences are not taken into account properly. The reason, revealed by 16 new push-out tests with transverse sheeting and 18 with parallel sheeting, is that the existing methods do not distinguish between the various failure modes.

New conceptual and mathematical models are developed with respect to the different failure modes. For transverse sheeting, up to nine parameters are involved, among which five are shown by statistic analyses to have negligible influence. Based on the other four, simpler expressions for reduction factors are derived, and the characteristic resistances (5% fractile) are given. For parallel sheeting, however, it is found that the reduction factor method used in the existing models is not suitable, because the mechanism of load transfer is different. On a whole, the new models improve the prediction of 95% of all the valid reported test results, from a range -40% to +100% to within ±11%.

The fatigue resistances of stud connectors in composite bridges are studied statistically using 115 sets of reported data. It is found that the testing methods have significant influence on the results, and are the reason for the discrepancies between the existing models. A new model is proposed, based on the most reliable group of data.

Acknowledgements

Declaration

I hereby declare that all the investigations presented in this thesis are my own except where specific reference has been made to the work of others. No part of this thesis has been submitted to any other university or institution for credit or award.

Notation

A_c	area of the surface of a concrete cone
A_r	cross section area of the transverse reinforcement per unit longitudinal length of the crack plane in the concrete slab
A_s	cross section area of the shank of a stud connector
b_{EC}, b_H, b_L	correction factors for the theoretical functions given by Eurocode 4, by Lawson and by Hanswille, respectively, as used in the statistical analyses
b_a	width of a patch or strip load
$b_{c,i}$, $b_{c,o}$	widths of the inner and outer prisms, respectively
b_e	effective upper width of the trough of steel sheeting; for single or staggered studs, $b_e = b_u$; for two transverse studs, $b_e = b_u/2$
b_o	average width of the trough of steel sheeting
b_u	upper width of the trough of steel sheeting
B_c, B_p	widths of stress regions in the concrete an the steel sheeting
d	diameter of the shank of a stud connector
d_c	depth of a concrete prism
d_r	diameter of a reinforcing bar
e	distance from the centre of a stud to the mid-depth of the nearer web of the trough of steel sheeting
e_f, e_r	for one stud per trough, the average covers of concrete in the trough in front and at the rear of the stud connector
e_u	distance from the centre of a stud to the nearer top flange of the trough of steel sheeting
E_{cm}, E_s	elastic modulus of concrete and the stud, respectively

f_c, f_{cu}	cylinder and cube strengths of concrete, respectively
f_{ct}	splitting tensile strength of concrete
f_y, f_{yd}	yield strengths of studs and steel sheeting
f_u	ultimate tensile strength of stud connectors
F, $F_{\alpha=5\%}$	F values found from a sample and at 5% significance level, respectively
g, G	failure function in X-space and in Z-space, respectively
h	overall height of a stud connector
h_a	depth of a patch load
h_c	overall depth of the concrete slab
h_{eff}	effective depth of the patch load, taking into account the vertical dispersal of the patch load; $h_{eff} = Q \cdot h_a$
h_{es}, h_{ep}	effective depths of the bearing area for splitting failure and for pulling out failure, respectively
h_p	depth of the trough of steel sheeting
h_r	distance from the reinforcement to the base of a stud
H	height of the fix-ended concrete beam, Figure 5.3
H_o, H_a	null and alternative hypotheses in the statistical analyses
k	shear-friction factor
k_α, k_s, k_d	fractile factors for α, characteristic and design resistances, respectively
K_d, K_s	factors used in the splitting theory of Oehlers, equations (2.19) and (2.20)
k_t, k_p	reduction factors for stud connectors with transverse and parallel sheeting; the other subscripts are for:
	c — concrete pulling out failure;
	f — the stud on the favourable side;
	r — rib punching failure;
	u — the stud on the unfavourable side.

$k_{t,\text{limit}}$	upper limit for k_t as given by Hanswille [16]
m, K	factors for predicting the fatigue resistances of studs
n	sample size
N_r, N_{rs}	number of studs per trough and per specimen
P_c, P_t	compressive and tensile forces in the concrete slab
P_e	resistance of a stud connector found from a push-out test
$P_{f,r}$, $P_{f,s}$	failure probabilities of the resistance and the load effects, respectively
P_r	predicted resistance of a stud connector with profiled sheeting; the other subscripts are:

<blockquote>

EC	—	Eurocode 4 model [7];
H	—	Hanswille's model [16];
L	—	Lawson's model [26];
p,i	—	splitting resistance of the inner prism given by Oehlers;
p,o	—	splitting resistance of the outer prism given by Oehlers;
ps	—	post-splitting resistance given by Oehlers;
u	—	for two studs per trough, the stud on the unfavourable side;
f	—	for two studs per trough, the stud on the favourable side.

</blockquote>

P_{rs}	predicted resistance of a stud in a solid slab
P_s	strip or patch load on a concrete prism
P_{sy}	resistance of a stud connector to pure shear
Q	proportional increase in resistance due to the vertical dispersal of the patch load

r	resistance function; subscripts are:
	α — value with failure fractile α;
	k — characteristic value;
	d — design value;
	t — mean value;
	e — value found from tests.
s	load effect
s_1, s_2	variances of two samples
s_c	weighted variance of two samples
s_r	transverse spacing of reinforcing bars
s_t, s_v	transverse and longitudinal spacings of stud connectors
t, $t_{\alpha=5\%}$	t values found from a sample and at 5% significance level, respectively
T, T_d	tensile forces in the stud and the steel sheeting, respectively
T_{su}, T_{sf}	for two staggered or transverse studs, tensile forces in the studs on the unfavourable and favourable sides, respectively
T_y	resistance of a stud connector to uniaxial tension
T_u	central torque on a beam
V	coefficient of variation; subscripts are the variables studied
$\bar{x}_1$, $\bar{x}_2$	means of two samples
α	significance level or failure fractile with subscript r for resistance and s for load effect
β	safety index

δ	error terms of a resistance function; subscripts are:

EC — Eurocode 4 model [7];

H — Hanswille's model [16];

L — Lawson's model [26].

σ	standard deviation; subscripts are the variables studied
σ_s	tensile stress in the shank of a stud connector
η_1, η_E	conversion factors for the tensile strength and the elastic modulus of lightweight concrete, respectively
η_h	factor for the height of a stud connector (equation 2.6))
η_f	friction factor between steel and concrete
η_t	thickness factor for steel sheeting
η, λ	the two factors for calculating the reduction factors for studs with transverse sheeting, as given by the new models; subscripts are:

c — concrete pulling out failure;

f — the stud on the favourable side;

r — rib punching failure;

u — the stud on the unfavourable side.

τ_r	shear stress on stud connectors
ν_t	torsional shear stress in the concrete slab
ν_{tu}	torsional shear strength of concrete
ν	degree of freedom
γ_M	partial safety factor
θ	slope of the trough of steel sheeting, in degree
θ_c	slope of the sides of a concrete cone, in degree
μ	mean of a population
ρ	measured density of concrete
ρ_u	upper limit of a density class (table 7.1)

Chapter 1

General introduction

Steel-concrete composite beams with profiled steel sheeting as permanent form-work for composite floor slabs have been used in building construction for some considerable time. To ensure the composite action between the steel beams and the concrete slabs, stud shear connectors are used. They are placed in the troughs of the sheeting and welded onto the top flanges of the steel beams through either sheeting or pre-cut holes in the sheeting.

In the design of such composite beams, the strength of the stud shear connectors is of great importance. Much of the research into the behaviour of stud shear connectors are based on push-out tests. Usually, there are two types of push-out specimens. One is the specimens simulating a shear connection in an interior composite beam, and the other is those simulating a shear connection in an exterior beam of a composite floor system. The research presented in this thesis concerns only the former.

The research consists of two parts. The first part is the static behaviour of stud shear connectors welded through profiled sheeting. It is based on experimental work, the object of which is to obtain physical understanding of load transfer and the failure criteria of the connectors, and hence to predict the shear resistance

1

of the connectors more rationally, compared with the existing models. This part of the research is presented in Chapters 2 to 9. The second part is the fatigue resistance of stud connectors in composite bridges. It is a conceptual study on the reported test results, aimed at revealing the reasons for the discrepancies in the existing models. Details are given in Chapter 10.

For the static resistance of stud connectors with profiled sheeting, the development of the existing models is briefly reviewed in Chapter 2. The most recent ones, Eurocode 4 model [7], Lawson's model [26] and Hanswille's model [16] are compared in Chapter 3 with a total of 183 reported results of push-out tests. This reveals the gaps in these reported data and the inappropriate regions of the three models.

Therefore, two series of push-out tests, altogether 34, were carried out. They were designed, according to the analyses of Chapter 3, to add fresh information in the gaps and the inappropriate regions. Details of the specimen layouts, manufacture, testing procedures, material properties, maximum loads and failure modes are described in Chapter 4. Compared with the three models mentioned above, these 34 tests show that none of them is appropriate, because they do not distinguish the various failure modes found in the tests.

The following work is to find new models. It is presented in Chapter 5 for transverse sheeting and in Chapter 6 for parallel sheeting. The most significant characteristic of these new models is that they are developed with respect to the different kinds of failure modes. For stud connectors with transverse sheeting, there are five kinds of failure modes: shank shearing, concrete pulling out, rib punching, rib punching combined with shank shearing and rib punching combined with concrete pulling out. The first two are predicted by a rotation model, the third by an arch model, and the last two combined failure modes by a combined model. For stud connectors with parallel sheeting, the two failure modes, splitting and pulling out, are predicted by a splitting model with a shear-friction concept.

These models are only for stud connectors in normal weight concrete. In the following chapter, Chapter 7, the influence of the density of concrete is studied. It proves that the models can still be used to predict the resistances of stud connectors in lightweight concrete, by introducing the conversion factors for the strengths and the elastic modulus of concrete, as given by Eurocode 2: Part 1-4 [5].

However, it is noted that the theoretical models are very complicated, especially those for transverse sheeting, with as many as nine variables involved simultaneously. A series of simplifications is carried out on the three models described in Chapter 5, by first finding out which variables have the most significant influence and then applying regression analyses. The results, with only three or four variables, are simple and straightforward. Details are given in Chapter 8.

As all of the new models described in Chapters 5 to 8 are developed to predict the mean resistances of the connectors, the partial safety factors γ_M are studied in Chapter 9, by means of the new statistical concept of Johnson and Huang [23], based on which the design resistance (0.1% fractile) for one stud per trough is given.

For the fatigue resistance of stud shear connectors, the study is presented in Chapter 10. A total of 115 data are selected, and are analysed by statistical methods of F-tests and two-sample t-tests to reveal the reasons for the discrepancies in the existing models.

The final chapter, Chapter 11, summarises the results of this research and gives suggestions for further studies.

Chapter 2

Literature review

2.1 Stud connectors with transverse sheeting

There are mainly two kinds of methods in predicting the shear resistances of stud connectors with transverse sheeting. One is the reduction factor method, and the other is the shear cone method.

The reduction factor method, as it is named, is characterised by a reduction factor relative to the resistance of the connector in solid (unsheeted) slab of uniform thickness. The factor is a function of the geometry of profiled sheeting, and does not exceed unity. This method stems from the research of Robinson [39] in 1967, and was formulated by Fisher in 1970 [12]. Since then, arguments have usually been over the function for the reduction factor. There are now models by Grant *et al.* [14] (commonly used in codes of practice USA and Canada), and those recommended by Eurocode 4 [7] and by BS 5950 [2], as well as some alternative models as given by Lawson [26] and by Hanswille [16].

The shear cone method assumes a kind of shear friction failure of the concrete over the surface of the shear cone developed around a stud connector. It was first

proposed by Hawkins and Mitchell [18]. Further efforts made by Jayas and Hosain [21] and by Lloyd and Wright [27] were to adjust either the shear-friction stress or the shape of the shear cone.

2.1.1 Reduction factor method

The reduction factor method can be expressed in a common form as

$$P_{\mathrm{r}} = k_t P_{\mathrm{rs}} \qquad (2.1)$$

where P_{r} and P_{rs} are the resistances of stud connectors with profiled sheeting and in a solid concrete slab, respectively; k_t is the reduction factor which is a function of rib geometry. The following are a number of different proposals for the function of the reduction factor.

Model of Grant et al.

In 1967, Robinson carried out 15 beam tests and 39 push-out tests [39], and concluded that for deep and narrow ribs the shear resistance of stud connectors is a function of the rib geometry, and is substantially less than that in a solid concrete slab. This observation was studied by Fisher in 1970 [12] with some other tests, which led to the finding that the function was the ratio of the average width of the trough of steel sheeting, b_{o}, to the depth of the trough, h_{p}:

$$k_t = \frac{b_{\mathrm{o}}}{h_{\mathrm{p}}} \leq 1.0 \qquad (2.2)$$

Recognising the many uncontrolled and ill-defined variables in the early investigations, Grant *et al.* carried out 17 full scale beam tests [14]. The results showed that k_t was related not only to b_{o} and h_{p} but also to the overall height of the stud connector, h. Supplemented by 58 beam tests of other investigators, the function was found to be

$$k_t = \frac{0.85}{\sqrt{N_{\mathrm{r}}}} \frac{b_{\mathrm{o}}}{h_{\mathrm{p}}} \left(\frac{h}{h_{\mathrm{p}}} - 1 \right) \leq 1.0 \qquad (2.3)$$

which was based on P_{rs} in equation (2.1) as given by equation (2.4).

$$P_{rs} = 0.5A_s\sqrt{f_c E_{cm}} \tag{2.4}$$

in which N_r is the number of studs per trough; A_s the cross section area of the shank of a stud connector; f_c the cylinder strength of concrete; E_{cm} the elastic modulus of concrete.

Equation (2.3) was widely accepted by the Standards of many countries, such as USA, Canada, the U.K., and in draft Eurocode 4.

BS5950: Part 3

After many years of application and especially after the appearance of the modern profiled sheeting, it is recognised that equation (2.3) is unconservative for:

- more than one stud in a trough;

- ribbed sheeting with off-centre studs.

Therefore, in the revised British Standard, BS 5950: Part 3 [2], additional limits were set on the application of equation (2.3). For more than one stud in a trough, the upper limit of the reduction factor k_t is lowered to 0.8 for $N_r = 2$ and 0.6 for $N_r = 3$.

For a stud in the trough with a central rib, there are two positions known as favourable and unfavourable. They are shown in Figures 4.7 and 4.8. In the direction of the shear force, when the stud is behind the central rib, it is in a favourable position, otherwise in an unfavourable position. The beneficial effect of the favourable position is taken into account in BS 5950: Part 3 by replacing b_0 in equation (2.3) with $2(b_0 - e)$, where e is the distance from the centre of the stud to the mid-depth of the nearer web. When a stud is placed on the unfavourable side, b_0 is replaced by $2e$.

Eurocode 4

This model was the result of the statistical analyses by Stark and von Hove [45] on four groups of data which were divided according to the following rules:

Group 1: through-deck welding and $N_r = 1$ (22 data);

Group 2: through-deck welding and $N_r = 2$ (14 data);

Group 3: through-hole welding and $N_r = 1$ (16 data);

Group 4: through-hole welding and $N_r = 2$ (4 data).

The analyses examined the use of equation (2.3), and found that the factor 0.85 in the equation should be reduced to 0.81 for Group 1, 0.72 for Groups 2 and 3 and 0.71 for Group 4. To make it safe, Eurocode 4 [7] adopted the lowest value 0.71 and simplified this to 0.7:

$$k_t = \frac{0.7}{\sqrt{N_r}} \frac{b_o}{h_p} (\frac{h}{h_p} - 1) \le \begin{cases} 1.0 & N_r = 1 \\ 0.8 & N_r \ge 2 \end{cases} \qquad (2.5)$$

with the reference resistance P_{rs} given by

$$P_{rs} = 0.29 \eta_h d^2 \sqrt{f_c E_{cm}} \le 0.8 \frac{\pi d^2}{4} f_u \qquad (2.6)$$

where

$$\eta_h = 0.2 \left[\frac{h}{d} + 1 \right], \quad 3 \le \frac{h}{d} \le 4$$

$$\eta_h = 1, \quad \frac{h}{d} > 4$$

in which d is the diameter of the shank of a stud, and f_u its ultimate tensile strength.

Equation (2.5) was recognised as being a poor approximation, because the factor 0.7 was based on only 4 sets of data (Group 4), which, from the statistical point of view, inevitably resulted in high scatter, but no better one was found.

Lawson's model

A detailed study was carried out by Lawson [26] to examine the use of BS 5950: Part 3 [2], which revealed problems in the following regions:

- wide trough profiles;

- two studs per trough;

- one stud per trough in the unfavourable position.

The reason for the problems was believed to be due to the effects of the various kinds of stud positions. Therefore, new models were proposed accordingly:

$$k_t = \frac{0.75}{\sqrt{N_r}} \frac{b_o}{h_p} \frac{h}{h + h_p} \leq 1.0, \quad \text{for} \quad b_o \leq 2h_p; \tag{2.7}$$

$$k_t = \frac{1.5}{\sqrt{N_r}} \frac{h}{h + h_p(2h_p/b_o)} \leq 1.0, \quad \text{for} \quad b_o \geq 2h_p. \tag{2.8}$$

Both equations are for single or pairs of stud connectors placed centrally in a trough.

For one stud in the favourable position, as in BS 5950: Part 3, b_o in the two equations is replaced by $2(b_o - e)$, while in the unfavourable position, equation (2.7) is used with b_o replaced by $(e + h_p)$ or equation (2.8) if $e > h_p$.

For two studs per trough, if they are transverse to the trough, equation (2.7) or (2.8) is used with $N_r = 2$; if they are in-line along the trough off-centrally, the method is as for one off-centre stud but with $N_r = 2$.

The reference resistance of the stud connectors, P_{rs}, is the tabulated value as given in BS 5950: Part 3 [2] (Clause 5.4.6).

Hanswille's model

In Hanswille's model [16], the effect of the thickness of steel sheeting was considered. A total of 46 reported results of push-out tests was collected, and was

classified into several groups according to the thickness of the sheeting, t_s, and the welding methods. Statistical analyses were then carried out on each group to examine the use of the Eurocode 4 model [7]. It was found that equation (2.5) is unconservative, especially for profiles with thickness less than 1.0 mm and for studs welded through pre-cut holes.

An alternative proposal to the function was given by Hanswille [16] by lowering the limits of equation (2.5) as follows:

$$k_t = \frac{0.7}{\sqrt{N_r}} \frac{b_o}{h_p} (\frac{h}{h_p} - 1) \leq k_{t,\text{limit}} \tag{2.9}$$

in which $k_{t,\text{limit}}$ is as given in Table 2.1.

Table 2.1: Hanswille's model for $k_{t,\text{limit}}$.

Number of studs per trough	Through-deck welding $t_s = 1.2$ mm	Through-deck welding $t_s \leq 1.0$ mm	Through-hole welding
$N_r = 1$	0.90	0.85	0.75
$N_r = 2$	0.75	0.70	0.60

2.1.2 Shear cone method

The shear cone method is restricted to failure by the stud(s) pulling out from the concrete. It assumes a kind of shear and friction failure precipitated on the surface area of a concrete cone or pyramid around the stud connector. It is expressed in a common form as

$$P_r = k\sqrt{f_c} \cdot A_c \tag{2.10}$$

where $\sqrt{f_c}$ represents the shear-friction stress, in N/mm^2 units, over a surface area A_c of the shear cone, as defined later, and k is an empirically derived shear-friction factor.

The method was first proposed by Hawkins and Mitchell in 1984 [18]. They obtained a value of k as 0.45 from eight push-out tests. In 1988, Jayas and Hosain [21] carried out 18 push-out tests and found that for 38-mm deck with b_o/h_p from 1.6 to 4.2, k is 0.61, and for 76-mm deck with $b_o/h_p = 2.0$, 0.35. Apart from this, they introduced another factor λ, varying according to the type of the concrete used: 1.0 for normal density concrete, 0.85 for semi-low density concrete and 0.75 for structural low density concrete. The definition of the density is as given in the CPCI Metric Design Manual (Canadian Prestressed Concrete Institute 1982) [3].

Both methods assumed a 45° pyramid-shaped failure surface intersecting with the profiled sheeting, as shown in Figure 2.1. Details of the calculation of A_c were given in [18] for single or double studs placed in a variety of metal deck geometries.
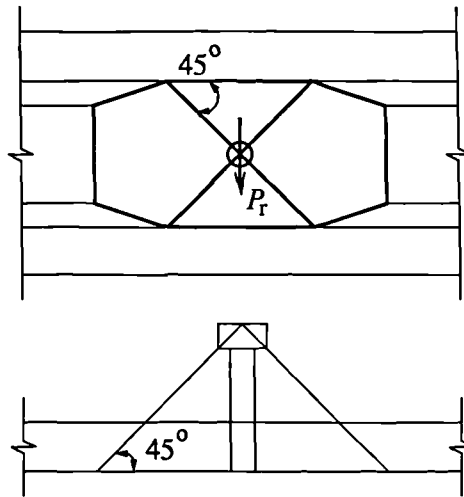
Figure 2.1: The 45° pyramid-shaped shear cone.

The most recent study on a shear cone method was done by Lloyd and Wright [27], in which 42 push-out specimens with 50-mm deck were tested. Checking with the methods mentioned above found k a value of 0.36 for these tests (b_o/h_p around 3.1). Clearly, there are considerable differences in the value of k. The reason for this, explained by Lloyd and Wright, is that approximating the concrete shear failure to a 45° cone is too insensitive to variations in rib geometry and the height

of the stud. Based on the dimensions of the failure cones measured from the 42 tests, a wedge-shaped concrete pyramid was proposed, as shown in Figure 2.2.

The shear strength was then found to be

$$P_r = 0.92(A_c\sqrt{f_{cu}})^{0.34} \tag{2.11}$$

in which $\sqrt{f_{cu}}$ is the shear-friction stress, in N/mm^2 units; f_{cu} the cube strength of concrete; A_c the area of the wedge-shaped concrete cone, in mm^2 units.

The factors 0.92 and 0.34 in equation (2.11) were the results of the regression analysis of $\log P_r$ on $\log(A_c\sqrt{f_{cu}})$ on the 42 data and those from [18] and [21].
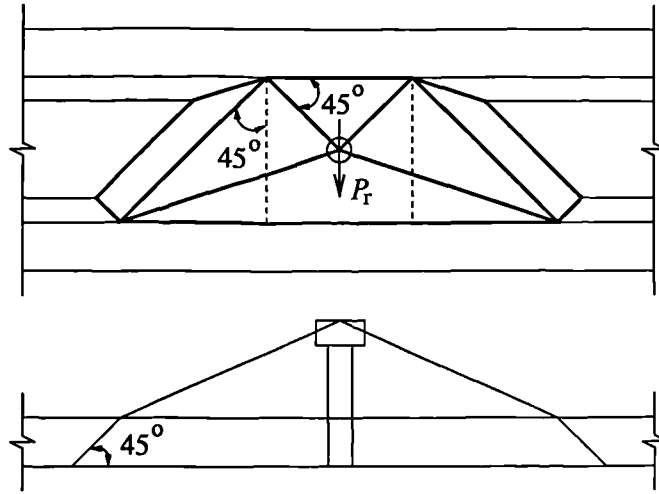
Figure 2.2: Wedge-shaped shear cone.

2.2   Stud connectors with parallel sheeting

There is limited experimental work on stud connectors with parallel sheeting. Based on it, studies have been mainly empirical, in order to find a reliable function for the reduction factor, as has been done for studs with transverse sheeting. Here there are two main models, Eurocode 4 [7] and Lawson's model [26].

Since 1981, a series of theoretical analyses has been carried out by Oehlers

to study the behaviour of stud connectors in composite beams [38]. They were based on finite element analyses [35].

2.2.1 Empirical studies - Reduction factor method

Eurocode 4 model

In 1977, Grant *et al.* found from beam tests with transverse sheeting that the reduction factor is in proportion to two ratios, b_o/h_p and h/h_p, as given by equation (2.3). The model was found to be applicable also to stud connectors with parallel sheeting. For wide troughs with $b_o/h_p > 1.5$, no reduction was required. In other cases, a single constant 0.6 was used to replace $0.85\sqrt{N_r}$ in equation (2.3), and this gave:

$$k_p = 1.0, \quad \frac{b_o}{h_p} > 1.5; \tag{2.12}$$

$$k_p = 0.6\frac{b_o}{h_p}(\frac{h}{h_p} - 1) \leq 1.0, \quad \frac{b_o}{h_p} \leq 1.5. \tag{2.13}$$

For studs with parallel sheeting, Eurocode 4 [7] gives only equation (2.13), without the condition on b_o/h_p, due to the fact that some push-out tests showed that $k_p = 1.0$ for $b_o/h_p > 1.5$ was unconservative.

Lawson's model

In Lawson's study [26], the reduction factors were found to depend on the arrangement of the stud connectors within a trough, and to be related to the rib geometry in terms of only b_o/h_p. The functions proposed are as below:

For a single central line of studs in a trough,

$$k_p = \begin{cases} 0.67\frac{b_o}{h_p} \leq 1.0 & b_o \leq 1.5h_p \\ 1.0 & b_o > 1.5h_p \end{cases} \tag{2.14}$$

For pairs of studs in a trough,

$$k_{\mathrm{p}} = 0.4\frac{b_{\mathrm{o}}}{h_{\mathrm{p}}} \leq 1.0 \tag{2.15}$$

2.2.2 Oehlers' theory

A series of systematic studies has been carried out by Oehlers since 1981. They started with shear resistance of stud connectors in solid concrete slabs, then in concrete slabs with haunches, and finally extended the idea into shear resistances of stud connectors welded through parallel sheeting, based on the assumption that the sheeting in the last case has a similar effect on the shear resistance of stud connectors as haunches and the reinforcement have in the other two cases. These studies were summarised in [38].

For stud connectors with parallel sheeting, three kinds of failure modes were identified. They were dowel failure, splitting failure and post-splitting failure.

Dowel failure

The dowel failure is the shearing of the shank of the stud connector with local damage to the surrounding concrete. It has the highest resistance, and usually occurs when wide-trough decking is used. In this case the rib geometry has no negative influence on the resistance, so the mean dowel strength for stud connectors in a solid concrete slab, P_{rs}, as proposed by Oehlers and Johnson [22], can be used, that is,

$$P_{\mathrm{rs}} = 4.3A_{\mathrm{s}}f_{\mathrm{u}}(\frac{f_{\mathrm{c}}}{f_{\mathrm{u}}})^{0.35}(\frac{E_{\mathrm{cm}}}{E_{\mathrm{s}}})^{0.4} \tag{2.16}$$

where A_{s} and E_{s} are the cross section area and the elastic modulus of the shank of a stud, respectively.

Splitting failure

Splitting failure is by the tensile cracks in the concrete slab in some regions. The transfer of the shear force into the concrete through stud connectors develops transverse tensile force in the slab. When the tensile strain of concrete reaches the ultimate value, the concrete slab splits and fails immediately if there is no effective reinforcement crossing the cracking region. This mode is very brittle.

The transfer of the shear forces through stud connectors is regarded as a concentric patch load with width b_a and depth h_a, as shown in Figure 2.3.
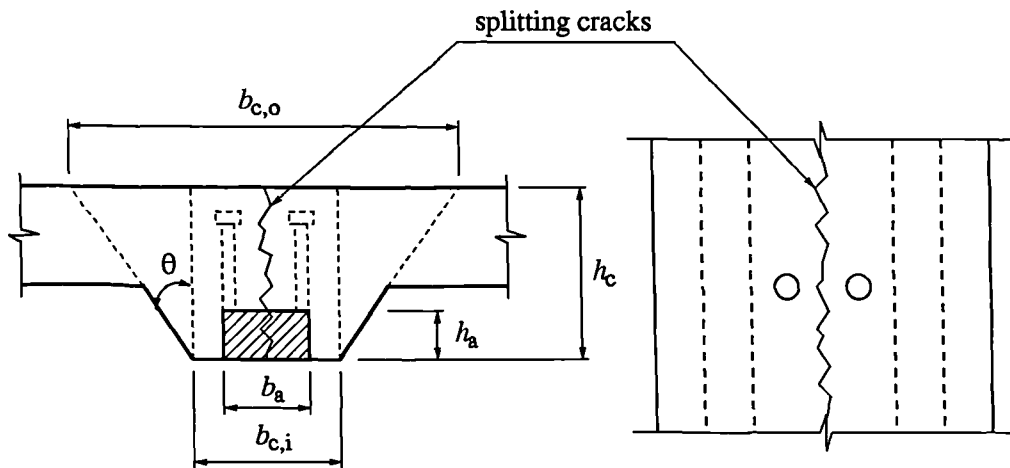
Figure 2.3: The concentric patch action of stud connectors.

The patch load is dispersed into the concrete in three dimensions: horizontal, vertical and in the direction into the paper. To simplify this three-dimensional problem, the patch load is assumed to be acting on two prisms, the inner one with width $b_{c,i}$ and the outer one with width $b_{c,o}$, as shown in Figure 2.4. It is also assumed that the width of the patch load b_a is the diameter of the stud for one line of connectors or the edge distance between the two or multiple lines of connectors. Shown in Figure 2.3 is the definition of b_a for two lines of studs.

The beneficial effect of vertical dispersal of the patch load is taken into account
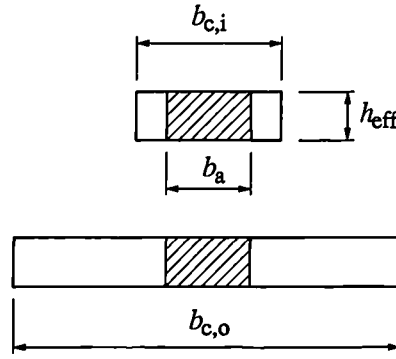
Figure 2.4: Oehlers' splitting analyses: inner and outer prisms.

by the effective depth h_{eff} of the patch load by defining

$$h_{eff} = Q \cdot h_a = Q \cdot 1.8d \qquad (2.17)$$

where Q is the proportional increase in resistance due to vertical dispersal. It is given as

$$Q = 1 + K_d \pi \frac{b_a}{b_c} K_s \qquad (2.18)$$

The factors K_d and K_s are determined by equations (2.19) and (2.20):

$$K_d = \frac{1}{\pi} \left[1 - \frac{b_a}{b_c} \right]^2 \qquad (2.19)$$

and

$$K_s = \left[\left[1 - \frac{1.8d}{h_c} \right]^2 \frac{1.8d}{h_c} \right]^{-1} \qquad (2.20)$$

where h_c is the overall height of the concrete slab.

If $P_{rp,i}$ and $P_{rp,o}$ are the splitting resistances of the inner and outer prisms, respectively, the resistance of splitting failure is determined by:

$$P_{rp} = P_{rp,i} + \frac{\theta}{90}(P_{rp,o} - P_{rp,i}) \qquad (2.21)$$

where θ is in degree. Details of calculating $P_{rp,i}$ and $P_{rp,o}$ are given in [38] (Section 11.5.3) for various stud arrangements: single line, two lines and multiple lines.

Post splitting failure

After splitting occurs, if there is reinforcement across the splitting zone, the released tensile force is taken by the reinforcement. Therefore, the resistance of the connector depends on the amount and position of the reinforcement. With sufficient reinforcement the dowel strength of the stud connector may be reached. The difference between this mode and dowel failure is the severe damage of the concrete in a wider region, due to the deformation of the reinforcement.

If A_r is the area of the transverse reinforcement per unit longitudinal length of the crack plane, and s_v is the longitudinal spacing of a longitudinal line of shear connectors, the post-splitting resistance of a shear connector P_{rps} was found [38] to be

$$P_{rps} = P_{rs}(0.6 + \frac{3A_r s_v}{h_a^2})$$ (2.22)

in which P_{rs} is from equation (2.16), and h_a (= 1.8d) is the depth of the patch load.

Equation (2.22) requires the diameter d_r of the reinforcing bar not greater than $0.4h_a$, and the distance h_r of the bar from the base of the shear connection not greater than $1.7h_a$, as shown in Figure 2.5.
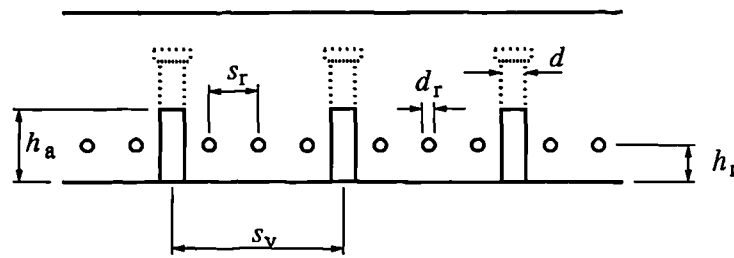
Figure 2.5: Distribution of transverse reinforcement.

In the absence of reinforcing bars in the splitting zone, as is the case for composite slabs, the haunch is fully encased by a trough of profiled sheeting of thickness t_s. Therefore, it is reasonable to assume the effective area of reinforcement A_r for use in equation (2.22) as $\eta_t t_s$, in which η_t is an influence factor for

the thickness of decking. From equation (2.22), the post-splitting resistance for a haunch formed by steel sheeting is

$$P_{\text{rps}} = P_{\text{rs}}(0.6 + \frac{3\eta_t t_s s_v}{h_a^2}) \tag{2.23}$$

The value of η_t can be determined from push-out tests, and P_{rs} from equation (2.16).

2.3 Summary

As this review has shown, design rules given by Eurocode 4 [7] are much more reliable than by BS 5950: Part 3 [2] and the one used in the USA (equation (2.3)), in that they are based on more recent test results.

Proposals for modification given by Lawson [26], Hanswille [16], Lloyd and Wright [27] and others concern the following problems in the design rules:

1. various positions of stud connectors in the modern profiled sheeting;

2. effects of the thickness of profiled sheeting;

3. various failure modes.

However, the physical understanding of the mechanism of load transfer and the failure criteria of stud connectors is still missing. Therefore, the most recent models: the Eurocode 4 model [7], Lawson's model [26] and Hanswille's model [16], are re-examined by reported results of push-out tests to find gaps and the inappropriate regions, as will be shown in the next chapter.

Chapter 3

Analyses of reported results of push tests

3.1 Introduction

Among a large number of reported push-out test data, 203 were selected with respect to their reliabilities, for the analyses carried out in this chapter.

Apart from the variables in concrete, steel decking and stud connectors, these selected data are also different in welding methods and specimen layouts (or numbers of studs per specimen). Naturally, questions are raised - are these test results affected by the welding methods or by the specimen layouts, and if they are, to what extent? In order to solve these problems, statistical methods for testing means and standard deviations were applied. It was found that welding methods have significant influence on test results. As to specimen layouts, the influences are negligible only when the number of studs in a specimen is greater than six.

According to the statistical results, the 203 data were re-divided into seven

significantly different groups. Two of these, with studs welded through pre-cut holes, were not studied, because the influence of welding methods is beyond the range of this research. The other five groups were analysed to examine the use of the reduction factors as given by Eurocode 4 [7], by Lawson [26] and by Hanswille [16].

The results show that none of the three models is satisfactory, especially for steel sheeting with the thickness less than 1.0 mm and for one stud in the unfavourable position, as well as for two studs in a trough.

3.2 Selection of data

The 265 sets of push-out test data are outlined in Table 3.1, in which the Roman numbers I, II and III denote the rows of studs per slab.

As mentioned earlier in Chapter 2, the shear resistances of stud connectors with profiled sheeting in Eurocode 4 are given in the form of reduction factors relative to those in solid concrete slabs P_{rs}, where P_{rs} is assumed to be controlled by the weaker of the concrete or the stud connectors (equation (2.6)). This is shown schematically in Figure 3.1, where f_c is the strength of concrete, and f_u the ultimate tensile strength of the stud. With low strength of concrete, an unknown f_u does not affect the estimation of P_{rs}. On the contrary, it may result in big errors when concrete strengths are higher. Therefore, for tests with unknown f_u, a careful check is needed.

Among the 42 tests reported by Lloyd and Wright [27], 30 have plain decking without embossment. These data are excluded from the analyses, because the embossment is needed to provide additional friction between the steel and the concrete, as is usually the case in the other reported push-out tests. The other 12 tests have stud connectors imported from Germany with an estimated range

of f_u from 450 to 470 N/mm^2. The cube strength of concrete is from 33.1 to 43.4 N/mm^2 (26.5 to 34.7 N/mm^2 if converted to cylinder strength). The shear resistances, then, are between 94.9 and 112.7 kN when f_c controls $(0.29d^2\sqrt{f_cE_{cm}})$, and are greater than 102.1 kN when f_u controls $(0.8\pi d^2 f_u/4)$. So, only those with resistances controlled by f_c are selected.

For the same reason, eight of the 16 tests reported by Roik and Hanenkamp [41] are selected.
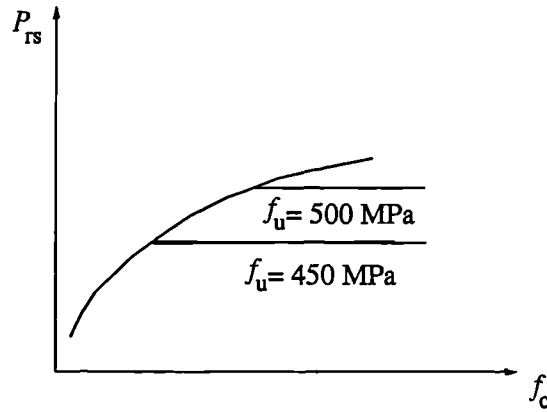
Figure 3.1: Resistances of studs in solid concrete slabs.

The 10 tests of Bode and Künzel [9] with relatively stronger concrete show the uncertainties from f_u much more clearly. Again, all these data have an estimated f_u from 450 to 470 N/mm^2. With the cylinder strengths from 36.5 to 39.1 N/mm^2, the shear resistance controlled by the stud connectors is 136.8 kN for $f_u = 450$ N/mm^2 and 142.9 kN for $f_u = 470$ N/mm^2, well below the resistances controlled by the concrete which is from 156.4 kN to 163.5 kN. So, these data are rejected.

For the Canadian tests with transverse sheeting, [18] to [21] and [40], though f_u was not reported, it is known to be 415 N/mm^2 for the commonly available stud connectors in Canada [11]. Comparing the shear resistances governed by the concrete and by the stud connectors, it is found that the concrete is always on the weaker side. Therefore, these data are selected.

Table 3.1: The outline of 203 reported results of push-out tests.

	Transverse deck								Parallel deck			No.
Ref	One stud per trough				Two studs per trough						Total	of data
	Hole	Deck			Hole	Deck			Gap	Deck		used
	II	I	II	III	II	I	II	III				
[18]			3			4				1	8	8
[21]		2				2	2	2	(5)		13	8
[27]				9					(3)		42	9
				(30)								
[41]	2		3		1		2				16	8
	(4)		(1)		(2)		(1)					
[9]	(10)										10	-
[42]					5						5	5
[34]			28				12				40	40
[10]	6		6								12	12
[20]										8	8	8
[40]		12				11				8	31	31
[17]				10				5		3	18	18
[47]			3				3				12	6
			(3)				(3)					
[29]			23			27					50	50
Total	22	14	70	49	8	44	23	7	8	20	265	
Used	8	14	66	19	6	44	19	7	-	20		203
Group	G12H	G11	G12	G13	G22H	G21	G22	G23				
$\bar{b}_{EC}$	0.82	1.19	1.02	1.01	0.71	1.08	1.03	1.12				
σ_{bEC}	0.10	0.17	0.21	0.09	0.03	0.23	0.36	0.26				

Note: I, II and III are the rows of studs per slab.

Among these reported results of push tests, the types of failure mode were shank shearing, concrete pulling out, rib punching, welding and tension cracking.

The first three types are the modes usually observed in full-scale beam tests. Failure in welding can be prevented by controlling the quality of welding. One result reported by Wright and Gallocher [47] that failed by this mode is rejected.

Tension cracking is the transverse tension cracks developed on the outer concrete surface at the thinner section. It is due to the narrow width of the concrete slab in a push specimen, so it is unlikely to happen in a composite beam where the concrete slab is usually very wide. Five results reported by Wright and Gallocher [47] that failed by this type of mode are rejected.

When a parallel sheeting is used, it can be continuous across the beam or discontinuous with one sheet on each side of the beam. This allows several options for the welding of the studs:

(a) continuous sheeting with stud connectors welded through it;

(b) continuous sheeting with stud connectors welded through holes in it;

(c) discontinuous sheeting with stud connectors welded through it;

(d) discontinuous sheeting with stud connectors welded directly on the steel beam through the gap between the sheeting.

These four options are illustrated in Figure 3.2.

A continuous sheeting can provide effective lateral restraints to the sides of the concrete haunch, as in cases (a) and (b). Similar restraint can also be achieved in case (c), because the sheeting is fixed to the beam by the stud connectors. However, in case (d), as the sheeting is only lightly fixed to the steel flange, it provides little lateral restraint to the concrete haunch. The shear resistance of stud connectors in this case is beyond the range of this study. Cases (a), (b) and (c) are denoted as through-deck welding, and case (d) through-gap welding.

Five tests reported by Jayas and Hosain [21] and three by Lloyd and Wright [27] belong to the latter case, so they are rejected.

(a)   (b)

(c)   (d)
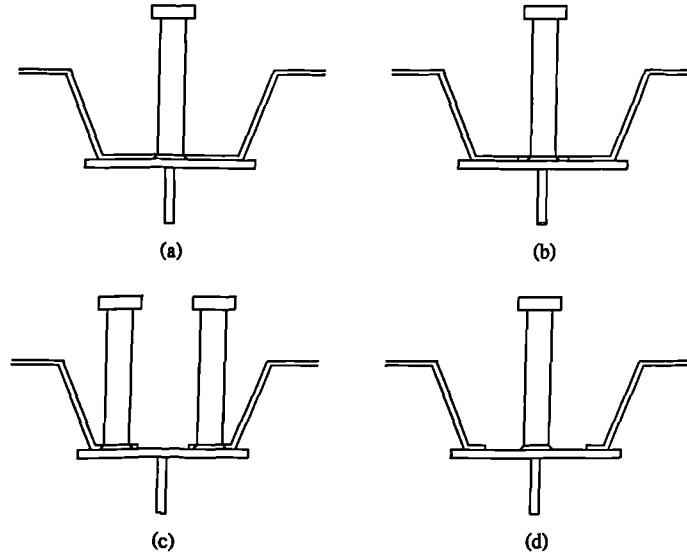
Figure 3.2: The options for stud connectors with parallel sheeting.

Altogether, 203 data are selected, among which 183 have transverse sheeting, and the other 20 parallel sheeting.

3.3 Statistical analyses of the data selected

3.3.1 Random variable b_{EC}

Variables in the selected 203 data can be classified into five areas:

1. concrete (strength and density);

2. stud connector (diameter, height, ultimate tensile strength, number per trough and position);

3. steel sheeting (thickness, width and depth of the trough, and orientation);

4. testing method (base conditions);

5. specimen layout (width, height of the specimen);

6. welding method (through pre-cut hole or through decking).

The first three areas are where the behaviour of stud connectors in a composite beam has been studied. Data with variables within these areas are compatible.

Among the selected 203 data, there are mainly two kinds of base condition of the push specimen. One is the friction base of British style, where the base of the specimen was bedded down on dental plaster directly onto the floor. The other is the friction recessed base of German style, where there was a small recession at the base of the specimen. The influences of these two base conditions were studied by Hicks and McConnel [19]. They concluded that the German style push tests gave only marginally smaller capacities than the British style tests. Considering that there are only 25 data (out of 203) with the base condition of German style, the influence of testing methods can be neglected.

As explained in Section 3.2, data with failure mode that associates with the width of the specimen have been rejected, the influence of the width can also be neglected.

The height of a push specimen usually depends on the rows of studs per slab. Up until now no standard form has been specified for push-out tests on stud connectors with profiled sheeting. The number of rows of stud connectors per slab has been chosen randomly by the researchers, usually from one to three. Therefore, the effects of different rows of studs need to be clarified.

As to the welding methods, though there is experimental evidence that studs welded through profiled sheeting tend to be stronger, Eurocode 4 gives a conservative recommendation on the reduction factors, based on the statistical analyses for two studs per trough welded through pre-cut holes. Their effects also need to be clarified.

Therefore, the selected data are analysed. Because there are only 20 data with parallel sheeting, the analyses are carried out on the 183 data with transverse sheeting.

As shown in Table 3.1, these 183 data are divided into eight groups, according to the number of studs per trough, welding methods and the rows of studs per slab. The names of the groups are defined in such a way that the first digit represents the number of studs per trough, and the second is the rows of studs per slab. For example, G12 means the Group of data with 1 stud per trough and 2 rows in each slab.

Comparing the experimental resistance P_e with the theoretical one P_{rEC} from the Eurocode 4 model (equations (2.1), (2.5) and (2.6)), the correction factor b_{EC} is given by:

$$b_{EC} = \frac{P_e}{P_{rEC}} \qquad (3.1)$$

The mean and the standard deviation of b_{EC}, $\bar{b}_{EC}$ and $\sigma_{b_{EC}}$, for each group are also given in Table 3.1. Differences are obvious among the groups. But are the differences due to welding methods and rows of studs per slab or only to chance? In order to solve this problem, statistical methods for testing means and standard deviations are applied.

3.3.2 Mean of b_{EC}

The statistical method of two-sample t-test is to test the significance of the means of two independently drawn random samples. If μ_1 and μ_2 are the means of the populations from which the samples are drawn, the null hypothesis is

$$H_0 : \mu_1 = \mu_2$$

against the alternative hypothesis

$$H_a : \mu_1 \neq \mu_2$$

When H_o is accepted, it means the two populations have equal means, and the difference in the sample means is purely by chance. When H_o is rejected, H_a is automatically accepted, that is, the two samples are from populations with significantly different means. However, there is a probability of rejecting a true null hypothesis, which is called the significance level α. For example, when $\alpha = 5\%$ and we come to the decision of $\mu_1 \neq \mu_2$, this means that there is 5% probability that μ_1 is actually equal to μ_2 and we make a wrong decision.

For the eight groups in Table 3.1, they can be treated as eight independent random samples, one from each of eight populations. The base samples are chosen as G12 for groups with one stud per trough, and G22 for two studs per trough, because they have similar specimen layouts to that recommended by Eurocode 4 for push-out tests with stud connectors in solid concrete slabs. Two-sample t-tests are carried out between the base sample and any other sample for groups with one and two studs per trough, respectively.

From the way b_{EC} is defined, as given in equation (3.1), it is rational to assume that b_{EC} is a randomly distributed variable with normal distribution. The differences caused by the concrete, steel decking and stud connectors are only by chance. Therefore, if the t-test shows significant difference in the means of b_{EC} of two groups with the same theoretical resistance function P_{rEC}, it can be concluded at 95 per cent confidence level that the variable investigated, either the welding method or the number of rows of studs per slab, has significant influence on the test results P_e. Otherwise, the influence is negligible, with 5 per cent risk of a wrong conclusion.

3.3.3 Standard deviation of b_{EC}

In the two-sample t-test, an assumption about the equality or inequality of the standard deviations is necessary, because two different ways of testing are fol-

lowed. Therefore, the relation between the standard deviations of the two samples are determined by applying the F-test prior to the two-sample t-test.

The F-test is to test the significance of the variations. It follows similar rules to the two-sample t-test, except that the null hypothesis is H_o: $\sigma_1 = \sigma_2$, and the alternative hypothesis is H_a: $\sigma_1 \neq \sigma_2$, where σ_1 and σ_2 are the standard deviations of the two underlying populations from which the samples are drawn.

The acceptance of the null hypothesis means the two populations have the same variance, and the difference in the two samples is due to chance only. On the contrary, the rejection of it proves with 95 per cent confidence level that some real cause is responsible for the difference in the variances of the two samples.

For the eight groups concerned here, the F-test is carried out on the base sample and one other sample. From equation (3.1), it can be seen that the variance of b_{EC} is due to partly to the randomness of the variables in concrete, steel decking and stud connectors, and partly to the imperfection of the theoretical models. The former is virtually the same for all theoretical models, so the differences in σ_{bEC} come mainly from the latter.

If the F-test shows significant differences in σ_{bEC} for the two groups tested, it means the theoretical model is less appropriate for the group with higher σ_{bEC} than for that with lower one. In other words, the variable investigated (either welding methods or rows of studs per slab) has significant influence on the test results, but is not taken into account by the theoretical model. In this case, a new theoretical function is needed.

If the F-test shows no significant difference in σ_{bEC} of the two groups, it only means the theoretical model predicts the two groups of tests with the same accuracy, with respect to their means. The significantly different means of the two groups, therefore, is due to the welding methods or rows of studs per slab, and it can be concluded that the influence is very simple: the tested values are

either higher or lower by a certain percentage.

3.3.4 Procedures of the statistical analyses

The procedures of the testing on the base sample and any other sample are as follows:

1. Calculating the value of b_{EC} (equation (3.1)) for each set of data of the two samples.

2. Finding out the mean and the standard deviation of b_{EC} for each sample.

3. Performing the F-test to test the significance of the standard deviations of b_{EC} of the two samples, with the null hypothesis H_o: $\sigma_1 = \sigma_2$ against the alternative hypothesis H_a: $\sigma_1 \neq \sigma_2$ at the 5 per cent significance level.

   If s_1 and s_2 are the standard deviations computed from the two samples, the random variable

   $$F = \frac{s_1^2/\sigma_1^2}{s_2^2/\sigma_2^2} \qquad (3.2)$$

   follows a distribution called the F distribution, with the degrees of freedom $\nu_1 = n_1 - 1$ and $\nu_2 = n_2 - 1$, where n_1 and n_2 are the sizes of the two samples, respectively [24].

   Invoking the null hypothesis H_o, equation (3.2) is reduced to

   $$F = \frac{s_1^2}{s_2^2}, \quad s_1 > s_2. \qquad (3.3)$$

   The value of F is compared with the one found from the F distribution at 5 per cent level, given in Table A.14 of [24]. If F is greater than the tabulated value, the null hypothesis H_o is rejected, and it is concluded with 95 per cent confidence level that the influence of welding methods or specimen layouts is significant. If, otherwise, F is less than the tabulated value, the null hypothesis is accepted, and step 4 is performed.

4. As $\sigma_1 = \sigma_2$ is accepted, the two-sample t-test is performed for equal standard deviations, with the null hypothesis H_o: $\mu_1 = \mu_2$ against the alternative hypothesis H_a: $\mu_1 \neq \mu_2$ at the 5 per cent significance level, where μ_1 and μ_2 denote the means of the *underlying populations*.

If $\bar{x}_1$ and $\bar{x}_2$ are the means of b_{EC} of the two samples, the statistic

$$t = \frac{|\bar{x}_1 - \bar{x}_2|}{s_c\sqrt{\frac{1}{n_1} + \frac{1}{n_2}}} \tag{3.4}$$

has a t distribution with $(n_1 + n_2 - 2)$ degrees of freedom, where

$$s_c^2 = \frac{(n_1 - 1)s_1^2 + (n_2 - 1)s_2^2}{n_1 + n_2 - 2} \tag{3.5}$$

Comparing t from equation (3.4) with the value in Table A.7 of [24] at 5 per cent level, if t is smaller, the null hypothesis is accepted, and the conclusion is that the influence of welding methods or specimen layouts is negligible. Otherwise, the null hypothesis is rejected, and the difference in the two samples is believed with 95 per cent confidence level to be the result of different welding methods or specimen layouts.

3.3.5 Results of the statistical analyses

The results are listed in Tables 3.2 and 3.3, relative to the number of studs per trough.

The influence of welding methods is significant for both one and two studs in a trough, and is found that studs welded through decks are stronger than through holes. This might be because the decking fixed by the weld collar stiffens the studs around the base area, though the weld collar itself is less pronounced, compared to the case of through-hole welding. However, the effect of welding methods is beyond the scope of this research, so the following analyses concern only studs welded through decking.

In the sequence of G11, G12, G21, G13, G22 and G23, the numbers of studs per specimen, N_{rs}, are 2, 4, 4, 6, 8 and 12. From both Tables 3.2 and 3.3, the F- and t-tests show that their influence on test results can only be neglected when there are more than six studs in a push-out specimen. So, G22 and G23 with 8 and 12 studs per specimen are combined into one single group, denoted as G223. The significantly different groups are:

G11: one row of one stud per trough;

G12: two rows of one stud per trough;

G13: three rows of one stud per trough;

G21: one row of two studs per trough;

G223: two or three rows of two studs per trough.

Table 3.2: F- and t-tests for groups with one stud per trough.

Group	n	N_{rs}	$\bar{b}_{EC}$	σ_{bEC}	F-test		t-test	
					F	$F_{\alpha=5\%}$	t	$t_{\alpha=5\%}$
G12	66	4	1.0187	0.2093				
G11	14	2	1.1911	0.1740	1.45 $<$	2.25	2.87 $>$	1.98
G13	19	6	1.0052	0.0927	5.09 $>$	2.02		
G12H	8	4	0.8274	0.0968	4.68 $>$	3.30		

n — size of group; N_{rs} — number of studs per specimen.

3.4 Discussion

The above five groups of test results are analysed to examine the use of the Eurocode 4 model and the alternative models given by Lawson and by Hanswille.

Table 3.3: *F*- and *t*-tests for groups with two studs per trough.

Group	n	N_{rs}	$\bar{b}_{EC}$	σ_{bEC}	\multicolumn{2}{c}{*F*-test}		\multicolumn{2}{c}{*t*-test}	
					F	$F_{\alpha=5\%}$		t	$t_{\alpha=5\%}$
G22	19	8	1.0292	0.3606					
G21	44	4	1.0764	0.2303	2.45	>	1.84		
G23	7	12	1.1249	0.2588	1.94	<	3.87	0.37 <	2.06
G22H	6	8	0.7071	0.0296	148.17	>	4.56		

n — size of group; N_{rs} — number of studs per specimen.

In Chapter 2, it was shown that compared to the Eurocode 4 model, Lawson's model is characterised by the consideration of different stud positions within a trough, and Hanswille's model by the introduction of a new variable, the thickness of the sheeting.

As explained in Section 3.3.3, the accuracy of the theoretical model is reflected by the standard deviation of b_{EC}. If, for each group, let $\delta_{EC} = b_{EC}/\bar{b}_{EC}$, noting that $\bar{\delta}_{EC} = 1$, then $\sigma_{\delta EC}$ are compatible among the groups, and hence the effects of stud positions and the thickness of sheeting can be studied on a more general basis.

For the two alternative models, the corresponding variables are developed in the same way, that is:

for Lawson's model

$$b_L = \frac{P_e}{P_{rL}}, \quad \delta_L = \frac{b_L}{\bar{b}_L}; \tag{3.6}$$

for Hanswille's model

$$b_H = \frac{P_e}{P_{rH}}, \quad \delta_H = \frac{b_H}{\bar{b}_H}. \tag{3.7}$$

Comparing these variables will show the improvements and also the problems of the two alternative models.

3.4.1 Stud positions

For one stud per trough, the stud connectors can be in three positions: central, favourable and unfavourable, and for two studs per trough, the positions are much more complex. In the direction of the troughs, they are centre, favourable, unfavourable, transverse and staggered.

These positions are not distinguished by Eurocode 4. For one stud in the central or favourable position, as shown respectively in Figures 3.3 and 3.4, when $b_o/h_p < 1.4$, Eurocode 4 is over conservative, and the scatter is from 0.9 to 2.0. In the region of $2 \leq b_o/h_p \leq 3.2$, the scatter is still very high, from 0.7 to 1.1 for the central position and 0.9 to 1.4 for the favourable position. Figure 3.5 shows the results of one stud in the unfavourable position. The unconservatism of Eurocode 4 is very obvious, especially when $b_o/h_p \geq 2.6$. The scatter still keeps at the high level, from 0.7 to 1.1.

For two studs per trough, similarly, Eurocode 4 is rather inappropriate for any position of the studs in narrow troughs, say $b_o/h_p \leq 2.0$, as shown in Figures 3.6 and 3.7. The scatter is as low as 0.6 and as high as 1.6. For wider trough with $b_o/h_p \geq 2.4$, most of the points fall below 1.0, which means Eurocode 4 is unsafe, especially when studs are in favourable, unfavourable and staggered positions.

On the whole, Lawson's model which allows for studs in different positions more or less reduces the scatter, as shown in Figures 3.8 to 3.12, but the problems are still the same: for one central stud (Figure 3.8), the model is over conservative when $b_o/h_p < 1.4$, and unsafe when $b_o/h_p \geq 2.0$; for one unfavourable stud (Figure 3.10) with $b_o/h_p \leq 2.4$, over conservative; little improvement for two central studs (Figure 3.11) in the range of $b_o/h_p \leq 2.4$; unconservative for two favourable, staggered or transverse studs in wide troughs with $2.4 < b_o/h_p \leq 3.2$ (Figures 3.11 and 3.12).

3.4.2 Thickness of sheeting

Unlike Eurocode 4 or Lawson's model, Hanswille's model takes into account the effects of the thickness of sheeting, by limiting the reduction factor of Eurocode 4 in accordance with several thickness groups. It does reduce the scatter for one stud per trough with reported thickness (Figure 3.13), but not for two studs per trough (Figure 3.14). Clearly, Hanswille's model is still inappropriate.

Examining Lawson's model against the thickness of sheeting, as shown in Figure 3.15 for one stud per trough, it can be seen that the resistances of studs increase as the thickness increases. The behaviour is the same for two studs per trough when $t_s \leq 1.0$ mm. However, for $t_s = 1.2$ mm, all the points are on the unsafe side (Figure 3.16), which is due to the inappropriateness of the model.

To summarise, the influences of the thickness of sheeting and stud positions are significant, and are not properly taken into account by the current models.

3.5 Conclusions

1. Welding methods and number of studs per specimen (≤ 6) have significant influence on the results of push-out tests.

2. Neither the reduction factors as given by Eurocode 4 nor those proposed by Lawson and by Hanswille are appropriate. The problems are in the following areas: influence of the thickness of steel sheeting; behaviour of studs in narrow troughs with $b_o/h_p \leq 2.0$; behaviour of studs in different positions within a trough.

3. For one stud per trough, there are only three data with $b_o/h_p < 2.0$.

4. Considering the above three reasons, there is a need for further testing to focus on the problems and to fill in the gaps of existing data.

δ_{EC}

Figure 3.3: Eurocode 4: One central stud.

δ_{EC}

Figure 3.4: Eurocode 4: One favourable stud.

δ_{EC}
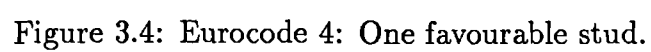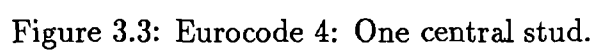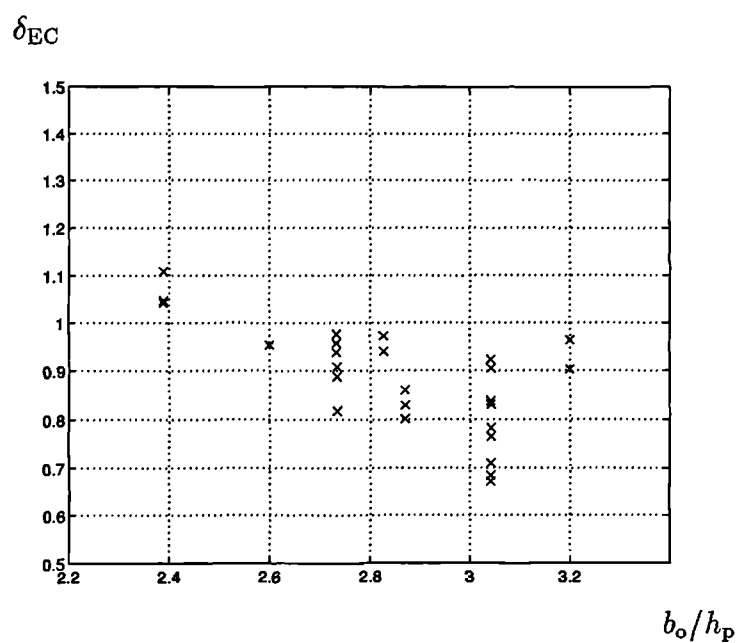
Figure 3.5: Eurocode 4: One unfavourable stud.

δ_{EC}
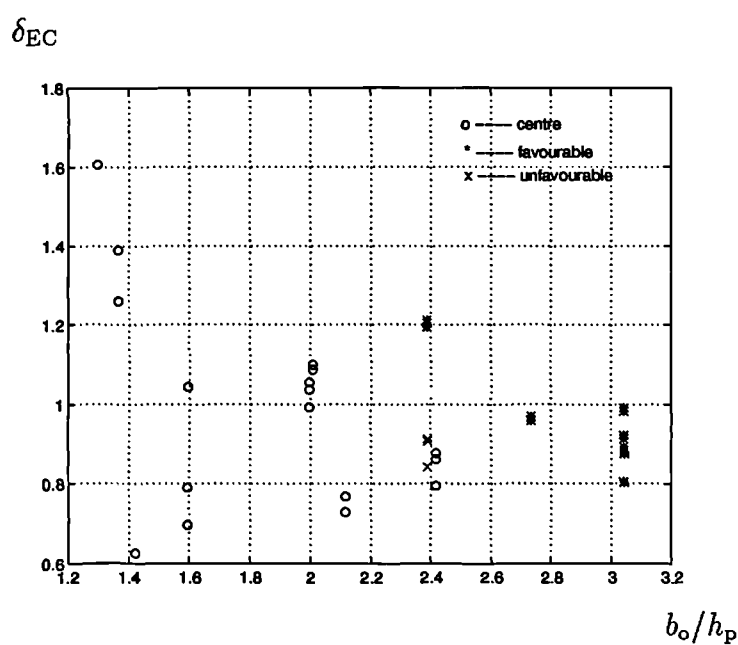
Figure 3.6: Eurocode 4: Two in-line studs.

δ_{EC}

Figure 3.7: Eurocode 4: Two transverse or staggered studs.

δ_{L}

Figure 3.8: Lawson's model: One central stud.

δ_{L}
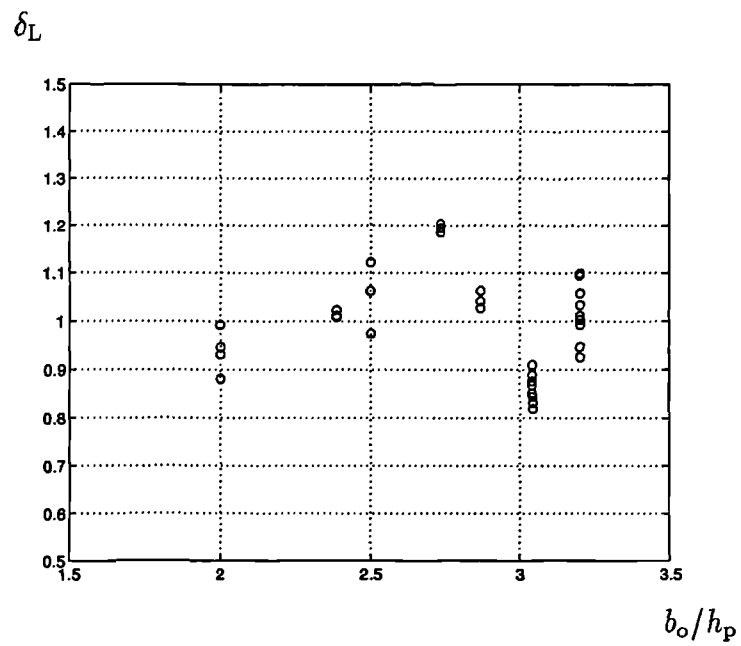
Figure 3.9: Lawson's model: One favourable stud.

δ_{L}
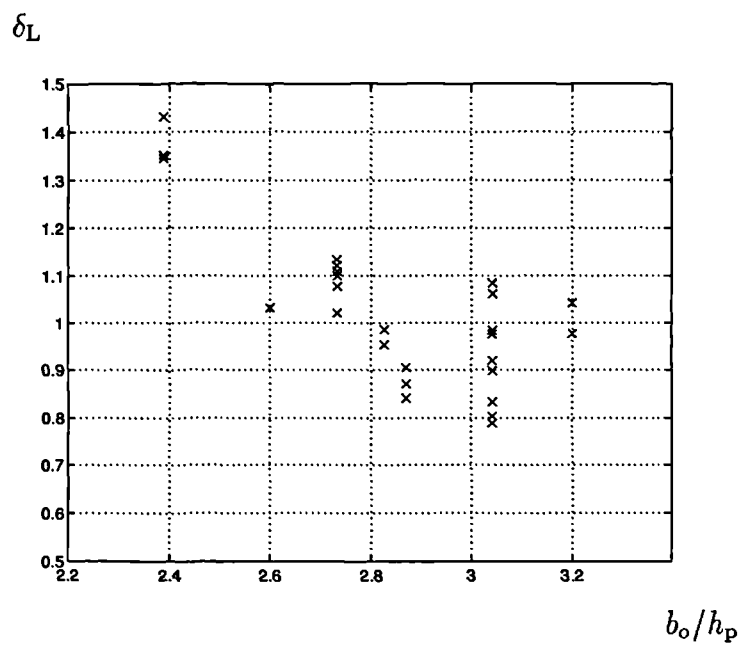
Figure 3.10: Lawson's model: One unfavourable stud.

δ_{L}
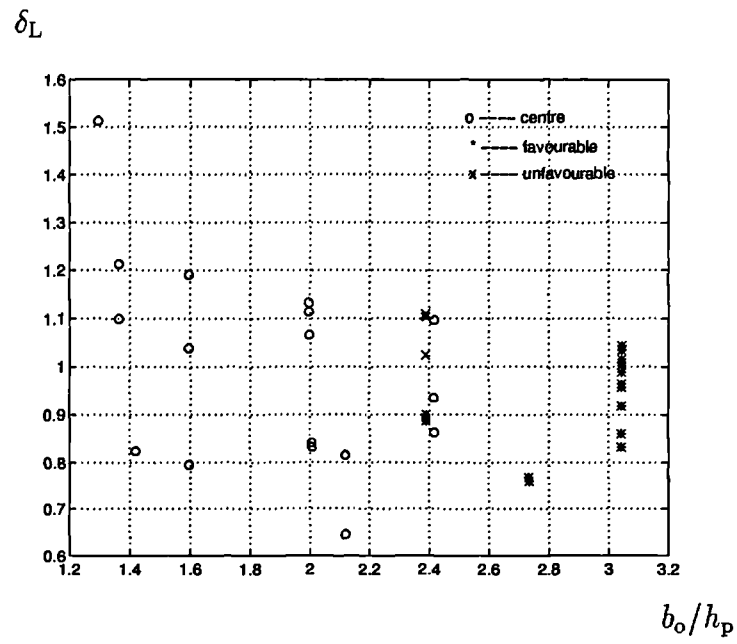
Figure 3.11: Lawson's model: Two in-line studs.

δ_{L}
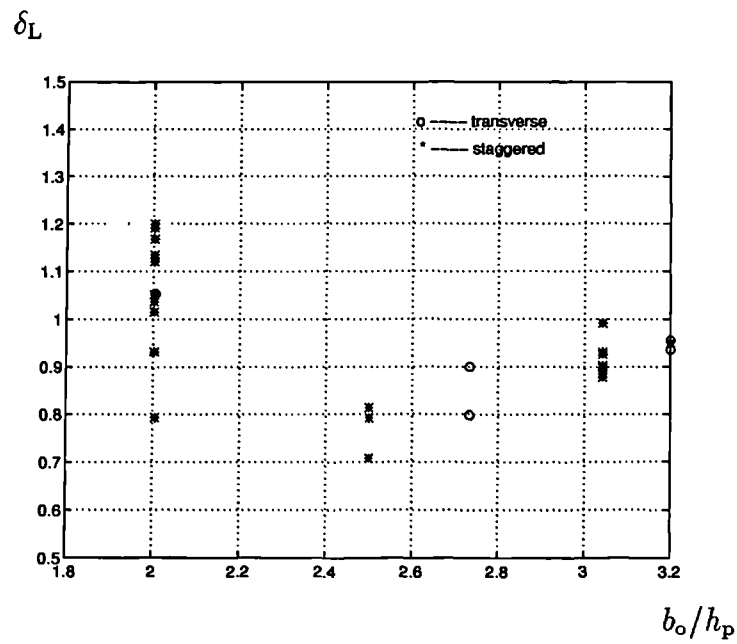
Figure 3.12: Lawson's model: Two transverse or staggered studs.

δ
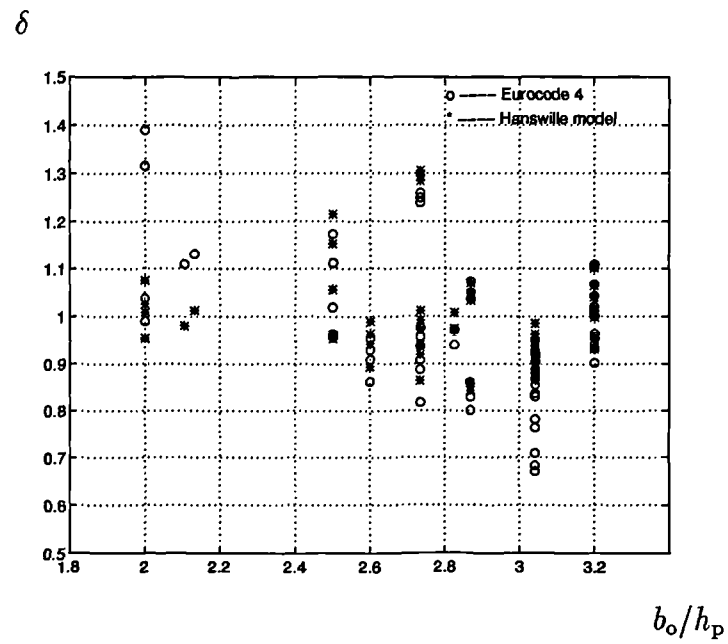
Figure 3.13: Hanswille's model compared with Eurocode 4: One stud per trough.

δ
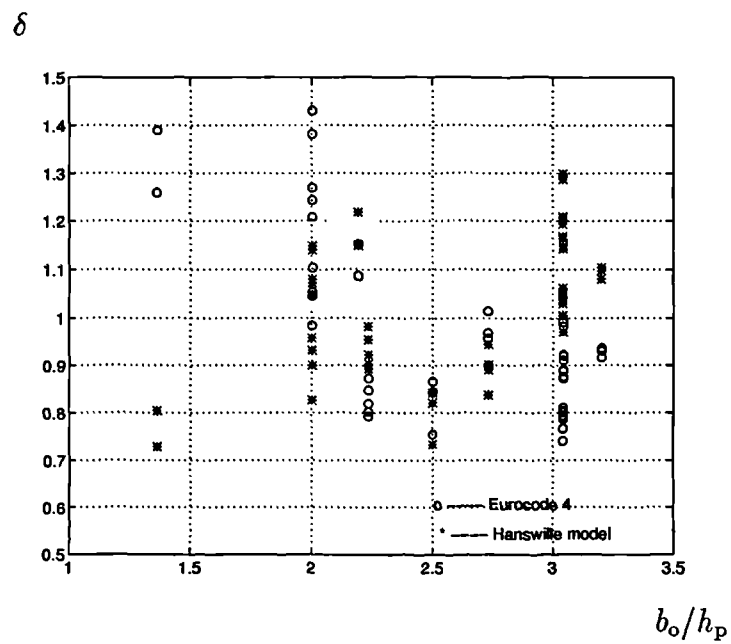
Figure 3.14: Hanswille's model compared with Eurocode 4: Two studs per trough.
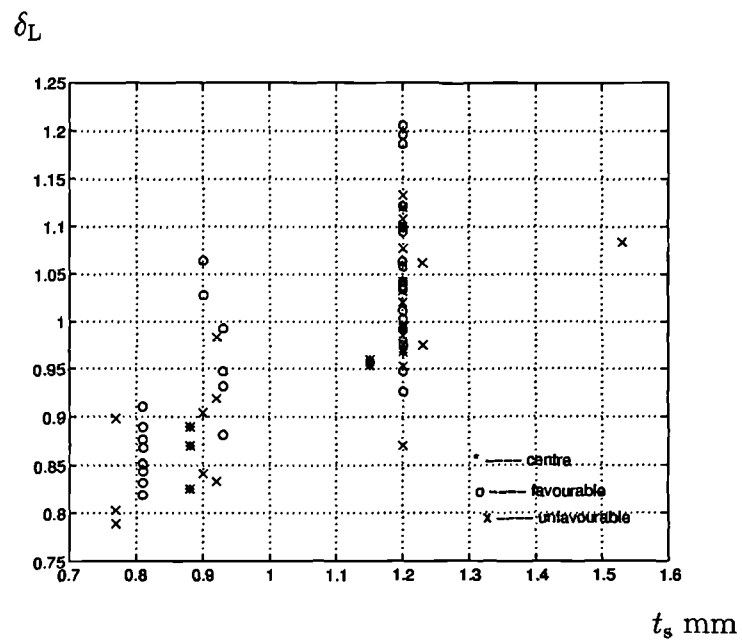
Figure 3.15: Lawson's model: Effects of t_s for one stud per trough.
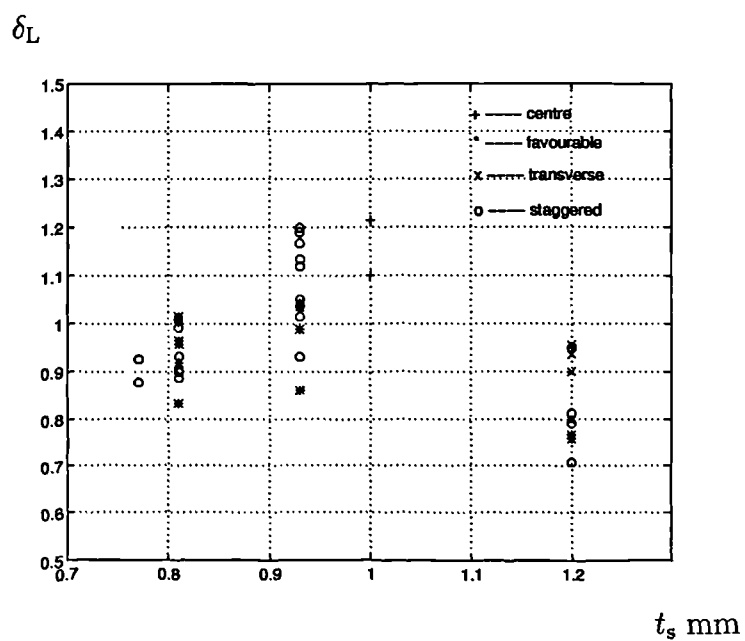
Figure 3.16: Lawson's model: Effects of t_s for two studs per trough.

Chapter 4

Push-out tests and their results

4.1 Introduction

Two series of push-out tests were carried out. They were designed, in accordance with the conclusions of the previous chapter, to fill in the gaps in the 203 data and to add fresh information in the regions where the existing models (Eurocode 4, Lawson's model and Hanswille's model) are inappropriate.

Series 1 consists of 16 specimens with transverse sheeting, and series 2 of 18 with parallel sheeting. Details of the specimen layouts, manufacture, testing procedures, material properties, maximum loads and failure modes of the two series are described in this chapter.

As found out from these tests, for transverse sheeting with one stud per trough, the failure modes can be shank shearing, concrete pulling out or rib punching, while with two studs per trough, rib punching combined with either shank shearing or concrete pulling out. For parallel sheeting, the modes of failure are splitting and pulling out.

Compared with the three existing models, the inappropriateness is obvious.

41

This is due to the fact that none of the previous models are sensitive to the variety of the failure modes. Apparently, new models are needed. In Chapters 5 to 8, several new models are developed based on these 34 test results together with the existing 203 data.

4.2 Preparation of specimens

4.2.1 Variables investigated

According to the analyses on the 203 data in Chapter 3, the new push-out tests were designed to investigate the following variables:

1. rib orientation: transverse sheeting (series 1) and parallel sheeting (series 2);

2. rib geometry: mainly concerning $b_o/h_p \leq 2.0$ and the thickness $t_s \leq 1.0$ mm;

3. number of stud connectors per trough: one or two;

4. stud positions: for series 1 with one stud per trough, centre, favourable and unfavourable, and with two studs per trough, transverse, in-line and staggered; for series 2, transverse and staggered;

5. concrete density: normal weight and lightweight concrete.

Altogether, there were 34 specimens. They were divided into 17 groups, each of which had two identical specimens in order to provide checks on the test results.

Series 1 - transverse sheeting

The 16 specimens of series 1 are outlined in Table 4.1 (all the tables and figures are given at the end of this chapter), where N_r is the number of studs per trough; f_{cu}, 100-mm cube strength of concrete, N/mm^2; ρ, density of concrete, kg/m^3; b_o and h_p, average width and overall depth of the trough of steel sheeting, mm; t_s, thickness of the sheeting, mm; h, height of studs, mm; e, distance of the stud to the mid-depth of the nearer web of the trough, mm.

Three kinds of decking, PMF CF60, PMF CF70 and Multideck 80 were tested. They were chosen to provide more information in the region of $b_o/h_p \leq 2.0$ in the existing data, and to check the effect of the thickness of profiled sheeting. Details of the decking are shown in Figure 4.1.

The influence of rib geometry was studied against the position of the stud: central and favourable position, G2C and G1F, unfavourable position, G5U and G6U, and against concrete density, G3FL and G4FL, as well as the number of studs in a trough, G7D and G8D.

Series 2 - parallel sheeting

The 18 specimens of series 2 are outlined in Table 4.2. All the symbols are the same as for Table 4.1, except that N_{rs} is the number of studs per specimen.

As there are very few data available to study the behaviour of stud connectors with parallel sheeting, five kinds of sheeting were tested. They were PMF CF46, PMF CF60, Multideck 80, Alphalock and Ribdeck 60. Details are shown in Figure 4.1.

G9P to G12PL were focussed on narrow and deep sheeting against the concrete density. The stud connectors were arranged in two rows, each with two connectors transverse to the trough. The transverse spacing was $2.8d$ for PMF

CF60 sheeting and 3.4d for Multideck 80 sheeting, respectively. As Eurocode 4 [7] requires the spacing of two transverse studs not less than 4d, studs in G13P and G14P with the same sheeting PMF CF60 and Multideck 80 were arranged staggered with the diagonal spacing meeting the requirement of 4d.

The longitudinal spacings for G9P to G16P were all greater than 6d, as required by Eurocode 4. In G17P, it was reduced to 5.8d, which was intended to check the effect of the narrow spacing.

4.2.2   Specimen configuration

Figures 4.4 to 4.18 show the details of the configuration for all the 34 specimens.

The basic layout, similar to that recommended by Eurocode 4 [7], consisted of two composite concrete slabs 620 mm wide, with one layer of A142 mesh in each slab. Two rows of studs were used to connect the slab to a 205 × 205 × 52 kg/m universal column. The heights of the slabs varied with the decking used: 900 mm for PMF CF70 and Multideck 80, and 620 mm for PMF CF60. For parallel sheeting, a uniform 620-mm height was used. The thicknesses of concrete slabs were all chosen to provide a 25-mm cover of concrete over the heads of the studs, except a 15-mm cover for G2C and G14P.

4.2.3   Welding of studs

All of the studs were 19 mm in diameter, and were provided by TRW Nelson Ltd in batches, with data on the mechanical properties. For the 95-mm studs, the ultimate tensile strength was 486 N/mm^2, and for the 125-mm studs, 472 N/mm^2.

Stud welding was performed by the technicians in the Department of Engineering of the University of Warwick.

The quality was controlled by the shape of the weld collar and the reduction of the height of stud. A good quality of welding has relatively large and uniform weld collar and about 5-mm reduction in the height after welding, which was achieved by most of the studs. However, the eight studs in specimens G1F and G5U did not satisfy this requirement. They were then bent over 15°, among which one in G1F-1 broken off. So the broken one and the other unbroken ones on the same side were removed. The sheeting was then turned around to provide fresh positions for the studs to be welded on the favourable sides.

4.2.4   Casting

All the specimens were cast horizontally. The edge trims for the sheeting served as form work. Initially one slab was cast. After 24 hours curing, the specimens were turned over and the slabs on the other sides were cast. Six or eight batches of concrete were needed for each set of four specimens (eight slabs). Two 100-mm concrete cubes were cast from each batch.

Trial mixes were made for an assumed 30 N/mm^2 strength at 28 days. It was intended to do each push-out test between 14 and 21 days after the casting of the first slab. But all the mixes gained strength more rapidly than expected. It was then necessary to test at an age of less than 14 days.

Ordinary Portland cement was used in all the specimens. For the normal weight concrete, the concrete strength was produced with the aggregate of maximum particle size 10 mm. For the lightweight concrete, Lytag Granular 12 mm with sand was used to provide the concrete density around 1900 kg/m^3, and with Lytag fines to provide the concrete density around 1600 kg/m^3.

The specimens and the cubes were cured togetherunder wet hessian until the day of testing.

4.3 Test procedure

4.3.1 Setting up of the specimen

Just before the specimen was set in position for testing, edge trims on G4FL, G6U, G7D, G10P and G12PL were pulled away to allow the propagation of the cracks on the sides of the slabs to be observed. The test rig with a specimen is shown in Figure 4.2. The slabs were bedded to the strong floor of the structures laboratory using dental paste. The spreader beams, which were simply supported by the flanges, were bolted against the web and the ball joint was placed above the centre of the web. Load was applied through a manually operated hydraulic jack and monitored with a 100-tonne capacity load cell for specimens with transverse sheeting and with a 200-tonne capacity load cell for those with parallel sheeting.

4.3.2 Instrumentation

Two linear voltage displacement transducers (LVDT's) placed at the base of the specimen were used to monitor the slip between the steel and concrete surface, as shown in Figure 4.2. They were connected to a Spectra Data Acquisition System (DAS) which also recorded the applied load from the jack.

4.3.3 Loading sequence

All tests were performed first under load control in 50-kN increments and then under deformation control in about 0.25-mm increments after the first crack appeared. When the load-slip curve progressed into the falling branch stage, a 0.5-mm increment of deformation was used for several increments, and then 1-mm increment until the specimens completely failed.

4.4   Test results

4.4.1   Transverse sheeting

The results of the 16 push-out tests are listed in Table 4.3, and their load-slip curves are given in Figures 4.19 to 4.26. These figures also show the loads at which cracks of types *a, b* or *c,* defined below, first appeared.

Crack patterns and load-slip curves

All the 16 tests behaved in a generally similar manner. The crack pattern is illustrated in Figure 4.3(a).

One stud in a trough

At about 70-80% of the maximum load, a transverse crack *a* was developed at the thinner section between the two rows of studs, but much closer to the upper row. It opened up with further loading. At about the maximum load, a longitudinal crack *b* appeared, from the centre of crack *a* up beyond the upper row of studs. The load dropped slightly, and then went up to about the maximum value again at which another longitudinal crack *c* appeared, from the centre of crack *a* down to the bottom of the slab. G2C and G6U had this kind of behaviour. Their load-slip curves clearly showed the down and up performance of the loads. There is an alternative that the longitudinal cracks *b* and *c* appeared simultaneously at the maximum loads, as observed in G1F, G3FL and G4FL.

The behaviour after the maximum load depends on the density of concrete. G3FL and G4FL with lightweight concrete showed quite brittle load-slip performances, especially for G3FL of which the slip at 80% of the maximum load was only 1.5 mm. This might be due to the fact that this group had very low concrete density, only 1640kg/m^3.

For G4FL, the failure was due to the studs pulling out of the slabs, carrying away wedge-shaped portions of concrete, and the failure surfaces were entirely below the reinforcement. However, for G3FL with the centre of the mesh 40 mm lower than the heads of the studs, there was no sign of the pulling out of the studs.

For normal weight concrete, when studs were placed on the favourable side or at the centre of the decking, G1F-1 and G2C showed good ductility, with over 10-mm deformation when loads dropped to about 80% of the maximum values. They ended up by the shearing off of the studs along the sections just above the weld collars, with little damage to the surrounding concrete.

The different behaviour of G1F-2 was the result of poor welding of the stud connectors. The four studs in this specimen were welded in the same batch as those in G1F-1. The welding problem in the latter was spotted before the casting of concrete, but not in the former (Section 4.2.3).

Two studs in a trough

With two studs in a trough, G7D and G8D behaved in a different way. The longitudinal cracks *b* and *c* appeared long before the maximum loads were reached. The dropping parts of the load-slip curves were gradually decreasing and smooth, but less ductile, with about 5-mm deformation at 80% of the maximum loads. G7D showed the similar failure to that observed in G4FL, in that the studs were pulled out with a portion of concrete around. G8D failed by severe deformation of the studs, showing much higher shear resistance than G7D.

In both groups, severe damage in the concrete between the stud connectors and the ribs of the profiled sheeting on the unfavourable sides were observed, and the ribs were found to be fractured to the mid-depth of the rib.

Failure modes

Three kinds of failure modes were observed in the tests with one stud per trough. They are shank shearing, concrete pulling out and rib punching. For two studs per trough, G7D showed a combined failure mode of rib punching with concrete pulling out, and G8D a combined failure mode of rib punching with shank shearing.

Shank shearing

This kind of failure has the highest resistance. As the head of the stud is deeply embedded in the upper slab, its rotation is restrained. This allows a plastic zone to be developed in the shank of the stud just above the weld collar. The stud first yields, then shears off. There is little damage to the surrounding concrete, because there is stronger restraint to the concrete in this area from the sufficient cover of concrete in front of the stud, such as G2C with wider troughs and G1F with studs in the favourable position. The load-slip curve for this kind of failure shows high ductility, maintaining about 80% of the maximum load at 10-mm deformation. A typical failure is shown in Figure 4.36.

Concrete pulling out

The movement of the base of the stud develops a bending moment on the head, which is resisted by the surrounding concrete. When the resistance is small, the head of the stud rotates. Finally, it is pulled out of the slab, carrying away a wedge-shaped portion of concrete. This is concrete pulling out failure, as shown in Figure 4.37.

Rib punching

Rib punching occurs when there is insufficient cover of concrete in front of the stud. In this case, the limited cover of concrete offers little restraint to the movement of the base of the stud. The concrete crushes, and the base of the stud

moves forwards, torn away from the deck at the weld collar. The rib in front of the stud first bulges, then tears as the stud pushes the crushed concrete through it. Finally, the stud is broken at the section just above the weld collar. This kind of failure is usually observed in the tests with narrow troughs or with studs on the unfavourable side, such as G5U and G6U, as shown in Figure 4.38.

4.4.2   Parallel sheeting

The results of the 18 push-out tests with parallel sheeting are listed in Table 4.4, and their load-slip curves are given in Figures 4.27 to 4.35.

Crack patterns and load-slip curves

Almost all the specimens showed longitudinal cracks along the two lines of the connectors in each slab at about 95% of the maximum loads. These cracks opened up quickly with further loading. Meanwhile, for the specimens with two connectors transverse to the trough, there were transverse cracks between the two connectors. A typical pattern is shown in Figure 4.3(b). When the connectors were staggered to the trough, as in G13P and G14P, there was no sign of the transverse cracks.

At the maximum loads or shortly after the maximum loads, local buckling of the profiled sheeting was observed in all the other specimens except G10P and G12PL. The buckling was in the area around the stud connectors, as shown in Figure 4.39.

For G10P and G12PL, before the occurrence of the longitudinal cracks, at about 80% of the maximum loads, the upper parts of the slabs started to separate from the main body, and the separation expanded very quickly. At the end of the tests, it was the completed separation that dominated the failure, not the

longitudinal cracks as observed in the other tests. The upper parts of the slabs were very easily removed, exposing cone-shaped failure surfaces of the concrete around the stud connectors.

The falling branch part of the load-slip curves for all the specimens showed good ductility, with the deformation over 5 mm when the loads dropped to about 80% of the maximum values.

Failure modes

Two kinds of failure modes were observed. One is splitting failure and the other is pulling out failure.

Splitting failure is the consequence of the laterally dispersed shear force in the concrete within the troughs of the profiled sheeting. First, the dispersal is just around the base of the connector. As the narrow haunch of the concrete in this area holds little resistance, concrete splits, but the expansion of the splitting cracks is resisted by the profiled sheeting. Therefore, the shear force is gradually transferred and dispersed deep into the concrete, until the profiled sheeting bulges, releasing the restraint.

Pulling out failure occurs when the stud connectors are arranged closely in relatively narrow troughs of the profiled sheeting. The dispersal of the shear force is provided by the axial stiffness of the connectors, which develops corresponding tensile forces. It is unlikely that the connectors fail in tension. But, because of the closely arranged connectors in narrow troughs, the surface of the concrete to resist the pulling action is small, the result of which is the pulling out of the stud connectors, carrying away a cone-shaped portion of concrete, as shown in Figure 4.40.

4.5 Discussion

4.5.1 Eurocode 4

Shear resistance

Figures 4.41 and 4.42 show the results of these 34 tests, P_e, compared with Eurocode 4 model, P_{rEC}.

On the whole, Eurocode 4 becomes overconservative as b_o/h_p reduces, especially when $b_o/h_p < 2.0$. The scatter is very high, from 0.8 for unfavourable position to 1.9 for two transverse studs. The inappropriateness of the model for parallel sheeting is also very obvious, in that the tested resistance can be as high as three times the predicted one.

The main reason for this is that Eurocode 4 model does not distinguish between the seven different failure modes found in these tests.

Spacing between stud connectors

As recommended by Eurocode 4, the centre-to-centre spacing between stud connectors transverse to the shear force should not be less than $4d$, and the one in line with the shear force should not less than $6d$. This is not quite the situation for the 18 tests with parallel sheeting.

For G15P and G16P, the spacing in both directions was as required by Eurocode 4. There was no sign of reduction in shear resistance, and the connectors showed good ductility. When the longitudinal spacing dropped below $5.8d$, as in G17P, there was still no penalty on the resistance of the connectors, nor any change in the ductility.

For G9P and G10P, the longitudinal spacings were as required by Eurocode 4,

but the transverse spacings were 3.4d and 2.8d, respectively. However, the shear resistances of the connectors in G9P were about twice the predicted values, and in G10P about 17% higher. The ductility of G10P had a little change, showing brittle behaviour to some extent, which is due to the change in failure mode.

Minimum width of a push-out specimen

The influence of the width of a push-out specimen is significant when it is below the limit beyond which rib shearing failure replaces concrete pulling out failure. The rib shearing failure is the shearing of the concrete slab along a plane level with the upper flange of the trough. It was found by Lloyd and Wright [27] from their tests that the limit was 415 mm.

In the 16 new push-out tests with transverse sheeting, all of the specimens had 620mm-wide slab. As shown in Figure 4.37, the cone in a concrete pulling out failure extended almost to the edges of the slab, which suggest that to prevent the rib shearing failure from occuring, the minimum width of a push-out specimen should be 620 mm.

4.5.2   Two alternative models

Though Lawson's model (equations (2.7) and (2.8)) considers the effects of different positions of studs within a trough, it is still not satisfactory, as shown in Figures 4.43 and 4.44, in that one unfavourable or two transverse studs are overpredicted, while central or favourable stud(s) with parallel sheeting are underpredicted.

As found in Chapter 3, Hanswille's model (equation (2.9)) makes certain improvement for one stud per trough by introducing different upper limits to the reduction factors given by Eurocode 4, but Figure 4.45 shows that only two tests

with wide troughs, $b_o/h_p = 2.9$, are affected by Hanswille's upper limits. The other 14 tests with $b_o/h_p < 2.0$ are well below the limits, which means Hanswille's model is no better than that of Eurocode 4 for studs in narrow troughs.

4.6   Conclusions

1. For transverse sheeting with one stud per trough, the failure modes are shank shearing, concrete pulling out and rib punching.

2. For transverse sheeting with two studs per trough, the failure modes are either rib punching with shank shearing or with concrete pulling out.

3. For parallel sheeting, there are two failure modes. One is splitting failure, the other is pulling out failure.

4. The 34 push-out tests are not well predicted by Eurocode 4, or other alternative models, such as those by Lawson and by Hanswille. This is because they do not distinguish between the seven different failure modes mentioned above. New models are needed.

Table 4.1: Specimens with transverse sheeting.

Group	Concrete		Decking				Studs (d=19mm)				Figure
	f_{cu}	ρ	Type	b_o	h_p	t_s	h	N_r	Position	e	
G1F	35.0		Multideck 80	140	80	1.2	125	1	favourable	37.5	4.4
G2C	27.3		PMF CF70	162	55	0.9	125	1	centre	81.0	4.5
G3FL	29.6	1640	Multideck 80	140	80	1.2	125	1	favourable	37.5	4.6
G4FL	36.9	1900	PMF CF60	113	60	0.9	95	1	favourable	30.0	4.7
G5U	35.0		Multideck 80	140	80	1.2	125	1	unfavourable	37.5	4.8
G6U	27.3		PMF CF60	113	60	0.9	95	1	unfavourable	30.0	4.9
G7D	32.3		PMF CF60	113	60	0.9	95	2	transverse	30.0	4.10
G8D	32.3		Multideck 80	140	80	1.2	125	2	transverse	37.5	4.11

Table 4.2: Specimens with parallel sheeting.

Group	Concrete		Decking				Studs (d=19mm)				Figure
	f_{cu}	ρ	Type	b_o	h_p	t_s	h	N_{rs}	Position	e	
G9P	35.8		Multideck 80	140	80	1.2	125	8	transverse	37.5	4.12
G10P	32.3		PMF CF60	113	60	0.9	95	8	transverse	30.0	4.13
G11PL	41.2	1580	Multideck 80	140	80	1.2	125	8	transverse	37.5	4.12
G12PL	36.9	1900	PMF CF60	113	60	0.9	95	8	transverse	30.0	4.13
G13P	31.4		PMF CF60	113	60	0.9	95	8	staggered	30.0	4.14
G14P	29.4		Multideck 80	140	80	1.2	125	8	staggered	37.5	4.15
G15P	37.8		PMF CF46	132	46	1.0	95	8	transverse	33.3	4.16
G16P	41.5		Alphalock 50	160	50	1.0	95	8	transverse	37.5	4.17
G17P-1	27.7		Ribdeck 60	173	60	1.2	95	12	transverse	36.3	4.18
G17P-2	30.2		Ribdeck 60	173	60	1.2	95	12	transverse	36.3	4.18

Table 4.3 56

Table 4.3: The results of the 16 push-out tests with transverse sheeting.

Group	b_o/h_p	P_e/stud (kN)	Failure mode
G1F-1	1.75	93.1	stud
G1F-2	1.75	90.6	stud
G2C-1	2.95	88.8	stud
G2C-2	2.95	88.0	stud
G3FL-1	1.75	86.3	stud
G3FL-2	1.75	87.0	stud
G4FL-1	1.88	64.7	concrete
G4FL-2	1.88	68.9	concrete
G5U-1	1.75	70.9	rib punching
G5U-2	1.75	67.5	rib punching
G6U-1	1.88	51.3	rib punching/concrete
G6U-2	1.88	53.8	rib punching/concrete
G7D-1	1.88	49.8	rib punching/concrete
G7D-2	1.88	51.6	rib punching/concrete
G8D-1	1.75	61.4	rib punching/stud
G8D-2	1.75	60.1	rib punching/stud

Table 4.4   *57*

Table 4.4: The results of the 18 push-out tests with parallel sheeting.

Group	b_o/h_p	P_e/stud (kN)	Failure mode
G9P-1	1.75	131.1	splitting
G9P-2	1.75	126.2	splitting
G10P-1	1.88	70.3	pulling out
G10P-2	1.88	72.1	pulling out
G11PL-1	1.75	124.2	splitting
G11PL-2	1.75	129.8	splitting
G12PL-1	1.88	77.6	pulling out
G12PL-2	1.88	82.9	pulling out
G13P-1	1.88	92.1	splitting
G13P-2	1.88	91.8	splitting
G14P-1	1.75	112.1	splitting
G14P-2	1.75	114.2	splitting
G15P-1	2.87	101.9	splitting
G15P-2	2.87	96.3	splitting
G16P-1	3.20	108.8	splitting
G16P-2	3.20	114.5	splitting
G17P-1	2.88	87.8	splitting
G17P-2	2.88	85.7	splitting
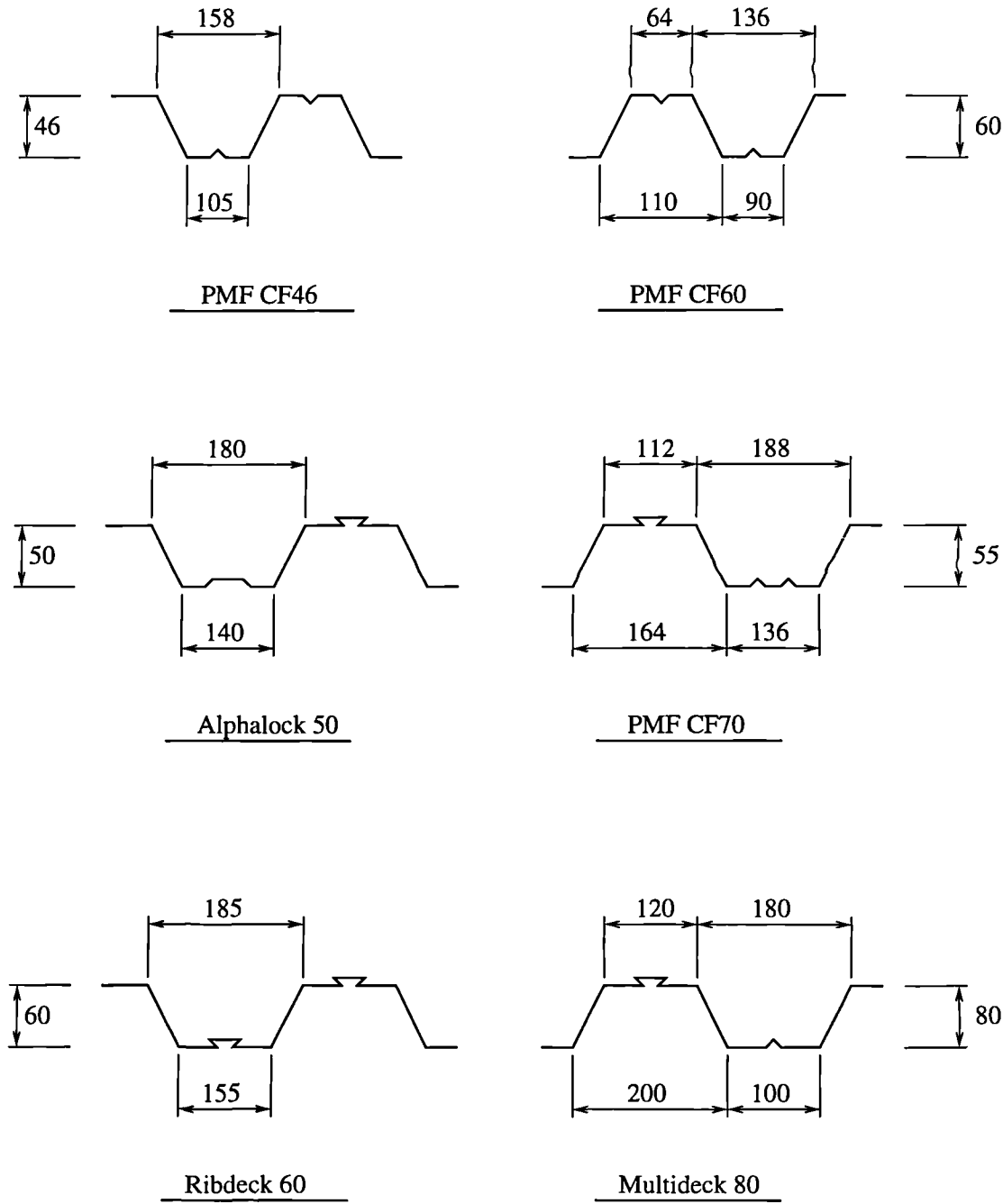
Figure 4.1 58

Figure 4.1: Details of the profiled sheeting.
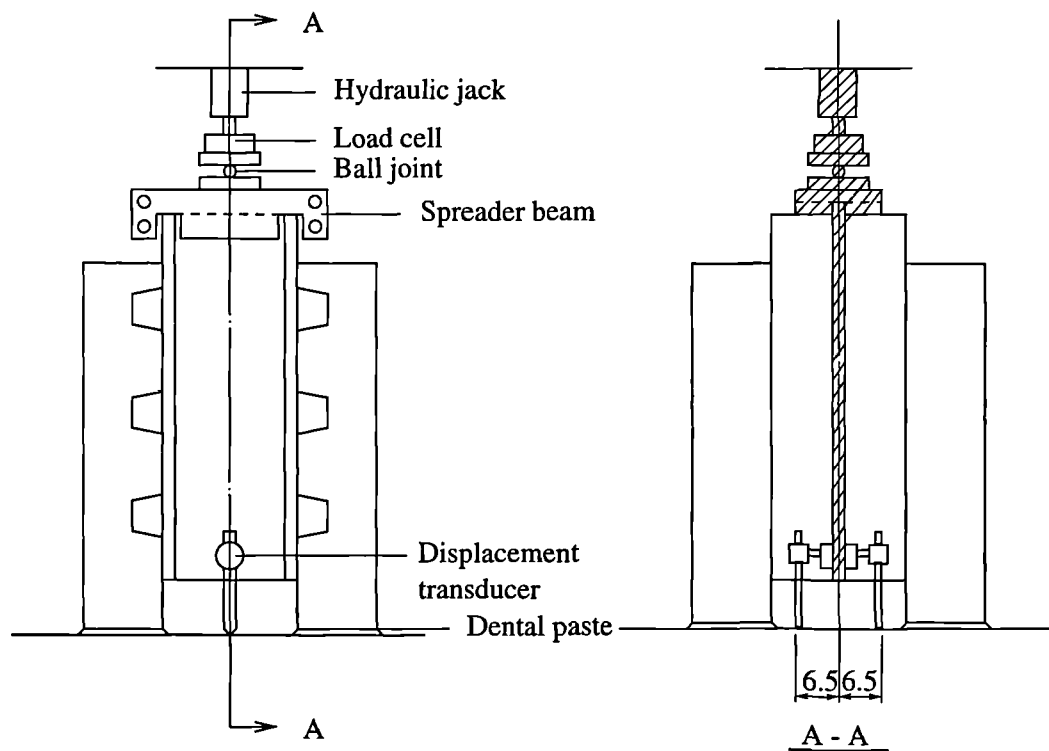
Figure 4.2: Test rig.
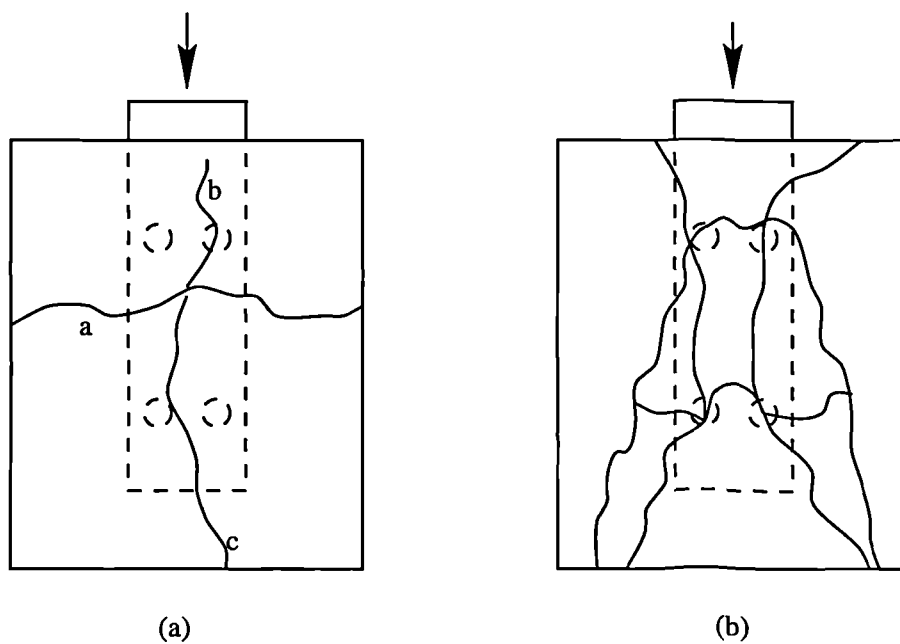
Figure 4.3: Crack patterns: (a) transverse sheeting; (b) parallel sheeting.
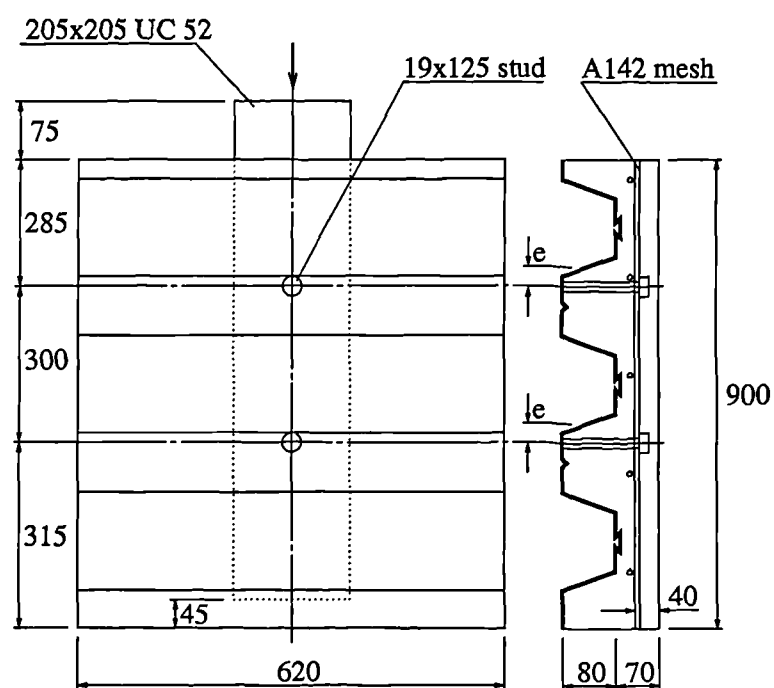
Figure 4.4: Test configuration of G1F.
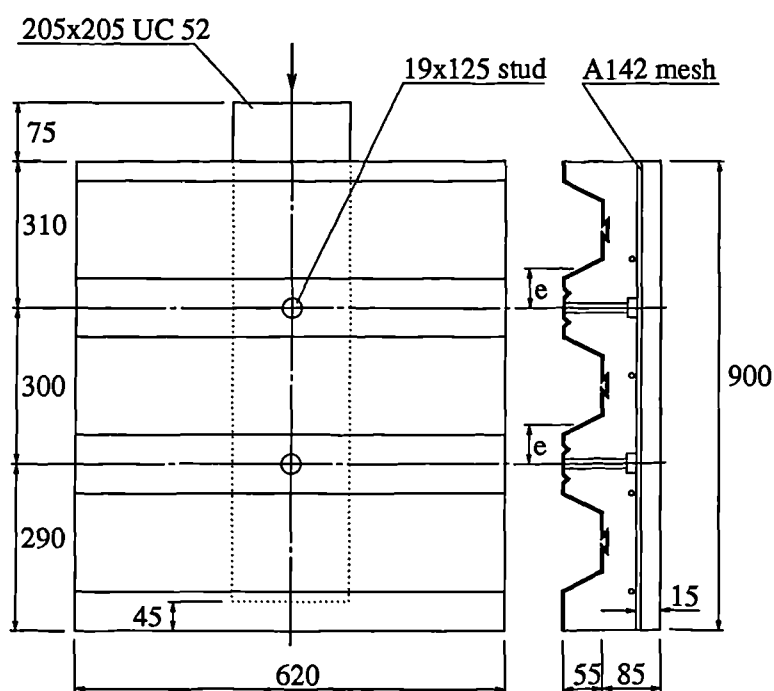
Figure 4.5: Test configuration of G2C.
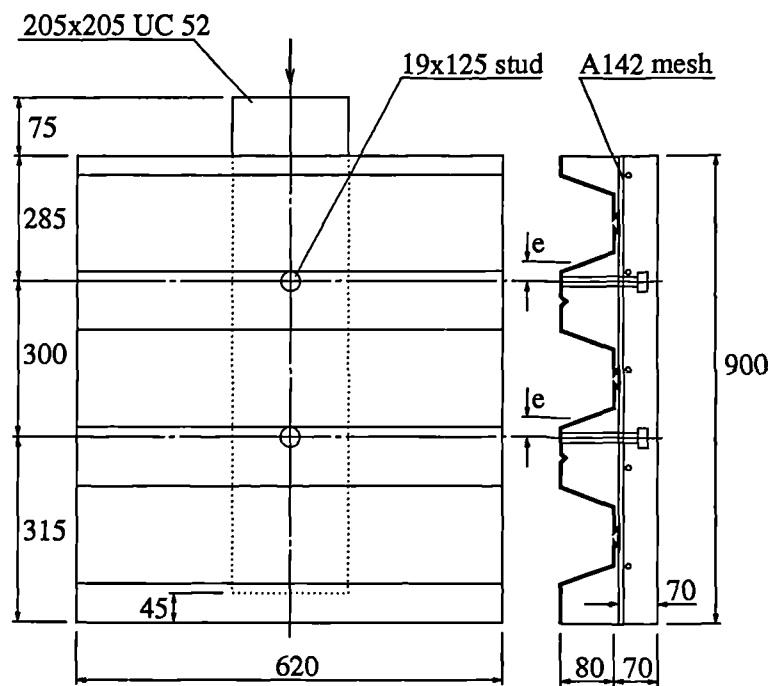
Figure 4.6: Test configuration of G3FL.
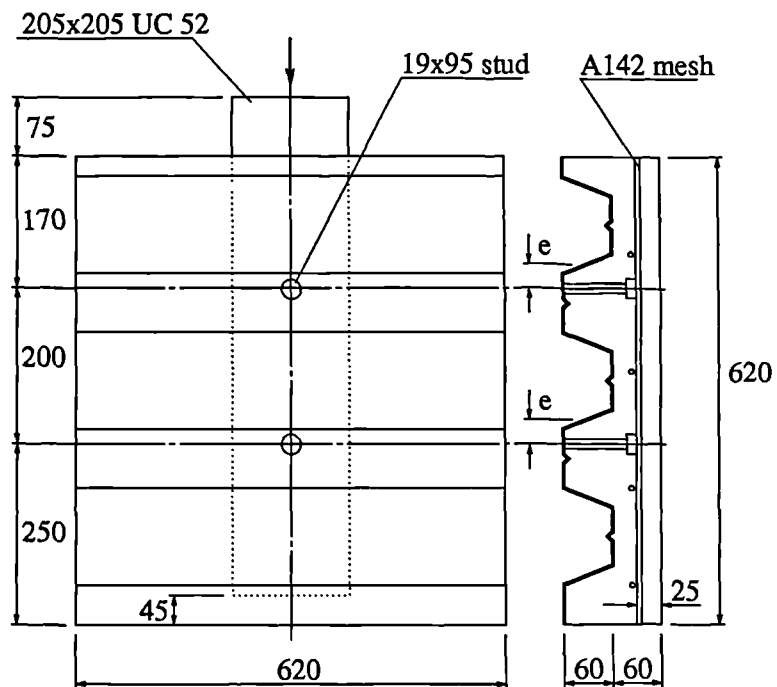
Figure 4.7: Test configuration of G4FL.
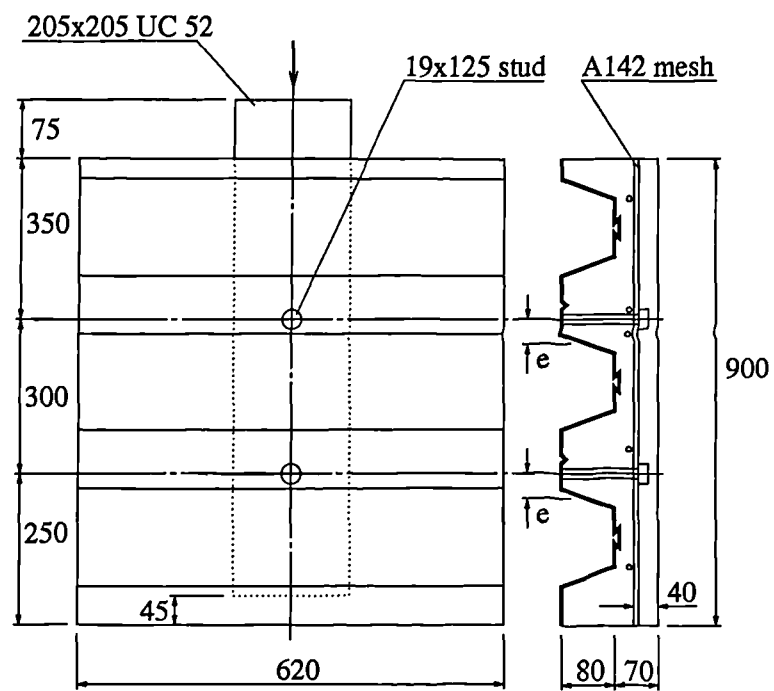
Figure 4.8: Test configuration of G5U.
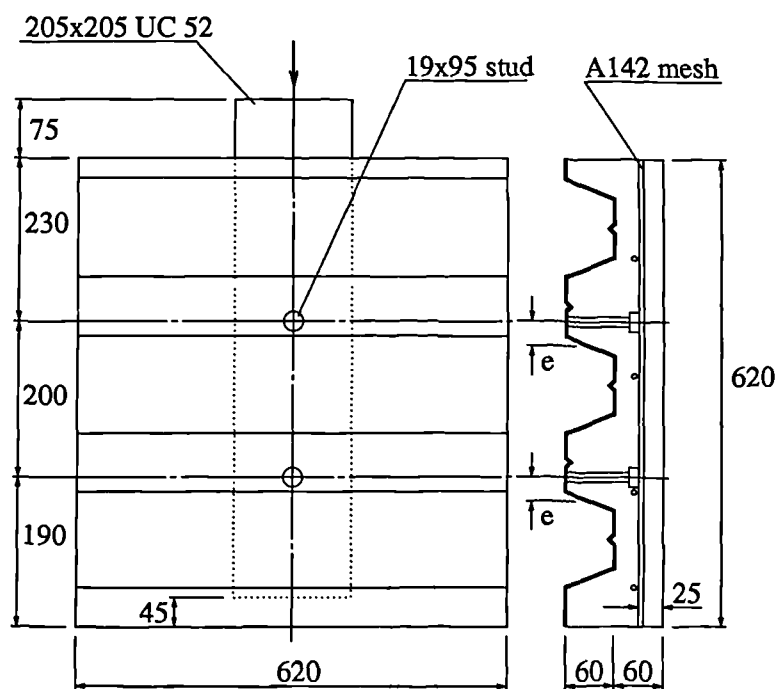
Figure 4.9: Test configuration of G6U.
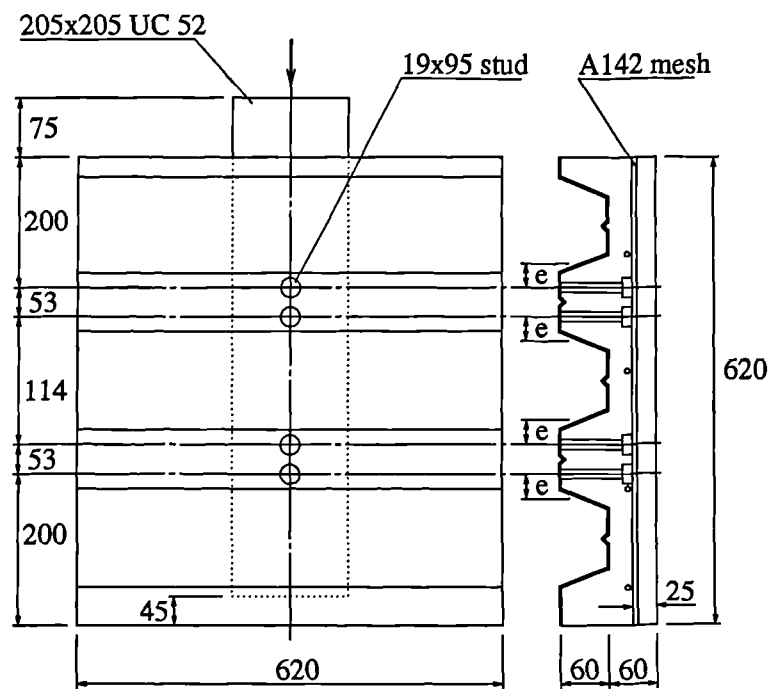
Figure 4.10: Test configuration of G7D.
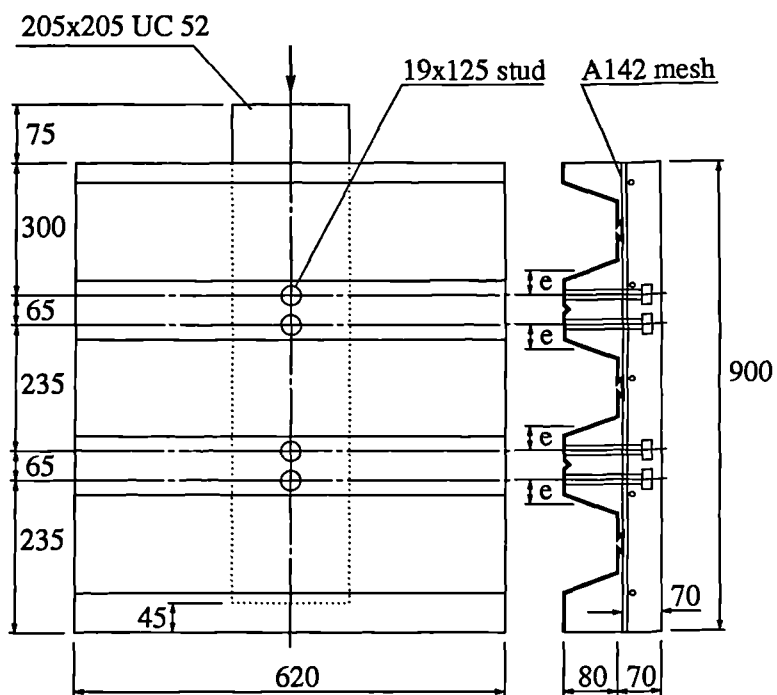
Figure 4.11: Test configuration of G8D.
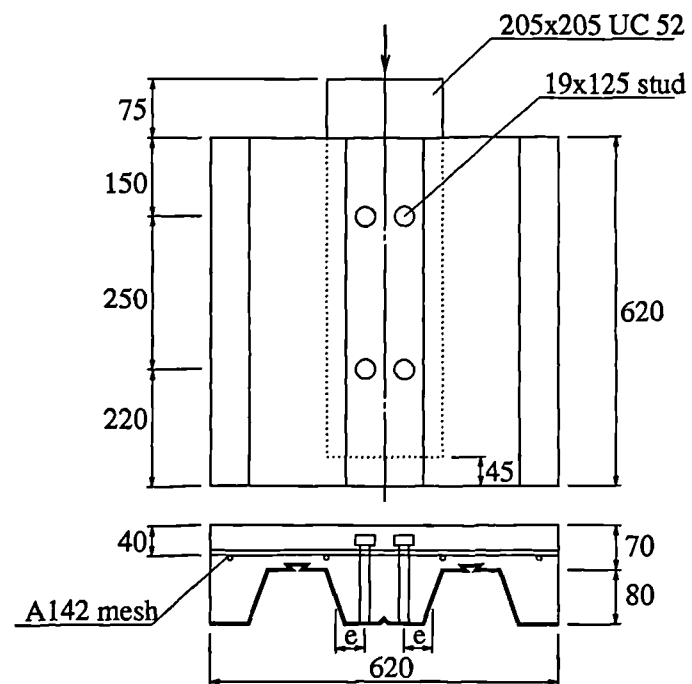
Figure 4.12: Test configuration of G9P and G11PL.
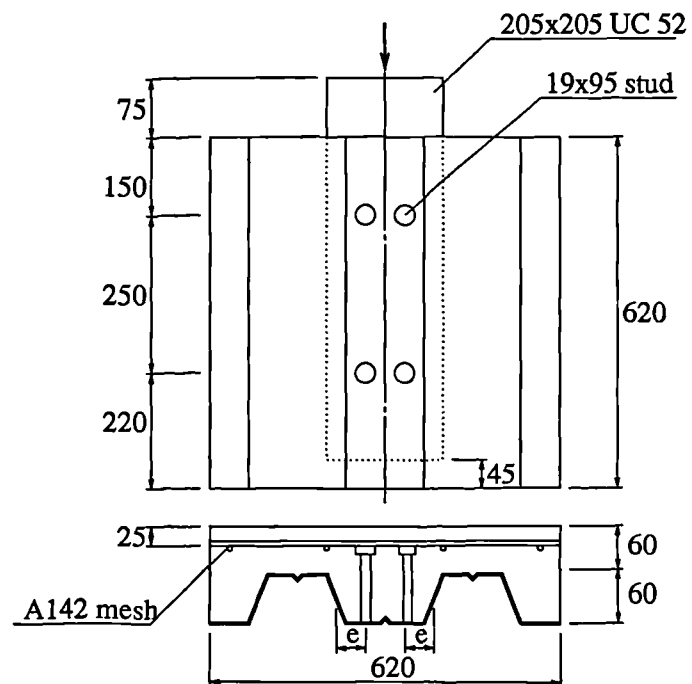
Figure 4.13: Test configuration of G10P and G12PL.
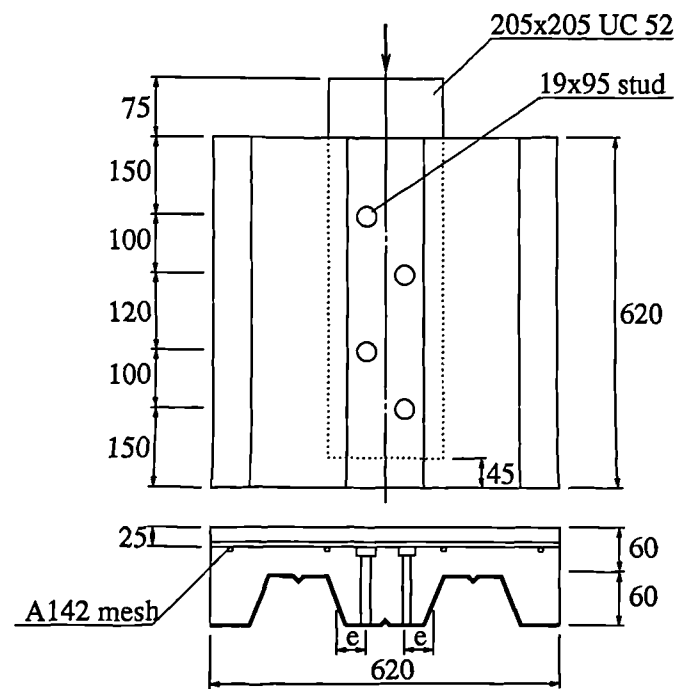
Figure 4.14: Test configuration of G13P.
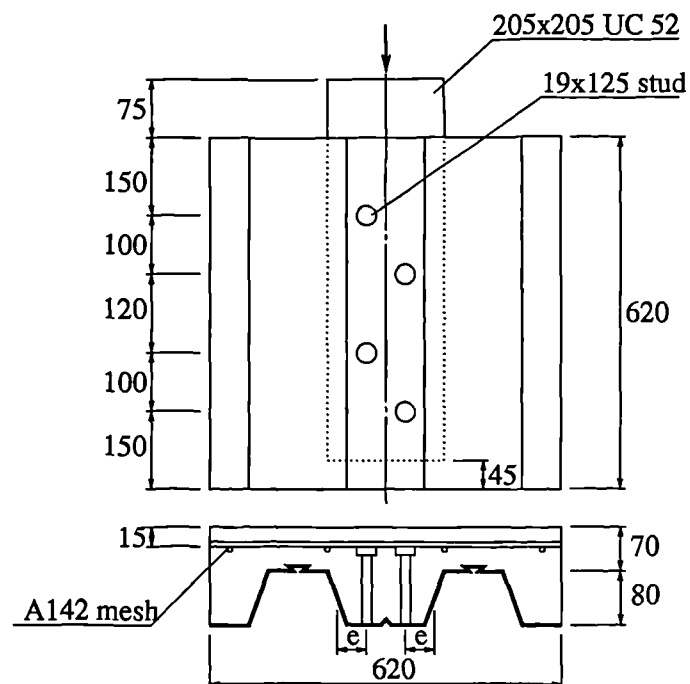
Figure 4.15: Test configuration of G14P.

Figure 4.16: Test configuration of G15P.

Figure 4.17: Test configuration of G16P.
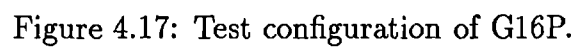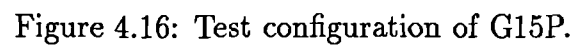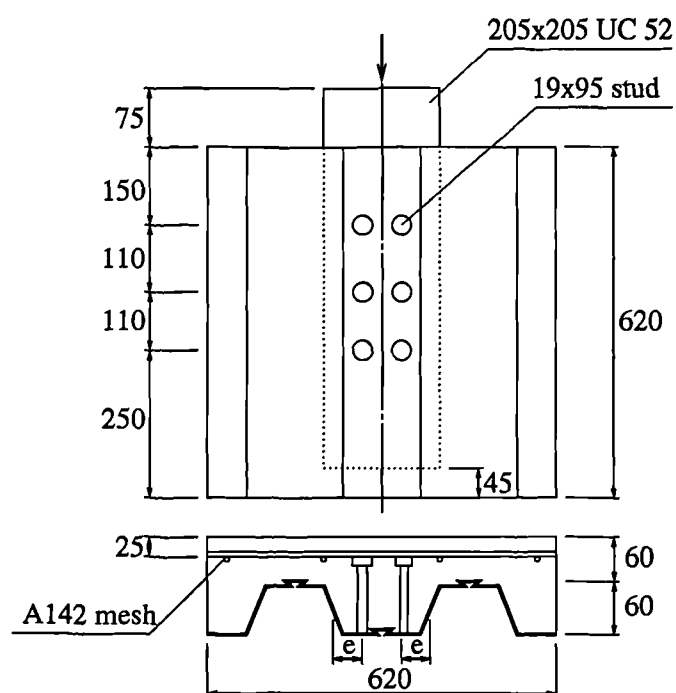
Figure 4.18: Test configuration of G17P.
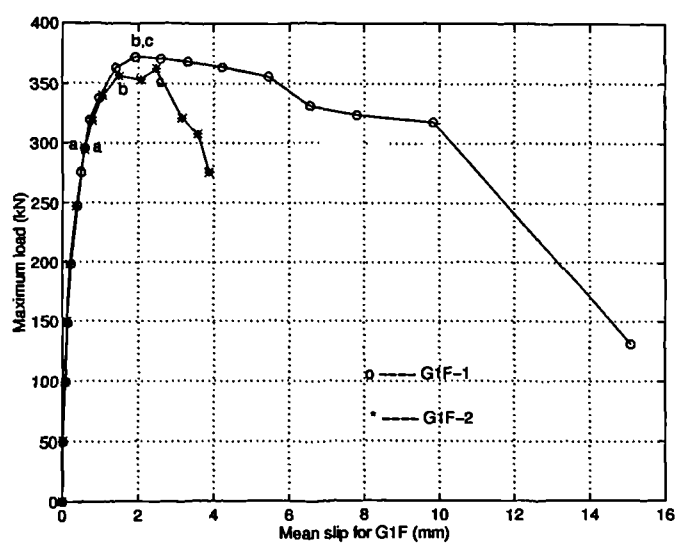
Figure 4.19: Load-slip curve of G1F.
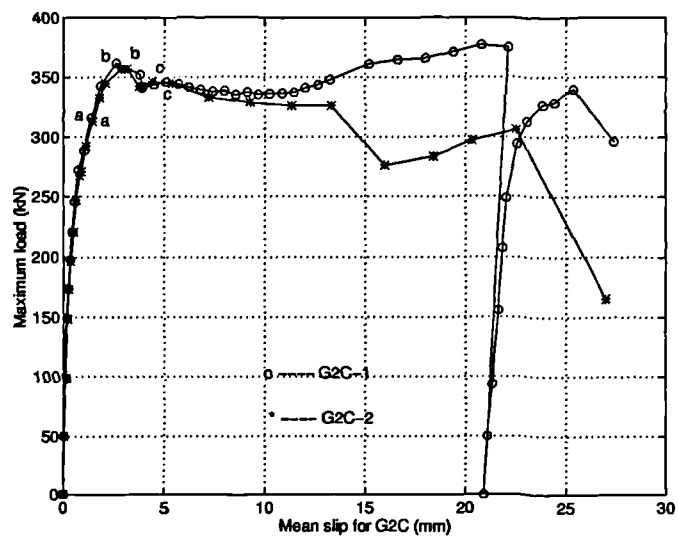
Figure 4.20: Load-slip curve of G2C.
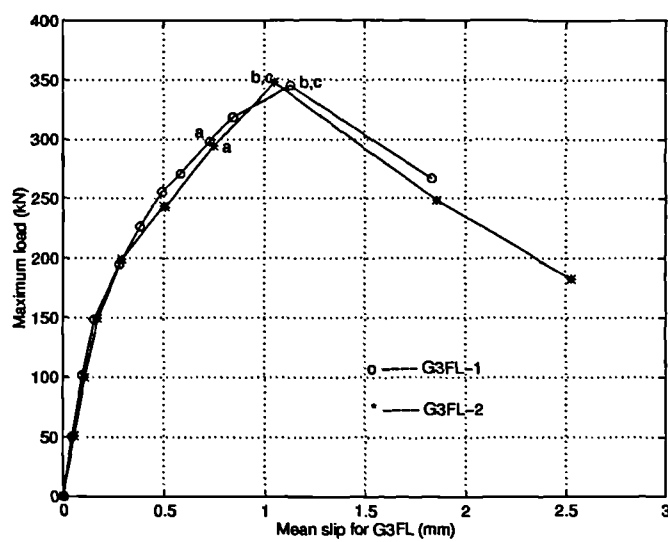
Figure 4.21: Load-slip curve of G3FL.
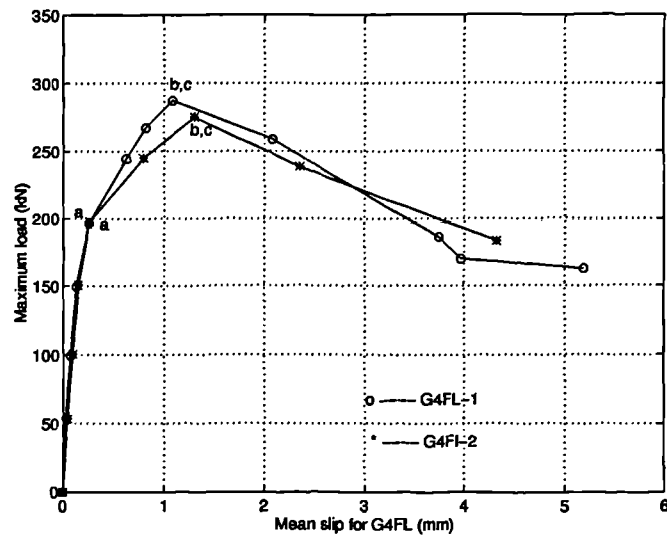
Figure 4.22: Load-slip curve of G4FL.
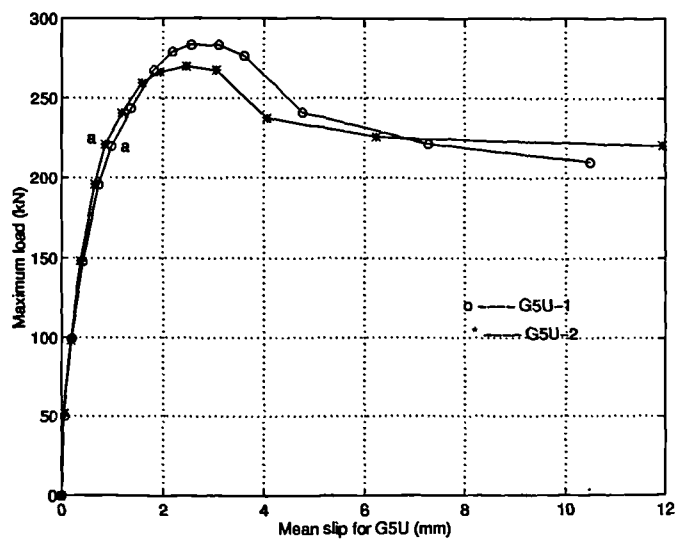
Figure 4.23: Load-slip curve of G5U.
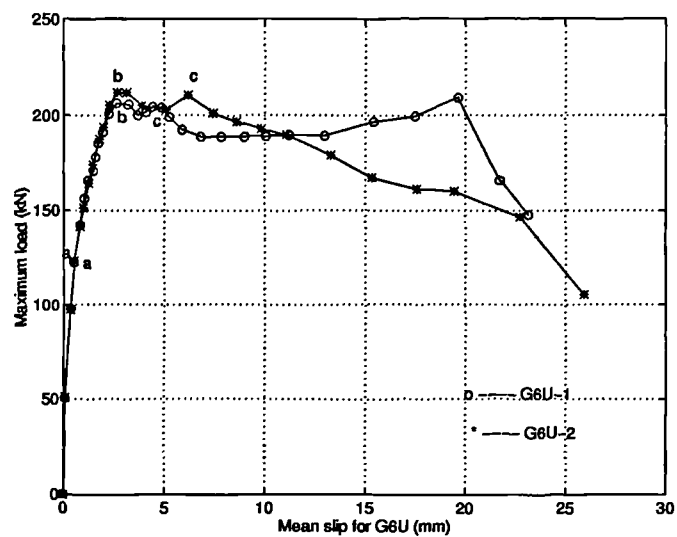
Figure 4.24: Load-slip curve of G6U.
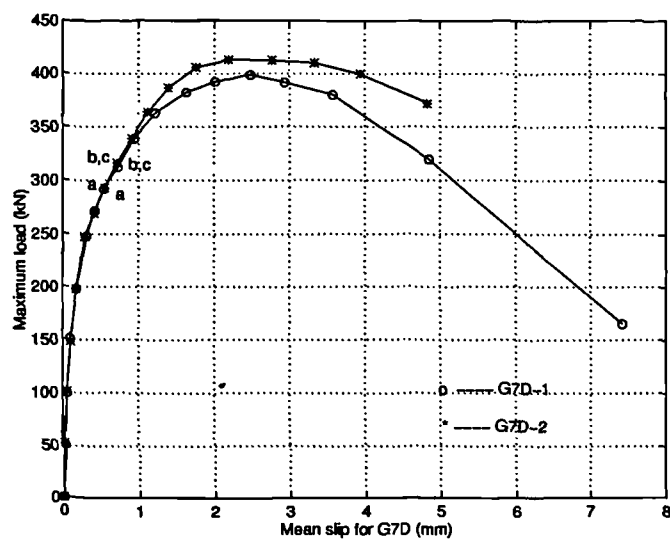
Figure 4.25: Load-slip curve of G7D.
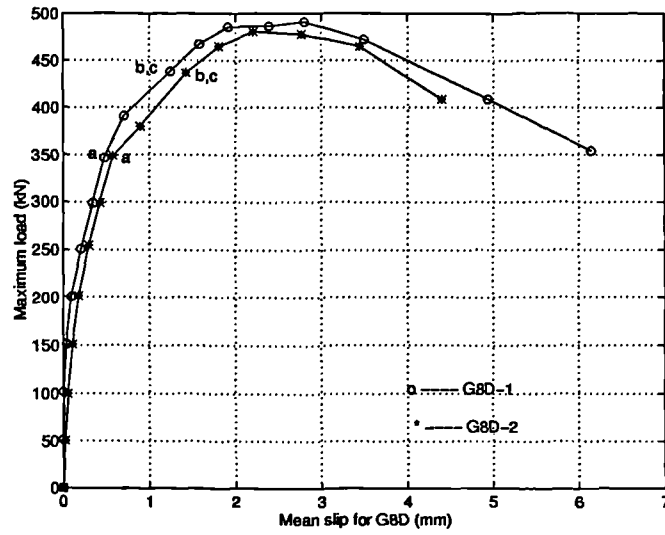
Figure 4.26: Load-slip curve of G8D.
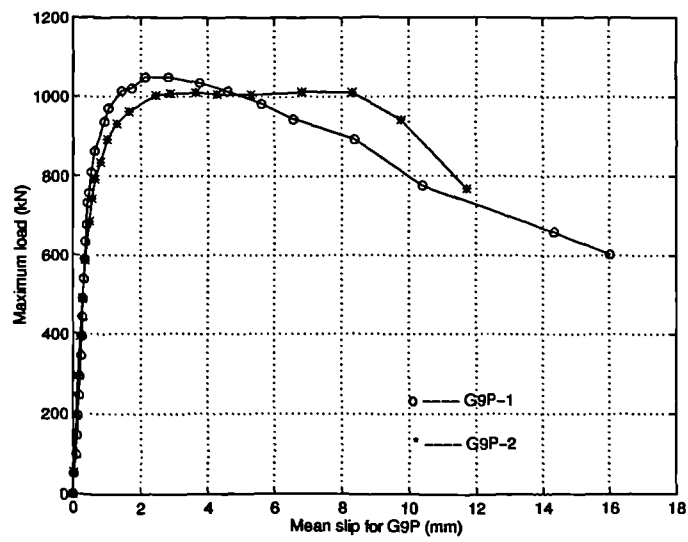
Figure 4.27: Load-slip curve of G9P.
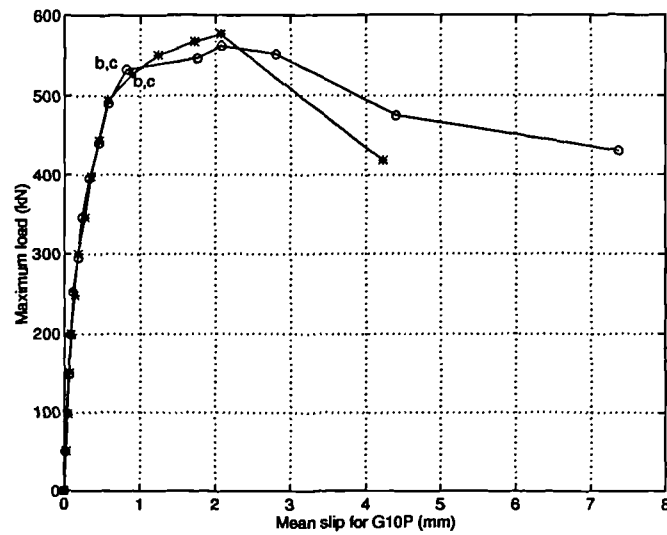
Figure 4.28: Load-slip curve of G10P.
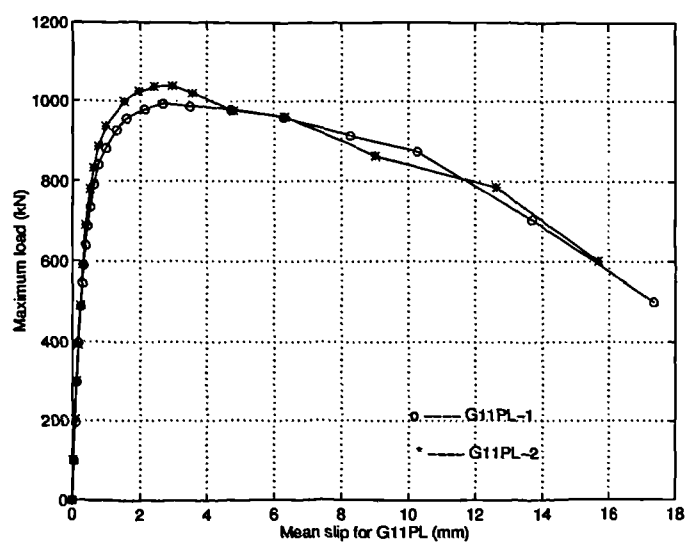
Figure 4.29: Load-slip curve of G11PL.
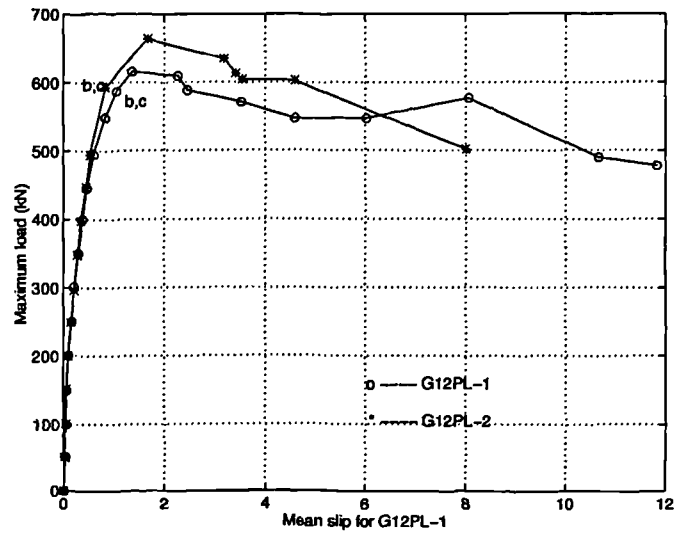
Figure 4.30: Load-slip curve of G12PL.
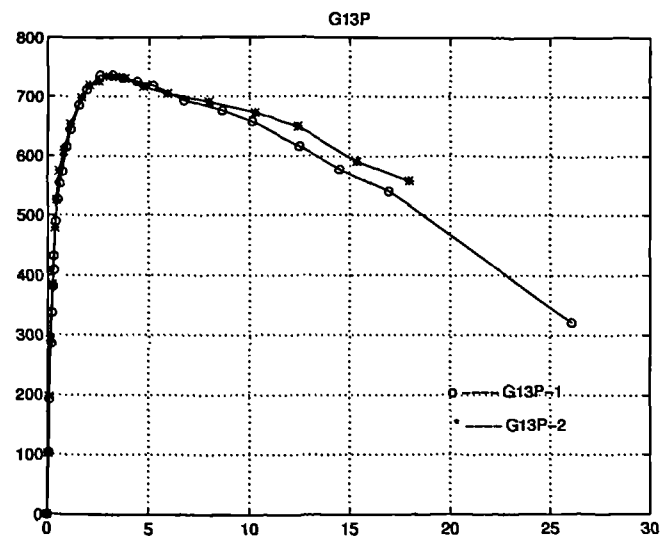
Figure 4.31: Load-slip curve of G13P.
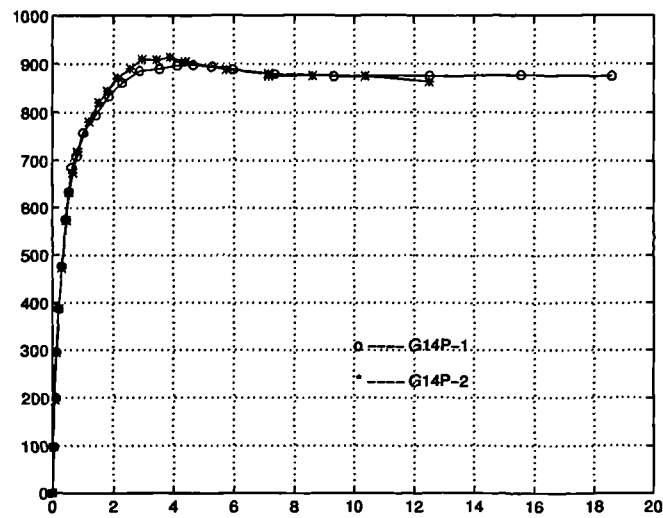
Figure 4.32: Load-slip curve of G14P.
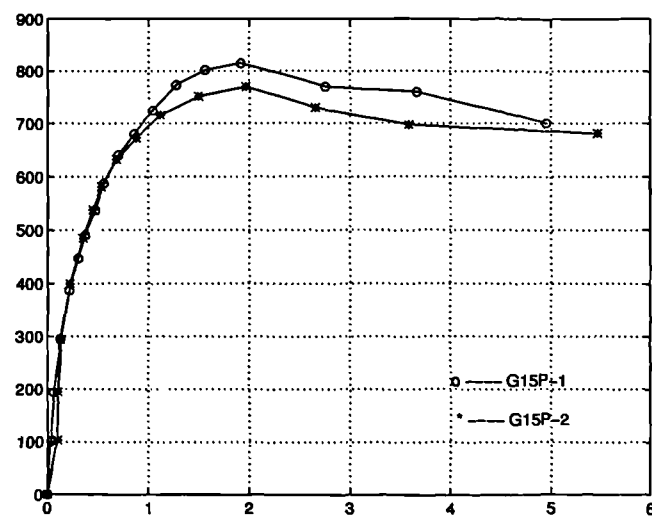
Figure 4.33: Load-slip curve of G15P.
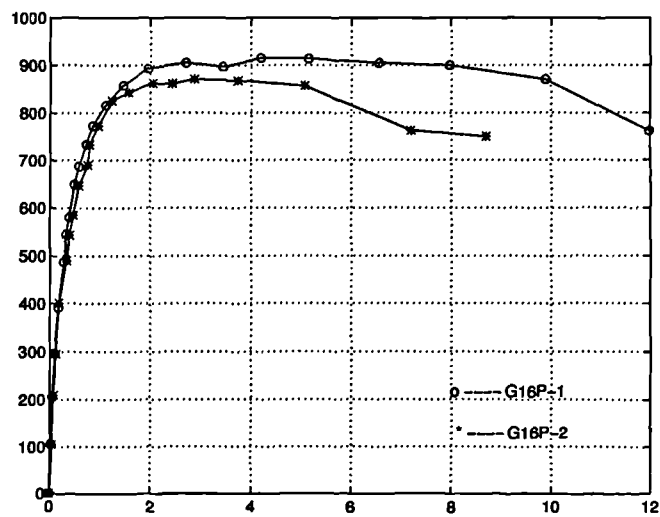
Figure 4.34: Load-slip curve of G16P.
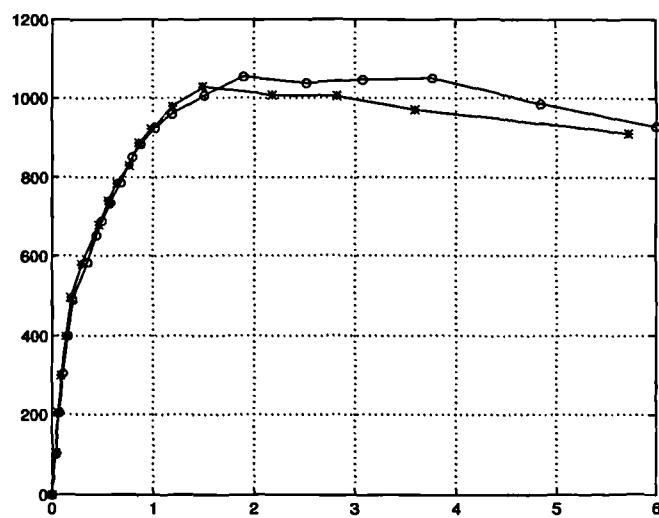
Figure 4.35: Load-slip curve of G17P.
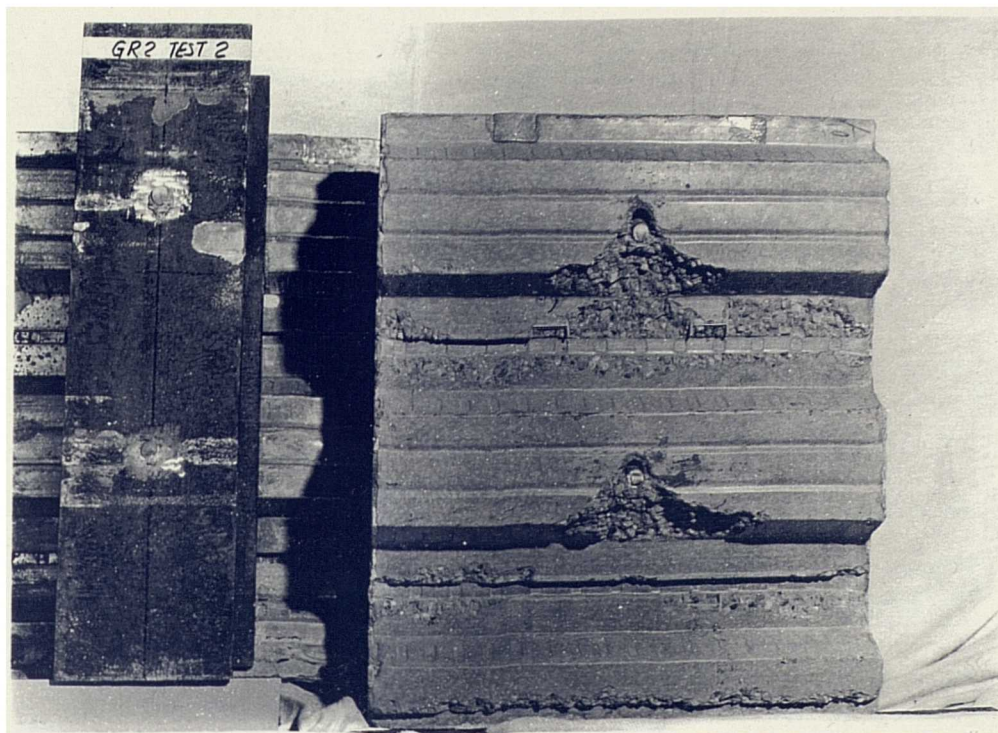
Figure 4.36: Shank shearing failure.
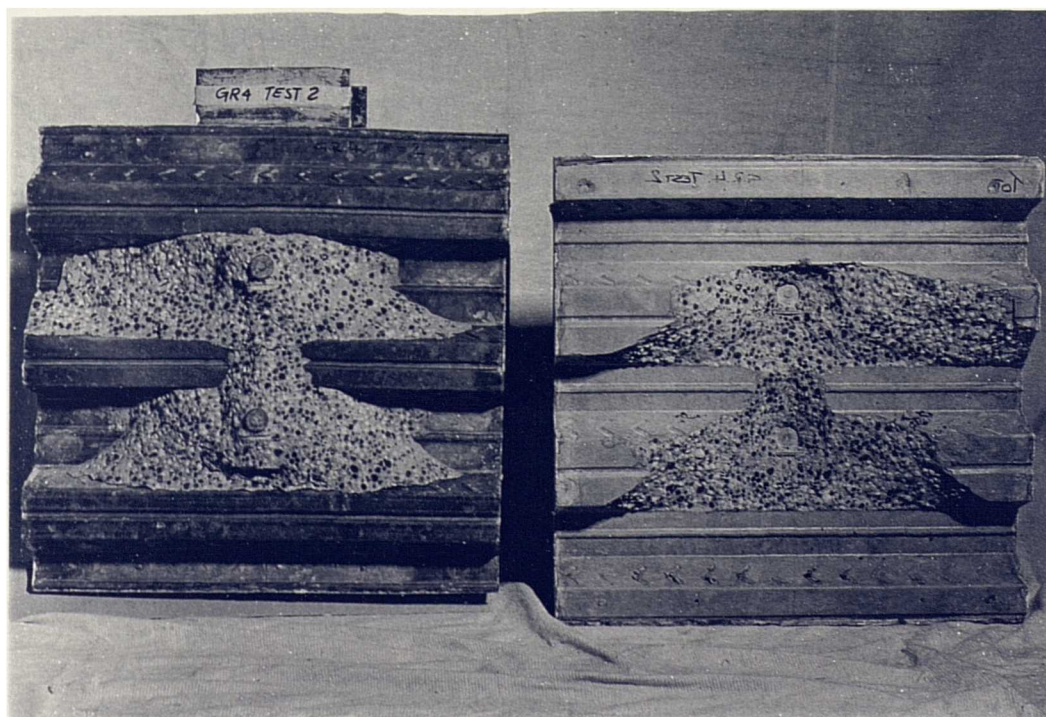
Figure 4.37: Concrete pulling out failure.
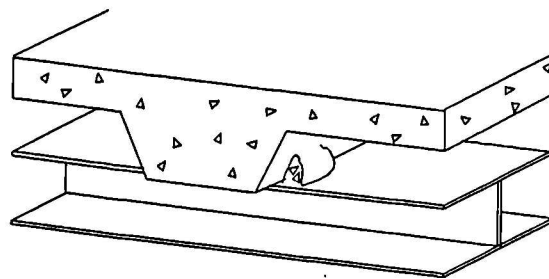
Figure 4.38: Rib punching failure.
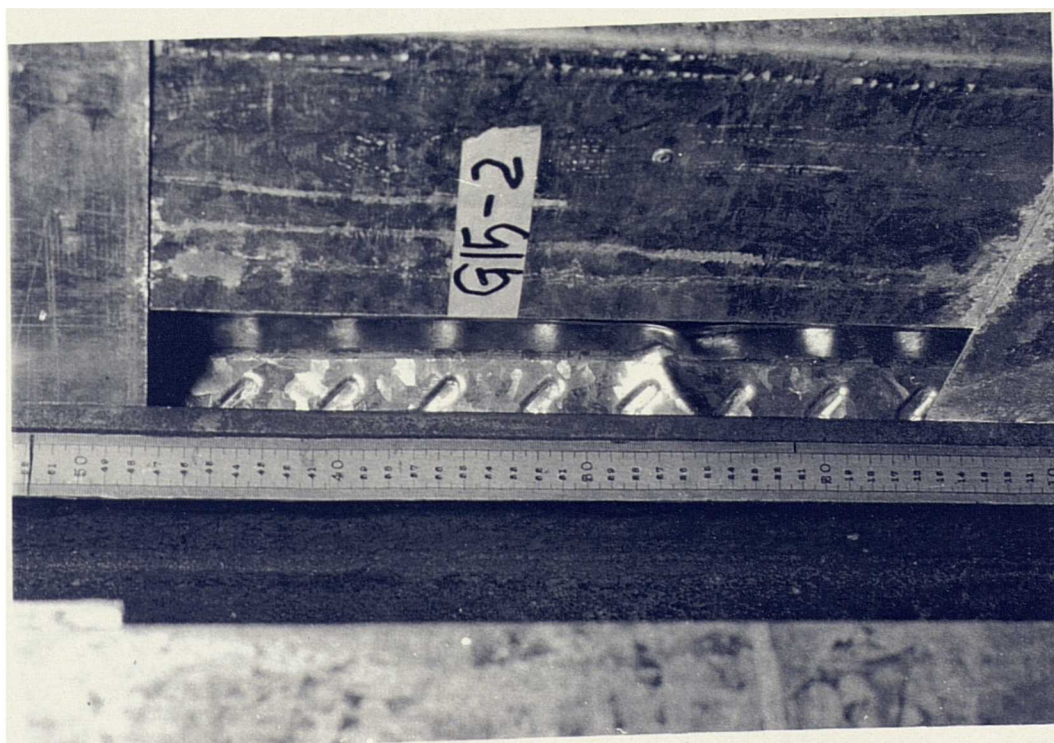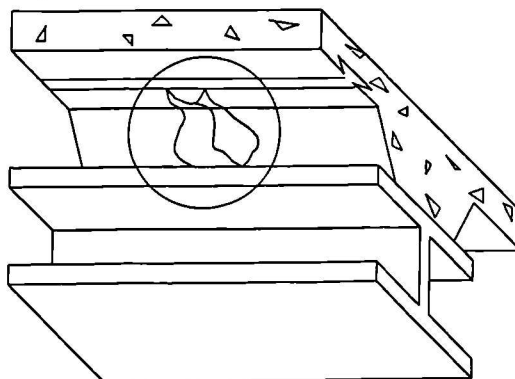
Figure 4.39: Local buckling.
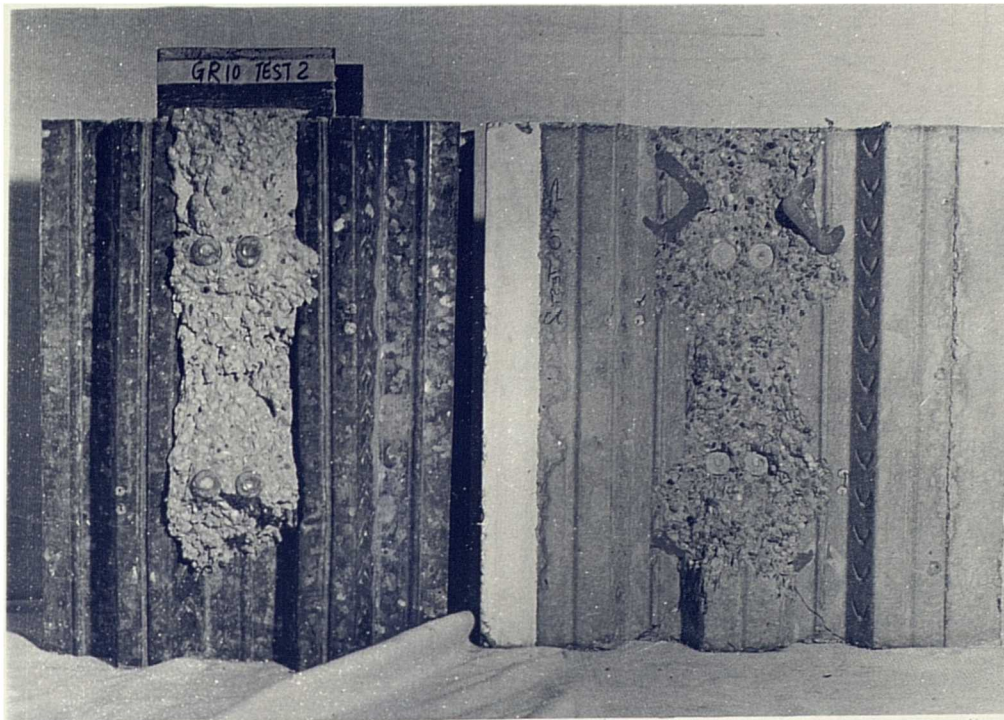
Figure 4.40: Pulling out failure.

P_e/P_r

b_o/h_p
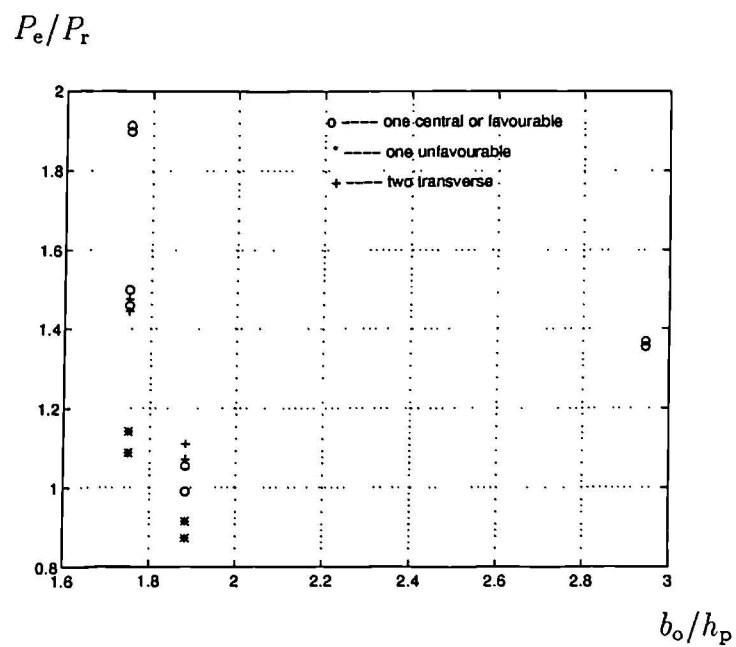
Figure 4.41: Eurocode 4 model for new tests with transverse sheeting.

$P_{\mathrm{e}}/P_{\mathrm{r}}$
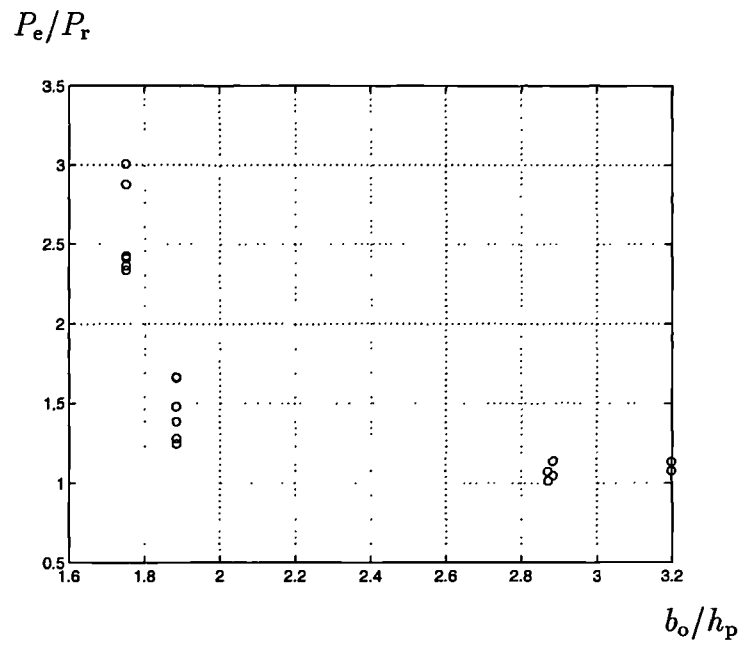
Figure 4.42: Eurocode 4 model for new tests with parallel sheeting.

$P_{\mathrm{e}}/P_{\mathrm{r}}$
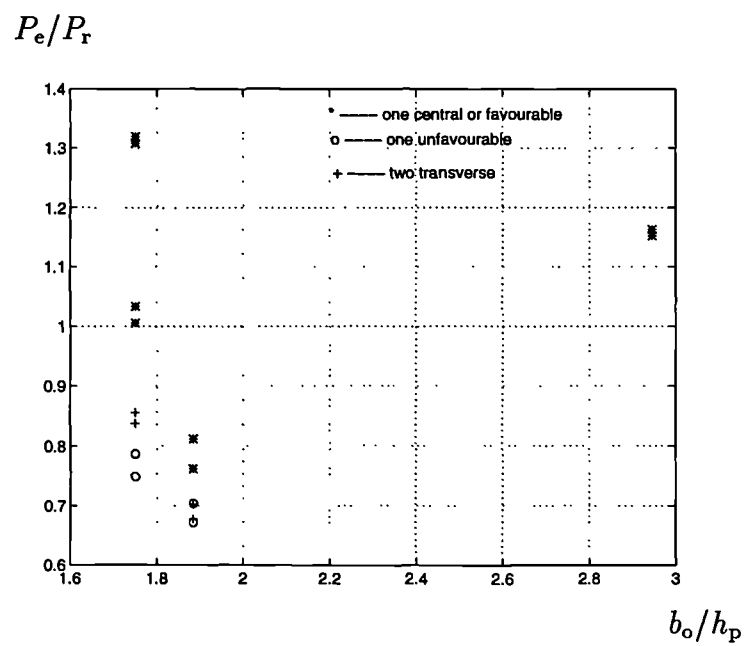
Figure 4.43: Lawson's model for new tests with transverse sheeting.

$P_{\rm e}/P_{\rm r}$
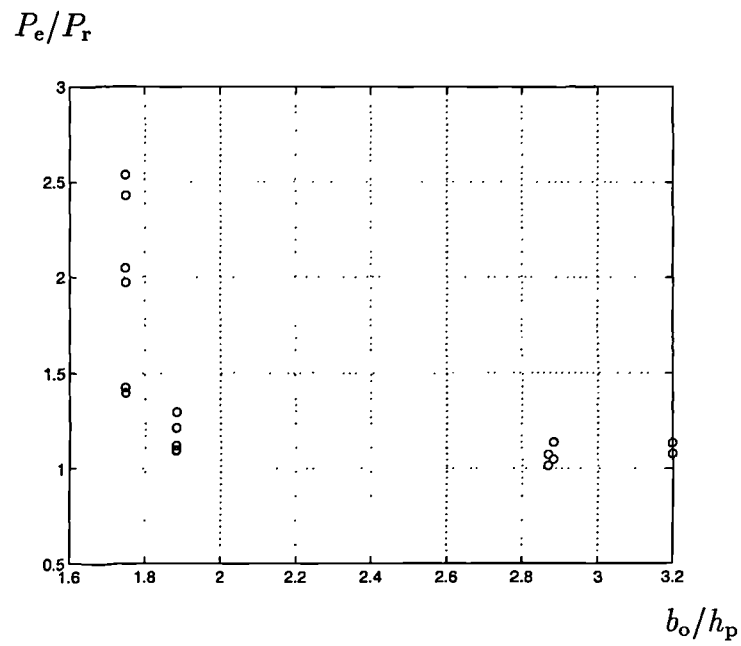
Figure 4.44: Lawson's model for new tests with parallel sheeting.

$P_{\rm e}/P_{\rm r}$
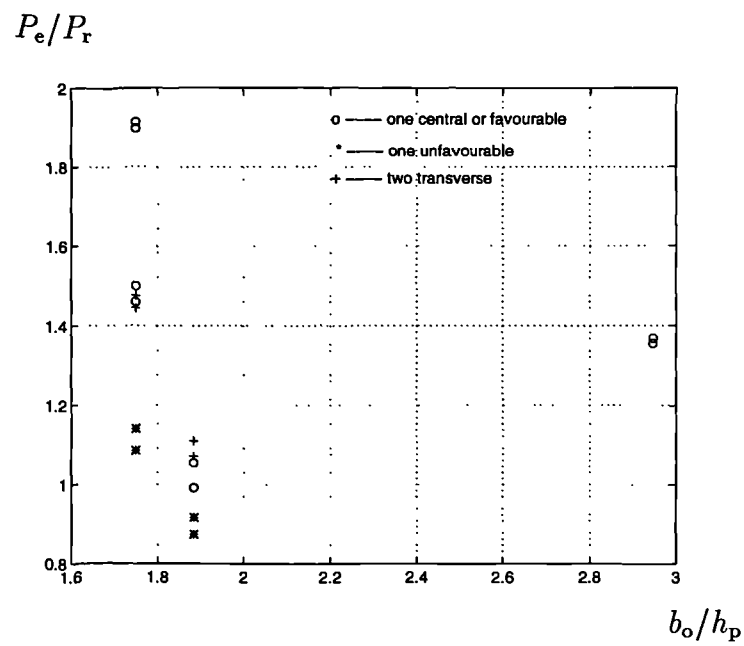
Figure 4.45: Hanswille's model for new tests with transverse sheeting.

Chapter 5

Theoretical analyses on push-out tests with transverse sheeting

5.1 Introduction

In a composite beam, stud connectors are used to transfer shear force from the steel beam to the concrete slab. Where profiled steel sheeting is present, the connectors can be welded onto the top flange of the beam either through the sheeting or through pre-cut holes in the sheeting. As discussed in Chapter 3, these two welding methods have significant influence on the test results. The following studies concern only the stud connectors welded through profiled steel sheeting.

The 16 push-out tests described in Chapter 4 (Table 4.3) showed five possible failure modes for studs with transverse sheeting. They are shank shearing, concrete pulling out, rib punching, and two combined modes of rib punching with either shank shearing or concrete pulling out.

In this Chapter, based on the hypothesis of a modified yield criterion for the connectors, either the upper bound or the lower bound theory is applied to the three basic failure modes, as well as the two combined failure modes. The solutions fit a total of 126 data very well. Compared with the Eurocode 4 model, the coefficient of variation is reduced from 17.1% to 10.9% for shank shearing or concrete pulling out failure, from 13.1% to 7.4% for rib punching failure and from 20.3% to 7.2% for two combined failure modes.

5.2 Yield criterion for stud connectors
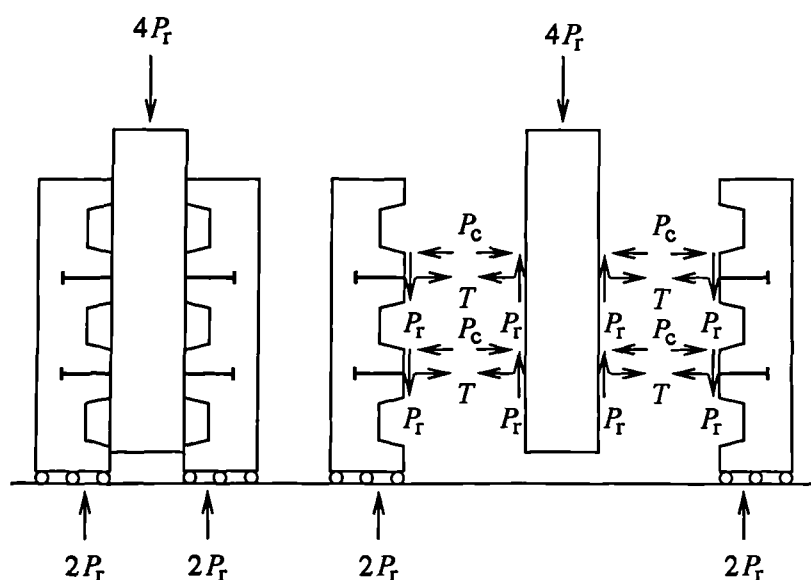
Figure 5.1: Forces on studs in a push-out test.

In order to simplify the problem, a push-out specimen on roller supports is considered, as shown in Figure 5.1. The vertical load $4P_r$ is borne evenly by the four stud connectors. The movement of the steel beam under the vertical load generates tensile force T in the shank of the connectors. For equilibrium, there must be a compressive force P_c between each trough and the steel beam.

Because a stud connector is under a combination of shear and tensile forces,

it is rational to assume that it follows von Mises' yield criterion:

$$\sigma_s^2 + 3\tau_r^2 = f_y^2 \qquad (5.1)$$

where τ_r and σ_s are the shear and tensile stresses on the connector, and f_y is the yield strength. If both τ_r and σ_s are assumed to be uniformly distributed over the cross section, equation (5.1) can be expressed in terms of the shear and tensile forces, P_r and T:

$$(\frac{P_r}{P_{sy}})^2 + (\frac{T}{T_y})^2 = 1 \qquad (5.2)$$

where T_y is the resistance of a stud connector to uniaxial tension,

$$T_y = f_y \pi d^2 / 4 \qquad (5.3)$$

and P_{sy} is the resistance of the connector to pure shear,

$$P_{sy} = \frac{f_y}{\sqrt{3}} \frac{\pi d^2}{4} \qquad (5.4)$$

It is specified in Eurocode 4 [7] that the ultimate tensile strength of the stud connector f_u is not less than $1.2 f_y$. So, f_y is taken as $f_u/1.2$, and equation (5.3) becomes

$$T_y = \frac{f_u}{1.2} \frac{\pi d^2}{4} \doteq 0.8 f_u \frac{\pi d^2}{4} \qquad (5.5)$$

According to the test result of G2C, as shown in Figure 4.36, the shank shearing failure is dominated by the severe shear deformation at the base of the stud connector, and its failure surface is quite similar to that of the pure shear failure. Therefore, it is assumed that the shank shearing failure happens when a stud connector is under pure shear force.

Considering that a shank shearing failure is the main failure mode when a solid concrete slab is used [22], it is further assumed that the shank shearing resistance equals that when the stud is in a solid concrete slab, P_{rs}, as given by Eurocode 4 [7],

$$P_{rs} = \min \begin{cases} 0.29 d^2 \sqrt{f_c E_{cm}} \\ 0.8 \pi d^2 f_u / 4 \end{cases} \qquad (5.6)$$

The two assumptions mean P_{sy} in equation (5.2) can be replaced by P_{rs} from equation (5.6). Therefore, the yield criterion given by equation (5.2) is modified as:

$$(\frac{P_r}{P_{rs}})^2 + (\frac{T}{T_y})^2 = 1 \qquad (5.7)$$

The main characteristic of this modified yield criterion is to take into account the influence of the concrete on the resistance of a stud connector to pure shear.

5.3 Concrete pulling out failure

5.3.1 One stud per trough

Failure mechanism

As observed in the push-out tests, concrete pulling out failure is due to the movement of the base of the stud and the rotation of the head developed by this movement. When the resistances to the movement and the rotation are small, the stud connector rotates, carrying away a wedge-shaped portion of concrete. A typical form of the failure surface is shown in Figure 4.37.

This failure mode is modelled by the mechanism shown in Figure 5.2, in which:

- All materials are rigid-plastic;

- Part I gets a vertical displacement δ_1;

- Part II slides δ_1 from B to B_1 and δ_2 from D to D_1, and the stud connector extends δ_3 at its base;

- Part III slides δ_2 horizontally;

- The influence of the decking is neglected.
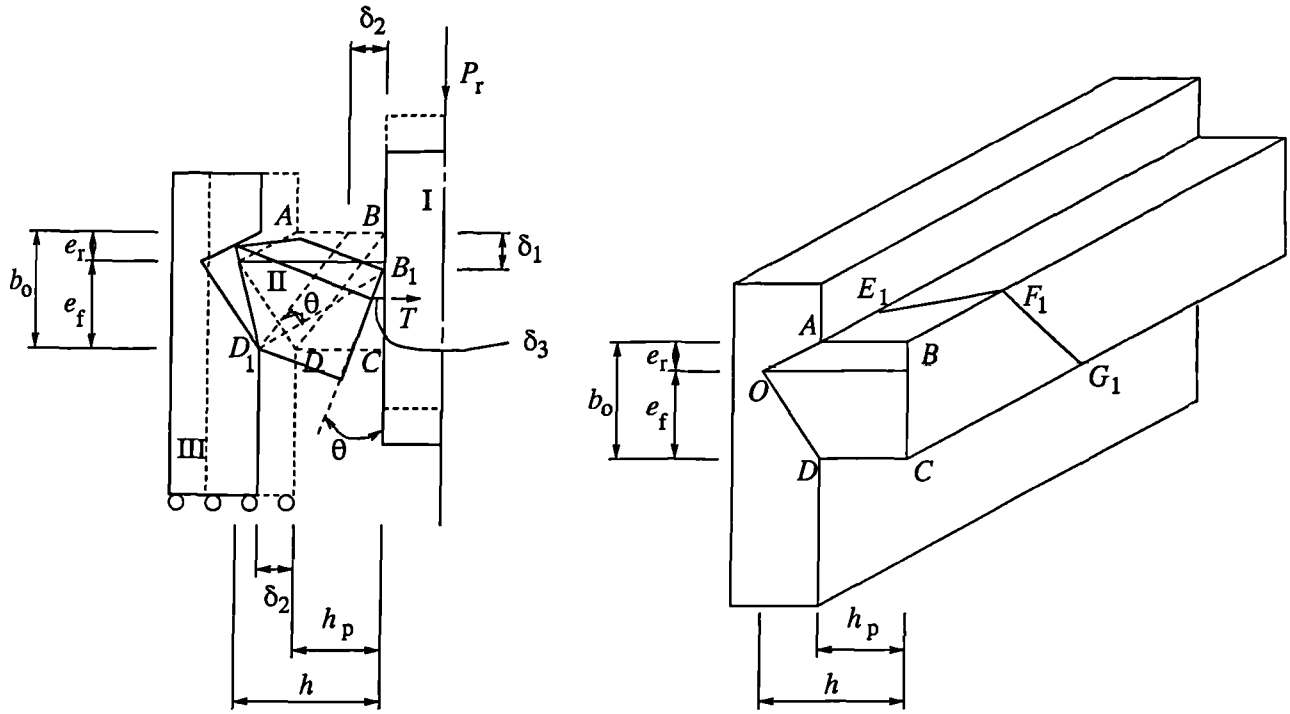
Figure 5.2: Rotation model for concrete pulling out failure.

Relation between the displacement of each part

The relation between δ_1 and δ_2 can be determined geometrically. As $BD = B_1D_1$, there is

$$(D_1C)^2 + (B_1C)^2 = (DC)^2 + (BC)^2 \tag{5.8}$$

Substituting in $D_1C = \delta_2 + h_p$ and $B_1C = b_o - \delta_1$, and regarding that $\delta_1^2 \doteq \delta_2^2 \doteq 0$ as they are very small, equation (5.8) is simplified into

$$\delta_2 = \frac{b_o}{h_p}\delta_1 \tag{5.9}$$

The displacement of part II relative to III is a rotation θ around D, which depends on δ_1 and δ_2:

$$\theta = \frac{\sqrt{\delta_1^2 + \delta_2^2}}{BD} = \frac{\sqrt{\delta_1^2 + \delta_2^2}}{\sqrt{b_o^2 + h_p^2}}$$

Substituting in δ_2 from equation (5.9),

$$\theta = \frac{\delta_1}{h_p} \tag{5.10}$$

In a similar way, it can be found that the displacement of part II relative to I is also a rotation θ but around B. The extension of the stud connector δ_3 therefore is easily determined by:

$$\delta_3 = e_r\theta = \frac{e_r}{h_p}\delta_1 \tag{5.11}$$

Work equation

The work equation is to equate the external work to the internal work. In the mechanism illustrated in Figure 5.2, the external work is $P_r\delta_1$. The internal work consists of two parts. One arises from the rotation θ of part II, w_{ic}, and the other from the extension of the stud connector under a tensile force T:

$$P_r\delta_1 = w_{ic} + T\delta_3 \tag{5.12}$$

Reference is now made to the picture of concrete pulling out failure shown in Figure 4.37. If we neglect the part of concrete slab which is above the head of the stud connector, the failure surface is rather similar to that found in a fixed-ended concrete beam subjected to a central torque T_u, as shown in Figure 5.3. Based on this similarity, it is assumed that the concrete cone in Figure 5.3 dissipates the same amount of work as the cone in Figure 5.2. Then, it is easy to get a relation between w_{ic} and T_u:

$$w_{ic} = T_u\theta \tag{5.13}$$

Referring to the plastic theory for concrete beams in torsion, if the torque T_u in Figure 5.3 produces complete plasticity, then the torsional shear stress ν_t on the cross section is everywhere equal, and can be expressed as

$$\nu_t = \frac{T_u}{H^2(b_o - H/3)}, \quad \text{for } H \leq b_o. \tag{5.14}$$

Here, further assumption is made that when ν_t reaches ν_{tu}, the torsional shear strength, a complete failure cone (part I) as shown in Figure 5.3 is developed.

The relation between ν_{tu} and the cube strength of the concrete f_{cu} is quoted from [25], with f_{cu} in N/mm^2 units:

$$\nu_{tu} = 0.8\sqrt{f_{cu}} \leq 5 \quad \text{N/mm}^2.$$

From equations (5.13) and (5.14),

$$w_{ic} = 0.8\sqrt{f_{cu}}H^2(b_o - H/3)\frac{\delta_1}{h_p} \tag{5.15}$$

where $f_{cu} \leq 40$ N/mm^2, $H \leq b_o$.
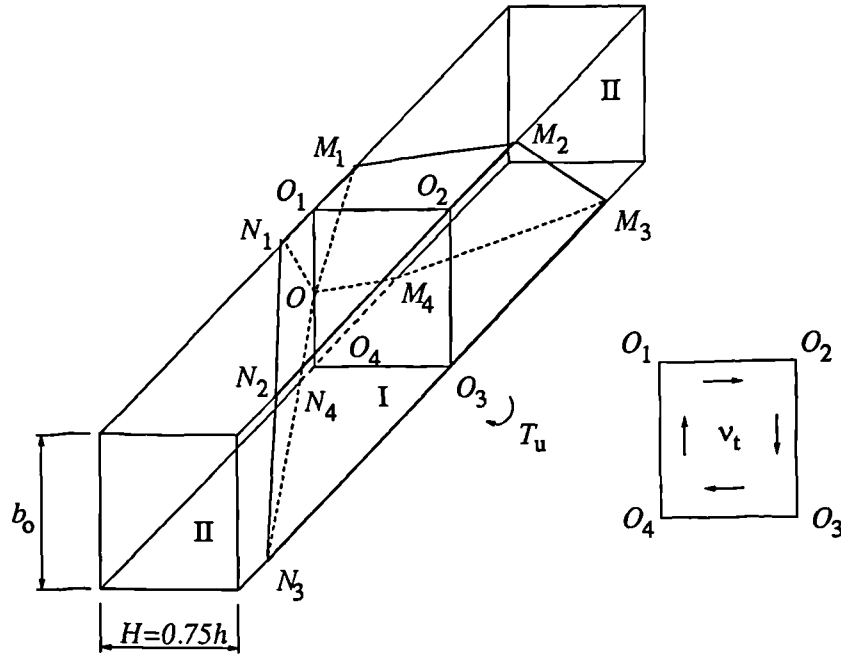
Figure 5.3: Fix-ended beam with central torque.

Though the concrete cone in Figure 5.3 rotates around the centre of the cross section, and the cone in Figure 5.2 rotates around the corner D, the assumption stated by equation (5.13) relates well to the test results, as will be shown later in Section 5.3.3, if the height of the beam in Figure 5.3 is given by $H = 0.75h$, where h is the overall height of the stud connector.

Substituting equations (5.15) and (5.11) into equation (5.12), and considering that $H = 0.75h$,

$$P_r = \frac{0.45\sqrt{f_{cu}}h^2(b_o - 0.25h)}{h_p} + \frac{Te_r}{h_p} \tag{5.16}$$

Introducing in P_{rs} and T_{y},

$$\frac{P_{\text{r}}}{P_{\text{rs}}} = \eta_{\text{c}} + \lambda_{\text{c}}\frac{T}{T_{\text{y}}} \tag{5.17}$$

if

$$\eta_{\text{c}} = \frac{0.45\sqrt{f_{\text{cu}}}h^2(b_{\text{o}} - 0.25h)}{h_{\text{p}}P_{\text{rs}}} \tag{5.18}$$

and

$$\lambda_{\text{c}} = \frac{e_{\text{r}}}{h_{\text{p}}}\frac{T_{\text{y}}}{P_{\text{rs}}} \tag{5.19}$$

where T_{y} and P_{rs} are as given by equations (5.5), (5.6), and $f_{\text{cu}} \leq 40$ N/mm^2, $h \leq 4b_{\text{o}}/3$.

By now, the shear resistance of a stud connector P_{r} is determined, by combining equation (5.17) with (5.7).

5.3.2 Two studs in-line along the trough

When two studs are used within a trough, and they are placed in-line along the trough at the centre or on the favourable side, the failure mechanism is the same as that found for one stud, except that the shear and tensile forces are shared by the two studs. In this case, P_{r} and T in equation (5.12) are replaced by $2P_{\text{r}}$ and $2T$, respectively, and so on and so forth. Finally, equation (5.17) is changed into

$$\frac{P_{\text{r}}}{P_{\text{rs}}} = \frac{\eta_{\text{c}}}{2} + \lambda_{\text{c}}\frac{T}{T_{\text{y}}} \tag{5.20}$$

Introducing a new factor N_{r}, the number of studs per trough, into equation (5.18), a more general expression can be obtained:

$$\eta_{\text{c}} = \frac{0.45\sqrt{f_{\text{cu}}}h^2(b_{\text{o}} - 0.25h)}{h_{\text{p}}N_{\text{r}}P_{\text{rs}}} \tag{5.21}$$ ·

Here, $N_{\text{r}} \leq 2$.

Replacing equation (5.18) with (5.21), the whole process for one stud per trough is also valid for two in-line studs.

5.3.3 Comparison with test results

Among the selected 183 data (Table 3.1) and the 16 new tests with transverse sheeting, there are 107 with one or two studs welded through the centre or the favourable side of the trough in normal weight concrete, in which 70 are used to check the new theoretical models developed in the preceding. The other 37 data are unused, because they are either with unreported f_u (9 from [27] and 5 from [41]) or with re-entraint Holorib steel decking (14 from [34] and 3 from [10]) or with unclear failure mode (5 from [18] and 1 from [21]).

Table 5.1 lists the results of the comparison of the 70 data, where N_r is the number of studs per trough; b_o, average width of a trough; h_p, depth of the trough; h, overall height of a stud; t_s, thickness of steel sheeting; P_e, tested resistance; P_{rs}, theoretical resistance of the stud in a solid concrete slab; P_r^a and P_{rEC}, the resistances of a stud from the new model and the Eurocode 4 model, respectively; P_r^b, same as P_r^a, but with $h = 2h_p$ when $h/h_p \geq 2.0$.

On the whole, the new theoretical models (P_r^a) are better than the Eurocode 4 model, in that the coefficient of variation is reduced from 17.1% to 12.9%.

For data 1-2, 5-9, 14-16, 28-30 and 53-54, the tested resistance P_e is much higher than that expected in a solid concrete slab P_{rs}. It is unreasonable to contribute this beneficial effect to the steel decking. What is most likely is that the steel decking has no influence on the connectors, and the connectors failed by shank shearing. This agrees with the theoretical model. For these data, the predicted resistances P_r^a by the model are near or equal to the shank shearing resistances P_{rs}. Therefore, it is considered that the lower predicted shear resistance P_{rs} is the initial error, and is the reason for the overconservatism of the theoretical model for these data.

Between each pair of data 33-34, 51-52 and 57-58, the differences of tested resistances are from 12% to 17%. This might be the reason of the scatter of the

prediction for these data. The reason for the unsafe prediction for data 23 and 24 is unclear.

The ratios of h/h_p for data 1-2, 35-47, 51-54 and 68-70 are all greater than 2.0, and the prediction for these data seems slightly unconservative. The reason for this is the contineous positive influence of h, the height of the stud connector, on the value of η (equations (5.18) and (5.21)). The tested resistances of these data suggested that when $h/h_p \geq 2.0$, the influence of h is less significant. Therefore, an upper limit for h is introduced into the new theoretical models, i.e., when $h/h_p \geq 2.0$, h is taken as $2h_p$. Considering this limit for h and re-checking all the 70 data, the results shown by P_e/P_r^b are much more better, reducing the coefficient of variation from 12.9% to 10.9%. The comparison of P_r^b with P_e is shown in Figure 5.4.
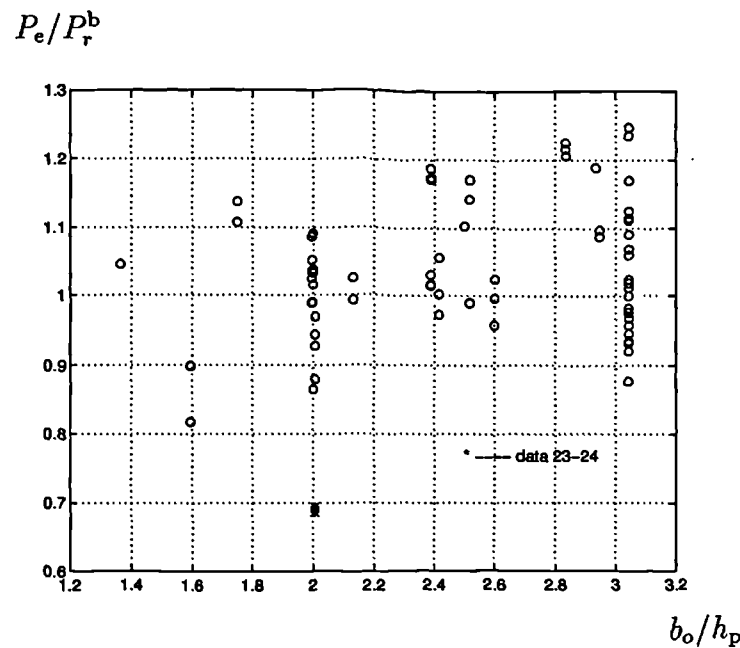
Figure 5.4: Predictions for concrete pulling out failure.

Table 5.1   91

Table 5.1: Predictions for shank shearing or concrete pulling out failure.

Ref	No.	Tests	N_r	b_o	h_p	h	t_s	P_e	P_{rs}	P_r	$\dfrac{P_e}{P_r^a}$	$\dfrac{P_e}{P_{rEC}}$	$\dfrac{P_e}{P_r^b}$
				(mm)				(kN)					
New	1	G2C-1	1C	162	55	125	0.9	88.8	81.1	81.1	1.09	1.09	1.09
	2	G2C-2		(PMF CF70)				88.0			1.08	1.08	1.08
	3	G1F-1	1F	140	80	125	1.2	93.1	94.6	82.3	1.13	1.43	1.13
	4	G1F-2		(Multideck 80)				90.6			1.10	1.39	1.10
[47]	5	60SS-1	1F	151	60	100	1.2	113.0	100.5	95.0	1.19	1.12	1.19
	6	60SS-2		(Multideck 60)				95.5			1.00	0.95	1.00
	7	60SS-3						110.3			1.16	1.10	1.16
[17]	8	PMF-NW -0.9-R-26.2	1F	135	46	95	0.9	93.8	82.2	77.1	1.22	1.14	1.22
				(PMF CF46)									
	9	QL-N-1T	1C	150	60	95	1.15	87.1	82.2	78.8	1.11	1.06	1.11
	10	MET-N-2T	2C	75	55	95	1.0	59.3	82.2	60.8	0.98	1.47	1.05
[40]	11	QI-A	1C	152.5	76	116	-	83.6	91.4	86.5	0.97	1.24	0.97
	12	QI-B						81.4			0.94	1.20	0.94
	13	QI-C						80.0			0.92	1.18	0.92
	14	TI-A	1F	181.5	76	116	-	106.4	91.4	89.6	1.18	1.32	1.18
	15	TI-B						104.9			1.17	1.30	1.17
	16	TI-C						105.2			1.17	1.31	1.17
	17	RI-A	1C	101.8	51	91	-	82.0	91.4	79.8	1.03	0.90	1.03
	18	RI-B						81.1			1.02	0.89	1.02
	19	RI-C						86.0			1.08	0.94	1.08
	20	TII-A	2F	181.5	76	116	-	64.3	84.8	68.6	0.94	1.22	0.94
	21	TII-B						64.2			0.94	1.22	0.94
	22	TII-C						65.2			0.95	1.24	0.95
	23	QII-A	2C	152.5	76	116	-	53.2	91.4	76.8	0.69	1.11	0.69
	24	QII-B						53.8			0.70	1.13	0.70
	25	RII-A	2C	101.8	51	91	-	76.6	91.4	72.2	1.06	1.08	1.06
	26	RII-B						75.3			1.04	1.06	1.04
	27	RII-C						72.1			1.00	1.02	1.00
[34]	28	R30-1-FA	1F	170	60	95	1.2	113.4	94.0	94.0	1.21	1.21	1.21
	29	R30-1-FB		(Ribdeck 60)				115.2			1.23	1.23	1.23
	30	R30-1-FC						114.3			1.22	1.22	1.22
	31	HD30-1-A	1C	162	76	120	1.2	83.9	91.1	89.3	0.94	1.07	0.94
	32	HD30-1-B						86.6			0.97	1.10	0.94
[29]	33	D2	1F	152.4	50.1	88.9	0.81	99.4	106.4	94.3	1.05	0.93	1.05
	34	D3						82.2			0.87	0.77	0.87
	35	D6	1F	152.4	50.1	101.6	0.81	94.0	106.4	100.3	0.94	0.88	0.95
	36	D7	1F	152.4	50.1	114.3	0.81	96.2	106.4	104.9	0.92	0.90	0.97
	37	D8						92.6			0.88	0.87	0.93
	38	D9						97.6			0.93	0.92	0.98

Table 5.1 92

Table 5.1: Continuing.

Ref	No.	Tests	N_r	b_o	h_p	h	t_s	P_e	P_{rs}	P_r	$\frac{P_e}{P_r^a}$	$\frac{P_e}{P_{rEC}}$	$\frac{P_e}{P_r^b}$
					(mm)				(kN)				
[29]	39	D10	1F	152.4	50.1	127	0.81	93.5	103.9	103.9	0.90	0.90	0.96
	40	D11						95.3			0.92	0.92	0.97
	41	D12						99.9			0.96	0.96	1.02
	42	D13	1F	152.4	50.1	140	0.81	91.3	103.9	103.9	0.88	0.88	0.94
	43	D14						97.6			0.94	0.94	1.00
	44	D15						89.9			0.87	0.87	0.92
	45	D33	2F	152.4	50.1	101.6	0.81	83.1	90.9	75.6	1.10	0.91	1.12
	46	D34	2F	152.4	50.1	114.3	0.81	81.3	90.9	77.6	1.03	0.89	1.09
	47	D37	2F	152.4	50.1	127	0.81	74.9	90.9	79.8	0.91	0.82	1.01
	48	D73	2F	152.4	50.1	88.9	0.81	71.7	76.6	65.1	1.11	0.94	1.11
	49	D74						68.1			1.06	0.90	1.06
	50	D75						70.8			1.10	0.92	1.10
	51	D82	2F	152.4	50.1	101.6	0.93	76.7	93.3	76.6	1.00	0.82	1.02
	52	D83						88.1			1.15	0.94	1.17
	53	D86	2F	152.4	50.1	114.3	0.93	94.9	93.3	79.4	1.18	1.02	1.24
	54	D87						94.0			1.17	1.01	1.24
	55	D52	1F	152.4	76.2	114.3	0.93	79.0	88.5	77.0	1.03	1.26	1.03
	56	D54						83.5			1.08	1.34	1.08
	57	D55	1F	152.4	76.2	127	0.93	82.6	88.5	81.7	1.01	1.00	1.01
	58	D56						70.4			0.86	0.85	0.86
	59	D58	1F	152.4	76.2	140	0.93	84.9	88.5	85.9	0.99	0.96	0.99
	60	D59						89.0			1.04	1.01	1.04
[21]	61	JDT-1	2C	60.6	38	76	-	41.1	64.5	45.8	0.90	0.80	0.90
	62	JDT-2	2C	91.8	38	76	-	58.6	64.5	55.5	1.06	0.91	1.06
	63	JDT-3	2C	60.6	38	76	-	37.4	64.5	45.8	0.82	0.73	0.82
	64	JDT-4	2C	91.8	38	76	-	54.0	64.5	55.5	0.97	0.84	0.97
	65	JDT-5	2C	60.6	38	76	-	44.8	76.7	50.0	0.90	0.74	0.90
	66	JDT-6	2C	91.8	38	76	-	62.9	76.7	62.9	1.00	0.82	1.00
	67	JDT-8	1C	152.5	76	127	-	74.5	85.8	83.2	0.90	0.91	0.90
[10]	68	T-4	1C	104	40	100	0.88	90.2	95.2	91.4	0.99	0.94	1.02
	69	T-5	1C	104	40	100	0.88	85.1	91.8	88.4	0.96	0.93	1.00
	70	T-6	1C	104	40	100	0.88	88.3	100.5	95.9	0.92	0.88	0.96
					Mean							1.03	1.03
				Coefficient of variation							12.9%	17.1%	10.9%

C — central position; F — favourable position;

P_r^a — resistance calculated from the new models (equations (5.2) and (5.17) to (5.21));

P_r^b — same as P_r^a, but $h = 2h_p$ when $h/h_p \geq 2.0$;

P_{rEC} — resistance calculated from the Eurocode 4 model.

5.4 Rib punching failure

5.4.1 Lower bound solution

The two groups with studs on the unfavourable sides, G5U and G6U described in Chapter 4 (table 4.3), all failed by rib punching failure. Similar phenomena were also observed in the tests reported by Lyons and Easterling [29]. The main reason for this kind of failure is the insufficient cover of concrete in front of the stud connector. In this case the concrete crushes easily, and the base of the stud moves forwards, torn away from the deck at the weld collar. With further deformation, first the rib in front of the stud bulges, and usually near the end of the tests, the bulges are broken by the thrusting of the connector and the crushed concrete in front of it. The rib punching failure is defined by this state (Figure 4.38).

For this kind of failure, a lower bound solution can be very easily derived. As shown in Figure 5.5, the stresses in the concrete are distributed mainly in three regions, ABF, $FBCE$ and CDE, which act as an arch. The region $FBCE$ is in uniaxial compression. The shear and tensile forces P_r and T in the stud connector, and the tensile force T_d in the steel decking are transferred to the arch through the regions ABF and CDE, which are in hydrostatic pressure. Both the hydrostatic and the uniaxial stresses are assumed to be equal to the concrete strength f_c. Therefore, the angle FBC is $\pi/2$. It is also assumed that the tensile stress in the steel decking reaches its yield strength f_{yd}.

If the width of the stressed region in the concrete is B_c, the equilibrium of the vertical force gives

$$P_r - T_d = B_c x f_c \qquad (5.22)$$

This equation implies that the maximum shear force P_r can be obtained when x
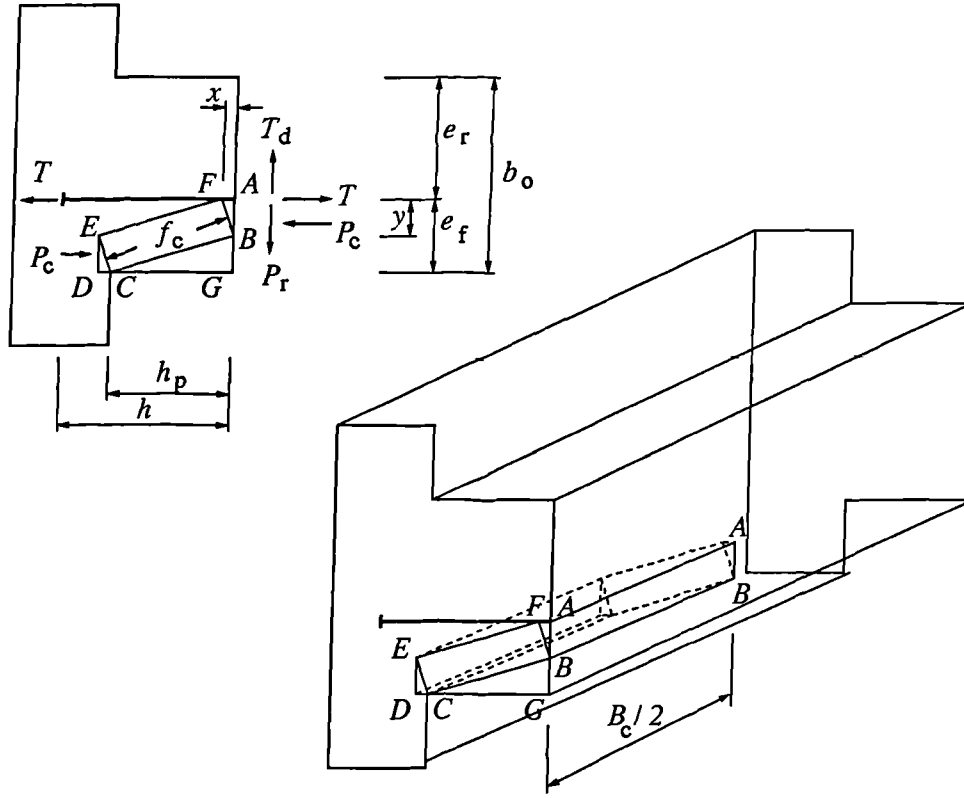
Figure 5.5: Arch model for rib punching failure.

is as large as possible. As $\angle FBC = \pi/2$, a geometrical equation is found,

$$(h_{\mathrm{p}} - x)^2 + e_{\mathrm{f}}^2 = x^2 + y^2 + h_{\mathrm{p}}^2 + (e_{\mathrm{f}} - y)^2 \qquad (5.23)$$

Developing and simplifying,

$$x = \frac{-y^2 + e_{\mathrm{f}} y}{h_{\mathrm{p}}} \qquad (5.24)$$

It is not difficult to show that when $y = e_{\mathrm{f}}/2$, x has its maximum value which is $x = e_{\mathrm{f}}^2/(4h_{\mathrm{p}})$. Substituting it into equation (5.22),

$$P_{\mathrm{r}} - T_{\mathrm{d}} = \frac{B_{\mathrm{c}} e_{\mathrm{f}}^2}{4h_{\mathrm{p}}} f_{\mathrm{c}} \qquad (5.25)$$

The equilibrium of horizontal forces is

$$T = C_{\mathrm{c}} = B_{\mathrm{c}} y f_{\mathrm{c}} = \frac{B_{\mathrm{c}} e_{\mathrm{f}}}{2} f_{\mathrm{c}} \qquad (5.26)$$

combining with equation (5.25),

$$P_{\mathrm{r}} = T_{\mathrm{d}} + \frac{e_{\mathrm{f}}}{2h_{\mathrm{p}}} T \qquad (5.27)$$

If the width of the stressed region in the steel sheeting is B_p, and the thickness of the sheeting is t_s, then,

$$T_d = B_p t_s f_{yd} \qquad (5.28)$$

Study of the push-out test results showed that the shear resistance of a stud connector which failed by rib punching depends to a great extent on the embedment of the head of the stud and the cover of the concrete in front of the connector. According to the mechanism in Figure 5.5, it is clear that the rib punching resistance increases with the width of the stressed region B_p. So, if the embedment is expressed as $(h - h_p)$ and the cover as e_f, B_p is a function of $(h - h_p)$ and e_f,

$$B_p = f(h, h_p, e_f) \qquad (5.29)$$

It is found from the test results shown in Section 5.4.2 that the function can be expressed as

$$B_p = 1.8(e_f + h - h_p) \qquad (5.30)$$

so, the tensile force in the steel decking

$$T_d = 1.8(e_f + h - h_p)t_s f_{yd} \qquad (5.31)$$

Substituting it into equation (5.27) and introducing two factors P_{rs} and T_y which are as given by equations (5.6) and (5.5):

$$\frac{P_r}{P_{rs}} = \eta_r + \lambda_r \frac{T}{T_y} \qquad (5.32)$$

where

$$\eta_r = \frac{1.8(e_f + h - h_p)t_s f_{yd}}{P_{rs}} \qquad (5.33)$$

and

$$\lambda_r = \frac{e_f}{2h_p} \frac{T_y}{P_{rs}} \qquad (5.34)$$

Combining equations(5.7) and (5.32), the shear resistance of a stud connector failed by rib punching is obtained.

5.4.2 Comparison with test results

Except six data reported by Robinson [40] which had unreported t_s, all the other 25 data with normal weight concrete, out of the selected 183 and the 16 new tests, are used to check the new model developed. The results are shown in Table 5.2 and in Figure 5.6. Symbols are as for Table 5.1.

P_e/P_r
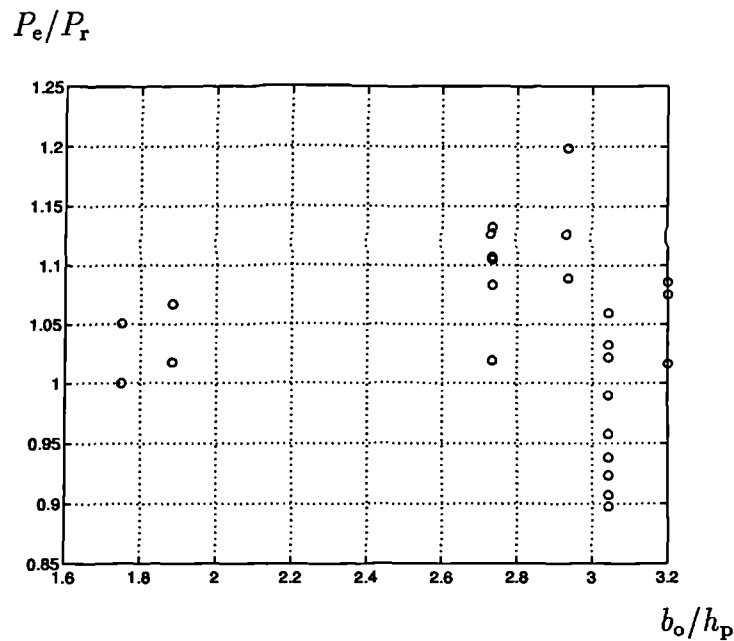
Figure 5.6: Predictions for rib punching failure.

Apparently, the new model is much better than the Eurocode 4 model, in that the coefficient of variation is reduced from 13.1% to 7.4%.

It should be mentioned that for these 25 data, the yield strengths of the steel sheeting are unknown for the new tests and those 11 from [34] and one from [17], but the minimum value is known to be 280 N/mm^2. For the nine tests from [29], the values of f_{yd} are all higher than 280 N/mm^2. In order to be comparable, for all the 25 tests the minimum value of f_{yd} is taken, that is, 280 N/mm^2.

Table 5.2 97

Table 5.2: Predictions for rib punching failure.

Ref	No.	Tests	N_r	b_o	h_p	h	t_s	P_e	P_{rs}	P_r	$\dfrac{P_e}{P_r}$	$\dfrac{P_e}{P_{rEC}}$
					(mm)				(kN)			
New	1	G5U-1	1U	140	80	125	1.2	70.9	94.5	67.5	1.05	1.09
	2	G5U-2						67.5			1.00	1.04
	3	G6U-1	1U	113	60	95	0.9	51.3	80.8	50.4	1.02	0.83
	4	G6U-2						53.8			1.07	0.87
[29]	5	D40	1U	152.4	50.1	88.9	0.77	50.8	78.0	55.0	0.92	0.65
	6	D41						49.9			0.91	0.64
	7	D42						56.8			1.03	0.73
	8	D43	1U	152.4	50.1	88.9	0.92	52.7	78.0	58.7	0.90	0.68
	9	D44						58.1			0.99	0.74
	10	D45						62.2			1.06	0.80
	11	D47	1U	152.4	50.1	88.9	1.23	67.2	78.0	65.7	1.02	0.86
	12	D48						61.7			0.94	0.79
	13	D49	1U	152.4	50.1	88.9	1.53	68.6	78.0	76.6	0.96	0.88
[34]	14	R30-1-UA	1U	164	60	95	1.2	73.2	94.0	71.8	1.02	0.78
	15	R30-1-UB						81.3			1.13	0.86
	16	R30-1-UC						79.5			1.11	0.85
	17	R30-1-UDA	1U	164	60	120	1.2	92.9	97.7	82.5	1.13	0.95
	18	R30-1-UDB						91.1			1.10	0.93
	19	R30-1-UDC						89.3			1.08	0.91
	20	P30-1-UA	1U	135	46	95	1.2	88.1	96.1	81.8	1.07	0.92
	21	P30-1-UB						91.1			1.11	0.95
	22	A30-1-UA	1U	160	50	95	1.2	82.2	88.8	76.4	1.08	0.93
	23	A30-1-UB						77.7			1.02	0.88
	24	A30-1-UC						83.0			1.09	0.93
[17]	25	PMF-NW -0.9-F-25.7	1U	135	46	95	0.9	76.9	81.4	65.0	1.18	0.94
Mean											1.04	0.86
Coefficient of variation											7.4%	13.1%

U — unfavourable position;

P_r — the resistance calculated from the new model;

P_{rEC} — the resistance calculated from the Eurocode 4 model.

5.5 Combined failure modes

5.5.1 Theoretical approach

When two studs are placed staggered or transverse to the trough, test results give two different types of failure modes, and these mostly depend on the transverse spacing between the two studs. As there is always one stud on the unfavourable side, both of the failure modes include rib punching failure for this stud. For the stud on the other side, when it is far enough away from the other, shank shearing is observed. Otherwise, when it is too close, both of the studs are pulled out of the concrete slab, carrying away a wedge-shaped concrete cone, showing the typical form of concrete pulling out failure.

Clearly, the stud on the unfavourable side yields first, because the concrete arch in front of the stud can carry relatively lower shear force. After the yielding of this stud, further shear force is transferred to the stud on the favourable side, until it fails either by shank shearing or by concrete pulling out.

Considering this failure mechanism, the trough with two studs is divided into two parts, each with one stud, as shown in Figure 5.7. The first part is the stud on the unfavourable side with the concrete cover in front of it. The resistance P_{ru} is calculated by equations (5.7) and (5.32), with $1.8(e_f + h - h_p)$ replaced by $(e + h - h_p)$; in other words, P_{ru} and T_{su}, are given by equations (5.35) and (5.36):

$$\left(\frac{P_{\mathrm{ru}}}{P_{\mathrm{rs}}}\right)^2 + \left(\frac{T_{\mathrm{su}}}{T_y}\right)^2 = 1 \tag{5.35}$$

and

$$\frac{P_{\mathrm{ru}}}{P_{\mathrm{rs}}} = \eta_{\mathrm{u}} + \lambda_{\mathrm{u}} \frac{T_{\mathrm{su}}}{T_y} \tag{5.36}$$

where

$$\eta_{\mathrm{u}} = \frac{(e + h - h_p) t_s f_{yd}}{P_{\mathrm{rs}}} \tag{5.37}$$

and

$$\lambda_{\mathrm{u}} = \frac{e}{2h_{\mathrm{p}}} \frac{T_{\mathrm{y}}}{P_{\mathrm{rs}}} \tag{5.38}$$

Again, f_{yd} is taken as 280 N/mm^2 for all the tests.
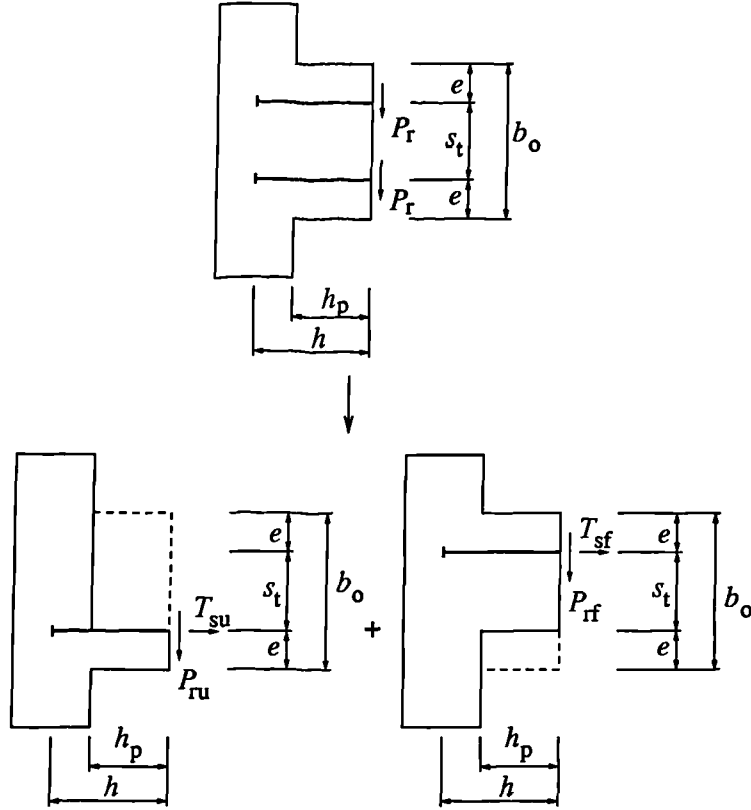
Figure 5.7: Combined model for two transverse or staggered studs.

The second part is the stud on the favourable side with the remainder of the concrete rib. The shear resistance P_{rf} is calculated by equations (5.7) and (5.17), with b_{o} replaced by $(e + s_t)$, and is given by equations (5.39) and (5.40):

$$(\frac{P_{\mathrm{rf}}}{P_{\mathrm{rs}}})^2 + (\frac{T_{\mathrm{sf}}}{T_{\mathrm{y}}})^2 = 1 \tag{5.39}$$

$$\frac{P_{\mathrm{rf}}}{P_{\mathrm{rs}}} = \eta_{\mathrm{f}} + \lambda_{\mathrm{f}} \frac{T_{\mathrm{sf}}}{T_{\mathrm{y}}} \tag{5.40}$$

where

$$\eta_{\mathrm{f}} = \begin{cases} 0.45\sqrt{f_{\mathrm{cu}}}h^2(e + s_t - 0.25h)/(h_{\mathrm{p}}P_{\mathrm{rs}}) & h \leq 4(e + s_t)/3 \\ 0.8\sqrt{f_{\mathrm{cu}}}(e + s_t)^2\,[0.75h - (e + s_t)/3]\,/(h_{\mathrm{p}}P_{\mathrm{rs}}) & (e + s_t) \leq 0.75h \end{cases} \tag{5.41}$$

and

$$\lambda_f = \frac{e}{h_p} \frac{T_y}{P_{rs}}$$
(5.42)

The shear resistance of each stud P_r is assumed to be the mean value of P_{ru} and P_{rf}:

$$P_r = \frac{P_{ru} + P_{rf}}{2}$$
(5.43)

5.5.2 Comparison with push-out test results.

The preceding approach for two transverse or staggered studs gives much better predictions than the Eurocode 4 model, as shown in Table 5.3. The coefficient of variation is reduced from 20.3% to 7.2%. The comparison is also shown in Figure 5.8.
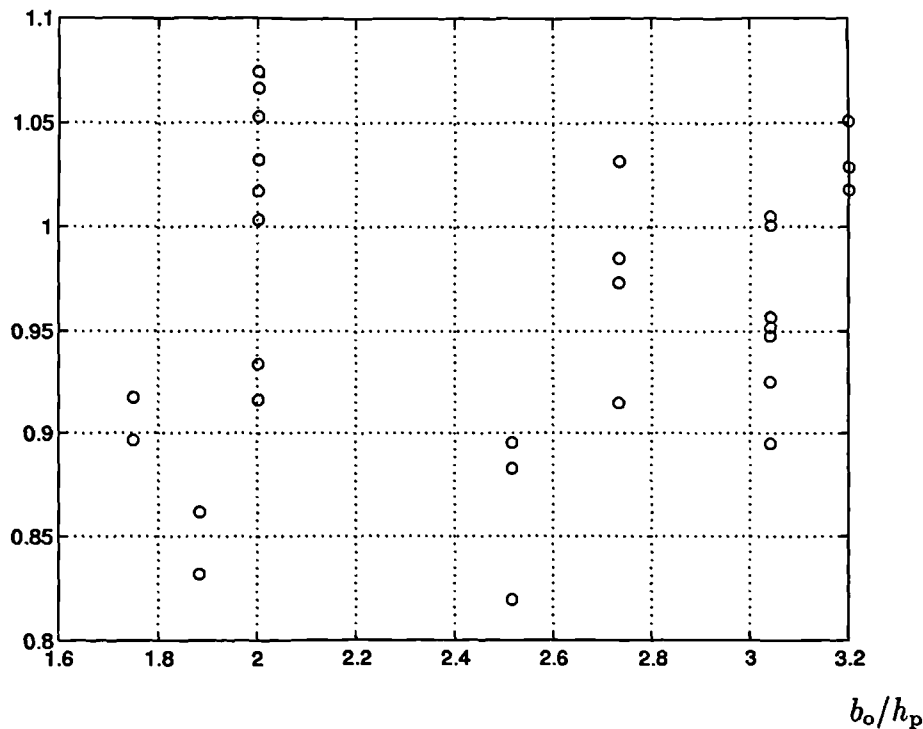
Figure 5.8: Predictions for combined failure modes.

Table 5.3 101

Table 5.3: Predictions for combined failure modes.

Ref	No.	Tests	N_r	b_o	h_p	h	t_s	P_e	P_{rs}	P_r	$\dfrac{P_e}{P_r}$	$\dfrac{P_e}{P_{rEC}}$
					(mm)				(kN)			
New	1	G7D-1	2T	113	60	95	0.9	49.8	89.9	59.8	0.83	1.02
	2	G7D-2						51.6			0.86	1.06
	3	G8D-1	2T	140	80	125	1.2	61.4	89.9	66.9	0.92	1.40
	4	G8D-2						60.0			0.90	1.37
[34]	5	R30-2-SSA	2S	164	60	95	1.2	70.5	90.9	77.1	0.91	0.98
	6	R30-2-SSB						79.5			1.03	1.11
	7	R30-2-SA	2T	164	60	95	1.2	75.0	90.9	77.1	0.97	1.05
	8	R30-2-SB						75.9			0.98	1.06
	9	A30-2-SA	2T	160	50	95	1.2	85.7	91.1	81.5	1.05	0.94
	10	A30-2-SB						83.9			1.03	0.92
	11	A30-2-SS	2S	160	50	95	1.2	83.0	91.1	81.5	1.02	0.91
[47]	12	60-SS-1	2S	151	60	100	1.2	70.8	96.0	79.1	0.90	0.89
	13	60-SS-2						69.9			0.88	0.88
	14	60-SS-3						65.1			0.82	0.82
[29]	15	D62	2S	152.4	50.1	88.9	0.81	69.5	88.6	72.6	0.96	0.78
	16	D63						67.2			0.93	0.76
	17	D71	2S	152.4	50.1	127	0.81	69.0	76.9	68.9	1.00	0.90
	18	D72						61.7			0.90	0.80
	19	D79	2S	152.4	50.1	114.3	0.77	73.5	93.2	77.2	0.95	0.79
	20	D81						77.6			1.01	0.83
	21	D67	2S	152.4	76.1	140	0.93	63.6	76.6	63.4	1.00	1.00
	22	D68						68.1			1.07	1.07
	23	D69						67.6			1.07	1.07
	24	D64	2S	152.4	76.1	127	0.93	62.2	76.6	62.0	1.00	1.22
	25	D65						64.0			1.03	1.26
	26	D66						56.8			0.92	1.12
	27	D76	2S	152.4	76.1	114.3	0.93	60.4	93.3	64.7	0.93	1.30
	28	D77						68.1			1.05	1.47
	29	D78						65.8			1.02	1.42
	30	D20	2S	152.4	50.1	101.6	0.81	69.5	86.5	72.6	0.96	0.80
	31	D23	2S	152.4	50.1	114.3	0.81	69.9	86.5	73.7	0.95	0.80
Mean											0.96	1.03
Coefficient of variation											7.2%	20.3%

T — two studs transverse to the trough; S — staggered;

P_r — the resistance from the new model; P_{rEC} — the resistance from the Eurocode 4.

5.6 Discussion

5.6.1 Upper limit for η

The previous sections have shown that the shear resistance of stud connectors in a composite beam with transverse sheeting can be determined theoretically by equations (5.44) and (5.45):

$$(\frac{P_{\mathrm{r}}}{P_{\mathrm{rs}}})^2 + (\frac{T}{T_y})^2 = 1 \tag{5.44}$$

and

$$\frac{P_{\mathrm{r}}}{P_{\mathrm{rs}}} = \eta + \lambda \frac{T}{T_y} \tag{5.45}$$

where P_{r} and T are the shear and tensile forces in the stud connectors, and P_{rs} and T_y are as given by equations (5.6) and (5.5). With different positions and numbers of the stud connectors, the expressions for η and λ are different.

Among the three failure modes, i.e., shank shearing, concrete pulling out and rib punching, the shank shearing failure has the highest resistance. As assumed in Section 5.2, it is equal to the resistance of the stud connector in a solid concrete slab P_{rs}, which means the shear force in the connectors P_{r} cannot be greater than P_{rs}, that is:

$$\frac{P_{\mathrm{r}}}{P_{\mathrm{rs}}} = \eta + \lambda \frac{T}{T_y} \leq 1.0 \tag{5.46}$$

From the expressions for η (equations (5.18), (5.21), (5.33), (5.37) and (5.41)), it is clear that η depends to a great extent on the geometry of the decking. In the process of comparing the models with the push-out test results, η was found to be greater than 1.0 for wide and shallow troughs, such as the tests with $b_o/h_{\mathrm{p}} \geq 2.9$. In this case η was taken as 1.0, and the calculation showed that $T = 0$ and $P_{\mathrm{r}} = P_{\mathrm{rs}}$, in consistent with the test results.

Apparently, there are two conditions for the occurrence of the shank shearing failure:

1. $\eta + \lambda \frac{T}{T_y} \geq 1.0$;

2. $\eta \geq 1.0$.

Therefore, the upper limit for η is 1.0.

5.6.2 Influence of the transverse reinforcement

A new point was raised by Mottram and Johnson [34] that the location of the mesh below the heads of the studs would increase the push strengths, because most of the failure surfaces observed in the tests were entirely below the mesh. This was considered in the new 34 push tests described in Chapter 4. For transverse sheeting, the locations of the mesh were at the tops of the studs (Figures 4.5, 4.7, 4.9 and 4.10), below them (Figures 4.4 and 4.8) or on the flanges of the sheeting (Figures 4.6 and 4.11). Comparing G3FL (Figure 4.6) with G4FL (Figure 4.7) and G5U (Figure 4.8) with G6U (Figure 4.9), it seems that the lower location of the mesh prevented the occurrence of concrete pulling out failure.

Now let us consider the rotation model for concrete pulling out failure shown in Figures 5.2 and 5.3. By taking into account the presence of the transverse reinforcement within the failure surface, the torsional resistance T_u in equation (5.13) is increased, so is the factor η_c in equation (5.17), which means the studs can be stronger.

Both the test evidence and the theoretical model suggest a positive influence of the transverse reinforcement, but neglecting it, as the model does, still gives satisfactory solutions. This might be because the amount of the reinforcement intersecting the failure surface is insufficient. To obtain further understanding, more tests are needed.

5.7 Conclusions

The shear resistances of stud connectors welded through transverse sheeting have been predicted theoretically by applying the upper or the lower bound theory. In a common form, they are expressed as

$$P_r = k_t P_{rs} \tag{5.47}$$

in which P_{rs} is the resistance of a stud to shank shearing failure, which is assumed to be equal to the resistance of the stud in a solid concrete slab (equation (5.6)); and the reduction factor k_t is determined by:

$$k_t = \frac{\eta + \lambda\sqrt{1 - \eta^2 + \lambda^2}}{1 + \lambda^2} \leq 1.0 \tag{5.48}$$

1. For one stud per trough, k_t is the smallest of 1.0 for shank shearing failure, k_{tc} for concrete pulling out failure and k_{tr} for rib punching failure, in which k_{tc} is calculated from η_c (equation (5.18)) and λ_c (equation (5.19)); k_{tr} from η_r (equation (5.33)) and λ_r (equation (5.34)).

2. For two in-line studs, the behaviour is similar to one stud per trough, but with lower resistance. This is taken into account by a factor N_r, the number of studs per trough, in the calculation of η_c as given by equation (5.21).

3. For two transverse or staggered studs, k_t is the average of k_{tf}, the reduction factor for the stud on the favourable side, and k_{tu}, the one for the stud on the unfavourable side. k_{tf} is calculated from η_f (equation (5.41)) and λ_f (equation (5.42)), and k_{tu} from η_u (equation (5.37)) and λ_u (equation (5.38)).

4. The predictions are valid for 19-mm stud(s) with in-line spacing (centre to centre) between $2.8d$ and $5d$.

5. Because of the insufficient information on the yield strengths of the steel sheeting, f_{yd}, it is taken as 280 N/mm^2 for all the tests.

Chapter 6

Theoretical analyses of push-out tests with parallel sheeting

6.1 Introduction

From the 14 push-out tests with normal weight concrete described in Chapter 4 (Table 4.4), two kinds of failure modes were observed for stud connectors with parallel sheeting. They are splitting failure and pulling out failure.

In this chapter, theoretical models for the two failure modes are developed, based on the splitting theory of Oehlers [38] and the shear-friction theory of Hawkins and Mitchell [18].

The splitting theory assumes that the shear force transfered by the stud connectors is resisted by two prisms which fail simultaneously by splitting. It is used to model the splitting failure. However, for narrow troughs, due to the weakness of the concrete around the stud, one of the prisms could not reach its splitting strength, and fails prematurely by a different mode. This mode is pulling out failure, which is modelled by introducing the shear-friction concept into the splitting theory.

The significant characteristic of the models is the different mechanism of load transfer compared with the Eurocode 4 model. Therefore, the connectors with parallel sheeting can be stronger than in a solid concrete slab, which agrees with the test results. In other words, it is inappropriate to apply the reduction factor method for studs with parallel sheeting, as in Eurocode 4.

The prediction fits a total of 31 data very well. Compared with the Eurocode 4 model, the coefficient of variation is reduced from 28.4% to 5.6% for splitting failure and from 40.7% to 10% for pulling out failure.

6.2 Splitting theory

A series of studies on the resistance of a prism to strip or patch load was reported by Oehlers [38]. Here is the summary of the general analyses for both types of the loads.

6.2.1 Local splitting

Figure 6.1(a) shows a concentric strip load of width b_a on a prism of width b_c and depth h_a. From finite element elastic analyses, as reported in [35], the vertical strip load P_s develops high compression stresses over a short length adjacent to the strip load and tensile stresses over a much greater length.

If the strip load is within the prism, as shown in Figure 6.1(b), the distribution of the lateral stresses is anti-symmetrical, with the shape of the part of the compressive stresses identical to the part of the tensile stresses.

The finite element analyses also showed that the tensile force P_t or the compressive force P_c can be determined as

$$P_t = P_c = 0.6 b_c h_a f_{ct} \qquad (6.1)$$

where f_{ct} is the splitting tensile strength of concrete, and is assumed to be related to the cylinder strength f_c, by:

$$f_{ct} = 0.5\sqrt{f_c}, \quad \text{N/mm}^2. \tag{6.2}$$
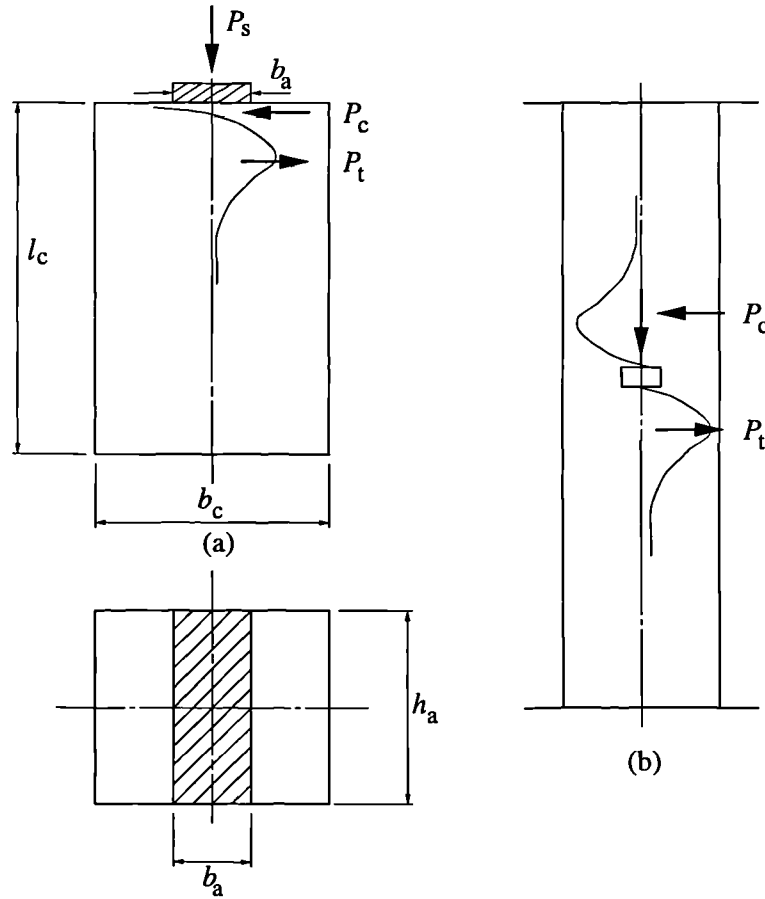
Figure 6.1: Central strip load on a prism.

The ratio of the tensile or compressive force to the strip load P_s was derived theoretically in [38]:

$$K_d = \frac{P_t}{P_s} = \frac{1}{\pi}(1 - \frac{b_a}{b_c})^2 \tag{6.3}$$

Equations (6.1) and (6.3) give the following general expression for local splitting due to a strip load:

$$P_s = \frac{0.6 b_c h_a f_{ct} \pi}{(1 - \frac{b_a}{b_c})^2} \tag{6.4}$$

When a concentric patch load $b_a \times h_a$ is applied to a prism $b_c \times d_c$, as shown in Figure 6.2, it is assumed to be supported by both prisms ABHG and CDFE, and the strip load P_s is the sum of the splitting resistances of the patch on each prism when the ratio of the area of patch load to $b_c \times d_c$ is between 0.04 and 0.36. The resistance of prism CDFE can be determined directly by equation (6.4), while for prism ABHG, it is calculated with b_c, h_a and b_a in equation (6.4) replaced by d_c, b_a and h_a. Hence,

$$P_s = \frac{0.6 b_c h_a f_{ct} \pi}{(1 - \frac{b_a}{b_c})^2} + \frac{0.6 b_a d_c f_{ct} \pi}{(1 - \frac{h_a}{d_c})^2} \qquad (6.5)$$
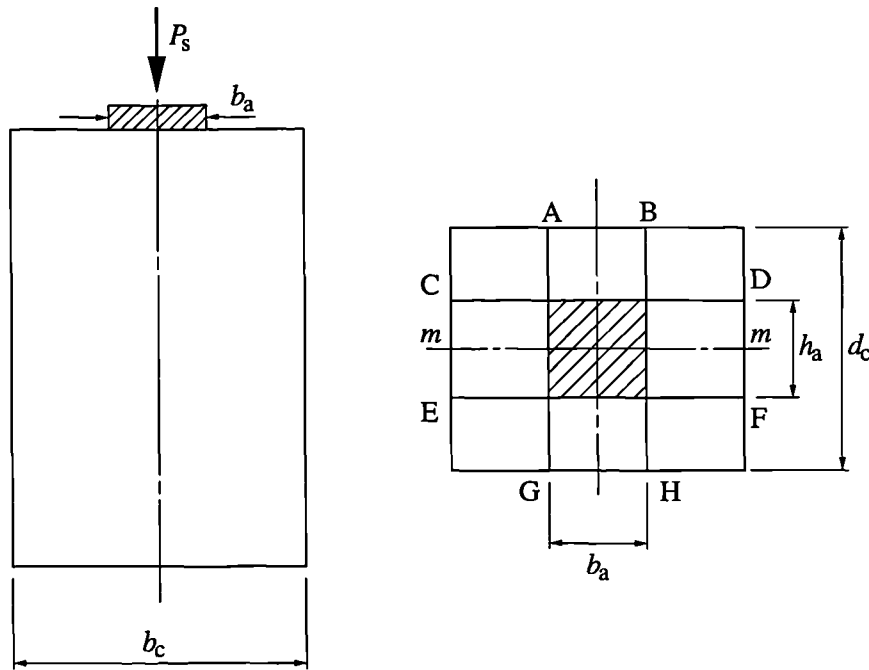
Figure 6.2: Central patch load on a prism.

6.2.2 Global splitting

If there are several strip loads along a certain length of a prism, as shown in Figure 6.3, the lateral stress zones will overlap with each other, and hence will

affect the loads at which splitting occurs. In this case, the splitting is called global splitting.

For a group of strip loads with uniform value P_s and even spacing s_v, according to [38],

$$P_s = \frac{s_v h_a f_{ct}}{K_d} = \frac{s_v h_a f_{ct} \pi}{(1 - \frac{b_a}{b_c})^2} \tag{6.6}$$

Comparing equation (6.6) with equation (6.4), it is easy to find that the occurrence of global splitting requires $s_v \leq 0.6 b_c$.

For a group of patch loads, the strip load P_s can be determined in a similar way as for single patch load, which is simplified into a group of strip loads on two prisms,

$$P_s = \frac{s_v h_a \pi f_{ct}}{(1 - \frac{b_a}{b_c})^2} + \frac{s_v b_a f_{ct} \pi}{(1 - \frac{h_a}{d_c})^2} \tag{6.7}$$

Apparently, global splitting occurs on the first prism when $s_v \leq 0.6 b_a$, and on the second prism when $s_v \leq 0.6 h_c$.
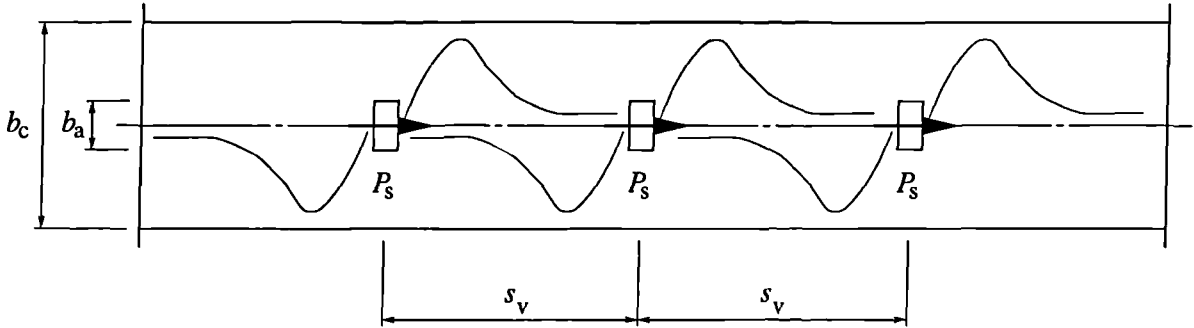
Figure 6.3: Global splitting.

6.3 Splitting analyses on stud connectors

6.3.1 Splitting resistance

As observed in the 14 push-out tests with normal weight concrete described in Chapter 4, all the other tests except G10P showed splitting failure, with longitudinal cracks that occurred at the maximum loads, and local buckling in the ribs of the profiled sheeting.
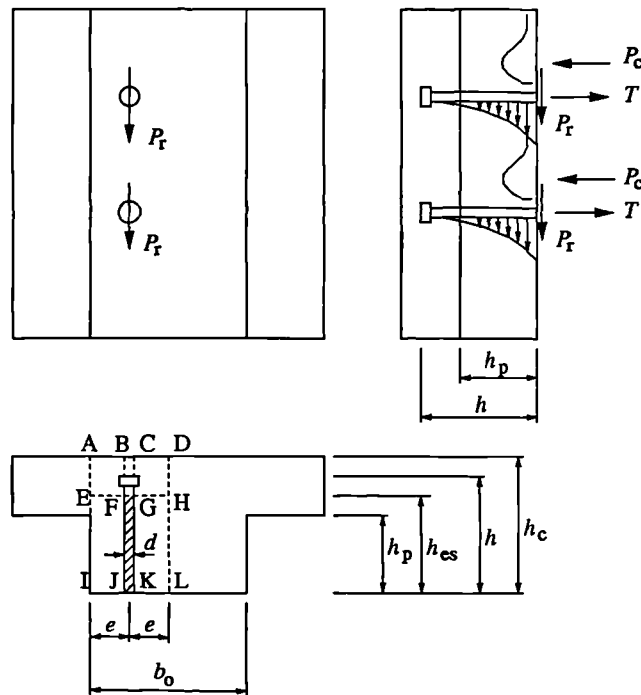
Figure 6.4: Patch load from the stud connector (parallel sheeting).

Figure 6.4 shows a push-out specimen with parallel sheeting. The shear force P_r is assumed to be transferred into the concrete in terms of a bearing pressure between the connector and the concrete over the area $d \times h_{es}$, where d is the diameter of the shank of a stud and h_{es} is the effective depth of the bearing area.

At first, the bearing area is just around the base of the connector, causing the concrete in this area to split, but the expansion of the splitting cracks is restrained by the ribs of the profiled sheeting. Therefore, with the increase of the

shear force P_r, the bearing area increases, until yielding of the ribs releases the restriction.

Due to the flexible behaviour of the stud connector, the bearing pressure is greatest adjacent to the base of the connector, and is gradually reduced to zero over h_{es}. However, we assume that the pressure is uniformly distributed. In this case, the resistance of the prism ADLI in Figure 6.4 to the pressure over $d \times h_{es}$ determines the shear resistance of the stud connector P_r, ignoring the restraint of the concrete to both sides AI and DL..

The prism ADLI can be regarded as the upper half of the prism above $m - m$ in Figure 6.2. The discrepancy between the two cases is that the dispersal of the splitting force in the prism of ABHG in Figure 6.2 is provided by the restraint along $m - m$, while in Figure 6.4 the concrete slab is only restrained by the axial stiffness of the stud connectors, which develops tensile forces T in the studs. As this tensile force is unlikely to cause the studs to fail in tension, the prisms EHLI and BCKJ in Figure 6.4 are assumed to fail simultaneously in splitting. This is not a bad assumption, especially for stud connectors with wide troughs, but for narrow troughs, it needs to be revised, as will be discussed in Section 6.4.

To equate the tensile forces T, there are compressive forces P_c distributed behind the studs. Clearly, the tensile and compressive regions are unlikely to overlap with each other. So, the prisms EHLI and BCKJ will be controlled only by local splitting. If, P_{r1} and P_{r2} are the resistances of the two prisms, respectively, the above assumption becomes

$$P_r = P_{r1} + P_{r2} \tag{6.8}$$

Referring to equation (6.4), P_{r1} and P_{r2} can be determined as follows:

$$P_{r1} = \frac{1.2 e h_{es} f_{ct}}{K_d} \tag{6.9}$$

and

$$P_{r2} = \frac{0.6 d h_{es} f_{ct}}{K_s} \tag{6.10}$$

where K_d is as given by equation (6.11), and K_s by (6.12):

$$K_d = \frac{1}{\pi}(1 - \frac{d}{2e})^2 \tag{6.11}$$

and

$$K_s = \frac{1}{\pi}(1 - \frac{h_{es}}{h_c})^2 \frac{h_{es}}{h_c} \tag{6.12}$$

in which e is the distance from the centre of the stud to the mid-depth of the nearer rib, and h_c the overall depth of the concrete slab. The splitting tensile strength of the concrete f_{ct} is as given by equation (6.2).

It was found from push-out tests [38] that K_s defined by equation (6.12) underestimates the test results, and that a better estimation can be obtained by replacing h_c with $2h_c$, that is,

$$K_s = \frac{1}{\pi}(1 - \frac{h_{es}}{2h_c})^2 \frac{h_{es}}{2h_c} \tag{6.13}$$

Substituting it into equation (6.10), equation (6.8) then becomes

$$P_r = \frac{2.4\pi e^3 h_{es}\sqrt{f_c}}{(2e - d)^2} + \frac{2.4\pi d h_c^3 \sqrt{f_c}}{(2h_c - h_{es})^2} \tag{6.14}$$

The effective depth of the bearing area h_{es} is determined based on the observation of the test results. As shown in Figure 4.39, the bulging in the sheeting is over the full depth of the rib, so h_{es} is assumed to be

$$h_{es} = \frac{h + h_p}{2} \tag{6.15}$$

where h is the overall height of the stud connector, and h_p the depth of the ribs of the profiled sheeting. This assumption gives very good prediction, as will be shown next by the comparison with the test results.

6.3.2   Comparison with test results

The shear resistance P_r for a stud connector with parallel sheeting is determined by equation (6.14). Among the 20 selected data (Table 3.1) and the 18 new tests,

there are 22 with normal weight concrete which failed by splitting. One result reported by Harding [17] is unused because of insufficient information. Details of the other 21 push-out tests and their comparison with the prediction are listed in Table 6.1, e the distance from the centre of the stud to the mid-depth of the nearer rib, mm; h the overall height of the stud, mm; h_p the depth of the trough, mm; h_c the overall depth of the concrete slab, mm; b_e the effective upper width of the trough, mm, as defined below; P_e the tested resistance, kN; P_r the predicted resistance from equation (6.14), kN. Also shown in this table is the resistance of the stud in a solid concrete slab, P_{rs} (kN), which is specified in Eurocode 4 [7] as the upper limit for the resistance of stud connectors with parallel sheeting. Clearly, this upper limit is too conservative.

The comparison is also shown in Figure 6.5. The predicted resistances for tests 13 to 15 are much higher than the tested values ('stars' in the figure). This is because the stud connectors in these tests are at the centres of relatively wide troughs, with $2e/h_p = 2.0$ for test 13, and 2.39 for tests 14 to 15. In this case, the effective depth of the bearing area h_{es} given by equation (6.15) is overestimated.

If h_{es} in equation (6.15) is replaced by equation (6.16) for stud connectors with $2e/h_p \geq 2.0$, the results, as shown in Table 6.1 in curved brackets, are very good, especially for tests 14 and 15 with $2e/h_p = 2.39$ ('circles' in Figure 6.5). For test 13, h_{es} from equation (6.16) seems underestimated.

$$h_{es} = h_p \tag{6.16}$$

Considering that $h_{es} = (h + h_p)/2$ gives better prediction for the other tests with $2e/h_p$ from 0.94 to 1.5, a linear interpolation between $[1.5, (h + h_p)/2]$ and $[2.4, h_p]$ will give

$$h_{es} = h_p + (2.4 - \frac{2e}{h_p})\frac{h - h_p}{1.8} \tag{6.17}$$

The value of h_{es} from equation (6.17) fits test 13 quite well, as shown in square brackets and the 'circle' in Figure 6.5.

Therefore, the assumption for h_{es} given by equation (6.15) is revised as:

$$h_{es} = \frac{h + h_p}{2}, \quad \frac{2e}{h_p} \leq 1.5; \tag{6.18}$$

$$h_{es} = h_p + (2.4 - \frac{2e}{h_p})\frac{h - h_p}{1.8}, \quad \frac{2e}{h_p} \geq 1.5. \tag{6.19}$$

Equations (6.14), (6.18) and (6.19) predict the results much better than the Eurocode 4 model, as shown in Table 6.1. The coefficient of variation is reduced from 28.4% to 5.6%.

The comparison is also shown in Figure 6.5 in 'circles'. However, equations (6.18) and (6.19) is based on very few data (21 altogether). More tests are needed to check the assumption made for h_{es}.
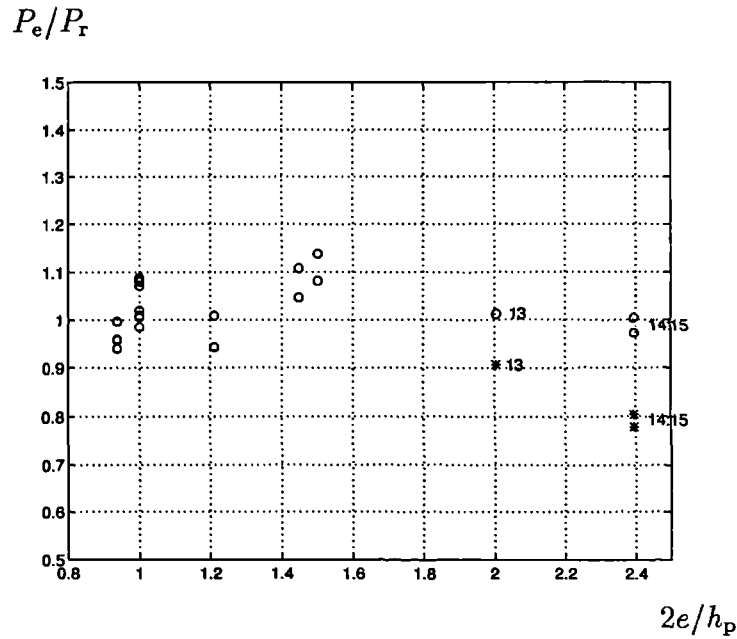
Figure 6.5: Splitting model for splitting failure.

Table 6.1: Comparison of splitting model with tests that failed by splitting.

No.	Ref.	Tests	e	h	h_p	h_c	b_e	P_e	P_r	P_{rs}	$\frac{P_e}{P_r}$	$\frac{P_e}{P_{rEC}}$
1	New	G9P-1	37.5	125	80	150	90	131.1	131.5	106.8	1.00	2.08
2		G9P-2						126.2			0.96	2.00
3		G13P-1	30.0	95	60	120	136	92.1	91.2	88.2	1.01	1.58
4		G13P-2						91.8			1.01	1.58
5		G14P-1	37.5	125	80	150	180	112.1	119.2	84.5	0.94	2.25
6		G14P-2						114.2			0.96	2.29
7		G15P-1	33.3	95	46	120	79	101.9	91.9	99.1	1.10	1.03
8		G15P-2						96.3			1.05	0.97
9		G16P-1	37.5	95	50	120	90	108.8	100.5	105.0	1.08	1.04
10		G16P-2						114.5			1.14	1.09
11		G17P-1	36.3	95	60	120	98	87.8	87.0	81.6	1.01	1.08
12		G17P-2	36.3	95	60	120	98	85.7	90.9	82.4	0.94	1.05
13	[18]	7M	76.2	114	76	140	178	156.8	172.9	112.9	0.91	2.31
									(139.8)		1.12	
									[154.8]		1.01	
14	[40]	TVI-A	91	114	76	141	203	128.4	159.8	91.2	0.80	1.97
									(127.8)		1.00	
15		TVI-B	91	114	76	141	203	124.3	159.8	91.2	0.78	1.90
									(127.8)		0.97	
16		TV-A	38	116	76	141	203	117.0	118.7	91.2	0.99	1.70
17		TV-B						128.9			1.09	1.87
18		TV-C						129.3			1.09	1.88
19		QIV-A	38	116	76	141	184	114.3	112.0	84.7	1.02	2.13
20		QIV-B						121.1			1.08	2.27
21		QIV-C						120.1			1.07	2.34
Mean											1.03	1.73
Coefficient of variance											5.6%	28.4%

P_r, P_{rEC} — the resistances from equations (6.14), (6.18) and (6.19), and the Eurocode 4 model.

6.4   Pulling out failure of stud connectors

The failure mode of G10P shown in Figure 4.40 is quite similar to the one found by Hosain in his eight push-out tests with stud connectors in narrow sheeting[20]. The latter is shown in Figure 6.6.

It is a kind of pulling out failure. One of the characteristics is that the separation of the upper parts of the slabs from the main body starts at about 80% of the maximum load, and extends quickly until the separation is complete. At the end of the tests, the upper parts of the slabs are very easily removed, exposing cone-shaped failure surfaces of the concrete around the stud connectors.

Figure 6.6: Hosain's test result.

Details of 10 tests with this failure mode are listed in Table 6.2, where f_{ct} is the tensile strength of the concrete, MPa, and the other symbols are as for Table 6.1. Also shown in this table is the splitting resistance P_r given by equation (6.14), kN, as well as the comparison with the test results. Evidently, pulling out failure has much lower resistance than splitting failure, especially for tests 1 to 6. It cannot be predicted simply by the splitting model.

Table 6.2: Splitting model for tests that failed by pulling out.

No.	Ref.	Tests	f_{ct}	e	h	h_p	h_c	s_v	b_e	P_e	P_r	P_{rs}	$\frac{P_e}{P_r}$
1	New	G10P-1	2.46	30.0	95	60	120	125	68	70.3	92.3	90.7	0.76
2		G10P-2								72.1			0.78
3	[20]	A-5	2.51	30.0	125	76	150	6·3d	65	45.3	99.7	92.3	0.45
4		A-6		.				5·4d		50.0	112.6		0.44
5		A-7						4·5d		62.5	122.1		0.51
6		A-8						4·6d		66.2	122.1		0.54
7		B-5	2.51	28.3	76	38	103	7·3d	70	44.4	52.9	65.5	0.84
8		B-6			(d= 16 mm)			6·4d		48.9	59.5		0.82
9		B-7						5·5d		55.4	59.5		0.93
10		B-8						4·6d		61.6	59.5		1.04

P_r — the resistance from equations (6.14), (6.18) and (6.19).

The failure surfaces in Figures 4.40 and 6.6 suggest that the concrete around the head of the stud has an important influence. It is further found that this influence can be reflected by the effective upper width of the trough b_e by defining $b_e = b_u$ for single or staggered studs or $b_e = b_u/2$ for pairs of studs which are transverse to the shear force, where b_u is the upper width of the trough. As shown clearly in Figure 6.7 where the 'stars' are tests 1 to 10 from Table 6.2 and the 'circles' the 21 tests from Table 6.1, when $b_e \leq 70$ mm, the pulling out failure controls.
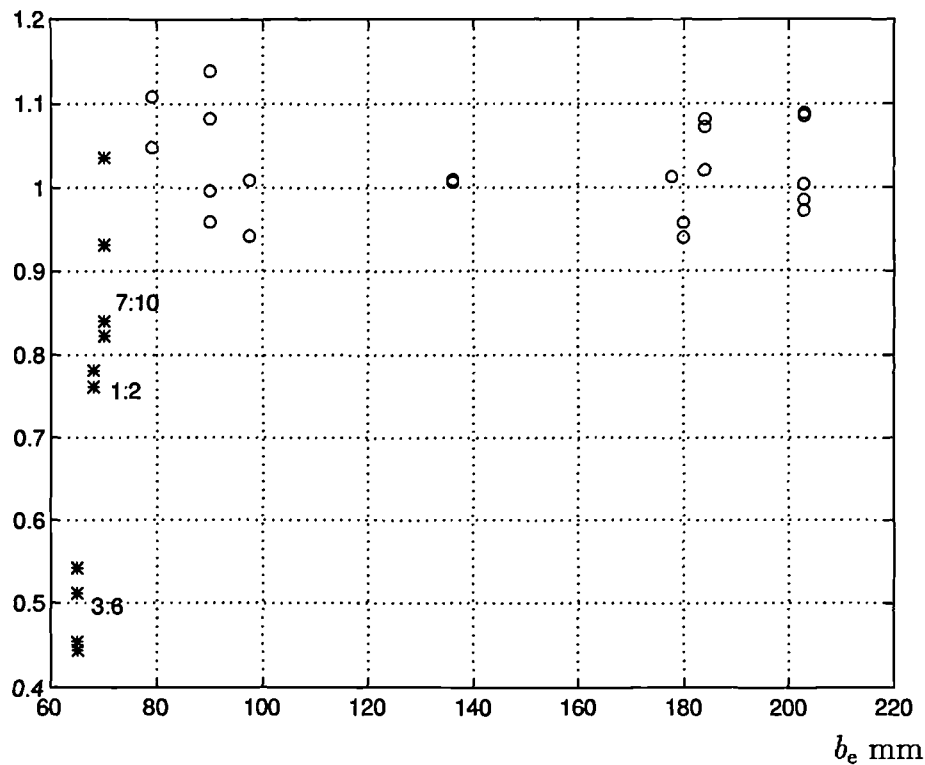
Figure 6.7: Splitting model for pulling out failure.

6.4.1 Mechanism of pulling out failure

The splitting model illustrated in Figure 6.4 is based on the assumption that the tensile forces developed in the stud connectors, T, due to the dispersal of splitting forces in the prism BCKJ, are unlikely to cause studs to fail in tension, and hence splitting failure governs the two prisms EHLI and BCKJ. This assumption is workable for stud connectors in wide troughs ($b_e \geq 80$ mm in Figure 6.7), because the concrete around the studs provides sufficient restraint to prevent the studs being pulled out of the concrete slab.

For stud connectors in narrow troughs, the shear force P_r still acts as a concen-

trated patch load on the prism ADLI, and is resisted by the two prisms EHLI and
BCKJ. With the increase of the shear force P_r, the effective depth of the bearing
area increases, and so does the tensile force T in the studs and the splitting force
in the prism EHLI. When T reaches the tensile resistance of the concrete, cracks
appear around the stud connectors, the result of which will be the pulling out
of the stud with a portion of concrete around, as observed in test G10P (Figure
4.40) and in Hosain's test (Figure 6.6).

If h_{ep} is the effective depth of the bearing area at which the premature failure
of concrete occurs, and P_{r1} and P_{r2} are the corresponding shear forces taken by
prisms EHLI and BCKJ, then the shear resistance of pulling out failure P_r is the
sum of P_{r1} and P_{r2}:

$$P_r = P_{r1} + P_{r2} \qquad (6.20)$$

in which P_{r1} is as given by equation (6.9) with h_{es} replaced by h_{ep}.
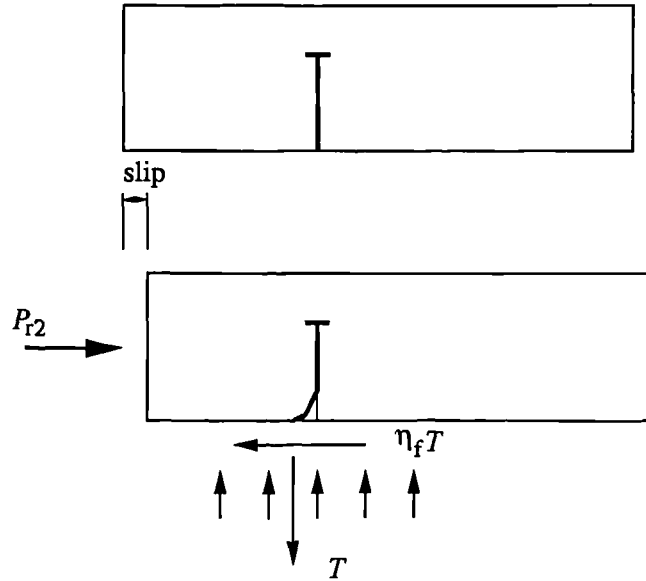
Figure 6.8: Shear-friction concept

The shear force taken by prism BCKJ which causes the tensile force in the
studs to exceed the resistance of the concrete can be predicted by introducing
the 'shear-friction concept' reported by Hawkins and Mitchell [18]. In Figure 6.8

a stud is shown, embedded in concrete and under a shear force P_{r2}. The slip caused by this shear force develops a tensile force T in the stud. In order to equilibrate T, compression also of magnitude T exists at the interface between the steel beam and the concrete slab. Therefore, the resistance to the shear force P_{r2} can be thought of as the frictional force arising from the normal force, T, and the coefficient of friction, η_f, of the concrete-steel interface, that is,

$$P_{r2} = \eta_f T \qquad (6.21)$$

The tensile force T acting on the stud can cause the stud to be pulled out of the concrete. The common approach to calculate T is to assume that the tensile strength of the concrete, f_{ct}, acts on a cone-shaped failure surface around the stud, and is related to the cylinder strength of the concrete, f_c, in N/mm^2 units, by:

$$f_{ct} = 0.5\sqrt{f_c} \qquad (6.22)$$

If A_c is the area of the failure surface,

$$T \propto A_c f_{ct} \qquad (6.23)$$

so, using equation (6.22), the shear force P_{r2} to cause the stud to be pulled out of the concrete can be expressed as $P_{r2} \propto \eta_f A_c \sqrt{f_c}$, or

$$P_{r2} = k A_c \sqrt{f_c} \qquad (6.24)$$

in which k is a coefficient to be determined from the tests.

From the mechanism of pulling out failure described early in this section, it is clear that when P_{r2} from equation (6.24) is smaller than the resistance from equation (6.10), pulling out failure controls, otherwise, splitting failure controls. Therefore, by equating equation (6.24) with (6.10) in which K_s is as given by equation (6.13), the effective depth of the bearing area h_{ep} for pulling out failure is obtained:

$$h_{ep} = 2h_c(1 - \sqrt{\frac{0.6 d h_c \pi}{k A_c}}) \qquad (6.25)$$

The failure surface for each row of stud(s) is assumed to be a wedge-shaped cone, as shown in Figure 6.9 (a). All the four surfaces have the same slope, which is controlled by e_u. The cone is unsymmetrical, with the surface behind the stud (in the direction of shear force) extending to the bottom of the trough and the one in front to the top flange of the sheeting. Under the combined action of shear and tensile forces in the shank of the stud, the cone rotates around AB. This is not a bad assumption, as will be shown later in Section 6.4.2.

When the rows of stud(s) are placed closely together, with the longitudinal spacing s_v less than $2e_u$, the slope of the front and rear surfaces of the cone is controlled by s_v. The slope of the other two surfaces is as before, as shown in Figure 6.9 (b). When the studs are placed off-centrally, the slope of the larger side surface is then controlled by $(s_t + e_u)$, as shown in Figure 6.9 (c).

Therefore, the area of the wedge-shaped failure surface A_c for each row of stud(s) is calculated as below:

$$A_c = \begin{cases} 2A_1 + b_o \dfrac{h_p}{\sin \theta_1}, & A_1 \le A_2 \\[2mm] 2A_2 + b_o \dfrac{h_p}{\sin \theta_2}, & A_1 > A_2 \end{cases} \qquad (6.26)$$

and A_1 and A_2 are the areas of surface ABCDEF controlled by θ_1 and θ_2, respectively, which are determined by:

$$A_1 = \begin{cases} (s_t + 2e_u)\dfrac{h - h_p}{\sin \theta_1} & \text{stud(s) placed symmetrically} \\[2mm] (s_t + 3e_u)\dfrac{h - h_p}{2\sin \theta_1} + e_u\dfrac{h - h_p}{2\sin \theta_3} & \text{stud(s) placed unsymmetrically} \end{cases}$$
$$(6.27)$$

and

$$A_2 = \begin{cases} s_v\dfrac{h - h_p}{2\sin \theta_1} + (s_t + e_u)\dfrac{h - h_p}{\sin \theta_2} & \text{stud(s) placed symmetrically} \\[2mm] s_v\dfrac{h - h_p}{4\sin \theta_1} + (s_t + 2e_u)\dfrac{h - h_p}{2\sin \theta_2} + s_v\dfrac{h - h_p}{4\sin \theta_3} & \text{stud(s) placed unsymmetrically} \end{cases}$$
$$(6.28)$$

where

$$\tan \theta_1 = \frac{h - h_p}{e_u}; \qquad \tan \theta_2 = \frac{h - h_p}{s_v/2}; \qquad \tan \theta_3 = \frac{h - h_p}{s_t + e_u} \qquad (6.29)$$

(a)

(c)

(b)
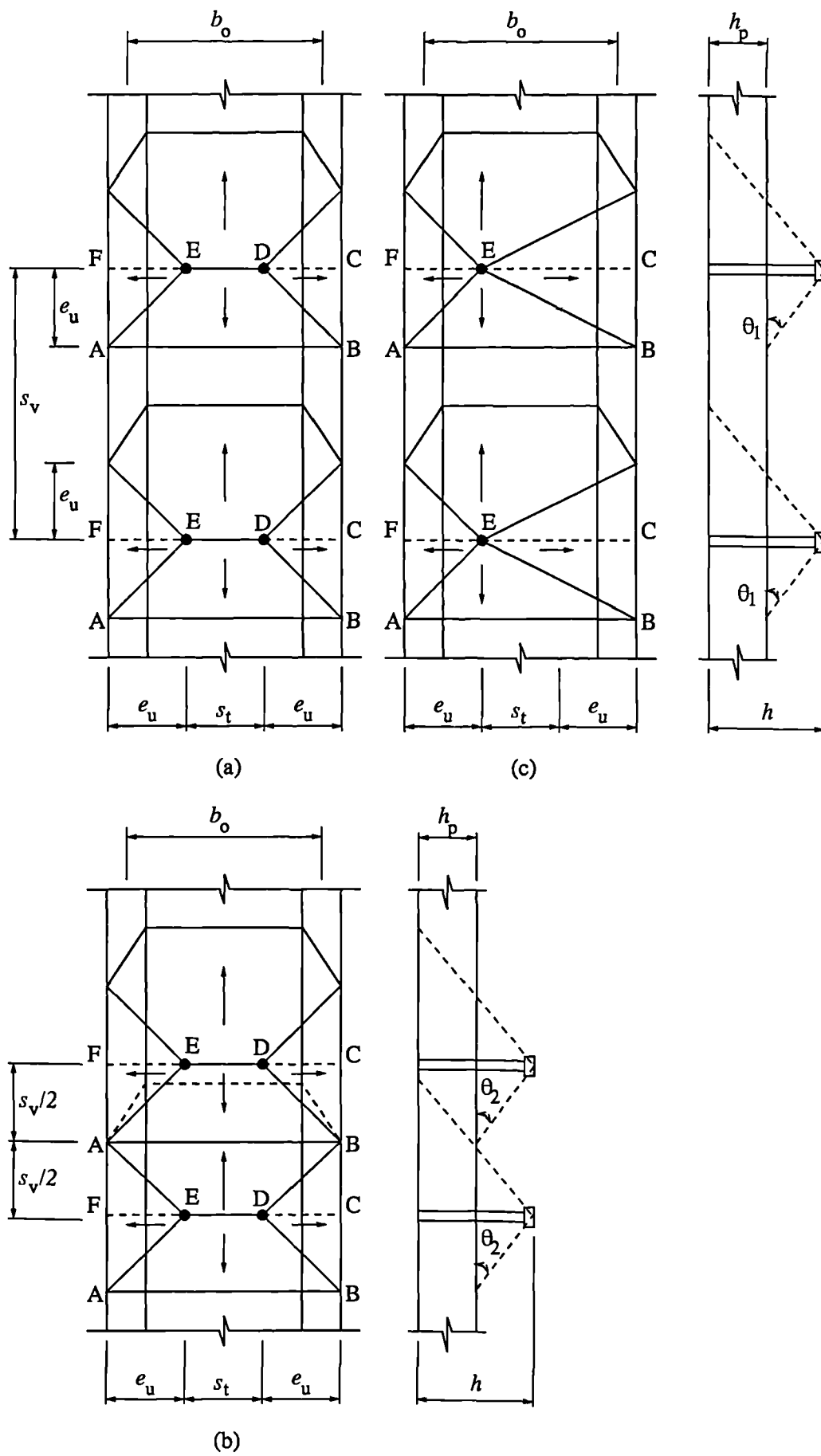
With h_{es} replaced by h_{ep}, P_{r2} can be calculated from equation (6.10), so equation (6.20) becomes

$$P_r = \frac{2.4\pi e^3 h_{ep}\sqrt{f_c}}{(2e - d)^2} + \frac{2.4\pi d h_c^3 \sqrt{f_c}}{(2h_c - h_{ep})^2}$$
(6.30)

Table 6.3: Friction-splitting model for tests that failed by pulling out.

No.	Ref.	Tests	f_{ct} (MPa)	d	b_u	s_t	s_v	h_{ep}^e (mm)	k	P_e	P_r (kN)	$\frac{P_e}{P_r}$	$\frac{P_e}{P_{rEC}}$
						(mm)							
1	New	G10P-1	2.46	19	136	53	125	56.9	0.58	70.3	66.4	1.06	1.18
2		G10P-2						55.7	0.58	72.1		1.09	1.21
3	[20]	A-5	2.51	19	65	-	6·3d	22.6	0.53	45.3	51.9	0.87	1.61
4		A-6					5·4d	28.1	0.50	50.0	63.1	0.80	1.78
5		A-7					4·5d	42.5	0.56	62.5	63.1	0.99	2.22
6		A-8					4·6d	46.7	0.58	66.2	63.1	1.04	2.35
7		B-5	2.51	16	70	-	7·3d	39.4	0.58	44.4	42.0	1.06	0.76
8		B-6					6·4d	44.9	0.53	48.9	52.8	0.93	0.84
9		B-7					5·5d	52.5	0.55	55.4	56.7	0.98	0.95
10		B-8					4·6d	59.5	0.60	61.6	56.7	1.09	1.05
Mean												0.99	1.40
Coefficient of variation												10%	40.7%

P_r — the resistance from equation (6.31);

P_{rEC} — the resistance from the Eurocode 4 model.

Replacing P_r with the tested resistance P_e, values of h_{ep} for tests that failed by pulling out mode are obtained, denoted as h_{ep}^e in Table 6.3, where the symbols are the same as for Table 6.1, except that d is the diameter of the shank of a stud; s_t and s_v are the transverse and longitudinal spacings between the studs, respectively. Substituting these h_{ep}^e into equation (6.25) finds the k value for each test which is also shown in the table.

The mean value of k is 0.56, so the pulling out strength is finally deduced:

$$P_r = \frac{2.4\pi e^3 h_{ep}\sqrt{f_c}}{(2e - d)^2} + 0.56 A_c\sqrt{f_c} \tag{6.31}$$

where

$$h_{ep} = 2h_c(1 - \sqrt{\frac{1.07 d h_c \pi}{A_c}}) \tag{6.32}$$

6.4.2 Comparison with test results

As described in the preceding section, the occurrence of splitting or pulling out failure is controlled by the effective depth of the bearing area:

- If h_{es} from equation (6.18) or (6.19) is less than h_{ep} from equation (6.32), splitting failure controls, and the shear strength is determined by equation (6.14).

- Otherwise, pulling out failure controls with the strength determined by equation (6.31).

The comparison is shown in Figure 6.10. For the 21 tests in Table 6.1, h_{es} is always smaller than h_{ep} (neither of the values are given in the table). This corresponds to the test results, in that all these specimens failed by splitting. The ten test resultes given in Table 6.2 are all governed by pulling out failure. Compared with the Eurocode 4 model, the new theoretical model for pulling out failure reduces the coefficient of variation from 40.7% to 10%.

The two points in Figure 6.10 with P_e/P_r less than 0.9 are tests A-5 and A-6 which had the spacing between the studs less than $5d$ and had no second identical tests to check the results. It is the author's opinion that tests No 3-10 in Table 6.1 are not as reliable as the others.

$P_{\mathrm{e}}/P_{\mathrm{r}}$

$b_{\mathrm{o}}/h_{\mathrm{p}}$
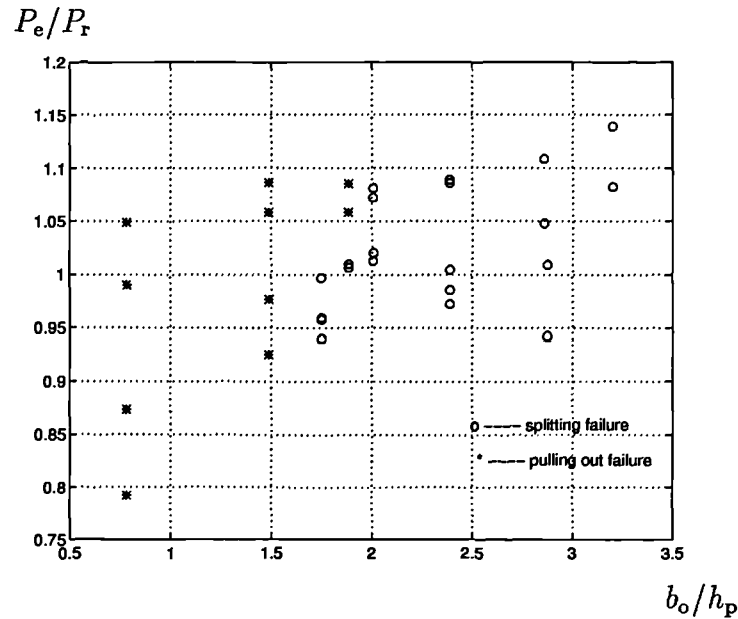
Figure 6.10: Comparison of both splitting and pulling out model with test results.

6.5 Discussion

As discussed in Section 6.3, the splitting occurs first at the base of the stud, but its development is restrained by the ribs of the profiled sheeting. When the cracks reach the surface of the concrete slab, the transverse reinforcement can provide additional restraint, as suggested by Oehlers [38] (Figure 2.5). If the reinforcement is below the head of the stud, pulling out failure might be prevented, depending on the amount of the reinforcement.

The occurrence of splitting and pulling out failure depends to a great extent on the upper width of the trough (Figure 6.7). Among the 31 tests studied in this chapter, only G9P in Table 6.1 has the reinforcement below the head of the stud. As it has profiled sheeting with relatively wide troughs, the splitting failure can hardly be attributed to the lower location of the reinforcement. For further understanding, more tests are needed.

6.6   Conclusions

1. The shear force on a composite beam with parallel sheeting is assumed to be transfered into the concrete slab in terms of a bearing pressure between the stud connector and the concrete over an certain height of the stud, defined as the effective depth of the bearing area. Based on this assumption, two models for splitting failure and pulling out failure have been found, and the shear resistances are predicted.

   If h_{es} denotes the effective depth for splitting failure (equations (6.18) and (6.19)) and h_{ep} for pulling out failure (equation (6.32)), the occurrence of failures will follow the following rules:

   - when $h_{es} \leq h_{ep}$, splitting failure controls, and the resistance is determined by equation (6.14);

   - when $h_{es} > h_{ep}$, pulling out failure controls, and the resistance is determined by equation (6.31).

2. The predictions have been found to be satisfactory for:

   - 16- and 19-mm studs with f_u from 410 to 470 N/mm^2;

   - the cylinder strength of concrete f_c from 20 to 35 N/mm^2;

   - b_o/h_p from 0.8 to 3.2;

   - $h - h_p \geq 35$ mm;

   - the centre-to-centre spacing between studs is from $2.8d$ to $4d$ in the direction transverse to the shear force, and from $3d$ to $6d$ inline along the shear force;

   - the centre-to-centre spacing between the studs greater than $4d$.

3. The two models were based on only 31 push-out data. More tests are needed for the further knowledge of the mechanism of load transfer, the failure modes and the influence of the transverse reinforcement.

Chapter 7

Push-out tests with lightweight concrete

7.1 Introduction

Among the 34 push-out tests described in Chapter 4, eight were carried out to study the behaviour of studs in lightweight concrete, four with transverse sheeting and the other four with parallel sheeting (Tables 4.3 and 4.4).

The behaviour, compared with that in normal weight concrete, can be characterised as similar failure modes and less ductility. In other words, the density of the concrete has little influence on the mechanism of load transfer. This will be proved in this chapter, by applying those theoretical models for transverse sheeting (Chapter 5) and for parallel sheeting (Chapter 6) to a total of 15 push-out tests with lightweight concrete (8 new tests and 7 from [17]).

The compressive strengths and the densities of the concrete for these 15 specimens were measured from air-dry concrete cubes. The conversion factors for tensile and shear strengths and for elastic modulus are assumed to be the same

as those for oven-dried concrete of the same density class as given by Eurocode 2: Part 1-4 [5].

It will be shown that the models developed in the previous chapters are also satisfactory for lightweight concrete by introducing material conversion factors. However, because there are only 15 data, it is suggested that more tests be carried out for further understanding.

7.2 Properties of lightweight concrete

Material properties for lightweight concrete in this chapter is indicated by the subscript *lc*.

Density

Density of concrete can contribute significantly to the loads that structural members are required to carry and therefore changes in this property can have important effects structurally and economically.

For lightweight aggregate concrete, the porosity of the coarse aggregates results in differing densities at different curing stages or for different curing methods. So, there are fresh density, air-dry density and oven-dry density. In Eurocode 2: Part 1-4, oven-dry density is the basis of the density classes (Eurocode 2: Part 1-4: Table 3.5-C [5]), which feature in the conversion of several other properties such as tensile strength and elastic modulus. Table 7.1 is a copy of part of Table 3.5-C.

For push-out tests using concrete with non-oven-dry density, the same classes in Table 7.1 are used, so that the conversion for other non-oven-dry properties can be obtained referring to Eurocode 2: Part 1-4. For example, if the air-dry density is 1700 kg/m^3, the concrete is assumed to belong to class 1.8, for which the conversion factors for tensile strength or elastic modulus are calculated. This

Table 7.1: Density classes as given by Eurocode 2: Part 1-4.

Density class	1.0	1.2	1.4	1.6	1.8	2.0
Oven-dry density ρ_u (kg/m³)	901-1000	1001-1200	1201-1400	1401-1600	1601-1800	1801-2000

will be explained below.

Elastic modulus

The mean value of the elastic modulus for normal weight concrete, E_{cm}, is given in Eurocode 2 [4] by the following equation, in N/mm² units:

$$E_{cm} = 9500 f_c^{1/3} \tag{7.1}$$

in which f_c is the mean cylinder strength of concrete.

For lightweight concrete [5], it is estimated by multiplying the value from the above equation by a factor

$$\eta_E = (\frac{\rho_u}{2200})^2 \tag{7.2}$$

where ρ_u is the upper limit of the oven-dry density for the relevant class in Table 7.1.

For non-oven-dry concrete, in the absence of better information it is now assumed that equation (7.2) is still valid, provided that the non-oven-dry density is classified using Table 7.1. Hence,

$$E_{cm-lc} = 9500 \eta_E f_{c-lc}^{1/3}, \quad N/mm^2. \tag{7.3}$$

Tensile and shear strength

For normal weight concrete, the tensile strength, f_{ct}, is estimated from the cylinder strength, f_c, by:

$$f_{ct} = 0.5\sqrt{f_c}, \quad N/mm^2. \tag{7.4}$$

When calculating the tensile strength of lightweight concrete, f_{ct-lc}, a conversion factor η_1 is introduced into the above correlation:

$$f_{ct-lc} = 0.5\eta_1\sqrt{f_{c-lc}} \quad \text{N/mm}^2, \tag{7.5}$$

where f_{c-lc} is the cylinder strength of lightweight concrete, and η_1 is as given by Eurocode 2: Part 1-4:

$$\eta_1 = 0.40 + 0.60\frac{\rho_u}{2200} \tag{7.6}$$

in which ρ_u is the upper limit of the density for the relevant class in Table 7.1.

To obtain the torsional shear strength of lightweight concrete, ν_{tu-lc}, the same conversion factor η_1 is applied:

$$\nu_{tu-lc} = 0.8\eta_1\sqrt{f_{cu-lc}}, \quad \text{N/mm}^2. \tag{7.7}$$

7.3 Transverse sheeting with lightweight concrete

Two groups of specimens in Table 4.1, G3FL and G4FL, were tested to study the influence of lightweight concrete. Both groups had stud connectors in the favourable position, but the density of the concrete and the profiled sheeting were different.

The obvious effect of lightweight concrete was the brittle behaviour after the maximum loads, as shown in Figures 4.21 and 4.22 compared with Figures 4.19. This resulted in abrupt failure, but the failure modes showed no difference from those with normal weight concrete of similar cube strengths, because G3FL failed by shank shearing, while G4FL by concrete pulling out. Therefore, it can be assumed that the mechanism of load transfer is the same as for normal weight concrete, and hence the shear resistance can be predicted by the theoretical models described in Chapter 5.

Introducing the properties of the lightweight concrete (Section 7.2) into those models, the shear resistance of a stud connector with lightweight concrete, P_{r-lc}, is predicted by equation (7.8):

$$P_{r-lc} = k_{t-lc} P_{rs-lc} \qquad (7.8)$$

where P_{rs-lc} is the resistance of a stud to shank shearing failure, as given by equation (5.6) with E_{cm} replaced by E_{cm-lc} from equation (7.3).

The reduction factor k_{t-lc} is still the same as given by equation (5.48), but with η and λ slightly different, due to the influences of lightweight concrete on the strengths of materials. Details are as follows:

Concrete pulling out failure

$$\eta_{c-lc} = \frac{0.45\eta_1 \sqrt{f_{cu-lc}} h^2 (b_o - 0.25h)}{N_r h_p P_{rs-lc}} \qquad (7.9)$$

and

$$\lambda_{c-lc} = \frac{e_r}{h_p} \frac{T_y}{P_{rs-lc}} \qquad (7.10)$$

in which η_1 is as given by equation (7.6). Except where modified in this chapter, all the other symbols are as defined in Chapter 5.

Rib punching failure

$$\eta_{r-lc} = \frac{1.8(e_f + h - h_p) t f_{yd}}{P_{rs-lc}} \qquad (7.11)$$

and

$$\lambda_{r-lc} = \frac{e_f}{2h_p} \frac{T_y}{P_{rs-lc}} \qquad (7.12)$$

For G3FL with measured density as 1640 kg/m^3, equations (7.8) to (7.12) are slightly conservative, while G4FL is well predicted, as shown by the comparison of P_{r-lc} with the tested value P_e in Table 7.2, where ρ is the measured density and ρ_u the upper limit of the density obtained from Table 7.1.

Table 7.2: Theoretical models for transverse sheeting with lightweight concrete.

Test	Ref.	b_o	h	h_p	t_s	e	ρ	ρ_u	P_e	P_{rs-lc}	P_{r-lc}	$\frac{P_e}{P_{r-lc}}$	$\frac{P_e}{P_{rEC-lc}}$
		(mm)					(kg/m³)		(kN)				
G3FL-1	New	140	125	80	1.2	37.5	1640	1800	86.3	86.4	72.6	1.19	1.45
G3FL-2		one favourable stud							87.0			1.20	1.46
G4FL-1		113	95	60	0.9	30.0	1900	2000	64.7	91.0	68.3	0.95	0.92
G4FL-2		one favourable stud							68.9			1.01	0.98
QL60 -1T	[17]	150	95	60	1.15	30.0	1880	2000	81.9	79.7	76.5	1.07	1.03
		one central stud											
MET -2T		75	95	55	1.0	37.5	1891	2000	58.0	76.9	54.6	1.06	1.54
		two in-line studs											
PMF-R -24.8		132	95	46	0.9	33.3	1889	2000	85.1	74.8	69.6	1.22	1.14
		one favourable stud											
PMF-R -27.0		132	95	46	1.2	33.3	1897	2000	88.2	78.9	72.6	1.21	1.12
		one favourable stud											
PMF-F -26.2		132	95	46	0.9	98.7	1881	2000	65.9	79.6	64.5	1.02	0.83
		one unfavourable stud											
PMF-F -25.4		132	95	46	1.2	98.7	1876	2000	66.8	76.0	71.4	0.94	0.88
		one unfavourable stud											
Mean												1.09	1.13
Coefficient of variation												10.2%	22.9%

P_{r-lc} — the resistances from the new models;

P_{rEC-lc} — the resistances from the Eurocode 4 model;

Apart from G3FL and G4FL, Table 7.2 also shows the details and the comparison of six more data reported by Harding [17]. These six specimens had similar density (around 1900 kg/m^3), but varied in stud position and profiled sheeting. Again, the predictions, P_{r-lc}, are satisfactory, except a little conservative for specimens PMF-R-24.8 and PMF-R-27.0, which had 46-mm-deep deck and favourable stud position.

Another reason for the conservatism of the prediction might be the original errors in P_{rs-lc}, the resistance of a stud to shank shearing failure which is assumed to be equal to the shear resistance of the connectors in solid concrete slabs (Chapter 5). For example, P_{r-lc} is 74.8 kN for tests PMF-R-24.8, and 78.9 kN for tests PMF-R-27.0. As $k_{t-lc} \leq 1.0$ results in $P_{r-lc} \leq P_{rs-lc}$, the errors in P_{rs-lc} will be added onto P_{r-lc}. However, on the whole, the predictions are satisfactory, reducing the coefficient of variation to 10.2%.

7.4 Parallel sheeting with lightweight concrete

Among the nine groups of specimens with parallel sheeting described in Chapter 4 (Table 4.4), G11PL and G12PL were carried out to study the behaviour of stud connectors in lightweight concrete. They were companion specimens for G9P and G10P which had normal weight concrete.

Comparing these four groups found that neither the load-slip curves (Figures 4.27 to 4.30) nor the final failure modes show any differences. The relatively narrow trough (PMF CF60 sheeting) caused G10P and G12PL to fail by the pulling out of studs, while G9P and G11PL with wide trough (Multideck 80 sheeting) failed by splitting. These two failure modes for normal weight concrete have already been satisfactorily predicted in Chapter 6. So, in a similar way as for transverse sheeting with lightweight concrete described in the previous section, the resistances for the two failure modes can be predicted by equations (6.14) and
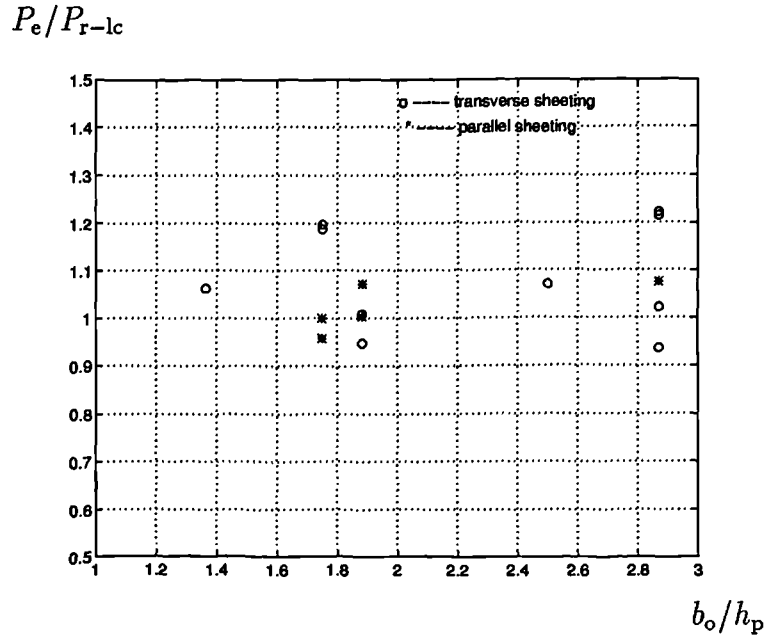
P_e/P_{r-lc}

Figure 7.1: Predictions for studs in lightweight concrete.

(6.31), respectively, with $\sqrt{f_c}$ replaced by $\eta_1\sqrt{f_{c-lc}}$. This modification is given by equations (7.13) and (7.14):

Splitting failure

$$P_{r-lc} = \frac{2.4\pi e^3 h_{es}}{(2e-d)^2}\eta_1\sqrt{f_{c-lc}} + \frac{2.4\pi h_c^3 d}{(2h_c - h_{es})^2}\eta_1\sqrt{f_{c-lc}} \qquad (7.13)$$

Pulling out failure

$$P_{r-lc} = \frac{2.4\pi e^3 h_{ep}}{(2e-d)^2}\eta_1\sqrt{f_{c-lc}} + 0.56A_c\eta_1\sqrt{f_{c-lc}} \qquad (7.14)$$

in which η_1 is from equation (7.6), and all the other symbols are as in Chapter 6.

Apart from G11PL and G12PL, only two additional results have been reported by Harding [17], in which one is not used because of insufficient information. Details of the other five sets of data are given in Table 7.3, where the symbols are as used in Chapter 7 or as defined for Table 7.2.

Figure 7.1 shows the comparison of the models with all the 15 test results.

They fit data very well. Compared with the Eurocode 4 model, the coefficient of variation is reduced from 44.3% to 5%. However, general conclusions can hardly be drawn from such a small set of data; more tests are needed.

Table 7.3: Theoretical models for parallel sheeting with lightweight concrete.

Test		G11PL-1	G11PL-2	G12PL-1	G12PL-2	PMF-25.2P		
Ref.		New				[17]		
b_o	(mm)	140	140	113	113	132		
b_u	(mm)	180	180	146	146	158		
e	(mm)	37.5	37.5	30	30	32.5		
e_u	(mm)	57.5	57.5	41.5	41.5	46.5		
h	(mm)	125	125	95	95	95		
h_p	(mm)	80	80	60	60	46		
h_c	(mm)	140	140	120	120	120		
s_v	(mm)	250	250	250	250	114		
f_{cu-lc}	(Mpa)	41.2	41.2	36.9	36.9	25.2		
ρ	(kg/m^3)	1580	1580	1900	1900	1840		
ρ_u	(kg/m^3)	1600	1600	2000	2000	2000		
P_e	(kN)	124.2	129.8	77.6	82.9	83.4		
P_{rs-lc}	(kN)	75.9	75.9	88.5	88.5	72.6		
P_{r-lc}	(kN)	129.8	129.8	77.4	77.4	77.6	Mean	COV
P_e/P_{r-lc}		0.96	1.00	1.00	1.07	1.07	1.02	5%
P_e/P_{rEC-lc}		2.78	2.89	1.33	1.42	1.14	1.91	44.3%

P_{r-lc}, P_{rEC-lc} — the resistances from the new models and the Eurocode 4, respectively.

7.5   Conclusions

1. Density of concrete, within the classes from 1.6 to 2.0, has no influence on the mechanism of load transfer. It only affects the resistance of the stud connector, in the following ways:

   (a) For transverse sheeting with one stud or two in-line studs in lightweight concrete, the shank shearing strength of a stud can be determined as for normal weight concrete by equation (5.6), but with E_{cm} replaced by E_{cm-lc} from equation (7.3).

   The resistance for concrete pulling out or rib punching failure relates to the shank shearing strength in lightweight concrete (equation (7.8)). The reduction factor follows the same function as for normal weight concrete with $\sqrt{f_{cu}}$ replaced by $\eta_1\sqrt{f_{cu-lc}}$ (equations (7.8) to (7.12)), where η_1 is the factor taking into account the influence of the density of concrete, as given by equation (7.6).

   (b) For parallel sheeting with lightweight concrete, the resistances are as given by equations (6.14) for splitting failure and (6.31) for pulling out failure, with $\sqrt{f_c}$ replaced by $\eta_1\sqrt{f_{c-lc}}$.

2. The predictions have been found to be satisfactory for:

   - 19-mm studs (UTS $f_u \geq 450$ MPa);

   - concrete with air-dry density of classes from 1.6 to 2.0 and cube strength from 25 to 40 MPa.

3. The models were supported by only 15 data. More tests are needed in the following regions:

   For transverse sheeting

   - concrete with air-dry density in classes 1.6 and 1.8 (according to Table 7.1);

- PMF CF46 sheeting, with stud connectors in favourable position;

- transverse, in-line or staggered position for two studs per trough.

For parallel sheeting

- concrete with air-dry density in classes 1.6, 1.8 and 2.0 (Table 7.1);

- all kinds of profiled sheeting available in the market;

- staggered stud position;

- different stud spacing.

Chapter 8

Reduction factors for transverse sheeting

8.1 Introduction

In Chapter 5, the five failure modes for studs with transverse sheeting were predicted theoretically by means of upper or lower bound theory. The solutions were given by a reduction factor relative to the shank shearing resistance of a stud. The reduction factor for each failure mode is a function of such variables as strengths of materials and geometry of studs and the steel sheeting. Although, the models were shown to fit a total of 172 sets of data satisfactorily, they are too complicated for practical use.

In order to solve this problem, in this chapter simplifications are carried out, by first finding out which variables are the most significant influence factors and then applying regression analyses. The results, simple and straightforward, are better than the Eurocode 4 models, in that the coefficient of variation for a total of 103 data (reported t_s) is reduced from 17.5% to 9.1%.

8.2 One stud in a trough

For one stud in a trough, it can be at the centre, on the favourable side or on the unfavourable side. The notations are as shown in Figure 8.1
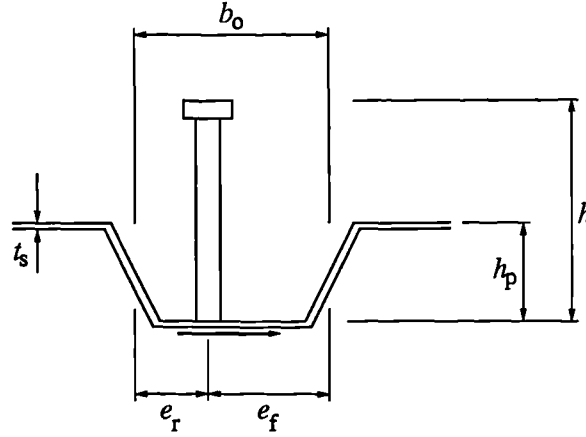
Figure 8.1: One stud in a trough.

8.2.1 Shank shearing or concrete pulling out failure

As found in Chapter 5, the reduction factor is determined by

$$k_t = \frac{\eta + \lambda\sqrt{1 - \eta^2 + \lambda^2}}{1 + \lambda^2} \leq 1.0 \tag{8.1}$$

For shank shearing failure or concrete pulling out failure,

$$\eta = \frac{0.45\sqrt{f_{cu}}h^2(b_o - 0.25h)}{h_p P_{rs}} \leq 1.0 \tag{8.2}$$

and

$$\lambda = \frac{e_r}{h_p}\frac{T_y}{P_{rs}} \tag{8.3}$$

in which f_{cu} is the cube strength of the concrete. T_y is the resistance of a stud connector to uniaxial tension, as given by equation (5.5), and P_{rs} is the shank shearing resistance of a stud, as given by equation (5.6).

Introducing $\eta_o = d^2\sqrt{f_{cu}}/P_{rs}$ into equation (8.2), in which d is the diameter of the shank of a stud connector:

$$\eta = 0.45\eta_o(\frac{h}{d})^2\frac{b_o - 0.25h}{h_p} \tag{8.4}$$

For data with one stud per trough in Table 5.1 (altogether 45), the values of η are plotted against $0.45(h/d)^2(b_o - 0.25h)/h_p$ in Figure 8.2, where the circles have P_{rs} controlled by the concrete and the stars by the stud connectors. The regression of η on $0.45(h/d)^2(b_o - 0.25h)/h_p$ finds η_o a constant 0.022.
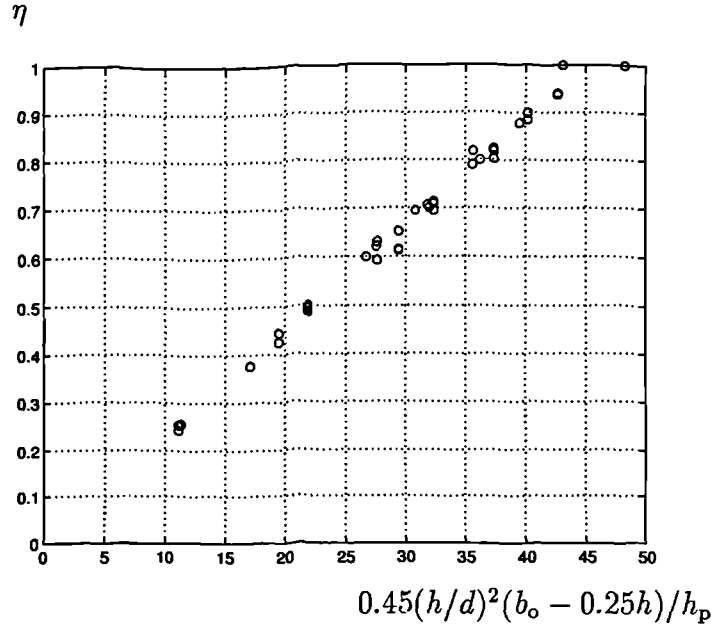
Figure 8.2: Slope η_o found from test results.

These 28 data have f_{cu} ranging from 25 to 40 N/mm^2 and f_u from 400 to 470 N/mm^2. For a wider range of f_{cu}, say from 25 to 50 N/mm^2, P_{rs} will always be governed by the concrete if $f_u \geq 546$ N/mm^2, and hence η_o will fall in the region from 0.021 to 0.023. This means $\eta_o = 0.022$ is acceptable, as long as P_{rs} is controlled by the concrete.

If P_{rs} is governed by the stud connector, it can be seen from the expression for η_o that f_{cu} controls the increase of η_o. The commonly used stud connectors

are the 19-mm Nelson studs with a guaranteed minimum f_u of 460 N/mm², corresponding to $f_{cu} = 40$ N/mm² (from equation (5.6)). When $f_{cu} \geq 40$ N/mm², P_{rs} is governed by studs. It is easy to find that η_o from 0.021 to 0.023 requires f_{cu} to be not greater than 45 N/mm², and this upper limit will increase as f_u increases.

Stud connectors used in Canada usually have f_u around 415 N/mm² [11]. So, if f_u is limited to not lower than 400 N/mm², η_o will range from 0.021 to 0.023 when $f_{cu} \leq 35$ N/mm², and $\eta_o = 0.024$ when $f_{cu} = 40$ N/mm². The difference is acceptable.

Therefore, $\eta_o = 0.022$ is correct for f_{cu} from 25 to 40 N/mm², and $f_u \geq 400$ N/mm². Considering the upper limit for f_u specified for use in calculations in Eurocode 4 [7], here the range of f_u is narrowed as $400 \leq f_u \leq 500$ N/mm².

Substituting $\eta_o = 0.022$ into equation (8.4),

$$\eta = 0.01 (\frac{h}{d})^2 \frac{b_o - 0.25h}{h_p} \qquad (8.5)$$

In a similar way, introducing $\lambda_o = T_y/P_{rs}$ into equation (8.3),

$$\lambda = \lambda_o \frac{e_r}{h_p} \qquad (8.6)$$

When P_{rs} is governed by studs, $\lambda_o = 1.0$, otherwise λ_o changes with the ratio of $f_u/\sqrt{f_c E_{cm}}$, but always greater than 1.0. Apparently, strong studs with weak concrete give high λ_o. For the ranges required by η_o, i.e., 25 N/mm² $\leq f_{cu} \leq$ 40 N/mm² and 400 N/mm² $\leq f_u \leq$ 500 N/mm², λ_o changes from 1.0 to 1.42.

If $\lambda_o = 1.0$, from equation (8.5) and $\lambda = e_r/h_p$, the reduction factor $k_{t,1.0}$ is calculated by equation (8.1). It relates data very well (Figure 8.3). In the same way, the results of $k_{t,1.42}$ with $\lambda_o = 1.42$ are shown in Figure 8.4. The difference is negligible. For simplification, λ_o is taken as 1.0, and equation (8.6) becomes

$$\lambda = \frac{e_r}{h_p} \qquad (8.7)$$

$P_e/(P_{rs}k_{t,1.0})$
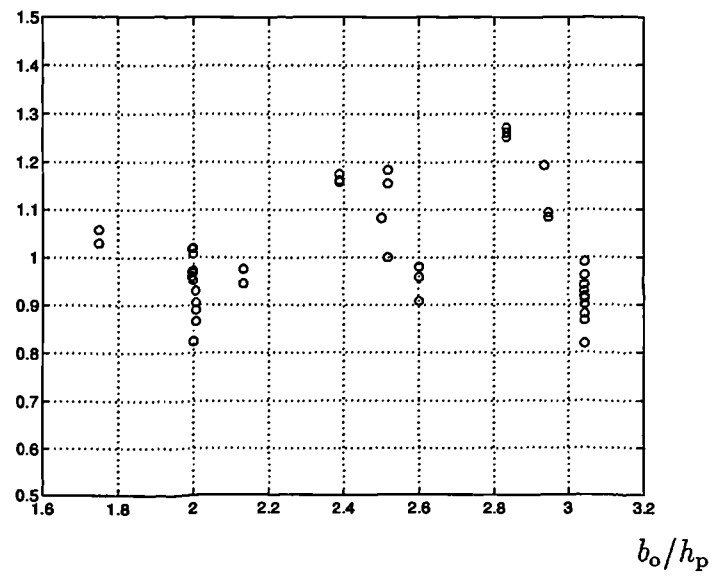
Figure 8.3: Results of comparison when $\lambda_o = 1.0$.

$P_e/(P_{rs}k_{t,1.42})$
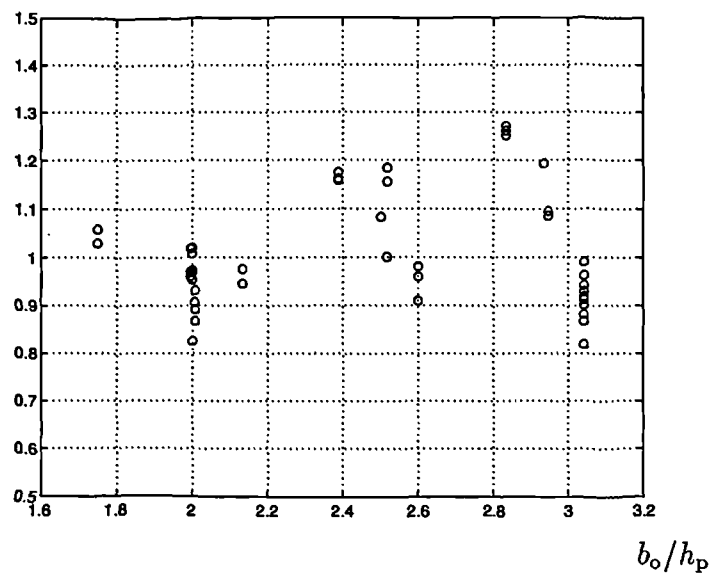
Figure 8.4: Results of comparison when $\lambda_o = 1.42$.

Though η and λ are simplified, the calculation for the reduction factor is still too complicated. Further simplification is needed.

Between the simplified η and λ, it is found that the reduction factor k_t depends to a great extent on η (Figure 8.5), while the influence of λ is not significant (Figure 8.6).

Equation (8.5) is a complex function of b_o, h and h_p. It can be simplified into a line (Figure 8.7). The variable $[0.5e_f + 3(h - h_p)]$ can be approximated by the non-dimentional variable $\dfrac{0.5e_f + 3h}{h_p}$. The relation between k_t and η and $[0.5e_f + 3(h - h_p)]$ suggests that k_t must be related to $\dfrac{0.5e_f + 3h}{h_p}$, as shown in Figure 8.8. The relation is found to be

$$k_t = 0.04\frac{0.5e_f + 3h}{h_p} + 0.7 \leq 1.0 \tag{8.8}$$

Figure 8.9 shows the comparison of equation (8.8) with the test results. The coefficient of variation is 12.7% and $\mu = 1.03$, while the Eurocode 4 model gives $\mu = 1.05$ and the coefficient of variation 16.3% (the comparison is not shown in the figure).
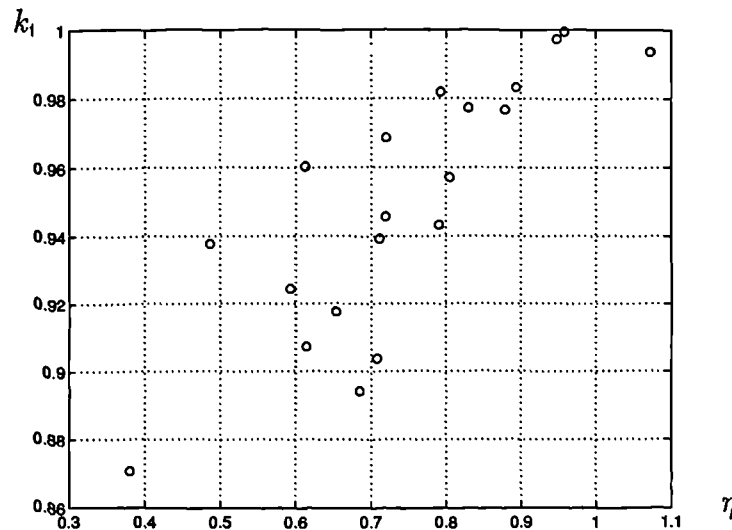
Figure 8.5: Relation between η and k_t for concrete pulling out failure.
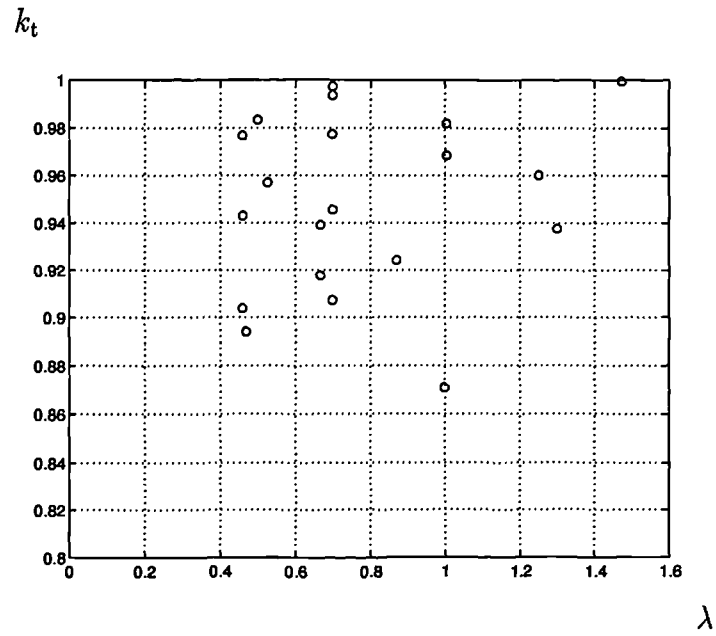
Figure 8.6: The effects of λ on k_t for concrete pulling out failure.
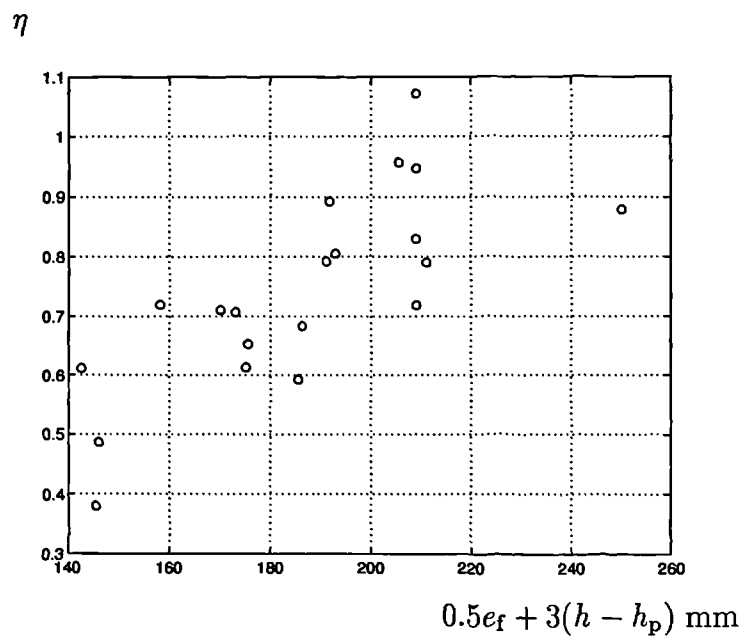
Figure 8.7: The relation between η and $0.5e_f + 3(h - h_p)$.

k_t
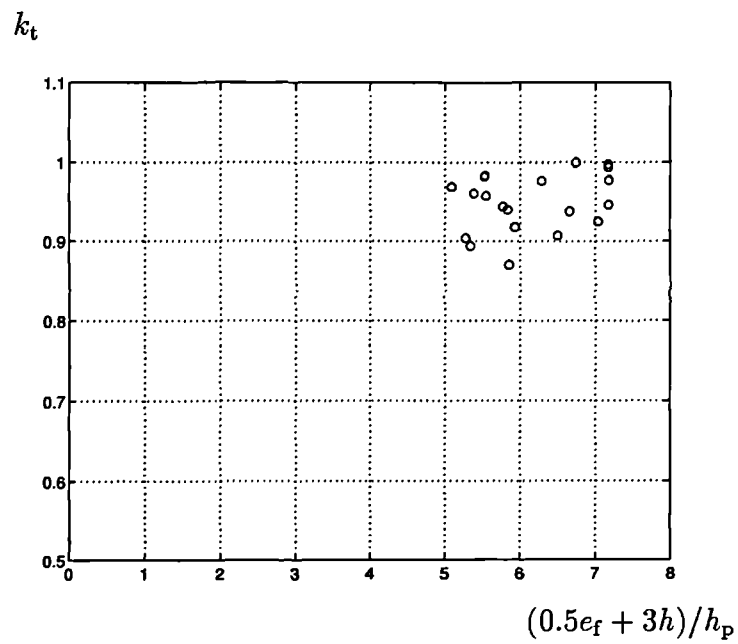
$(0.5e_f + 3h)/h_p$

Figure 8.8: The relation between k_t and $(0.5e_f + 3h)/h_p$.

$P_e/(P_{rs}k_t)$

b_o/h_p
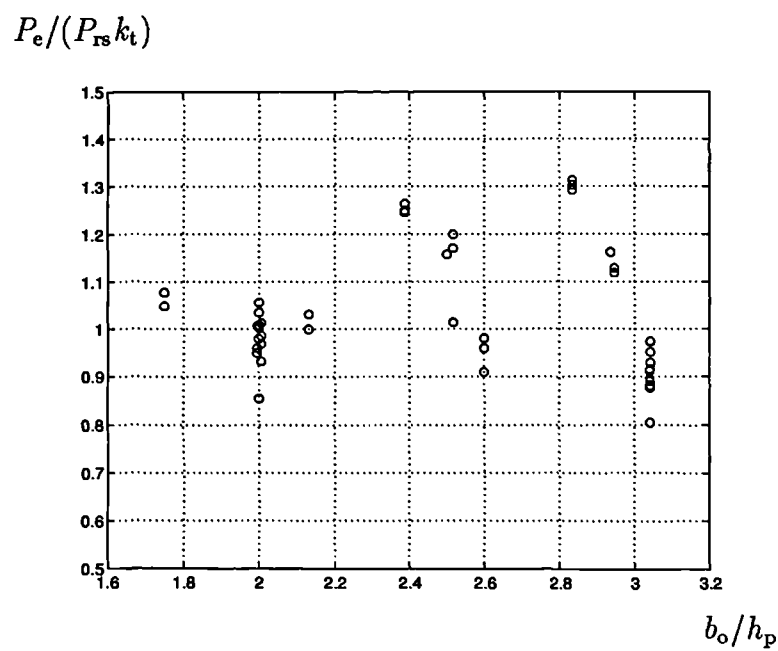
Figure 8.9: The simplified reduction factor for concrete pulling out failure.

8.2.2 Rib punching failure

The theoretical reduction factor for rib punching failure is also determined by equation (8.1), but with η and λ replaced by equations (8.9) and (8.10):

$$\eta = \frac{1.8(e_\mathrm{f} + h - h_\mathrm{p})t_\mathrm{s}f_\mathrm{yd}}{P_\mathrm{rs}} \tag{8.9}$$

and

$$\lambda = \frac{e_\mathrm{f}}{2h_\mathrm{p}}\frac{T_\mathrm{y}}{P_\mathrm{rs}} \tag{8.10}$$

Similarly, η and λ depend on the strengths of concrete, f_c, stud connectors, f_u and steel decking, f_yd. Again, their influences are studied first, by comparing η with $(e_\mathrm{f} + h - h_\mathrm{p})t_\mathrm{s}$ in Figure 8.10 and λ with $\frac{e_\mathrm{f}}{h_\mathrm{p}}$ in Figure 8.12.

η

$(e_\mathrm{f} + h - h_\mathrm{p})t_\mathrm{s}$ mm^2
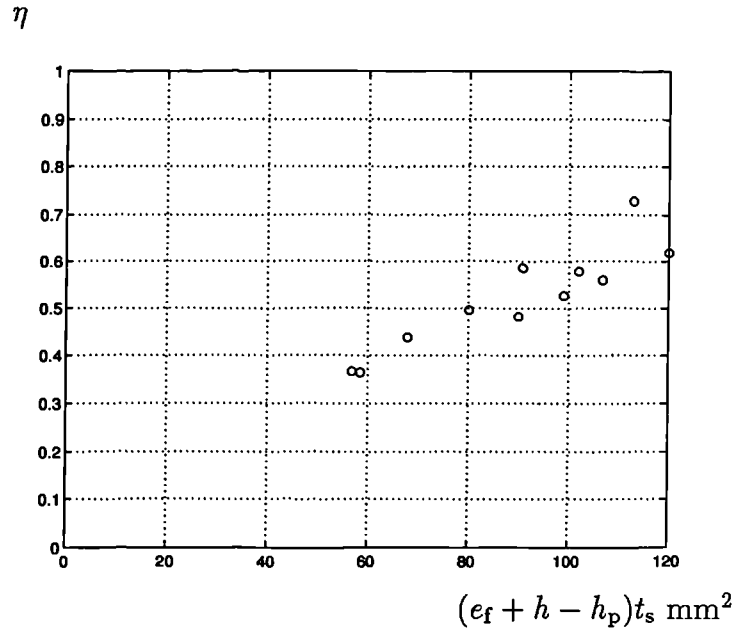
Figure 8.10: The influence of $f_\mathrm{yd}/P_\mathrm{rs}$ on η.

For the 25 data in Table 5.2 with f_c from 20 to 30 N/mm^2 and $f_\mathrm{u} \geq 470$ N/mm^2, Figure 8.10 clearly shows the linear relationship between η and $(e_\mathrm{f} + h - h_\mathrm{p})t_\mathrm{s}$, that is, the influences of material strengths f_c and f_u in the above range are negligible. Here, it should be noted that the yield strengths of steel sheeting

f_{yd} are taken as a constant 280 N/mm^2 for all of the 25 data, because some of them were not measured. If compared with those measured f_{yd} which were as high as 430 N/mm^2, the constant value of 280 N/mm^2 means the influence of f_{yd} can also be neglected.

From the relationship shown in Figure 8.10, it is clear that an increase of h_p reduces the value of η, so $(e_f + h - h_p)t_s$ is replaced by $\dfrac{e_f + h}{h_p}\eta_t$, as shown in Figure 8.11, where η_t is the thickness factor with its value equal to the value of the thickness of sheeting. The relation between η and $\dfrac{e_f + h}{h_p}\eta_t$ is still linear, and is found to be:

$$\eta = 0.2\eta_t \frac{e_f + h}{h_p} \tag{8.11}$$

For the 25 data, η_t ranges from 0.77 to 1.53.
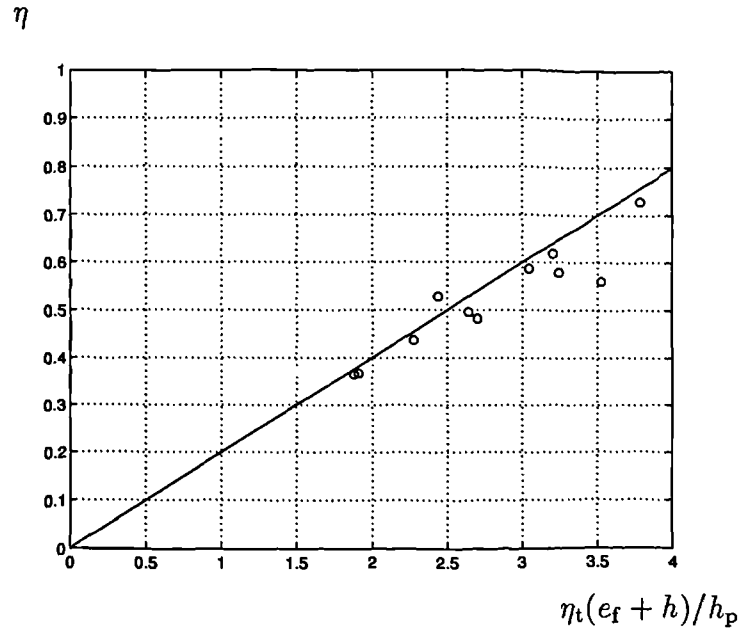
Figure 8.11: Relation between η and $\eta_t(e_f + h)/h_p$.

Also, for the value of λ, the material strengths can be proved to have negligible effects by plotting λ directly against $\dfrac{e_f}{h_p}$, as shown in Figure 8.12. So, λ is found

to be:

$$\lambda = 0.7 \frac{e_f}{h_p} \tag{8.12}$$
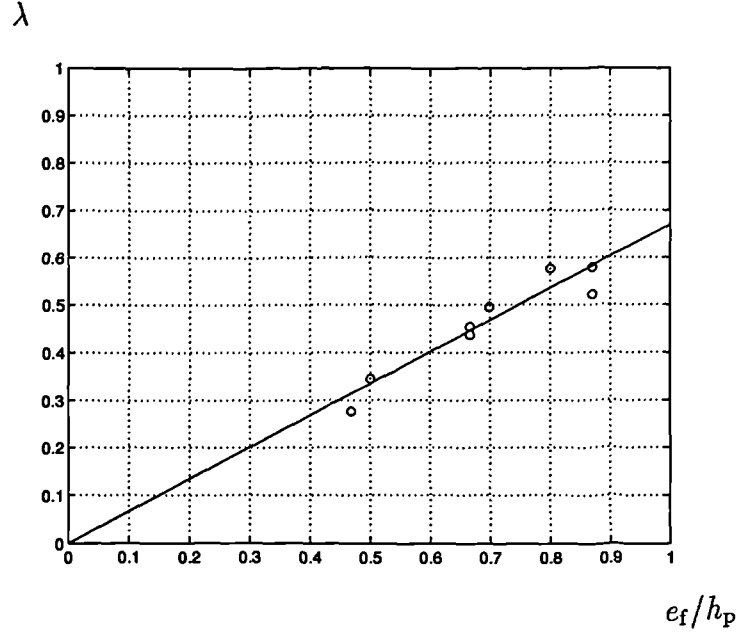
Figure 8.12: Relation between λ and e_f/h_p.

The reduction factor k_t for rib punching failure can now be calculated by equation (8.1) with η and λ from equations (8.11) and (8.12). This is proved to be very good, as shown in Figure 8.13, with errors within $\pm 10.5\%$.

However, the expression for k_t is still too complicated. Further simplification is made on the terms of $\sqrt{1 - \eta^2 + \lambda^2}$ and $1 + \lambda^2$ in equation (8.1).

First, let us consider $\sqrt{1 - \eta^2 + \lambda^2}$. As shown in equations (8.11) and (8.12), both η and λ consist of e_f/h_p, so the most significant influence on $\sqrt{1 - \eta^2 + \lambda^2}$ comes from η_t, as illustrated in Figure 8.14. The regression of $\sqrt{1 - \eta^2 + \lambda^2}$ on η_t gives:

$$\sqrt{1 - \eta^2 + \lambda^2} = -0.25\eta_t + 1.24 \tag{8.13}$$

$$P_e/(P_{rs}k_t)$$
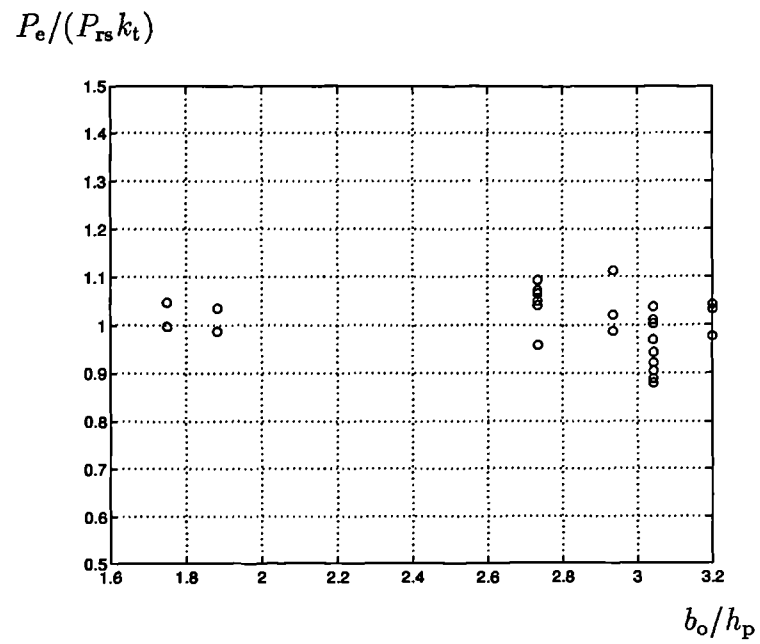
Figure 8.13: Comparison of the reduction factor with the test results.

$$\sqrt{1 - \eta^2 + \lambda^2}$$

η_t
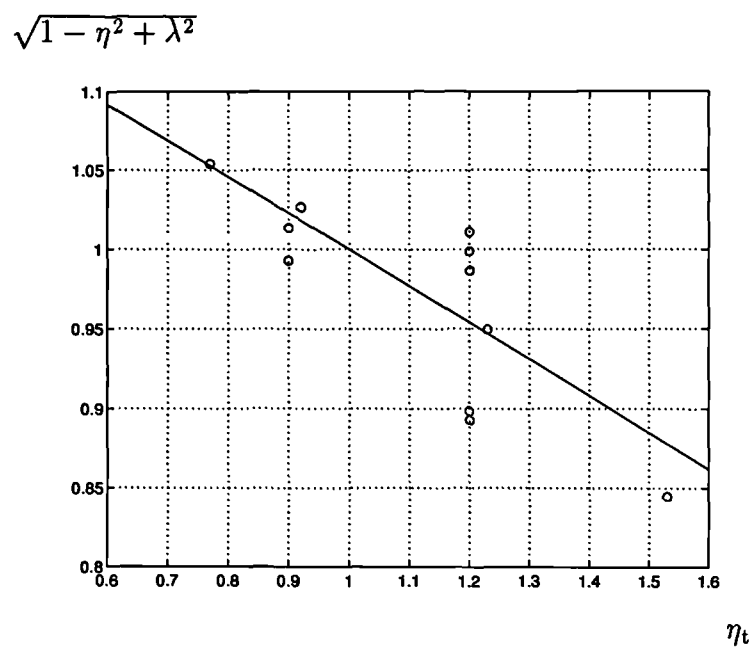
Figure 8.14: Regression on η_t.

As λ relates directly to e_f/h_p, therefore, $1 + \lambda^2$ is also a function of e_f/h_p. Within the range of the studied 25 data, the function is approximately a line (Figure 8.15), that is,

$$1 + \lambda^2 = 0.6\frac{e_f}{h_p} + 0.8 \tag{8.14}$$

$1 + \lambda^2$
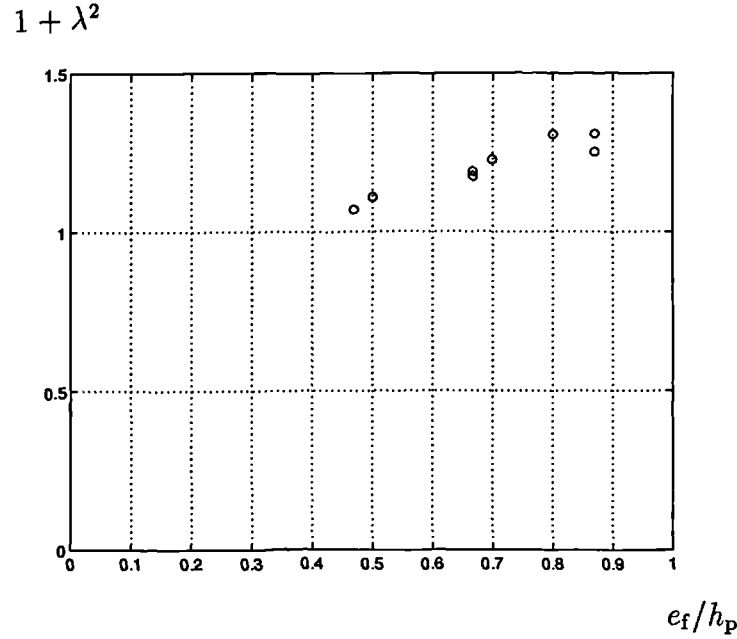
e_f/h_p

Figure 8.15: Relation between $1 + \lambda^2$ and e_f/h_p.

Substituting equations (8.11) to (8.14) into equation (8.1),

$$k_t = \frac{0.02e_f\eta_t + 0.2h\eta_t + 0.87e_f}{0.6e_f + 0.8h_p} \tag{8.15}$$

Because $0.02e_f\eta_t$ is much smaller than the other parts, it is neglected. Equation (8.15) turns out to be:

$$k_t = \frac{\eta_t h + 4.3e_f}{3e_f + 4h_p} \tag{8.16}$$

It gives very good predictions for the tests that failed by rib punching failure, as shown in Figure 8.16, in that $\mu = 1.01$ and the coefficient of variance is 6.2%, while the Eurocode 4 model gives $\mu = 0.86$ and the coefficient of variation 13.1% (the comparison is not shown in the figure).

$$P_e/(P_{rs}k_t)$$
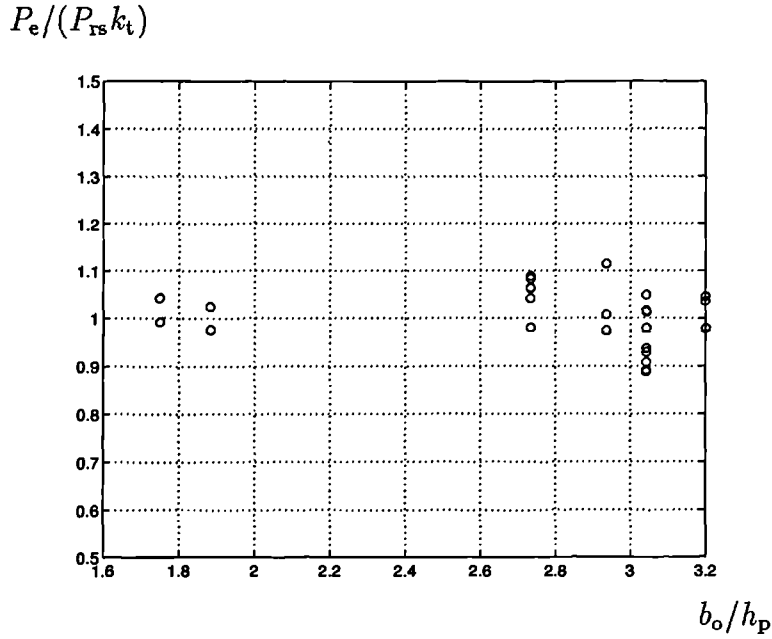
Figure 8.16: The simplified reduction factor for rib punching failure.

8.2.3   Discussion

Equations (8.8) is based on the concrete pulling out failure or the shank shearing failure, and equation (8.16) based on the rib punching failure.

For the steel sheeting commonly used in practice, the values of h/h_p ranges from 1.5 to 2.1. If the thickness of the decking is 1.0 mm, equation (8.8) gives the curves in Figure 8.17, and equation (8.16) the straight lines, where the solid lines have $h/h_p = 1.5$ and the dashed lines have $h/h_p = 2.1$.

The intersection of the solid lines is at $e_f/h_p = 1.35$. When $e_f/h_p \leq 1.35$, the reduction factor is determined by the curve, in other words, the failure mode of the stud connector is controlled by the rib punching failure. When $e_f/h_p \geq 1.35$, the concrete pulling out failure is the dominant failure mode until the line reaches $k_t = 1.0$ where the failure mode is replaced by the shank shearing failure. Therefore, the lower boundaries of the solid lines determine the failure mode of

the stud connector, and the intersection of the lines is the control point for the failure modes.

For $h/h_p = 2.1$, the dashed lines show similar behaviour, with the failure modes controlled by the lower boundaries. Also, it is noted that the intersection of the lines, at $e_f/h_p = 1.33$, is almost the same.

When the thickness of the decking $t_s = 0.8$ mm ($\eta_t = 0.8$), the control point is 1.56 for $h/h_p = 1.5$ and 1.66 for $h/h_p = 2.1$, and for $t_s = 1.2$ mm, it is 1.14 and 1.02, respectively. The influence of the height of the stud connector is negligible. Therefore, the control point for the failure modes depends on the position of the stud connector and the thickness of the steel decking.
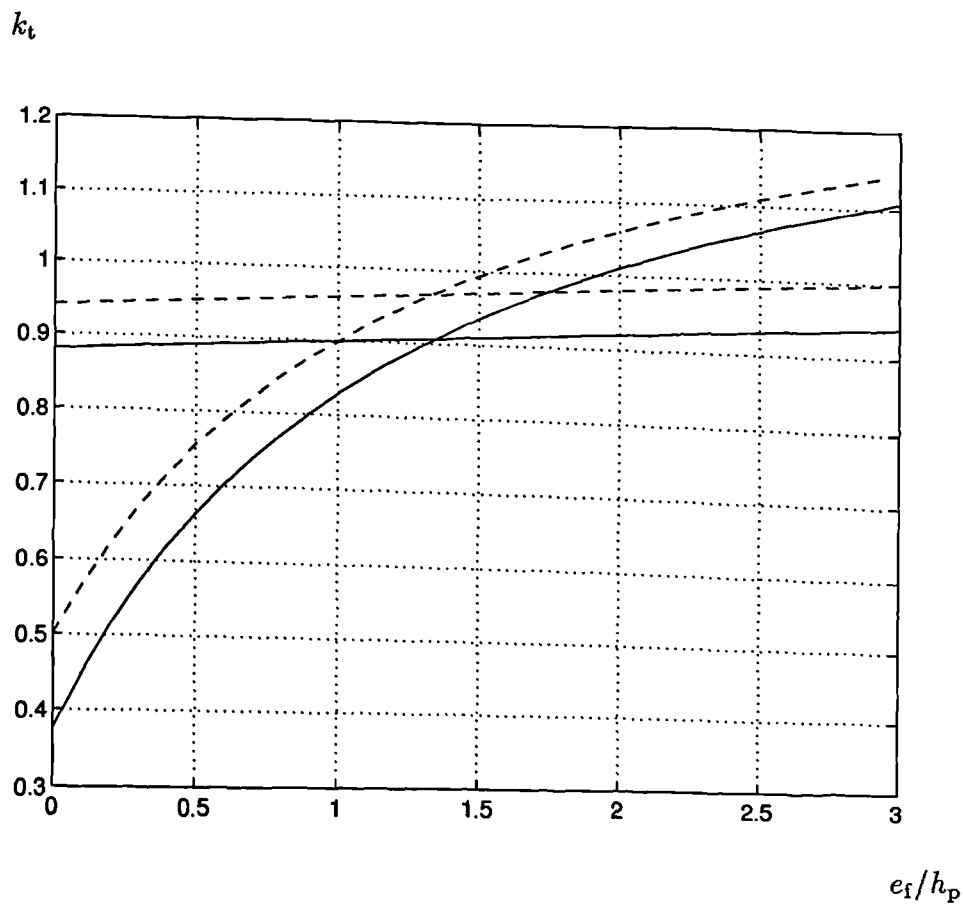
Figure 8.17: The control point for rib punching and concrete pulling out failure.

8.2.4 New reduction factor for one stud per trough

Because the lower boundaries of equations (8.8) and (8.16) control the failure mode of the stud connector, the reduction factor for one stud per trough is proposed as

$$k_t = \min \begin{cases} \dfrac{\eta_t h + 4.3 e_f}{3 e_f + 4 h_p} \\ 0.04 \dfrac{0.5 e_f + 3h}{h_p} + 0.7 \end{cases} \leq 1.0, \tag{8.17}$$

where η_t is the thickness factor, with its value equal to the thickness of the sheeting.

There are 60 data in Tables 5.1 and 5.2 which have one stud per trough with reported t_s. For these 60 data, the above simplified method gives satisfactory predictions, as shown in Figure 8.18, with $\mu = 1.02$ and the coefficient of variance 10.9%. The Eurocode 4 model for these data (not shown in the figure) gives $\mu = 0.98$ and the coefficient of variation 18.2%.

$P_e/(P_{rs}k_t)$

b_o/h_p
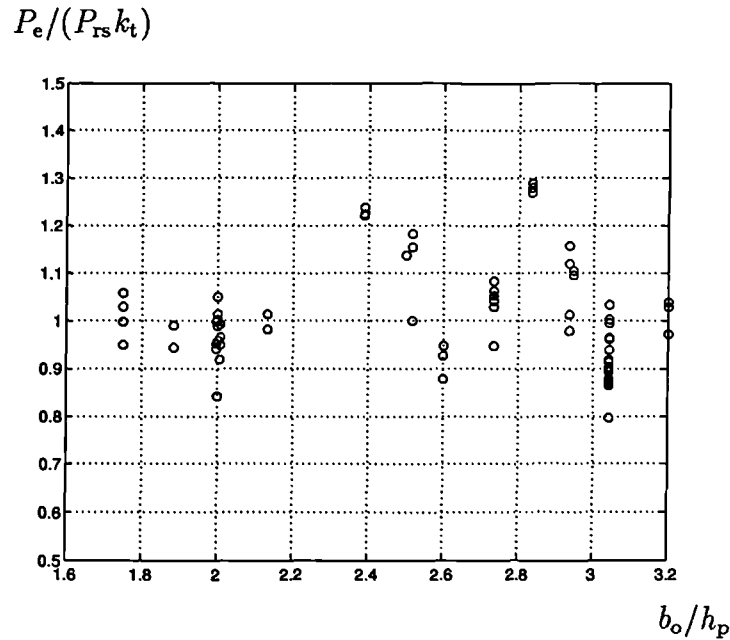
Figure 8.18: The simplified reduction factors for one stud per trough.

8.3   Two studs per trough

When two studs are used per trough, they can be arranged in three ways:

(a) in-line along the trough;
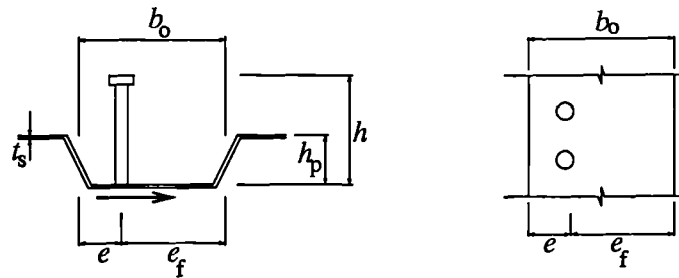
(b) transverse to the trough;
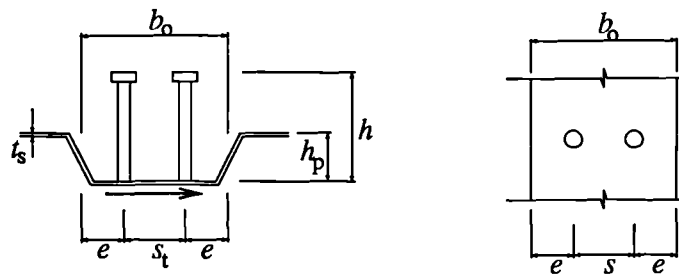
(c) staggered.
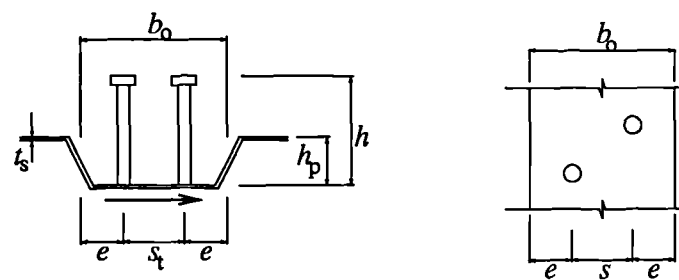
8.3.1   Two in-line studs

For two in-line studs, according to the theory described in Chapter 5, the reduction factor is only slightly different from that for one stud per trough, with

equation (8.2) replaced by equation (8.18):

$$\eta = \frac{0.45\sqrt{f_{cu}}h^2(b_o - 0.25h)}{N_r h_p P_{rs}} \qquad (8.18)$$

where $N_r(\leq 2)$ is the number of studs per trough. Again, η is simplified according to the relation shown in Figure 8.19.

$$\eta = \frac{0.01}{N_r}(\frac{h}{d})^2\frac{b_o - 0.25h}{h_p} \qquad (8.19)$$
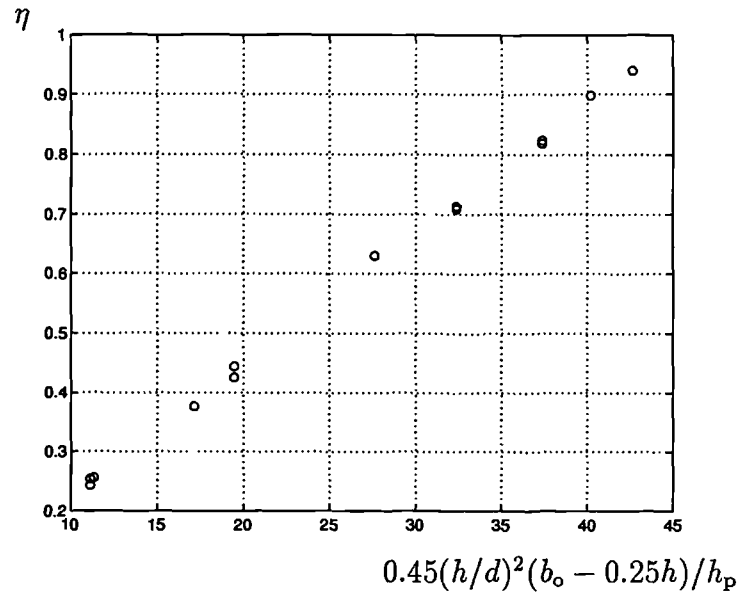
Figure 8.19: The effects of the strengths of materials on η.

In a similar way as for one stud at the centre or on the favourable side, η from equation (8.19) is found to be in relation with $0.5e_f + 3(h - h_p)/\sqrt{N_r}$, and the reduction factor k_t a function of $(0.5e_f + 3h/\sqrt{N_r})/h_p$, as shown in Figure 8.20.

$$k_t = 0.1\frac{0.5e_f + 3h/\sqrt{N_r}}{h_p} + 0.3 \leq 1.0, \quad N_r \leq 2 \qquad (8.20)$$

The comparison with the test results is shown in Figure 8.21 ($\mu = 1.04$, coefficient of variation=12.5%). For these data, the Eurocode 4 model (not shown in the figure) gives $\mu = 0.98$ and the coefficient of variation 18%. Because of insufficient number of test data, equation (8.20) is only valid for $b_o/h_p \geq 2.4$ with the two studs on the favourable side or at the centre.

k_t

$$(0.5 e_f + 3h/\sqrt{N_r})/h_p$$
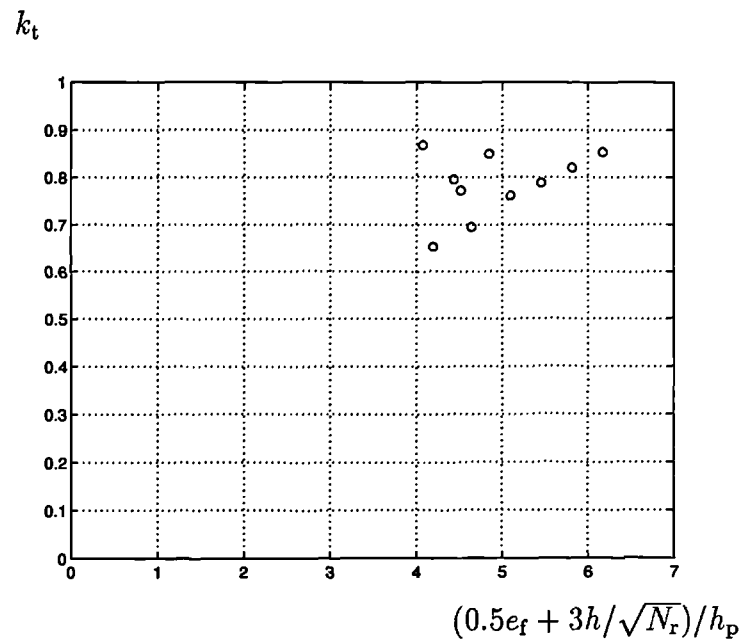
Figure 8.20: The reduction factor k_t for two in-line studs.

$P_e/(P_{rs} k_t)$

$$b_o/h_p$$
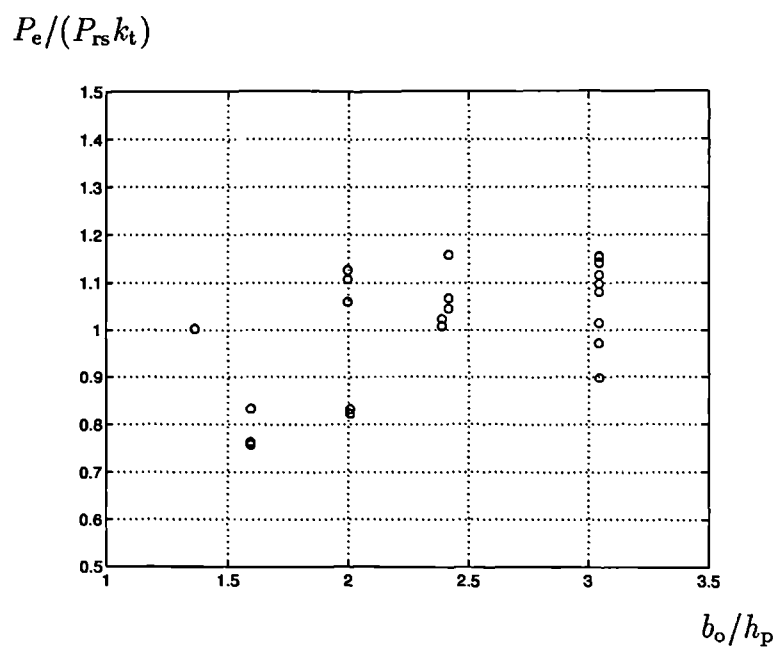
Figure 8.21: The simplified reduction factor for two in-line studs.

8.3.2 Two transverse or staggered studs

For two transverse or staggered studs, as found in Chapter 5, the reduction factor is the combined effect of the unfavourable position with the favourable position. So, from equations (8.8) and (8.16), the reduction factor for two transverse or staggered stud connectors is found to be

$$k_t = 0.28\frac{2s_t + 1.5\eta_t h}{1.5e + h_p} \leq 1.0 \tag{8.21}$$

Figure 8.22 shows that equation (8.21) is very good ($\mu = 1.02$ and the coefficient of variation=7.2%). The Eurocode 4 model (not shown in the figure) gives $\mu = 1.03$ and the coefficient of variance 20.3%.

$P_e/(P_{rs}k_t)$

b_o/h_p
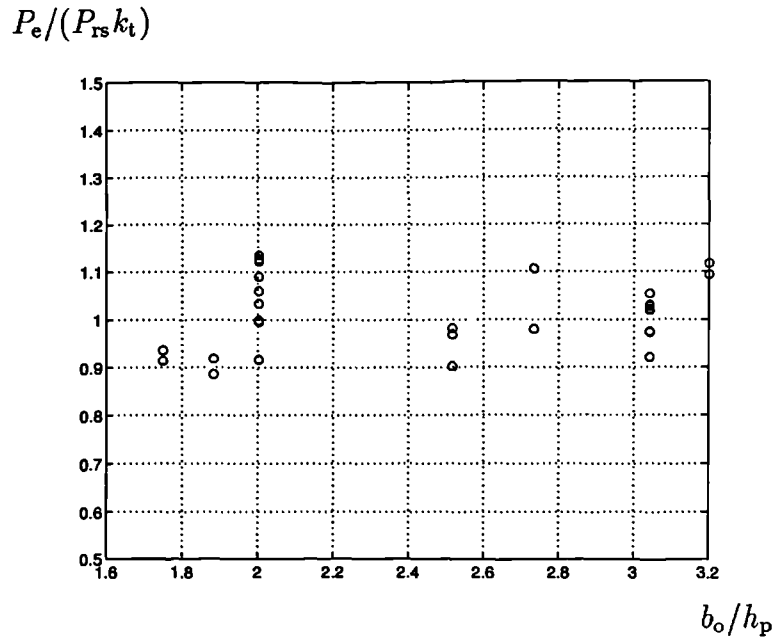
Figure 8.22: The simplified reduction factor for two transverse or staggered studs.

8.4   Conclusions

By applying regression analyses on the reduction factors obtained from the the-
oretical models in Chapter 5, it is found that the following factors have the
strongest influence: height of stud, h; depth of the trough, h_p; thickness of the
decking, t_s, in terms of the thickness factor η_t with the value equal to the thick-
ness; concrete cover in front of the stud, e_f for one stud or two in-line studs, or e
for two transverse or staggered studs; transverse spacing between the studs, s_t.
The reduction factors for transverse sheeting are, therefore, proposed as follows:

1. For one stud per trough,

$$k_t = \min \begin{cases} \dfrac{\eta_t h + 4.3 e_f}{3 e_f + 4 h_p} \\[2mm] 0.04 \dfrac{0.5 e_f + 3h}{h_p} + 0.7 \end{cases} \leq 1.0 \qquad (8.22)$$

2. For two in-line studs,

$$k_t = 0.1 \frac{0.5 e_f + 3h/\sqrt{N_r}}{h_p} + 0.3 \leq 1.0 \qquad (8.23)$$

which is only valid for two central or favourable studs in a wide trough with
$b_o/h_p \geq 2.4$.

3. For two transverse or staggered studs,

$$k_t = 0.28 \frac{2 s_t + 1.5 \eta_t h}{1.5 e + h_p} \leq 1.0 \qquad (8.24)$$

The proposals are satisfactory for f_c from 25 to 40 N/mm^2, and f_u not less than
400 N/mm^2.

Among the 126 data studied in this chapter, 102 have reported values for t_s,
the thickness of sheeting. For these 102 data, the new models give predictions
with $\mu = 1.02$ and the coefficient of variance as 9.1%, much lower than 17.5%
which is from the Eurocode 4 model which gives $\mu = 0.98$.

Chapter 9

Design resistances of studs with transverse sheeting

9.1 Introduction

So far, three theoretical models have been developed to predict the shear resistances of stud connectors with transverse sheeting in respect of different failure modes. As shown in previous chapters, the coefficient of variation of the predictions for a total of 102 data is 9.1%. From the statistical point of view, the scatter is inevitable, because those basic variables in the theoretical models are random variables. Apart from this, the imperfection of the models themselves also contributes to the variations.

In Eurocode 4, where ultimate limit design is specified for stud connectors, such kinds of uncertainties on the resistance side are represented by a single safety factor γ_M, applied to characteristic resistances (5% failure fractile) to give design resistances corresponding approximately to the 0.1% lower fractile. It was obtained from a new statistical concept [45] and [23].

In this chapter, this new concept is applied to the theoretical models for transverse sheeting. Data on parallel sheeting are not sufficient for statistical analyses.

The redistribution of the shear force in a push-out specimen is studied by dividing the available data into several groups according to the number of studs in the specimen. Though most of the groups are of relatively small size, the results are of use conceptually. It is found that for one stud per trough, the design resistances increase as the number of the studs increases, while for two studs in a trough, with the same number in a specimen, the design resistance is higher for staggered studs than for transverse ones. This confirms Oehlers and Johnson's conclusion [36] that due to the redistribution of the shear force, the characteristic and design resistances of a group of studs depend on the number in the group, or in other words, that the probability of failure at a given load/stud increases as the number of studs in a shear span reduces.

The design resistance is given here only for one stud per trough, based on the results for the group with four studs/specimen, because, on the one hand, the large size of this group (51 data) ensures higher accuracy. On the other hand, four could be the minimum number of studs in a shear span in practice, so the results are on the conservative side.

The analyses also suggest that the number of studs in a specimen should be treated as a variable in future studies.

9.2 New concept for reliability analyses

Since the 1920s, structural reliability has been studied extensively, and the most famous and influential theory is Hasofer and Lind's reliability index method, or more precisely, the advanced first order second moment method [30]. It treats all

the basic variables (generic symbol X) involved in the theoretical failure function, such as material strengths and geometric dimensions, as uncorrelated random basic variables. The reliability index is calculated from the first order Taylor expansion of the failure function around the design point.

Recently, a new concept was developed for the statistical determination of the design values of structural resistances [45], and was improved by Johnson and Huang [23] into a general calibration procedure for partial safety factors for resistances of composite members. The most significant characteristic of this new concept is that the resistance as a whole and the load effect as a whole are regarded as two uncorrelated random variables with log-normal distributions. Their coefficients of variations are determined from the first order Taylor expansion around the mean points.

In the following sections, Johnson and Huang's method for determining the partial safety factor will be used for stud connectors. Here is a summary of some basic concepts of the method.

If r and s are the resistance and the load effect, as they are two uncorrelated random variables with log-normal distributions (the fundamental assumption of the method), the failure function or g-function can be simply expressed as

$$g = \ln r - \ln s \begin{cases} > 0 & \text{safe} \\ = 0 & \text{critical} \\ < 0 & \text{unsafe} \end{cases} \qquad (9.1)$$

The measure of risk is the probability of the 'unsafe' event ($g < 0$),

$$P_\text{f} = P\{g < 0\} \qquad (9.2)$$

Let

$$Z = \frac{g - \mu_\text{g}}{\sigma_\text{g}} \qquad (9.3)$$

then $g < 0$ gives

$$Z < -\frac{\mu_\text{g}}{\sigma_\text{g}} = -\beta \qquad (9.4)$$

Thus

$$P_{\mathrm{f}} = P\{Z < \beta\} = \Phi(-\beta) \qquad (9.5)$$

where $\Phi(x)$ is the cumulative probability of the standard normal distribution; μ_{g} and σ_{g} are the mean and the standard deviation of the g-function, respectively; β is the safety index.

Referring to equation (9.1): because r and s are log-normal variates $N(\mu_{\ln r}, \sigma_{\ln r})$ and $N(\mu_{\ln s}, \sigma_{\ln s})$, it is easy to find that $\mu_{\mathrm{g}} = \mu_{\ln r} - \mu_{\ln s}$ and $\sigma_{\mathrm{g}}^2 = \sigma_{\ln r}^2 + \sigma_{\ln s}^2$. So,

$$\beta = \frac{\mu_{\mathrm{g}}}{\sigma_{\mathrm{g}}} = \frac{\mu_{\ln r} - \mu_{\ln s}}{\sqrt{\sigma_{\ln r}^2 + \sigma_{\ln s}^2}} \qquad (9.6)$$

Let

$$\begin{cases} Z_{\mathrm{r}} = \dfrac{\ln r - \mu_{\ln r}}{\sigma_{\ln r}} \\[2mm] Z_{\mathrm{s}} = \dfrac{\ln s - \mu_{\ln s}}{\sigma_{\ln s}} \end{cases} \qquad (9.7)$$

The g-function (9.1) is then transformed into Z-space:

$$G(Z_{\mathrm{r}}, Z_{\mathrm{s}}) = (Z_{\mathrm{r}}\sigma_{\ln r} + \mu_{\ln r}) - (Z_{\mathrm{s}}\sigma_{\ln s} + \mu_{\ln s}) \begin{cases} > 0 & \text{safe} \\ = 0 & \text{critical} \\ < 0 & \text{unsafe} \end{cases} \qquad (9.8)$$

Equation (9.8) is illustrated as in Figure 9.1, and it is easy to prove that the distance from point O to the failure surface, OA, is the safety index β. As given in equation (9.5), the failure probability reduces as the safety index or OA increases. Therefore, point A is defined as design point. Its coordinates are

$$\begin{cases} Z_{\mathrm{r}}^{\mathrm{A}} = -\alpha_{\mathrm{r}}\beta \\ Z_{\mathrm{s}}^{\mathrm{A}} = \alpha_{\mathrm{s}}\beta \end{cases} \qquad (9.9)$$

where

$$\begin{cases} \alpha_{\mathrm{r}} = \dfrac{\sigma_{\ln r}}{\sqrt{\sigma_{\ln r}^2 + \sigma_{\ln s}^2}} \\[3mm] \alpha_{\mathrm{s}} = \dfrac{\sigma_{\ln s}}{\sqrt{\sigma_{\ln r}^2 + \sigma_{\ln s}^2}} \end{cases} \qquad (9.10)$$
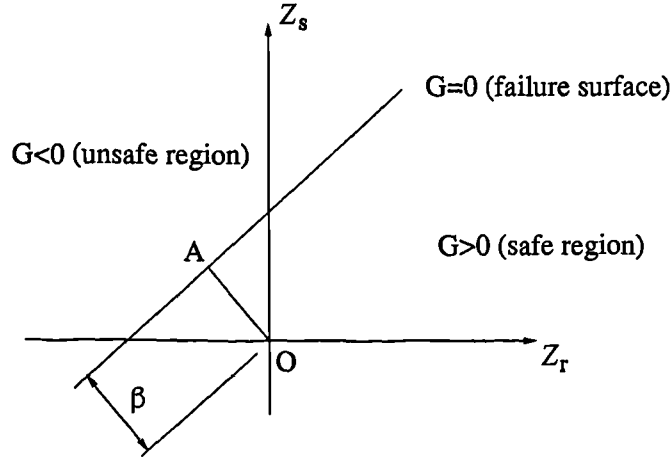
Figure 9.1: G-Function in Z-space.

The failure probability given by equation (9.5) then can be split into two parts. One is for the resistance:

$$P_{f,r} = P\{Z_r < Z_r^A = -\alpha_r\beta\} = \Phi(-\alpha_r\beta) \tag{9.11}$$

and the other for the load effect:

$$P_{f,s} = P\{Z_s > Z_s^A = \alpha_s\beta\} = 1 - \Phi(-\alpha_s\beta) \tag{9.12}$$

Considering the resistance side alone, and noting that $\mu_{\ln r} = \ln \bar{r} - 0.5\sigma_{\ln r}^2$, in X-space equation (9.11) becomes

$$P_{f,r} = P\{r < r_\alpha\} = \Phi(-k_\alpha) = \alpha \tag{9.13}$$

where

$$r_\alpha = \bar{r}\exp(-k_\alpha\sigma_{\ln r} - 0.5\sigma_{\ln r}^2) \tag{9.14}$$

and $k_\alpha = \alpha_r\beta$ is a factor with failure fractile α; $\bar{r}$ is the mean resistance. Therefore equation (9.13) defines the resistance r_α as the value which the probability of the resistance failing to reach is $\Phi(-k_\alpha) = \alpha$.

To calculate the characteristic resistance r_k, α is prescribed as 5%, with k_α in equation (9.14) replaced by k_s:

$$r_k = \bar{r}\exp(-k_s\sigma_{\ln r} - 0.5\sigma_{\ln r}^2) \tag{9.15}$$

and for the design resistance r_d, $\alpha = 0.12\%$, and k_α replaced by k_d:

$$r_d = \bar{r}\exp(-k_d\sigma_{\ln r} - 0.5\sigma_{\ln r}^2)$$ (9.16)

Both k_s and k_d depend on the sample size n. For large size with $n > 60$, $k_s = 1.64$ and $k_d = 3.04$. The calculation of $\sigma_{\ln r}$ will be explained later.

9.3 Design resistances of stud connectors from the new method

Idealised case

The design of stud connectors, as recommended in Eurocode 4, is based on the characteristic resistances with a single partial safety factor. First let us consider the idealised case to apply the new method on stud connectors. A set of push-out tests (total number $n > 60$) is carried out. All the basic variables are measured and their intended values are the same for all specimens. Such a set is defined as a sample with size n.

If $X_{mi} = (X_{1i}, X_{2i}, \cdots, X_{Ji})$ are the basic variables, for each specimen, the theoretical resistance of a stud connector is

$$r_{ti} = r_{ti}(X_{mi}), \quad i = 1 \quad \text{to} \quad \text{n}.$$ (9.17)

Comparing r_{ti} with the experimental resistance r_{ei}, the correction factor for each specimen

$$b_i = \frac{r_{ei}}{r_{ti}}$$ (9.18)

then the corrected theoretical resistance function is

$$r_i = \bar{b}\delta_i r_{ti}(X_{mi})$$ (9.19)

where $\bar{b}$ is the mean of the correction factors, and δ_i is the error term for each specimen, given by:

$$\delta_i = \frac{b_i}{\bar{b}} = \frac{r_{ei}}{\bar{b}r_{ti}}$$ (9.20)

Using the first order Taylor expansion around the mean point, $\{\bar{\delta}(=1), \bar{X}_{\mathrm{m}}\}$, and assuming $X_1, \cdots, X_J$ to be mutually uncorrelated, the mean value of the corrected theoretical resistances

$$\bar{r} = \bar{b}r_{\mathrm{t}}(\bar{X}_{\mathrm{m}}) \tag{9.21}$$

and the coefficient of variation of r depends on the coefficients of variations of the error term, V_{δ}, and of the theoretical function, V_{rt}:

$$V_{\mathrm{r}}^2 = V_{\delta}^2 + V_{\mathrm{rt}}^2 \tag{9.22}$$

V_{rt}, as suggested by the new method, can be determined by the first order Taylor expansion of the theoretical function around the mean point:

$$V_{\mathrm{rt}}^2 = \frac{1}{r_{\mathrm{t}}^2(\bar{X}_{\mathrm{m}})} \sum_{j=1}^{J} \left(\frac{\partial r_{\mathrm{t}}}{\partial X_j} V_{\mathrm{X}j} \bar{X}_j\right)^2 \tag{9.23}$$

As the resistance as a whole is treated as a random variable with log-normal distribution, so the mean and the standard deviation of $\ln r$ are

$$\mu_{\ln r} = \ln \bar{r} - 0.5\sigma_{\ln r}^2 \tag{9.24}$$

and

$$\sigma_{\ln r} = \sqrt{\ln(1 + V_{\mathrm{r}}^2)} \tag{9.25}$$

For the design of stud connectors, a single partial safety factor γ_{M} is used in relation to the characteristic resistance:

$$r_{\mathrm{d}} = \frac{r_{\mathrm{k}}}{\gamma_{\mathrm{M}}} \tag{9.26}$$

From equations (9.15) and (9.16),

$$\gamma_{\mathrm{M}} = \exp[(k_{\mathrm{d}} - k_{\mathrm{s}})\sigma_{\ln r}] \tag{9.27}$$

Practical case

The practical laboratory work is much more limited due to the cost of testing. The available test data are the results of a group of n specimens from different samples with sizes n from 1 to 3. None of the statistics deduced in the preceding can be obtained from the samples or the group. Therefore to apply the above statistical methods to the available test data, the following assumptions are made:

1. All the specimens with the same resistance function is called a group. Its size n is the number of the specimens. The correction factor b for the group is a random variable with normal distribution.

2. Each sample in the group represents the population of that particular design, so the coefficients of variation of the basic variables V_{Xj} in equation (9.23) are estimated from practice, not from variability in the laboratories where the test specimens were made.

3. The correction factors b for all the samples within a group are from a single population. Therefore, V_δ in equation (9.22) is determined from the n specimens in the group:

$$V_\delta^2 = \frac{1}{n-1}(\sum_{i=1}^{n} \delta_i^2 - n) \tag{9.28}$$

4. The fractile factors for characteristic and design resistances, k_s and k_d in equation (9.27), are replaced by:

$$k_s = \frac{1.64V_{rt}^2 + k_{s,g}V_\delta^2}{V_r^2} \tag{9.29}$$

and

$$k_d = \frac{3.04V_{rt}^2 + k_{d,g}V_\delta^2}{V_r^2} \tag{9.30}$$

where $k_{s,g}$ and $k_{d,g}$ are the factors with 5% and 0.1% fractiles, respectively, found from one tail t-distribution with the degree of freedom $\nu = n - 1$.

Therefore, from equations (9.17) to (9.27) together with the four assumptions, the partial safety factor γ_M for stud connectors can be found from the push-out test results.

9.4 Results of the analyses

9.4.1 One stud per trough

The theoretical model simplified in chapter 8 for one stud per trough is expressed as a reduction factor k_t relative to the shank shearing resistance of the stud. It was assumed in chapter 5 that the shank shearing resistance equals to the resistance of the connector in a solid concrete slab P_{rs} given by Eurocode 4 (equation (5.6)). As for all the data considered, P_{rs} is controlled by concrete, so the function is

$$P_r = k_t \cdot 0.29 d^2 \sqrt{f_c E_{cm}} \tag{9.31}$$

where k_t is given by equation (8.17), and is:

$$k_t = \min \begin{cases} \dfrac{h\eta_t + 4.3 e_f}{3 e_f + 4 h_p} & \text{(rib punching controls)} \\ 0.04 \dfrac{0.5 e_f + 3h}{h_p} + 0.7 & \text{(concrete pullout controls)} \end{cases} \leq 1.0 \tag{9.32}$$

Symbols are shown in Figure 8.1. The elastic modulus E_{cm} is determined with equation (9.33) in N/mm² units, which is given in Eurocode 2 [5]:

$$E_{cm} = 9500 f_c^{1/3} \tag{9.33}$$

Therefore, when concrete pulling out failure controls, the basic variables are (e_f, h, h_p, d, h_p). According to equation (9.23),

$$
\begin{aligned}
V_{rt}^2 &= \frac{1}{P_r^2}\left[\left(\frac{\partial P_r}{\partial e_f} V_{e_f} e_f\right)^2 + \left(\frac{\partial P_r}{\partial h} V_h h\right)^2 + \left(\frac{\partial P_r}{\partial h_p} V_{h_p} h_p\right)^2 + \left(\frac{\partial P_r}{\partial d} V_d d\right)^2 + \left(\frac{\partial P_r}{\partial f_c} V_{f_c} f_c\right)^2\right] \\
&= \left(\frac{0.02 V_{e_f} e_f}{k_t h_p}\right)^2 + \left(\frac{0.12 V_h h}{k_t h_p}\right)^2 + \left[\frac{0.04 V_{h_p}(0.5 e_f + 3h)}{k_t h_p}\right]^2 + (2V_d)^2 + \left(\frac{2}{3} V_{f_c}\right)^2
\end{aligned}
\tag{9.34}
$$

When rib punching failure controls, one more variable, t_s, is involved, in terms of η_t which has the same value as t_s:

$$
\begin{aligned}
V_{rt}^2 &= \frac{1}{P_r^2} \left[\left(\frac{\partial P_r}{\partial h} V_h h \right)^2 + \left(\frac{\partial P_r}{\partial t_s} V_{t_s} t_s \right)^2 + \left(\frac{\partial P_r}{\partial e_f} V_{e_f} e_f \right)^2 + \left(\frac{\partial P_r}{\partial h_p} V_{h_p} h_p \right)^2 + \left(\frac{\partial P_r}{\partial d} V_d d \right)^2 \right. \\
&\quad \left. + \left(\frac{\partial P_r}{\partial f_c} V_{f_c} f_c \right)^2 \right] \\
&= \left[\frac{t_s h}{(3e_f + 4h_p)k_t} \right]^2 (V_h^2 + V_{t_s}^2) + \left[\frac{(17.2 h_p - 3h t_s) V_{e_f} e_f}{(3e_f + 4h_p)^2 k_t} \right]^2 + \left(\frac{4 h_p V_{h_p}}{3e_f + 4h_p} \right)^2 + (2V_d)^2 \\
&\quad + \left(\frac{2}{3} V_{f_c} \right)^2
\end{aligned}
\tag{9.35}
$$

The coefficients of variation of the basic variables, V_{e_f}, V_h, V_{h_p}, V_{t_s} and V_{f_c}, are given in Table 9.5, which relies on the values given in Table A.1 of [23].

There are a total of 71 data. They are divided into three groups in accordance with the number of studs in a specimen, these being 2, 4 and 6. The group properties, $\bar{b}$, V_δ, $k_{s,g}$ and $k_{d,g}$ are listed in Table 9.1, where n is the group size and N_{rs} is the number of studs per specimen. Each group consists of several samples, on which the statistical analyses described in the previous section are carried out. Details are given in Table 9.3, where R_k is as defined below.

Table 9.1: Properties of groups with one stud per trough

Group	n	N_{rs}	$\bar{b}$	V_δ	$k_{s,g}$	$k_{d,g}$	$\bar{R}_k$	$\bar{\gamma}_M$	$\bar{b}\bar{R}_k/\bar{\gamma}_M$
G1	9	2	1.0717	0.1286	2.306	5.041	0.6892	1.4520	0.5087
G2	51	4	0.9989	0.0906	2.010	3.510	0.7464	1.2559	0.5937
G3	11	6	1.0691	0.0609	2.228	4.587	0.7713	1.2520	0.6586

$$R_k = \exp(-k_s \sigma_{\ln r} - 0.5 \sigma_{\ln r}^2)$$

The partial safety factor for two studs/specimen (G1) is 1.45, much higher than the other two cases. The smaller group size is one of the reasons. The other reason is the higher values of $\sigma_{\ln r}$, which is controlled by V_δ, or σ_δ as

$\bar{\delta} = 1$. Usually, the tested resistance of a stud connector in a push-out specimen is obtained by dividing the total shear force by the number of studs in the specimen. Therefore, a test of Group 1 gives the mean resistance of two studs, so does Group 2 of four studs and Group 3 of six. If δ is denoted as the standard deviation of the total population of stud connectors, it can be estimated as $\sqrt{2}V_{\delta 2} = \sqrt{2} \times 0.1286 = 0.1819$ from Group 1, $\sqrt{4}V_{\delta 4} = \sqrt{4} \times 0.0906 = 0.1811$ from Group 2 and $\sqrt{6}V_{\delta 6} = \sqrt{6} \times 0.0609 = 0.1491$ from Group 3. This means the standard error of the mean predicted resistance reduces as the number of studs per specimen increases, which inevitably results in the higher partial safety factor for Group 2 than for the others, even if all the other properties in the three groups are the same. So, the conclusion is that the design resistance increases with the number of studs per specimen.

According to equations (9.15) and (9.26), the design resistance for stud connectors can be expressed as

$$P_{\mathrm{d}} = \frac{\bar{b}R_{\mathrm{k}}}{\gamma_{\mathrm{M}}}P_{\mathrm{r}} \tag{9.36}$$

where $R_{\mathrm{k}} = \exp(-k_{\mathrm{s}}\sigma_{\ln\mathrm{r}} - 0.5\sigma_{\ln\mathrm{r}}^2)$. Comparison of the means of $\bar{b}R_{\mathrm{k}}/\gamma_{\mathrm{M}}$ of the three groups, as also shown in Table 9.1, confirms the above conclusion.

In practice, the number of studs used in a shear span varies in a broad range, from about 5 to over 100. It is not practicable to take account of this variable in design. Therefore, for one stud per trough, the design resistance is given based on the results of Group 2, as this group has the largest size ($n = 51$), which increases the reliability. Besides, considering that four could be the minimum number of studs in a shear span in practice, the design resistance such developed will give conservative prediction.

Though the calculated partial safety factor for Group 2 is 1.26, it is taken as 1.25 to achieve a uniform value for all types of connection, as was done in

Eurocode 4. So, the design resistance for one stud per trough is given by:

$$P_{\mathrm{d}} = \frac{0.75 k_t P_{\mathrm{rs}}}{\gamma_{\mathrm{M}}} \qquad (9.37)$$

where $\gamma_{\mathrm{M}} = 1.25$, and k_t from equation (9.32). P_{rs} is the shank shearing resistance of a stud, as given by equation (5.6).

9.4.2 Two studs per trough

As found in Chapters 5 and 8, the shear resistances for two studs per trough can still be predicted by equation (9.31), but with the reduction factor k_t replaced by equations (9.38) and (9.39). Symbols are as used in Section 8.3.

For two transverse or staggered studs,

$$k_t = 0.28 \frac{2s_t + 1.5 h \eta_t}{1.5e + h_{\mathrm{p}}} \le 1.0 \qquad (9.38)$$

for two in-line studs,

$$k_t = 0.1 \frac{0.5 e_f + 3h/\sqrt{2}}{h_{\mathrm{p}}} + 0.3 \le 1.0 \qquad (9.39)$$

With E_{cm} as given by equation (9.33), the resistance of two staggered or transverse studs becomes

$$P_{\mathrm{r}} = P_{\mathrm{r}}(s_t, h, t_{\mathrm{s}}, e, h_{\mathrm{p}}, d, f_c). \qquad (9.40)$$

Its coefficient of variation of the resistance is

$$
\begin{aligned}
V_{\mathrm{rt}}^2 &= \frac{1}{P_{\mathrm{r}}^2} \left[\left(\frac{\partial P_{\mathrm{r}}}{\partial s} V_{s_t} s_t \right)^2 + \left(\frac{\partial P_{\mathrm{r}}}{\partial h} V_h h \right)^2 + \left(\frac{\partial P_{\mathrm{r}}}{\partial t} V_{t_s} t_s \right)^2 + \left(\frac{\partial P_{\mathrm{r}}}{\partial e} V_e e \right)^2 \right. \\
&\qquad \left. + \left(\frac{\partial P_{\mathrm{r}}}{\partial h_{\mathrm{p}}} V_{h_{\mathrm{p}}} h_{\mathrm{p}} \right)^2 + \left(\frac{\partial P_{\mathrm{r}}}{\partial d} V_d d \right)^2 + \left(\frac{\partial P_{\mathrm{r}}}{\partial f_c} V_{f_c} f_c \right)^2 \right] \\
&= \left[\frac{0.56 V_{s_t} s_t}{(1.5e + h_{\mathrm{p}}) k_t} \right]^2 + \left[\frac{0.42 t_{\mathrm{s}} h}{(1.5e + h_{\mathrm{p}}) k_t} \right]^2 (V_h^2 + V_{t_s}^2) + \left(\frac{1.5 V_e e}{1.5e + h_{\mathrm{p}}} \right)^2 \\
&\qquad + \left(\frac{V_{h_{\mathrm{p}}} h_{\mathrm{p}}}{1.5e + h_{\mathrm{p}}} \right)^2 + (2 V_d)^2 + \left(\frac{2}{3} V_{f_c} \right)^2 \qquad (9.41)
\end{aligned}
$$

For two in-line studs,

$$P_r = P_r(e_f, h, h_p, d, f_c) \qquad (9.42)$$

and its coefficient of variation is determined by:

$$
\begin{aligned}
V_{rt}^2 &= \frac{1}{P_r^2} \left[\left(\frac{\partial P_r}{\partial e_f} V_{e_f} e_f \right)^2 + \left(\frac{\partial P_r}{\partial h} V_h h \right)^2 + \left(\frac{\partial P_r}{\partial h_p} V_{h_p} h_p \right)^2 + \left(\frac{\partial P_r}{\partial d} V_d d \right)^2 \right. \\
&\quad \left. + \left(\frac{\partial P_r}{\partial f_c} V_{f_c} f_c \right)^2 \right] \\
&= \left(\frac{0.02 V_{e_f} e_f}{h_p k_t} \right)^2 + \left(\frac{0.08 V_h h}{h_p k_t} \right)^2 + \left[\frac{0.04(0.5 e_f + 2.12 h) V_{h_p}}{h_p k_t} \right]^2 \\
&\quad + (2 V_d)^2 + \left(\frac{2}{3} V_{f_c} \right)^2 \qquad (9.43)
\end{aligned}
$$

The coefficients of variation of the basic variables are taken from Table 9.5.

Table 9.2: Properties of groups with two studs per trough

Group	n	N_{rs}	$\bar{b}$	V_δ	$k_{s,g}$	$k_{d,g}$	$\bar{R}_k$	$\bar{\gamma}_M$	$\bar{b}\bar{R}_k/\bar{\gamma}_M$
G4	11	8	0.9823	0.0863	2.228	4.587	0.7262	1.3236	0.5390
G5	17	4	1.0296	0.0630	2.120	4.015	0.7481	1.2695	0.6067
G6	13	4	0.9676	0.0845	2.179	4.318	0.7501	1.2820	0.5661

$$R_k = \exp(-k_s \sigma_{\ln r} - 0.5 \sigma_{\ln r}^2)$$

The available data are divided into three groups, as shown in Table 9.2 together with the group properties. Group 4 consists of 11 specimens, each with eight studs staggered or transverse in four troughs, while all the 17 specimens in group 5 have four studs staggered in two troughs. Group 6 are those with four studs in line in two troughs.

Similarly, the statistical analyses are carried out on each sample in the groups. Details of the results are given in Table 9.4, and the mean values of R_k, γ_M and $\bar{b}R_k/\gamma_M$ for each group are shown in table 9.2. It can be seen from G5 and G6

that with the same number of studs, the partial safety factor is higher for in-line studs than for staggered ones.

In G4, the larger number of studs ($N_{rs} = 8$) results in a higher partial safety factor γ_M, which is inconsistent with the conclusion for one stud per trough. This is because eight out of 11 specimens in G4 have transverse studs. So, the results suggest that the failure probability at a given load/stud is higher for transverse position than for staggered or in-line position.

9.5 Discussions

As the shear resistances of stud connectors obtained from experiments are treated as estimates of the means of the populations, the theoretical functions to be evaluated by the new statistical method described in Section 9.3 should represent predicted means. However, in Section 9.4 those theoretical functions studied do not give mean predictions, because they are based on the characteristic P_{rs} from Eurocode 4 (equation (5.6)). For example, equation (9.31) is in fact a prediction about $\frac{1}{\mu_o}$ of the predicted mean of the population with one stud per trough, in which $\mu_o (> 1)$ is unknown. Here, we will prove that the partial safety factors γ_M and the design resistance function given in equation (9.37) do not depend on any assumed value for μ_o, that is, the statistical results given in Section 9.4 are reliable.

For the theoretical function given by equation (9.31), if P_e is the tested resistance, the statistical analyses in Section 9.4 were actually based on the corrected theoretical resistance function:

$$P_{Ri} = \bar{B} \Delta_i P_{ri} \tag{9.44}$$

where

$$\bar{B} = \sum B_i = \sum \frac{P_{ei}}{P_{ri}} \tag{9.45}$$

and

$$\Delta_i = \frac{B_i}{\bar{B}} \tag{9.46}$$

If P_{rm} is the predicted mean estimated from equation (9.31), there is

$$P_{rm} = \mu_o P_r \tag{9.47}$$

Based on the estimated mean P_e and the predicted mean P_{rm}, equation (9.18) becomes

$$b_i = \frac{P_{ei}}{P_{rmi}} = \frac{1}{\mu_o} \frac{P_{ei}}{P_{ri}} = \frac{1}{\mu_o} B_i \tag{9.48}$$

and

$$\bar{b} = \frac{1}{\mu_o} \bar{B} \tag{9.49}$$

The error term, then, is the same as given by equation (9.46):

$$\delta_i = \frac{b_i}{\bar{b}} = \frac{\frac{1}{\mu_o} B_i}{\frac{1}{\mu_o} \bar{B}} = \frac{B_i}{\bar{B}} = \Delta_i \tag{9.50}$$

and so is the corrected theoretical resistance function:

$$r_i = \bar{b} \delta_i P_{rmi} = \frac{1}{\mu_o} \bar{B} \Delta_i \cdot \mu_o P_{ri} = \bar{B} \Delta_i P_{ri} = P_{Ri} \tag{9.51}$$

This means that the corrected theoretical resistance function from the predicted mean (equation (9.47)) is the same as from equation (9.31). So, none of those variables obtained from the corrected function, such as the coefficient of the resistance function, V_r from equation (9.22) and the standard deviation σ_{lnr} from equation (9.25), and the partial safety factor γ_M from equation (9.27), are affected by μ_o.

9.6   Conclusions

The three theoretical models developed in previous chapters for stud connectors with transverse sheeting have been evaluated by the new concept of the statistical method from [23].

1. The number of studs per specimen has significant influence on the characteristic and design resistances.

2. The design resistance for one stud per trough is recommended as:

$$P_{\rm d} = \frac{0.75 k_t P_{\rm rs}}{\gamma_{\rm M}} \qquad (9.52)$$

where the partial safety factor γ is 1.25, and k_t and $P_{\rm rs}$ are as given in equations (9.32 and (5.6)), respectively.

This recommendation is based on four studs per specimen, which is believed to be on the conservative side. It is valid for:

- 19-mm studs with the ultimate tensile strength greater than 450 N/mm^2;

- the cylinder strength of concrete from 20 to 35 N/mm^2.

3. With the given load/stud for the same number of studs, the failure probability is higher for in-line studs than for staggered ones.

4. The partial safety factor for two transverse studs per trough ($\gamma_{\rm M} = 1.32$) is higher than for the other two stud positions. Further study is needed to verify whether the higher $\gamma_{\rm M}$ is due to the inappropriate theoretical model or to the stud position.

Table 9.3: Results for one stud per trough.

Group	Sample	n	V_{rt}	V_r	$\sigma_{\ln r}$	R_k	k_s	k_d	γ_M
G1	1	3	0.1287	0.1819	0.1804	0.6892	1.9728	4.0399	1.4520
	2	3	0.1287	0.1819	0.1805	0.6892	1.9726	4.0393	1.4521
	3	3	0.1288	0.1820	0.1805	0.6891	1.9724	4.0388	1.4521
G2	1	2	0.1291	0.1577	0.1568	0.7494	1.7620	3.1950	1.2519
	2	2	0.1287	0.1574	0.1564	0.7498	1.7626	3.1957	1.2513
	3	1	0.1291	0.1577	0.1567	0.7495	1.7621	3.1951	1.2518
	4	3	0.1293	0.1578	0.1569	0.7493	1.7618	3.1948	1.2520
	5	3	0.1295	0.1580	0.1570	0.7490	1.7615	3.1940	1.2524
	6	3	0.1298	0.1582	0.1573	0.7488	1.7612	3.1957	1.2527
	7	2	0.1287	0.1574	0.1564	0.7498	1.7626	3.1957	1.2512
	8	2	0.1289	0.1575	0.1566	0.7497	1.7623	3.1954	1.2515
	9	3	0.1290	0.1576	0.1566	0.7496	1.7622	3.1952	1.2516
	10	3	0.1287	0.1574	0.1564	0.7498	1.7626	3.1957	1.2512
	11	3	0.1287	0.1574	0.1564	0.7498	1.7625	3.1956	1.2513
	12	2	0.1367	0.1640	0.1629	0.7417	1.7529	3.1834	1.2624
	13	2	0.1372	0.1644	0.1623	0.7412	1.7523	3.1826	1.2632
	14	3	0.1363	0.1637	0.1626	0.7421	1.7533	3.1839	1.2619
	15	3	0.1357	0.1631	0.1621	0.7427	1.7540	3.1849	1.2610
	16	2	0.1349	0.1625	0.1615	0.7435	1.7549	3.1860	1.2599
	17	1	0.1347	0.1623	0.1612	0.7438	1.7552	3.1864	1.2596
	18	3	0.1354	0.1629	0.1618	0.7430	1.7544	3.1853	1.2606
	19	3	0.1350	0.1626	0.1615	0.7435	1.7549	3.1859	1.2600
	20	2	0.1339	0.1616	0.1606	0.7446	1.7562	3.1876	1.2584
	21	3	0.1343	0.1620	0.1610	0.7441	1.7556	3.1869	1.2591
G3	1	3	0.1291	0.1427	0.1420	0.7725	1.7470	3.3214	1.2505
	2	3	0.1291	0.1427	0.1420	0.7725	1.7470	3.3214	1.2505
	3	3	0.1291	0.1427	0.1420	0.7725	1.7470	3.3214	1.2505
	4	1	0.1291	0.1427	0.1420	0.7725	1.7470	3.3214	1.2505
	5	1	0.1345	0.1476	0.1468	0.7663	1.7399	3.3030	1.2579

Table 9.4: Results for two studs per trough.

Group	Sample	n	V_{rt}	V_r	$\sigma_{\ln r}$	R_k	k_s	k_d	γ_M
G4	1	2	0.1475	0.1709	0.1697	0.7275	1.7899	3.4344	1.3219
	2	2	0.1459	0.1695	0.1683	0.7292	1.7924	3.4410	1.3198
	3	2	0.1502	0.1733	0.1720	0.7248	1.7859	3.4238	1.3254
	4	2	0.1513	0.1729	0.1729	0.7236	1.7843	3.4197	1.3268
	5	3	0.1491	0.1723	0.1711	0.7259	1.7875	3.4280	1.3240
G5	1	2	0.1535	0.1659	0.1647	0.7444	1.7091	3.1804	1.2743
	2	2	0.1510	0.1636	0.1626	0.7472	1.7110	3.1843	1.2706
	3	2	0.1520	0.1646	0.1635	0.7461	1.7103	3.1827	1.2721
	4	3	0.1472	0.1601	0.1591	0.7518	1.7142	3.1908	1.2648
	5	3	0.1477	0.1605	0.1595	0.7512	1.7138	3.1899	1.2655
	6	3	0.1483	0.1611	0.1601	0.7505	1.7133	3.1889	1.2664
	7	2	0.1525	0.1650	0.1639	0.7455	1.7099	3.1820	1.2728
G6	1	1	0.1285	0.1538	0.1529	0.7503	1.8028	3.4260	1.2817
	2	1	0.1287	0.1540	0.1531	0.7500	1.8024	3.4251	1.2820
	3	1	0.1288	0.1541	0.1532	0.7499	1.8023	3.4247	1.2821
	4	3	0.1289	0.1541	0.1532	0.7499	1.8021	3.4243	1.2822
	5	2	0.1286	0.1539	0.1530	0.7501	1.8026	3.4255	1.2819
	6	2	0.1286	0.1539	0.1530	0.7501	1.8026	3.4255	1.2819
	7	3	0.1287	0.1540	0.1531	0.7500	1.8024	3.4251	1.2820

Table 9.5: Coefficients of variation of basic variables.

Variable		Coefficient of variation
Dimensions of studs	d	0.04
	h	0.04
Position of studs	e_f	0.10
	e	0.10
	s_t	0.10
Dimensions of sheeting	h_p	0.04
	t_s	0.04
Compressive strength of concrete	f_c	0.15

Chapter 10

Fatigue strength of stud connectors

10.1   Introduction

In the design of composite beams for railway and road bridges or for industrial construction exposed to cyclic loads, such as cranes and fork-lift trucks, the endurance of stud connectors under repeated loading becomes the principal problem.

Usually, fatigue failure of stud connectors is regarded as a fatigue phenomenon in a welded detail of a steel structure. The mean strength is given by relating the constant range of shear stress $\Delta\tau$ caused by loading cycles to the number of cycles N of that range that result in fatigue failure:

$$N\Delta\tau^m = K \tag{10.1}$$

where m and K are the constants found from fatigue push-out tests.

A review of recent researches and Standards finds wide discrepancies in the values of both m and K. For example, the British Code for Bridges, BS 5400: Part 10 [1] has the value of m as 8, while Roik gives 9.2 [44] and Oehlers gives 5 [37].

This chapter presents a study of F-tests and t-tests of the available test results, and reveals the reasons for the discrepancies as the influences of different specimen layouts and test procedures.

A new proposal for design is then developed, based on the most reliable set of data.

10.2 Models for the design of stud connectors to fatigue

BS 5400: Part 10

The method was based on a study on 67 fatigue push-out tests [1]. It was found that the endurance of stud connectors N was governed by the stress range of unidirectional cyclic loading, and was influenced by the static strength of the connectors. Regression analyses found the relation (in N/mm^2 units) to be

$$N\sigma_r^8 = 2.08 \times 10^{22}, \tag{10.2}$$

where

$$\sigma_r = 425\frac{\Delta P}{P_{rs}}, \quad N/mm^2 \tag{10.3}$$

and ΔP is the range of the cyclic load applied on the stud connectors with ultimate static strength P_{rs} which is as given by BS5400: Part 3 [1].

Equation (10.2) gives characteristic values which ensure a less than 2.3% failure probability during the design life. It was derived from mean minus two

standard deviations. The partial safety factor γ_M is taken as 1.0, because the design is based on calculations of cumulative damage on a bridge, and on an estimated or specified spectrum of design loads that makes some provision for changes of traffic in the future.

Eurocode 3

In the draft of Eurocode 3 [6] for the design of composite bridges, the endurance of stud connectors is assumed to be controlled only by the stress range, $\Delta\tau$, and takes no account of the strength of the concrete. The characteristic values in N/mm² units are given by:

$$N\Delta\tau^5 = 6.554 \times 10^{15} \qquad (10.4)$$

where $\Delta\tau$ is calculated from the load range ΔP on the nominal cross sectional area A of the stud connectors, that is,

$$\Delta\tau = \frac{\Delta P}{A}, \quad \text{N/mm}^2 \qquad (10.5)$$

A similar method, with $\gamma_M = 1.0$, is used by Eurocode 3 for the design purpose.

Oehlers' method

Realising the discrepancies between the predicting methods, Oehlers [37] carried out a series of regression analyses to determine the endurance of stud connectors failing by dowel action under fatigue.

The multi-variable regression analyses revealed the significant influence factors on the endurance to be the static dowel strength P_{rs}, the range of unidirectional cyclic loading ΔP and the peak of the cyclic load P_{max}. The endurance was predicted in terms of mean values as

$$N(\frac{\Delta P}{P_{rs}})^5 = 1000(1 - \frac{P_{max}}{P_{rs}}) \qquad (10.6)$$

where P_{rs} is as defined by Oehlers in [22].

Roik's method

A series of studies on 62 fatigue push tests were carried out by Roik and Hanswille [44] to examine the use of Eurocode 3 (equation (10.4)), leading to the following conclusions:

1. the endurance increases with the higher concrete grade;

2. stud connectors behave more favourably under reversal of loading than under unidirectional loading;

3. the peak of the cyclic load has no influence on the endurance if it is less than 60% of the static strength.

Characteristic values of the endurance were derived by means of regression analyses on 18 data (out of 62) which had unidirectional cyclic loading with the peaks less than 60% of the static strengths, as given by equation (10.7) in N/mm^2 units:

$$N\Delta\tau^{9.2} = 1.88 \times 10^8 \qquad (10.7)$$

The concrete strengths for all these 18 data were between 20 and 30 N/mm^2, so equation (10.7) was believed to give conservative predictions (according to Conclusion 1).

These four methods for predicting the endurance of stud connectors vary widely. One obvious reason is the different parameters that are assumed to govern the endurance. Apart from this, it is also noticed that the fatigue push-out tests studied by the four methods are quite different in specimen geometry, reinforcements, restraints at the bottom of the slabs, casting of the concrete and testing methods. The question now is whether these factors are responsible for the discrepancies between the four methods. If they are, are they statistically significant? Before further statistical analyses to solve the problem, the reported data are checked and several rules for selecting data are prescribed, as explained in the following section.

10.3   Data selecting

A total of 211 reported results of fatigue push-out tests is collected, among which 115 ([13], [15], [28], [31], [32], [33] and [37]) are selected according to the following rules.

Testing methods

Push-out tests are the main testing method used through out the world. Usually, the concrete slabs in a push-out specimen are restrained at their bottoms to provide a pair of forces F which oppose the compressive forces C, as shown in Figure 10.1(a). In this way, it is believed that the behaviour of stud connectors in a composite beam is closely represented.
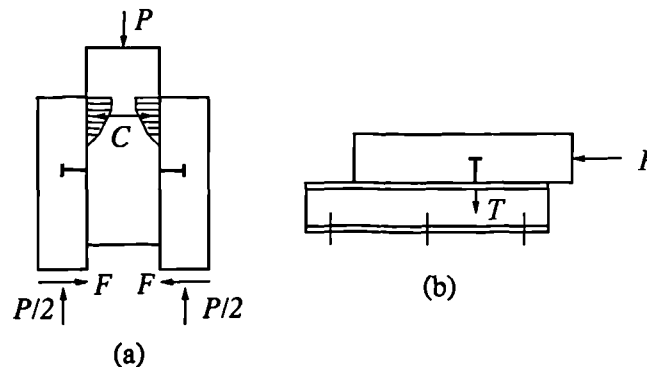
Figure 10.1: (a) Standard test arrangement; (b) Slutter and Fisher's specimen.

In the absence of a more reliable method, this kind of test arrangement is recommended by Eurocode 4 [7], and was used by most of the researchers. However, Slutter and Fisher [46] used a quite different test arrangement in that the concrete slabs were free to separate. This induced additional tensile forces T in ' the stud connectors, as shown in Figure 10.1(b). These tests are not selected.

Cyclic loads

There are two kinds of cyclic loads. One is reversed loading, where the shear forces applied to the stud connectors repeat in opposite directions, while the other is unidirectional loading, where the shear forces repeat only in one direction. From the reported studies, a common conclusion has been reached that stud connectors behave more favourably under reversed loading than under unidirectional loading. As design is based on the most critical state, only those tests under unidirectional loading are selected.

Peaks of cyclic loads

As mentioned in Section 10.2, the influence of the peak loads was considered by Oehlers as a governing factor for determining the endurance of stud connectors, while it was neglected by Roik, provided that the peak loads were less than 60% of the static strength of the connectors. In the following study, Roik's conclusion is accepted with the conditions that the concrete strengths f_c are between 15 and 50 N/mm^2, and the static strengths are as given by Eurocode 4 [7] (equation (2.5)). Therefore, only those data meet this rule are selected.

Casting of concrete

The fracture of stud connectors is initiated by the damage of concrete at the base of the stud, so the quality of concrete in this area is of great importance. One significant influence factor is the casting of concrete slabs. The best way is to cast them horizontally as in practice for a composite beam. However, some reported tests had concrete slabs cast vertically. With this position, an air pocket or weak concrete may establish around the base of stud, which have an unfavourable effect. These tests are not selected.

Failure modes

Three kinds of failure modes were reported in the previous studies. These are:

Type A: Cracks starts at the base of the stud shank, and gradually extend through the base or through the weld collar (Figure 10.2);
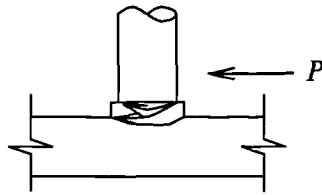
Figure 10.2: Type A fatigue failure.

Type B: Cracks start at the base of the weld collar and extend through the region of welding influence in the flange material (Figure 10.3);
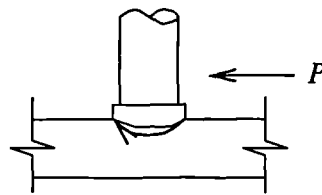

Figure 10.3: Type B fatigue failure.

Type C: Cracks start at the base of the weld collar, and developed either directly through the flange or first alongside the welding influence zone and then through the flange (Figure 10.4).
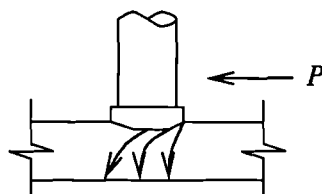

Figure 10.4: Type C fatigue failure.

Types A and B are due to the shear forces only. Type C has the lowest endurance, and is usually observed in beams with high tensile stress in the flange or with flanges of thickness much less than the diameter of the stud, which is beyond the range of this study. So, tests failed by Types A and B are selected.

10.4   Statistical analyses

The study is based on the design method of Eurocode 3. Expressed in terms of mean values, equation (10.4) becomes

$$N\Delta\tau^m = K \tag{10.8}$$

or

$$\log N = -m \log \Delta\tau + k \tag{10.9}$$

In graphical form, equation (10.9) is known as the τ-N line for stud connectors. All logarithms used in this chapter are to base 10.

The selected 115 data are divided into six types, as shown in Figure 10.5, according to their dimensions, reinforcement in concrete slabs and testing methods. Type 1 groups the tests reported by Mainstone and Menzies ([32], [33]), which were conducted with the concrete slabs bedded in mortar over papers laid on the greased steel base-plate of the loading frame. Type 2 are those reported by Hallam [15]. The basic specimen used differed from the other types mainly by casting a rod into the slabs at the base of the specimen to prevent separation of the slab from the joist. Types 3 and 4 are different from the others in that studs were arranged in two rows (type 3) and that the two concrete slabs were replaced by an un-reinforced one (type 4). Foley's tests (type 5) had the standard form of push-out specimens as recommended by Code of Practice CP 117. The difference in type 6 (tests reported by Maeda [31]) is that in these tests the bond between steel and concrete was not broken before testing began.
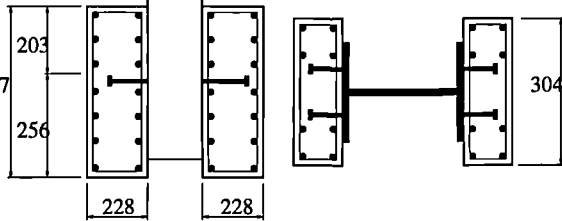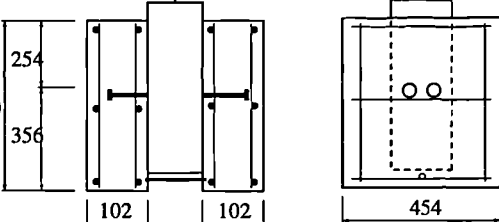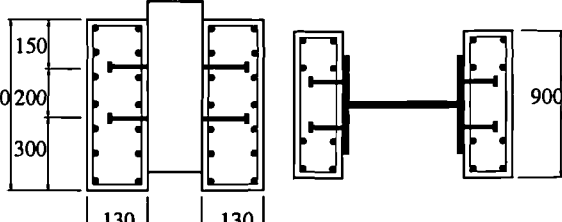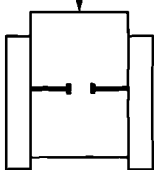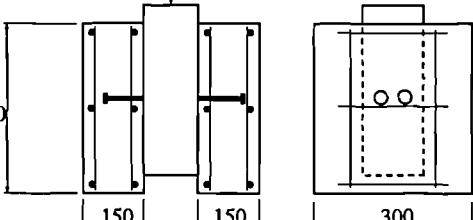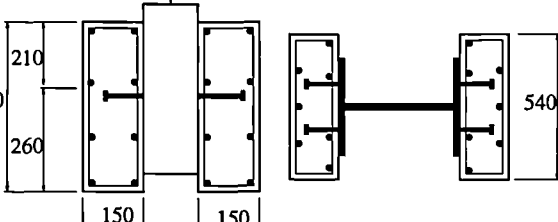
Figure 10.5 185

Type	Group	Dimensions	Number	Ref
1	1	457, 203, 256, 228, 228, 304	8	[31] [32]
2	2	610, 254, 356, 102, 102, 454	9	[15]
3	1	600, 150, 200, 300, 130, 130, 900	4	[36]
4	1		34	[27]
5	3	460, 150, 150, 300	6	[13]
6	4	470, 210, 260, 150, 150, 540	54	[30]

Figure 10.5: Classification of specimens for fatigue push tests.

The corresponding mean τ-N lines for all the types are shown in Figure 10.6. Except for type 3 where $\Delta\tau$ was not a variable, the differences between the other types are clear. To clarify whether the influence of specimen dimensions, reinforcement and testing methods are significant or only by chance, statistical methods for testing means and standard deviations are applied.
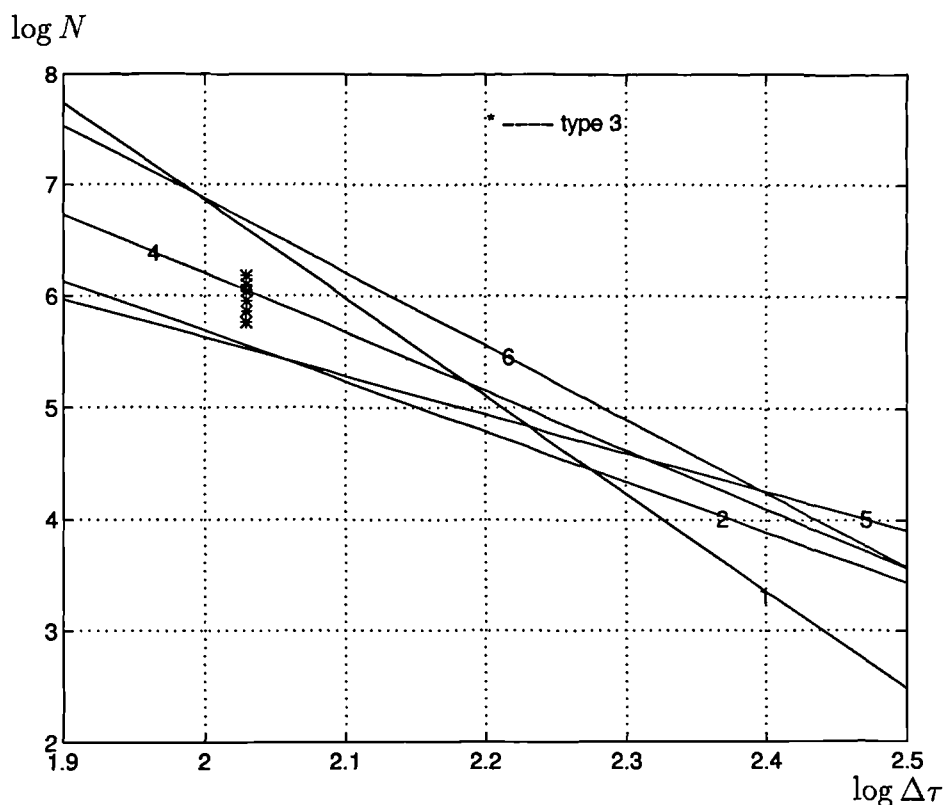
Figure 10.6: τ-N lines for all the types.

10.4.1 Variable tested

The six types are regarded as six uncorrelated samples. If one of them is chosen as the base sample, according to equation (10.9) the τ-N line for this sample is

$$\log N = -m_{\rm b} \log \Delta\tau + k_{\rm b} \qquad (10.10)$$

then for each data in a sample with size n, the error between the tested endurance and the theoretical one from equation (10.10) can be found as

$$Z_i = \log N_i - \log N = \log N_i + m_b \log \Delta\tau - k_b, \quad (i = 1, \cdots, n). \quad (10.11)$$

For the base sample, the mean and the standard deviation of Z are ($\mu_{Z_b} = 0$, σ_{Z_b}), and for another sample, or called compared sample, they are (μ_{Z_c}, σ_{Z_c}).

Suppose the τ-N line for the compared sample (m_c, k_c) is parallel to the one for the base sample, that is, $m_b = m_c$ and $k_b \neq k_c$, as shown in Figure 10.7(a). It is clear that the closer k_c is to k_b, the smaller is the difference between μ_{Z_c} and μ_{Z_b}. Now, suppose $m_b \neq m_c$ while $k_b = k_c$ as shown in Figure 10.7(b). In this case, the difference between μ_{Z_c} and μ_{Z_b} will reflect the difference between m_c and m_b. Therefore, if μ_{Z_c} and μ_{Z_b} are significantly different, then the two samples come from distinct populations. The difference between μ_{Z_c} and μ_{Z_b} can be tested by the two-sample t-test.
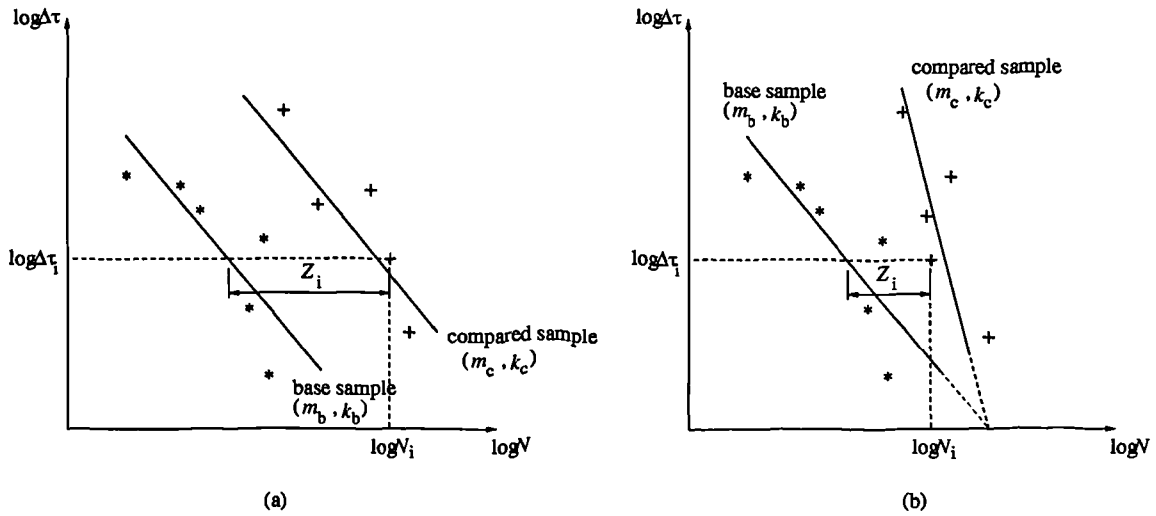
Figure 10.7: (a) $m_b = m_c$ and $k_b \neq k_c$; (b) $k_b = k_c$ and $m_b \neq m_c$.

However, there exists another case that the τ-N lines for the two samples intersect at a point as shown in Figure 10.8. Suppose the test data of the compared sample are evenly distributed above and below the τ-N line for the base sample. Then, μ_{Z_c} may be so close to μ_{Z_b} that the two-sample t-test will conclude that

there is no significant difference between the two samples, even though k_c and k_b are different. However, the difference can be reflected by σ_{Z_c} and σ_{Z_b}, in that σ_{Z_c} becomes close to σ_{Z_b} as the acute angle between the two lines reduces. The closeness can be tested by the F-test.
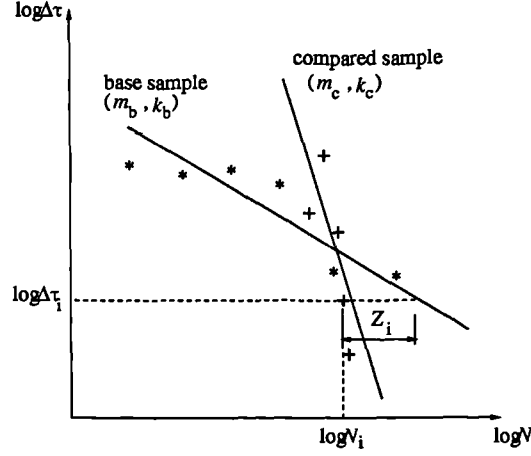
Figure 10.8: $m_b \neq m_c$ and $k_b \neq k_c$.

In summary, the provision for testing differences due to specimen dimensions, reinforcement and testing methods is that there is no significant difference between the two types of specimens compared, only when both F-tests and t-tests prove it.

10.4.2 Procedures

1. Choose a sample with large size ($n > 30$) as the base sample, and find its τ-N line:

$$\log N = -m_b \log \Delta \tau + k_b \qquad (10.12)$$

2. Let

$$Z_i = \log N_i - \log N = \log N_i + m_b \log \Delta \tau_i - k_b \qquad (10.13)$$

and calculate the values of Z_i for the base sample and another sample (compared sample).

3. Use the F-test to compare the standard deviations σ_{Z_b} and σ_{Z_c} of the two samples, with the null hypothesis H_o: $\sigma_{Z_b} = \sigma_{Z_c}$ against the alternative hypothesis H_a: $\sigma_{Z_b} \neq \sigma_{Z_c}$ at the 5% level of significance.

When the null hypothesis is rejected, the conclusion is, with 95% confidence, that the two samples (or two types) are from distinct populations affected by certain reasons. When the null hypothesis is accepted, it only means the two samples have homogeneous standard deviation. To establish if they are from the same population, two-sample t-tests are needed.

4. Use the two-sample t-test to compare the means μ_{Z_b} and μ_{Z_c} of the two samples with homogeneous standard deviation ($\sigma_{Z_b} = \sigma_{Z_c}$). The null hypothesis is H_o: $\mu_{Z_b} = \mu_{Z_c}$ and the alternative hypothesis H_a: $\mu_{Z_b} \neq \mu_{Z_c}$. Tests are done at the 5% level of significance.

At this stage, the acceptance of the null hypothesis means the two samples (or two types) are from the same population, and the influences of the differences between the two types are only by chance, while the rejection of the null hypothesis means the two samples are from distinct populations which are characterised by the differences between the types.

10.4.3 Results of F-tests and t-tests

Table 10.1: Results of statistical testing.

Base sample	Type 1	Type 2	Type 3	Type 4	Type 5	Type 6
Type 4	A	R	A	-	R	R
Type 6	R	R	R	R	R	-

A — accept the null hypothesis;

R — reject the null hypothesis.

Among the six types, only types 4 and 6 have sizes greater than 30. Each of

them is selected as the base sample, and the results are listed in table 10.1, in which A means the acceptance of the null hypothesis that the two types are from the same population, while R the rejection of the null hypothesis. Details of the testing are given in Tables 10.3 and 10.4.

It can be concluded at the 5% level of significance that the 115 data fall into four significantly different groups, as shown in Table 10.2 and also in Figure 10.5.

Table 10.2: Four significantly different groups.

Group	Type in the group	n	τ-N line
Group 1	Types 1, 3 and 4	46	$\log N = -5.4 \log \Delta\tau + 17.1$
Group 2	Type 2	9	$\log N = -4.5 \log \Delta\tau + 14.7$
Group 3	Type 5	6	$\log N = -3.4 \log \Delta\tau + 12.5$
Group 4	Type 6	54	$\log N = -6.6 \log \Delta\tau + 20.0$

10.5 A new approach to a design method

According to the results of statistical analyses given in Table 10.2, the significant differences among the groups are due to the bond between steel and concrete (Group 4) and the restraint to the separation of the slabs (Group 2), while the differences due to different dimensions, rows of studs and reinforcement (the three types of Group 1) are only by chance. The low influence of reinforcement is probably because the peaks of cyclic loads for all those six types are less than half of the static strengths, under which the transverse tensile strain in the concrete slabs could not reach the ultimate value. For the same reason, the bond between steel and concrete could not be broken at the low peak loads, so that it plays a significant part in the endurance of the studs.

From the classification shown in Figure 10.5, Group 3 and Group 1 are only

different in dimensions, so there must be some unclassified factors to cause the two groups to be significantly different.

As mentioned in Section 10.2, Oehlers found the peak of the cyclic load P_{max} had significant influence on the endurance of stud connectors, while Roik concluded that the influence can be neglected if it is less than 60% of the static strength P_{rs}. Re-examining the data in each of the four groups, it is found that Group 3 has very high peak loads with P_{max}/P_{rs} from 0.55 to 0.6, while all the other groups have $P_{max}/P_{rs} \leq 0.5$. It is therefore the author's oppinion that the difference between Group 3 and the other Groups could be due to the higher peak loads.

To establish a design method, Groups 2 and 3 are excluded because of the small size. Group 4 is also excluded, even though it has the largest size, because it is very difficult to know if the bond between steel and concrete in a composite bridge stays unbroken in the whole life. To make it safe, design method is based on test results without the influence of the bond, so only Group 1 is considered. Its τ-N line gives mean values of the endurance as

$$\log N = -5.4 \log \Delta\tau + 17.1 \qquad (10.14)$$

The characteristic values are the values below which the probability is 2.3%, and are obtained from the mean minus two standard deviations:

$$\log N = -5.4 \log \Delta\tau + 16.5 \qquad (10.15)$$

or expressed as

$$N\Delta\tau^{5.4} = 10^{16.5}, \quad \text{in N/mm}^2 \text{ units} \qquad (10.16)$$

To reduce the scatter, the design method should be based on data from one population. So, the two alternative methods proposed by Oehlers (equation (10.6)) and by Roik (equation (10.7)) are believed to be unreliable. The data used by Oehlers were from types 1, 2, 3 and 6 and were from three populations

(Groups 1, 2 and 4), while those used by Roik were from two different populations (Groups 1 and 2). Another point to be mentioned is that 7 data from Hallam [15] used by Roik were the failure results of both slabs of the push-out specimens. Hallam continued his tests on the other slab after one slab had failed. It is the author's opinion that data from the second slabs should be excluded, since failure in the first slab may alter the range of stress applied.

Clearly, the reason for the discrepancies in the existing methods is the different extent of the mix of data from the four distinct Groups.

10.6 Conclusions

Statistical analyses of testing means and standard deviations have proved that fatigue push-out tests are significantly influenced by the testing methods, such as the bond between steel and concrete and the restraints on the concrete slabs. Another influence factor is the peak of the cyclic load, but it can be neglected, provided that the peak load is not more than half of the static strength of the connector.

The existing methods are unreliable, due to the fact that they were not deduced from the data of a single population. In other words, they are affected to some extent by different testing methods.

To reduce the scatter, the design method should be based on data from a single population. This leads to the characteristic values of the endurance with 2.3% failure probability to be,

$$N\Delta\tau^{5.4} = 10^{16.5}, \quad \text{in N/mm}^2 \text{ units} \tag{10.17}$$

Table 10.3: Type 4 as base sample

Type	n	μ_Z	σ_Z	F	$F_{\alpha=5\%}$	t	$t_{\alpha=5\%}$
4	34	0.00	0.27				
1	8	0.11	0.32	1.34 $<$	2.25	1.02 $<$	2.02
2	9	-0.45	0.22	1.58 $<$	3.04	4.53 $>$	2.02
3	4	-0.16	0.45	2.71 $<$	2.84	1.72 $<$	2.02
5	6	-0.42	0.64	5.49 $>$	2.53		
6	54	0.42	0.39	2.03 $>$	1.79		

In tables 10.3 and 10.4, $F = \frac{\sigma_1}{\sigma_2}$, $\sigma_1 \geq \sigma_2$; $F_{\alpha=5\%}$ is the value found from Table A.14 [24] at 5% level with $\nu_1 = n_1 - 1$ and $\nu_2 = n_2 - 1$; $t = \dfrac{\mu_1 - \mu_2}{s_c\sqrt{\dfrac{1}{n_1} + \dfrac{1}{n_2}}}$,

where $s_c^2 = \dfrac{(n_1 - 1)\sigma_1^2 + (n_2 - 1)\sigma_2^2}{n_1 + n_2 - 2}$; $t_{\alpha=5\%}$ is the value found from Table A.7 [24] at 5% level with $\nu = n_1 + n_2 - 2$.

Table 10.4: Type 6 as base sample

Type	n	μ_Z	σ_Z	F	$F_{\alpha=5\%}$	t	$t_{\alpha=5\%}$
6	54	0.00	0.37				
1	8	-0.35	0.27	1.89 $<$	3.30	2.58 $>$	2.00
2	9	-1.00	0.30	1.51 $<$	3.01	7.62 $>$	2.00
3	4	-0.65	0.45	1.44 $<$	2.84	3.30 $>$	2.02
4	34	-0.44	0.32	1.36 $<$	1.64	5.70 $>$	2.00
5	6	-0.98	0.71	3.61 $>$	2.37		

Chapter 11

Conclusions

11.1 Static resistance of studs welded through profiled sheeting

The resistance of stud shear connectors welded through profiled sheeting is influenced by the geometry of the ribs and the position of the studs within them. This is allowed for in codes by applying a reduction factor to the resistance of the stud in a solid slab.

The apparent inappropriateness of the current reduction factors is shown by a study of 183 reported results of push-out tests, in that the errors between the predicted and tested values in some situations exceed 60%. The reason, revealed by 34 new push-out tests, is that they do not distinguish between the various modes of failure.

There are five possible failure modes for stud connectors with transverse sheeting and two with parallel sheeting. New models are developed with respect to each of these failure modes.

Transverse sheeting with one stud per trough

For transverse sheeting with one stud per trough, the failure modes can be shank shearing, concrete pulling out and rib punching.

Shank shearing failure is fracture of the shank of a stud above its weld collar, with a smooth failure surface and hardly any permanent deformation of the shank. In the slab, there is only local damage at the front of the stud (Figure 4.36).

Concrete pulling out failure is the pulling out of the stud from the concrete slab, together with a wedge-shaped portion of concrete. The damage in the slab extends to a much larger area (Figure 4.37).

Rib punching failure is also fracture of the shank of a stud above its weld collar, but with large amount of deformation in the shank and crushing of concrete at the front of the stud. Also, the rib in front of the stud tears up to its mid-depth (Figure 4.38).

The occurrence of these three failure modes depends on the tensile force developed in the shank of the stud, which follows the criterion expressed by equation (5.7). In graphic form, this criterion is schematically shown in Figure 11.1, where P_r and T are the shear and tensile forces in the stud, respectively. P_{rs} is the shank shearing resistance (equation (5.6)), and T_y is the resistance of the stud to uniaxial tension (equation (5.5)). At point A, with no tensile force in the stud, shank shearing failure occurs. When the tensile force T increases, the failure mode changes from concrete pulling out to rib punching.

The mean resistances for these three failure modes can be predicted with a reduction factor k_t relative to the shank shearing resistance P_{rs}; that is,

$$P_r = k_t P_{rs} \tag{11.1}$$

where the reduction factor k_t is given by equation (11.2):

$$k_t = \frac{\eta + \lambda\sqrt{1 - \eta^2 + \lambda^2}}{1 + \lambda^2} \leq 1.0 \tag{11.2}$$

Factors η and λ reflect the different failure modes. They are functions of the material strengths and the geometry of the ribs, as given by equations (5.18) and (5.19) for concrete pulling out failure, and (5.33) and (5.34) for rib punching failure.
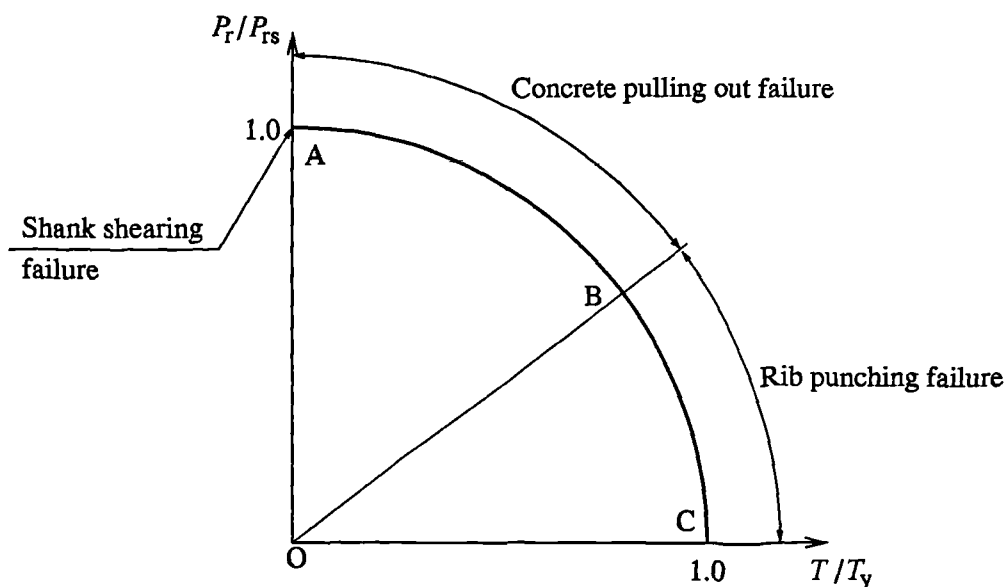

Figure 11.1: Failure criterion for stud connectors with transverse sheeting.

For the commonly used materials ($20 \leq f_c \leq 35$ N/mm^2 and $f_u \geq 400$ N/mm^2), the influences of the strengths are negligible, in that the strength ratios η_o (equation (8.4)), λ_o (equation (8.6)), f_{yd}/P_{rs} (equation (8.9)) and T_{sy}/P_{rs} (equation (8.10)) are found to be constants, as shown correspondingly in Figures 8.2, 8.3, 8.10 and 8.12. The failure modes are controlled only by four factors (equation (8.17)): concrete cover in front of the stud e_f, height of the stud h, thickness of the sheeting in terms of the thickness factor η_t and depth of the trough h_p. These symbols are as shown in Figures 5.2 and 5.5.

When determining the characteristic and design resistances of a stud connector, the number of studs per shear span is of great importance, because the resistances reduce as the number decreases (Table 9.1). However, it is not practicable to take account of this variable in design. Considering that four is the minimum number of studs per shear span in practice, to make it safe, design

resistance is given based on the data with four studs per specimen (equation (9.37)).

Transverse sheeting with two studs per trough

For two studs per trough, the failure criterion as given by equation (5.7) is still followed, so the resistance can also be predicted by a reduction factor relative to the resistance to shank shearing failure as given by equation (11.1).

If the two studs are in-line along the trough, they behave in much the same way as one stud per trough, except with lower resistances (equation (5.20)), because the resistance of the concrete to the pulling out action of the two studs is reduced, and hence the tensile forces in the shanks of the studs increase.

If the two studs are staggered or transverse to the trough, redistribution of shear forces occurs until the average resistance of the two studs is reached. The failure mode is rib punching (for the stud on the unfavourable side) combined with either shank shearing or concrete pulling out (for the opposite stud). Similar to one stud per trough, the influence of the strengths of the materials is negligible, so the redistribution is actually governed by: transverse spacing of the studs s_t, height of stud h, thickness of sheeting in terms of the thickness factor η_t and depth of the trough h_p, as given by equation (8.21). The symbols are as shown in Figure 5.7.

Parallel sheeting

The behaviour of stud connectors with parallel sheeting is unlike that with transverse sheeting, in that there is no plastic hinge developed in the shank of the stud, and the studs do not follow the failure criterion given by equation (5.2), because the mechanism of load transfer is completely different.

With parallel sheeting, the shear force is dispersed into the concrete in terms of a bearing pressure between the concrete and the stud connector over a certain height of the stud. The dispersal is three-dimensional, which develops tensile forces in both the concrete and the shank of the stud. The resistances of the concrete to the tensile forces and the pulling action of the studs govern the failure modes, either splitting or pulling out.

When the tensile strain of concrete reaches its ultimate value, concrete slabs split longitudinally, usually along the lines of the studs or between them. This is splitting failure. The resistance relates to: side cover of concrete to the stud e, height h and diameter d of the stud, depth of the trough h_p, overall depth of the slab h_c and strength of the concrete f_c, as given by equation (6.14).

The pulling out failure is due to the low resistance of the concrete to the pulling action of the stud. It depends mainly on the projection of the stud above the flanges of the sheeting $(h - h_p)$ and the top width of the trough b_u $(= s_t + 2e_u)$ (equations (6.26) to (6.28) and (6.31)).

Lightweight concrete

The use of lightweight concrete has no effect on the mechanism of load transfer. It affects only the ductility of the stud (Figures 4.21 and 4.22 cf. Figures 4.19 and 4.20) and the material properties, such as the strengths and the elastic modulus of the concrete.

Therefore, the resistances of stud connectors with lightweight concrete can be predicted by all the models for normal weight concrete by using the conversion factors as given by Eurocode 2: Part 1-4 [5]: η_1 for concrete strengths (equation (7.6)) and η_E for the elastic modulus (equation (7.2)).

Scopes of the results

The results summarised above are valid for:

- 16- and 19-mm stud connectors with the ultimate tensile strengths not less than 400 N/mm^2;

- centre-to-centre spacing between the studs is from 2.8d to 5d in the direction transverse to the shear force, and not less than 3d in-line along the shear force;

- concrete strengths from 20 to 35 N/mm^2 and the air-dry densities in the classes not less than 1.6 (the density classes (Table 7.1) are as given by Eurocode 2: Part 1-4 [5]);

- the projection of the head of the stud above the flanges of the decking $(h - h_\mathrm{p})$ not less than 35 mm;

- trapezoidal profiled sheeting with thickness from 0.7 to 1.5 mm and the ratio of the average width of the trough b_o to the depth h_p from 0.8 to 3.2;

- not less than four stud connectors per shear span.

11.2 Fatigue resistances of stud shear connectors in composite bridges

Push-out tests are the major method to study the resistance of stud connectors to fatigue. The testing methods, such as the presence or absence of bond between steel and concrete under low peak loads (less than 20% of the static strengths), and the restriction to the separation of concrete slabs from the steel beam, have significant influences on the results. Therefore, data with different testing methods and restraints should not be considered as a single population.

The current methods for predicting the fatigue resistances of stud connectors (Eurocode 3 [6], Oehlers' method [37] and Roik's method [44]) are unreliable, because they are affected to some extent by different testing methods and restraints.

A new method based on the data from a single population is derived (equation (10.16)). It is valid for cyclic loads with the peaks not greater than 50% of the static strengths of the connectors.

11.3 Suggestions for further studies

The statistical analyses (chapter 9) have shown that the number of stud connectors per specimen has significant influence on the characteristic and design resistances of stud connectors. As push-out tests are the major method to study the behaviour of stud connectors in composite beams, the number of studs per specimen should reflect the minimum possible number per shear span in practice. However, the available data from push-out tests that meet this requirement are very limited, especially for those with transverse sheeting (two studs per trough), parallel sheeting and lightweight concrete. The new models based on these data, though satisfactory, can only be of use conceptually.

For further understanding, more tests are needed to clarify the following uncertainties:

1. For transverse sheeting with two in-line studs, the spacing at which the two studs can be treated as two single studs. The new model developed in chapter 5 which allows for the reduction in strengths due to the in-line position is valid for the spacing not more than 5d, but it is based on only 13 data.

2. For transverse sheeting with two studs per trough, the effects of the two

positions: transverse or staggered. The statistical analyses carried out in chapter 9 show that the partial safety factor γ_M is higher for transverse studs than for staggered ones (table 9.2). It is based on only 28 data, among which there are eight with eight transverse studs per specimen, three with eight staggered studs and 17 with four staggered studs. This results in uncertainties as whether or not the higher γ_M is due to the inappropriate theoretical model.

3. For parallel sheeting, the assumption of the failure surface of the concrete cone. The two new models are based on a total of 41 data with number of studs per specimen ranging from 2 to 12.

4. The effects of lightweight concrete. Though the analyses presented in chapter 7 have proved that the new models are also valid for stud connectors in lightweight concrete, they are based on only 15 data, with the number of studs per specimen ranging from 2 to 6.

5. The influence of the transverse reinforcement on the failure modes.

Bibliography

[1] BS 5400 *Steel, concrete and composite bridges. Part 10: Code of practice for fatigue*, British Standards Institution, 1980

[2] BS 5950 *The structural use of steel in buildings: Part 3: Section 3.1: Code of practice for design of composite beams*, British Standards Institution, 1990

[3] Canadian Prestressed Concrete Institute: 'Metric design manual precast and prestressed concrete', 1st edition, Ottawa, Ontario, 1982, pp6-9

[4] DD ENV 1992-1-1 Eurocode 2: 'Design of concrete structures, Part 1: General rules and rules for buildings', British Standards Institution, London, 1992.

[5] DD ENV 1992-1-4, Eurocode 2: 'Design of concrete structures, Part 1-4: The use of lightweight aggregate concrete with closed structure', British Standards Institution, London, 1994.

[6] DD ENV 1993-1-1: 'Design of steel structures; General rules and rules for building', British Standards Institution, 1993

[7] DD ENV 1994-1-1, Eurocode 4: 'Design of composite steel and concrete structures, Part 1.1: General rules and rules for buildings', British Standards Institution, London, 1994.

202

[8] The Institution of Structural Engineers: 'Guide to the Structural use of lightweight aggregate concrete', London, 1987

[9] Bode, H., and Künzel, R.: 'Steifigkeit und Verformbarkeit von Verbundmitteln im Hochbau', International Symposium Composite Steel and Concrete Structures, Vol 1, Bratislava, 132/1987

[10] Bode, H., and Künzel, R.: 'Zur Anwendung der Durchschweißtechnik im Verbundbau', Forschungsbericht 2/1991, Universität Kaiserslautern

[11] Chien, E. Y. L., and Ritchie, J. K.: 'Design and construction of composite floor systems', Canadian Institute of Steel Construction, Universal Offset Limited, Markham, Ontario, 1984

[12] Fisher, J. W.: 'Design of composite beams with formed metal deck', *AISC Engineering Journal*, 7(3), 1970, pp88-96

[13] Foley, L.: 'The fatigue strength of stud shear connectors in push specimens', MEngSc thesis, University College, Cork, Aug. 1983

[14] Grant, J. A., Fisher, J. W., and Slutter, R. G.: 'Composite beams with formed metal deck', *Eng. J., Amer. Inst. of Steel Construction*, First Quarter, Vol 14, 1977, pp24-42

[15] Hallam, M. W.: ' The behaviour of stud shear connectors under repeated loading', Research Report 281, University of Sydney, School of Civil Engineering, Aug. 1976

[16] Hanswille, G.: 'Shear resistance of headed studs with profiled steel sheeting', Technical Paper H7, Bergische Universität, Gesamthochschule Wuppertal, December 1993

[17] Harding, P. W.: 'Composite floors with profiled steel sheeting', PhD Thesis, Department of Civil and Structural Engineering, University of Wales, Cardiff, March 1990

[18] Hawkins, N. M., and Mitchell, D.: 'Seismic response of composite shear con-
nections', *J. of Structural Engineering, ASCE*, 110, No.9, September 1984,
pp2121-2140

[19] Hicks, S. J., and McConnel, R. E.: 'Behaviour of shear studs in compos-
ite beams: push-out tests', Department of Engineering, University of Cam-
bridge, November 1995

[20] Hosain, M. U.: 'Composite beams with headed studs in narrow ribbed metal
deck', Composite construction in steel and concrete II, Proceedings of an
Engineering Foundation Conference, Potosi, 1992, American Society of Civil
Engineers, 1993, pp771-782

[21] Jayas, B. S., and Hosain, M. U.: 'Behaviour of headed studs in composite
beams: push-out tests', *Can. J. Civ. Eng.*, 15, 1988, pp240-253

[22] Johnson, R. P., and Oehlers, D. J.: 'Analysis and design for longitudinal
shear in composite T-beams', *Proc. ICE*, Part 2, 71, Dec. 1981, pp989-1021

[23] Johnson, R. P., and Huang, D. J.: 'Partial safety factors γ_M for composite
steel and concrete beams in bending', *Proc. of Institution of Civil Engineers,
Structurals and Buildings*, Vol. 104, May 1994, pp193-203

[24] Kennedy, J. B., and Neville, A. M.: 'Basic statistical methods for engineers
and scientists', 3rd edition, Harper and Row, New York, 1986

[25] Kong, F. K., and Evans, R. H.: 'Reinforced and prestressed concrete', 3rd
edition, Chapman and Hall, London, 1987

[26] Lawson, R. M.: 'Shear connection in composite beams', *Steel Construction
Today*, July 1992, pp171-176

[27] Lloyd, R. M., and Wright, H. D.: 'Shear connection between composite slabs
and steel beams', *J. Construct. Steel Research*, 15, 1990, pp255-285

[28] Lo, K. K.: 'Fatigue testing of stud shear connectors', MEng thesis, University of Melbourne, 1978

[29] Lyons, J. C., and Easterling, W. S.: 'Strength of welded shear studs: Vols I and II', Research Report No. CE/VPI-ST 94/07, Department of Civil Engineering, Virginia Polytechnic Institute and State University, December 1994

[30] Madsen, H. O., Krenk, S., and Lind, N. C.: 'Methods of structural safety', Prentice-Hall, Inc., Englewood Cliffs, NJ 07632, 1986

[31] Maeda, Y., and Matsui, S.: 'Effects of concrete placing direction on static and fatigue strengths of stud shear connector', Technical reports of the Osaka University, Vol. 33, No. 1733, Oct. 1983, pp397-406

[32] Mainstone, R. J., and Menzies, J. B.: 'Shear connectors in steel-concrete composite beams for bridges, Part 1: Static and fatigue tests on push-out specimens', Concrete, Vol. 1, No. 9, Sept. 1967, pp291-302

[33] Menzies, J. B.: 'CP117 and shear connectors in steel-concrete composite beams made with normal-density or lightweight concrete', The Structural Engineer, 49, No. 3, March 1971, pp137-154

[34] Mottram, J. T., and Johnson, R. P.: 'Push tests on studs welded through profiled steel sheeting', Structural Engineer, 68, No. 10, May 1990, pp187-193

[35] Oehlers, D. J., and Johnson, R. P.: 'The splitting strength of concrete prisms subjected to surface strip or patch loads', Magazine of Concrete Research, Vol. 33, No. 116, September 1981, pp171-179

[36] Oehlers, D. J., and Johnson, R. P.: 'The strength of stud shear connections in composite beams', The Structural Engineer, Vol 65B, No. 2, June 1987, pp44-48

[37] Oehlers, D. J.: 'Deterioration in strength of stud connectors in composite bridge beams', *ASCE J. of Structural Engineering*, Vol. 116, No. 12, Dec. 1994, pp3417-3431

[38] Oehlers, D. J., and Bradford, M. A.: 'Composite steel and concrete structural members: fundamental behaviour', Pergamon, Oxford, 1995

[39] Robinson, H.: 'Tests of composite beams with cellular deck', *ASCE Journal of Structural Division*, 93(ST4), 1967, pp139-163

[40] Robinson, H.: 'Multiple stud shear connections in deep ribbed metal deck', *Can. J. Civ. Eng.*, 15, 1992, pp553-567

[41] Roik, K. H., Hanenkamp, W., and Bürkner, K. E.: ' Erfassung spezieller Einflüsse auf die Tragfähigkeit von kopfbolzendübeln in Verbundträgern bei Verwendung von Stahlprofilblechen', Ruhr-Universität-Bochum, Bericht Nr. 7902/I/Versuchsbericht and Bericht Nr. 7902/II/Gutachten, februari 1979

[42] Roik, K. H., and Hanswille, G.: 'Gutachten für die Holorib GmbH Zur Frage der Tragfähigkeit von Kopfbolzendübeln bei auf dem Verbundträgerobergurt gestoßenen Profilblechen', Ruhr-Universität-Bochum, July 1988

[43] Roik, K., and Lungershausen, H.: 'Verbundträger mit Stahltrapezprofilblechen mit Rippenhöhen > 80 mm', Studiengesellschaft für Anwendungstechnik von Eisen und Stahl e. v, Projekt 99, Düsseldorf, 1988

[44] Roik, E. H., and Hanswille, G.: 'Backgroud report on Eurocode 4: Limited state of fatigue for headed studs', Report EC4/11/90, Bochum, Sept. 1990

[45] Stark, J. W., and von Hove, B. W. E. M.: 'Statistical analysis of push-out tests on stud connectors in composite steel and concrete structures', TNO Building and Construction Research, Report BI-91-163, Sept. 1991

[46] Slutter, R. G., and Fisher, J. W.: 'Fatigue strength of shear connectors', Highway Research Record, No. 147, 1966

[47] Wright, H. D., and Gallocher, S. C.: 'The capacity of the shear connection between composite slabs and steel beams', Private communication, H. D. Wright, University of Strathclyde, Department of Civil Engineering, Glasgow, August 1994